JYU DISSERTATIONS 559

Markku Hyrkäs

Cutting Rules in Non-Equilibrium Many-Body Theory

UNIVERSITY OF JYVÄSKYLÄ
FACULTY OF MATHEMATICS
AND SCIENCE

JYU DISSERTATIONS 559

Markku Hyrkäs

Cutting Rules in Non-Equilibrium Many-Body Theory

Esitetään Jyväskylän yliopiston matemaattis-luonnontieteellisen tiedekunnan suostumuksella
julkisesti tarkastettavaksi Ylistönrinteen luentosalissa KEM1
syyskuun 29. päivänä 2022 kello 12.

Academic dissertation to be publicly discussed, by permission of
the Faculty of Mathematics and Science of the University of Jyväskylä,
in building Ylistönrinne, lecture hall KEM1, on September 29, 2022, at 12 o'clock noon.

JYVÄSKYLÄN YLIOPISTO
UNIVERSITY OF JYVÄSKYLÄ

JYVÄSKYLÄ 2022

Editors
Ilari Maasilta
Department of Physics, University of Jyväskylä
Päivi Vuorio
Open Science Centre, University of Jyväskylä

ISBN 978-951-39-9202-6 (PDF)
URN:ISBN:978-951-39-9202-6
ISSN 2489-9003

Permanent link to this publication: http://urn.fi/URN:ISBN:978-951-39-9202-6

Abstract

Quantum many-body theory is a tool for modeling the behaviour of systems of many interacting quantum particles. It breaks transitions of the many-particle system from one state to another down to the possible ways this transition can occur in terms of interactions between individual particles. These possible transitions are depicted using diagrams, and can be further broken down into diagrams depicting the basic interaction processes from which the full transition process is build of. Any set of possible interaction processes can then be chosen and applied as corrections to a non-interacting system, thus building an approximate model of the interacting system, that only allows transitions via the included processes. What can reasonably be included in this way is necessarily a tiny subset of the full complexity of the many-body system. Still, in practice quantum many-body theory can be applied successfully to many real-world cases, since often the interactions involved in a specific process are primarily of the simplest types.

The variety of different approximations that quantum many-body theory allows raises the question of choosing the best option for a particular application. The choice of an approximation is important not only in order to include the interaction processes that contribute to the phenomenon under investigation, but also to retain relevant properties of the exact system. Certain approximations can, for example, violate conservation laws (of energy, particle number etc.). This thesis addresses in particular another important property that can be violated in approximations: the positivity of probabilities.

A recipe to construct positive approximations, i.e. approximations that are guaranteed to give non-negative probabilities, has been previously developed for system in equilibrium at zero-temperature [1, 2]. This recipe is based on diagrammatic cutting-rules, which are used to cut diagrams depicting basic interaction processes further into so called scattering diagrams. Expressing an approximation in terms of scattering diagrams makes its positivity, or lack of it, apparent. Furthermore, this approach makes the physical content of the diagrams more clear, providing further aid in the choice of the correct approximation.

In this thesis cutting rules that can be applied to systems in finite temperature are developed, and used to generalize the recipe for building positive approximations. This generalized recipe works not only for finite temperature systems, but also for systems that are perturbed to non-equilibrium state from an initial equilibrium. Several general results related to working with complicated diagrams are also derived.

Tiivistelmä (Abstract in Finnish)

Monen kappaleen kvanttiteoria on työkalu vuorovaikuttavien alkeishiukkasten käyttäytymisen mallintamiseen. Se rikkoo monista hiukkasista koostuvan järjestelmän transitiot tilasta toiseen erilaisiin tapoihin joilla tämä transitio voi tapahtua yksittäisten hiukkasten välisten vuorovaikutusten tasolla. Nämä erilaiset mahdollisuudet kuvataan diagrammeilla, jotka voidaan edelleen rikkoa diagrammeihin jotka kuvaavat erilaisia perustason vuoravaikutusprosesseja joista transitio kokonaisuudessaan koostuu. Mikä tahansa valikoima vuorovaikutusprosesseja voidaan sitten valita ja lisätä korjauksena vuorovaikuttamattomaan järjestelmään. Tästä seuraa approksimatiivinen malli vuorovaikuttavalle järjestelmällä, joka sallii transitiot ainoastaan sisällytettyjen vuorovaikutusprosessien kautta. Vuorovaikutukset jotka voidaan sisällyttää tällä tavoin ovat väistämättä vain pieni osa koko monihiukkasjärjestelmän monimutkaisuudesta. Siitä huolimatta monen kappaleen kvantti-teoriaa on sovellettu menestyksellä moniin todellisiin järjestelmiin, sillä usein tietyn ilmiön synnyttävät vuorovaikutukset ovat enimmäkseen yksinkertaisia.

Erilaisten approksimaatioiden lukumäärä jotka monen kappaleen kvanttiteoria sallii nostaa esiin kysymyksen oikein vaihtoehdon valinnasta kuhunkin tarkoitukseen. Oikean approksimaation valinta on tärkeää paitsi oikeiden vuorovaikutusprosessien sisällyttämiseksi tutkittavan ilmiön mallintamiseksi, myös tiettyjen todellisen systeemin fysikaalisten ominaisuuksien säilyttämiseksi. Jotkin approksimaatiot voivat esimerkiksi rikkoa säilyvyyslakeja (energian, hiukkaslukumäärän jne.). Tämä väitöskirja käsittelee erityisesti toista tulosten tulkinnan kannalta tärkeää ominaisuutta joka saattaa puuttua approksimaatiosta: todennäköisyyksien positiivisuus.

Approksimaatioiden jotka takaavat positiiviset todennäköisyydet, ns. positiivisten approksimaatioiden, rakentamiseksi on aiemmin kehitetty resepti [1, 2] joka toimii tasapainotilassa nollalämpötilassa oleville järjestelmille. Tämä resepti perustuu diagrammien leikkaussääntöihin, joiden avulla vuorovaikutusprosesseja kuvaavat diagrammit leikataan edelleen niin sanottuihin sirontadiagrammeihin. Approksimaation esittäminen sirontadiagrammien avulla tekee sen positiivisuuden, tai sen puutteen, ilmeiseksi. Sen lisäksi tämä lähestymistapa tekee approksimaation fysikaalisen sisällön hahmottamisen selkeämmäksi, helpottaen siten edelleen oikean approksimaation valintaa.

Tässä väitöskirjassa kehitetään leikkaussäännöt joita voidaan soveltaa järjestelmiin jotka ovat alussa tasapainotilassa äärellisessä lämpötilassa, mutta voidaan myöhemmin saattaa epätasapainotilaan. Näitä leikkaussääntöjä käytetään sitten yleistämään vastaavasti resepti positiivisten approksimaatioiden rakentamiseen. Sen lisäksi johdetaan useita yleisiä tuloksia monimutkaisten diagrammien käsittelyyn.

Author Markku Hyrkäs
Department of Physics and Nanoscience Center
University of Jyväskylä
Finland

Supervisor Robert van Leeuwen
Department of Physics and Nanoscience Center
University of Jyväskylä
Finland

Pre-examiners Yaroslav Pavlyukh
Department of Theoretical Physics
Wrocław University of Science and Technology
Poland

Michael Galperin
Department of Chemistry and Biochemistry
University of California, San Diego
USA

Opponent Gianluca Stefanucci
Department of Physics
University of Rome Tor Vergata
Italy

Preface

I started my journey as a doctoral student in the University of Jyväskylä in December 2011. This work is therefore a result of a decade of my life. What was originally intended to be a thesis built on numerical simulations ran first into a need to generalize existing methods in order to obtain novel results worthy of a doctoral thesis. These generalization attempts required theoretical tools that were either difficult to piece together from the existing research, or else non-existent. In deriving the results we needed these results were found to be applicable to much more than our original problem, and in fact could be used to solve some long-standing issues in the field. In the end no numerical calculations were performed, since these theoretical ventures resulted in enough material for a thesis in themselves.

I wish to thank first and foremost my supervisor Robert van Leeuwen, with whom I spent countless hours in discussion on topic of the thesis and off it. He was heavily involved with my research, especially during the final two years when I was the only other member of our research group. Robert took the readability of our papers very seriously, and whenever we thought of a more clear way to represent a particular issue, the time was always taken to do so. Thus large parts of our papers were rewritten multiple times, resulting not only in more understandable text for the reader, but also in deepened understanding for the authors. He remained patient and supportive when my own progress sometimes felt agonizingly slow. This allowed me to produce, despite my occasional doubts, a thesis that I can be proud of.

Among my other colleagues I wish to thank especially Daniel Karlsson both for his friendship and for his significant help with my research. From the countless other people that provided companionship during this journey I'd like to mention Luis Cort, Rosalba Juarez Mosqueda and Riku Tuovinen. A special mention in this regard goes to Janne Nevalaita, with whom I shared an office when I started, and who, after finishing his thesis in proper time and spending some time elsewhere, was still around when I finished.

I'm grateful for support from the Väisälä Foundation and the Finnish Cultural Foundation during the making of this thesis.

Lopuksi haluan kiittää vanhempiani, joiden luona saatoin aina rauhallisessa ilmapiirissä irtautua väitöskirjatyöstä hetkeksi.

Markku Hyrkäs, August 2022, Jyväskylä

List of publications

This thesis consists of an introductory part and of the following publications:

[I] M. Hyrkäs, D. Karlsson and R. van Leeuwen, Contour calculus for many-particle functions, J. Phys. A Math. Theor. **52** 215303 (2019).

[II] M. Hyrkäs, D. Karlsson and R. van Leeuwen, Diagrammatic Expansion for Positive Spectral Functions in the Steady-State Limit, Phys. status solidi **256** 1800615 (2019).

[III] M. Hyrkäs, D. Karlsson and R. van Leeuwen, Cutting rules and positivity in finite temperature many-body theory, J. Phys. A Math. Theor. **55** 335301 (2022).

Author's contribution

For all the publications the author has played a significant role in the derivation of the results and been the main author of the manuscript.

Contents

Chapter 1

Introduction

1.1 The Many-Body Problem

The many-body problem concerns understanding the behaviour of systems consisting of multiple mutually interacting parts. The region of systems presenting the many-body problem is flanked on the other hand by systems where the interactions are weak enough that one can describe the full system by considering a single piece at a time, and on the other hand by systems in which the number of parts is so large that the effects of their mutual interactions can be reduced to statistical concepts, such as when the movement of a large number of atoms is described by temperature and pressure.

Between the extremes there exist many important physical problems that resist simple attempts to cut them into manageable parts. In these cases one needs to consider the specifics, i.e. what is the property that needs to be calculated, and which aspects of the many-body system are likely to affect it meaningfully. The mathematical model of the system then needs to be put in such a form that the unimportant parts can be discarded without destroying the properties that are needed.

In practice such problems are often treated using so called perturbative methods. In these approaches one identifies the property of the system that prevents its solution, and starts by solving the system in its absence. One then introduces the property that was removed back as a weak perturbation, and calculates correction terms caused by its presence. Thus the solution to the original difficult problem can be approached step by step from an easier starting point.

This thesis concerns such a perturbation theory being applied to elementary particles in order to calculate properties of materials. The perturbation in this case is the electromagnetic interaction, either between particles in the material or as an external field corresponding for example to laser light directed to the material in an experiment. Although the methods discussed here are very general, to make the discussion more concrete we are going to consider in particular the so called photo-emission experiments.

1.2 Photo-Emission Experiments

A typical solid crystalline material consists of a lattice of atoms/molecules with their core electrons bound tightly to their nucleai while the outer electrons are either shared between neighbouring nucleai to form bonds, or move across the lattice from nucleus to nucleus. Often the free electrons can be studied independently of the nucleai/core electron system which is relative immobile and can to a good approximation be taken as an unmoving background. Still the sea of free electrons contains a massive number of particles all interacting with each other via electromagnetic forces. These free electrons conduct electric currents and their behaviour determines the electric properties of the material in question.

Let us consider first a single electron around a nucleus. The state of the electron is described by a wave (called the wave-function), so that the height of the wave corresponds to the probability to find the electron in a particular place in a measurement. Due to the attractive interaction between the electron and the protons, the low energy wave-functions will be those that quickly fall to zero away from the nucleus. This creates a situation similar to a guitar string that is fixed at its end points. Like harmonic frequencies of the string, the low energy states of the electron will have one, two, three etc. oscillations over the nucleus. Thus the energies of the electron take on discrete values.

The tendency for the wave-function to localize around the nucleus is balanced by the fact that quickly varying wave-functions lead to higher kinetic energy for the electron. The lowest energy states are therefore found by a balancing act between the potential energy of the interaction, minimized by a localized wave-function, and the kinetic energy of the electron, minimized by a slowly varying wave-function.

When many atoms are brought together in a lattice the wave-function of an electron begins to oscillate also over the lattice, which brings another energy contribution and causes the discrete energy levels of the atom to spread out into bands. Between these bands there are often energy ranges that contain no possible states for the electrons. Thus for every material there is a specific band-structure that is the result of the properties of the atoms/molecules that it consists of along with the nature of the bonds that bind together the lattice.

The band-structure determines among other things the electric properties of the matter. For example if the material has two bands with a gap between them, the lower (so called valence band) being filled with electrons and the upper (so called conduction band) being empty, it will be an electrical insulator, since electricity is conducted by moving electrons, and in this case the electrons in the lower band cannot move due to the band being full, and they cannot cross the gap to the upper band without receiving a large amount of energy. If these bands get close enough for hops across the gap to occur we have a semi-conductor, and if the bands overlap giving the electrons room to move freely we have a conductor.

The band structure of a material can be experimentally probed with so called photo-emission experiments. In these experiments the material is illuminated by monochromatic light (for example from a laser). Monochromatic light consists of photons with specific energy, and therefore as they interact with electrons in

the system they deposit to an electron a known quantity of energy. If the photon is energetic enough it will kick an electron out of the material, where it can be observed and its energy measured. The difference between the photon energy and the energy of the leaving electron then tells how much energy it took to extract the electron from the material and therefore what sort of energy it initially had. Repeating such experiments one can therefore obtain a spectrum of the energies the electrons in the material occupy, and thus find out, for example, the extent of the valence band in an insulator.

On the other hand the conduction band can be studied with inverse photoemission experiments, in which electrons are shot into the material. They settle on some energy level in the material, and then relax to the lowest energy state (called the ground-state) while emitting a photon that carries off the leftover energy. By measuring the energy of the emitted photon the energy of the level the electron was put on can be figured out, and thus the unoccupied levels of the material mapped out.

Trying to model these experiments theoretically is a many-body problem, since the electrons in a material interact and the removal or addition of an electron therefore affects the system in complicated ways. Above we have spoken loosely of energy levels that individual electrons can occupy, but to be precise since interactions with other electrons affect each electron, we cannot separate a single electron and instead have to consider all electrons of the system as occupying a specific many-body state. The removal of an electron then causes the remaining electrons to transition to a different many-body state with a different energy, and the energy carried of by the leaving electron corresponds to the energy difference between the initial and final many-body states.

In perturbative many-body quantum theory the system is first solved in absence of interactions, and the correction due to the interactions is then calculated by considering different ways the interactions between particles can occur in order of increasing complexity.

The process by which the system transitions from a particular many-body state to another one through certain interactions is called a scattering process. In perturbative many-body quantum theory the various scattering processes are depicted visually using the so called Feynman diagrams. Many different approximations can then be constructed by including different sets of diagrams, and these approximations succeed in describing the experiment better or worse depending on how many of the scattering processes that are most likely to occur in the experiment have been included.

1.3 Scattering and Feynman Diagrams

Feynman diagrams are a general way to categorize different collision processes between objects, and we can discuss these diagrams using a very concrete example of colliding billiard balls. Let us consider a billiard table containing some number of randomly placed balls. We strike one of the balls with our cue stick, and attempt to calculate the probability of a ball entering a pocket by considering the various possibilities of ball collisions and representing them using Feynman diagrams.

This can be related to the photo-emission experiment by taking the balls to represent the electrons, the cue stick the incoming laser light and the pockets the electron detectors. To make the analogy to the photo-emission experiment closer we could also require this to be done in the dark, so that we cannot say for certain where any of the other balls are, although we know how they are distributed on the table on a statistical level.

We attempt to find our answer step-by-step starting from the simplest possibilities. The first thing to consider is that the ball may simply enter a pocket directly without encountering any other balls on the way. We denote the simplest ball movement process diagrammatically by an arrow such as

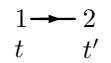

the probability for a ball to travel from state 1 to state 2 (1.1)

Here 1 denotes the ball in position $\mathbf{x}_1$ moving at velocity $\mathbf{v}_1$, and likewise for 2. Any combination of position and a velocity is a possible single-ball state (a state that any single ball can occupy). The arrow (1.1) represents the probability for a ball that is added to the table in state 1 at time t_1 to occupy state 2 at time t_2 when no collisions with other balls are taken into account (that is the when the balls are imagined to simply pass through each other unimpeded). To find our pocket-entering probability we take $\mathbf{x}_2$ to be the position of the pocket and $\mathbf{x}_1/\mathbf{v}_1$ to be the position/velocity of the ball we hit immediately after the hit. We can then plot the probabilities as a function of the velocity $\mathbf{v}_2$ to find the energy spectrum of the balls entering the pocket under this no-collision approximation.

But this does not yet correspond exactly to the picture of the photo-emission experiment. We do not want to add a new ball to the table, but instead deposit energy to one of the balls already on the table. We therefore do not want the number of balls on the table to change. This can be achieved conveniently by saying that at the time we add the ball we also remove a ball, or in other words we add a lack-of-ball (which we simply call a 'hole'). This is represented by an arrow going in the other direction, so that we have the diagram

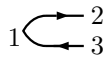

the probability for a ball to travel from state 1 to state 2 while a hole travels from state 1 to state 3 (1.2)

To understand what we mean by a hole, we must consider the full many-ball state of the table. A many-ball state consists of a list of all occupied single-ball states. What the diagram more precisely denotes is the probability for the system on the whole to transition from a specific many-ball state at time t_1 to another at time t_2, when it is perturbed by our strike with the cue. This is expressed as a change relative to what the initial many-ball state would have been at time t_2 had we left it alone. The perturbation, in this case our strike with the cue, causes a ball where there would be no ball in the unperturbed state, and likewise a hole, or a lack of ball, where there would be a ball in the unperturbed state. If the ball we hit would have traveled in the unperturbed state, the relative lack of ball correspondingly travels in the perturbed state. The diagram (1.2) for example can be seen as the probability for the system to transition from the initial state on the left-hand side to

a state on the right-hand side that differs from the initial state at t_2 in that a ball has been added in state 2 and a ball has been removed from state 3 (obviously this probability is only defined if the unperturbed initial state in fact would have a ball in state 3 at time t_2). Put yet another way, the diagram (1.2) represents the probability that our hit causes a ball that would have travelled to state 3 to instead travel to state 2. We can again calculate the pocket-entering probability from this. Since we do not care where the ball would have gone had we not hit it, we can simply sum over all possible end states 3 for the hole, while taking state 2 located in the pocket.

Non-interacting models such as this are used regularly in physics, and can be quite sufficient if the interactions do not significantly affect the quantity being calculated. But let us suppose this is not the case, and the collisions are too important to ignore. The simplest thing we can do is to assume that the ball we hit collides with another ball once. We denote this process diagrammatically by

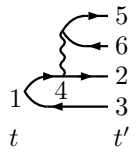

the probability for a ball to travel from state 1 to state 2 while colliding on the way with a ball on state 4 (1.3)

Here we denote the collision by a wavy-line. This process causes a more complicated change to the initial state, we have at time t_2 balls at states 2 and 5, while without our hit these balls would have been in states 3 and 6 respectively.

This raises another relevant issue. To make the analogy with electrons more precise, we have to require that all our balls are exactly identical, and we really cannot say if the ball that went to the pocket is the same one that we hit. It is possible that our ball hit another one, causing it to travel to the pocket. Such exchange processes will need to be taken into account in a theoretical calculation since they cannot be distinguished from direct processes in an experiment. For example in addition to (1.3) the same end state could also be reached by the process described by

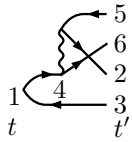

(1.4)

Obviously there are still more complicated ways for a ball to end in a pocket. In theory the total probability can be calculated by adding up the probability of all possible ball collision processes that can result in the ball going to a pocket. But there is an impractical number of possible ways the collisions may go, especially if there are a great many balls on the table. Not to mention the possibility that multiple balls may end up in a pocket. If, however, we may take the collisions to be in some sense rare, we may consider the more complicated collision processes to be less likely, and that most times when a ball ends up in a pocket there will have been relatively few contacts in the process. Then the number of processes that need to be added up to obtain a reasonably good estimate may be manageable.

There are also multiple ways by which we can maximise the mileage we get from the collision processes we do decide to calculate. We will here briefly present

some such approaches, since they will end up raising the main issue discussed in this thesis.

1.4 Interaction Processes and the Self-Energy

The laws of physics are reversible in time, and therefore if a collision process can happen in one direction, it is always possible in the reverse direction as well. It follows that gluing two collision processes together as in

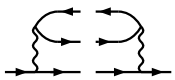

(1.5)

creates a diagram describing a possible interaction process in which a ball is collided with, moves about, and then returns back to its original location (or to wherever the hole left behind has moved), depositing the energy it received from the collision back to the colliding ball. Such a process may seem far too unlikely to bother with for our billiard balls, but for electrons they may be very important, since due to the discretization of energy levels and the requirement to conserve energy the types of collisions that can happen are much more restricted. Note that unlike billiard balls that experience friction and air resistance, electrons in these diagrams have no way to dissipate energy unless we explicitly add diagrams to describe that process. Furthermore whereas a billiard ball can transfer any percentage of its energy in a collision, from a full transfer in a perfectly head on collision to a very small amount if the balls only brush each other, electrons only do so in specific quantities corresponding to the available discrete energy states to scatter into. This is because with fundamental particles we are ultimately talking about energy transfer between oscillating systems. No matter how hard one shakes the first system, energy transfer does not occur if we are far from any resonant frequencies of the other system.

An electron system may thus go through any number of interaction processes that end up back in the original state before the final collision that sends an electron to the detector. To take these into account we can replace simple arrows in our diagrams by dressed arrows involving interaction processes along the way, such as

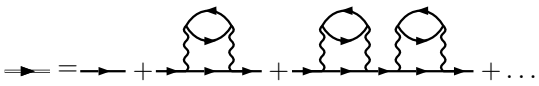

(1.6)

This equation can be written in a recursive form as

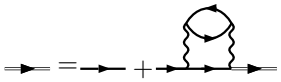

(1.7)

or more generally as

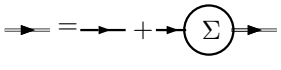

(1.8)

where Σ is an object known as self-energy (the reason for the name will become apparent later), which contains a sum of possible interaction processes; for example

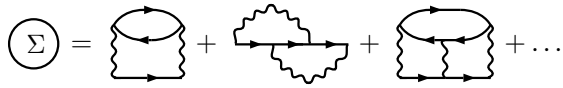

(1.9)

Equation (1.8) can be iterated by starting from

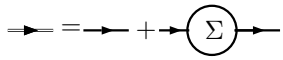

(1.10)

and placing the result repeatedly back into the right-hand side of (1.8), until the resulting probability reaches a stable value. In this way we have effectively calculated a probability for electron propagation from one state to another including an arbitrary number of interaction processes along the way. After having calculated the so called dressed propagator from (1.8) we can draw our scattering diagrams using it, and thus effectively include an infinite number of diagrams in each such dressed diagram.

The self-energy approximations can also be summed to infinite order through various recursive systems of equations. Thus one can for example nest interaction diagrams within themselves to generate diagrams such as

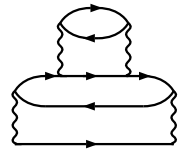

(1.11)

and so on. This generates an effectively infinite set of diagrams based on repeated scattering by the initial choice of scattering processes, but does not introduce new fundamental ways to scatter.

Alternatively one can consider interaction processes that involve a repeating piece, such as repeated collisions between two particles as in

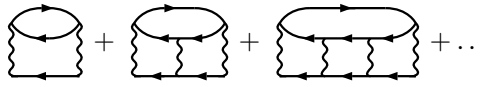

(1.12)

This can be calculated recursively by first calculating the probability for a two particle scattering

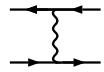

(1.13)

and linking them iteratively through

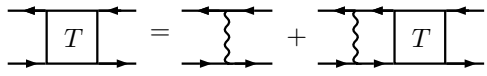

(1.14)

Joining the upper legs of T then leads to a self-energy of the form (1.12) that includes effectively infinite interactions.

It may of course be that the result of such summations does not lead to any finite result. We are expanding our results as a series of correction terms to a non-interacting system, which involves an assumption that the interacting system is in some sense not too different from the non-interacting one and can therefore be approached small step at a time. It may be, for example, that turning on the interaction causes the melting temperature to decrease and triggers a phase transition from solid to liquid, in which case a perturbative approach would certainly fail. We will throughout this thesis assume that such complications do not arise.

Such schemes to resum terms in various ways are an important way to improve the quality of results one obtains from perturbative theories. The diagrammatic approach is very powerful in making creation of these schemes intuitive. Sometimes, however, these tricks for nesting and chaining diagrams can end up obscuring the clear physical picture that was originally one of the main strengths of the diagrammatic approach.

1.5 Adding Up Probabilities

To explain this issue we will need to finally discuss something that is purely a property of quantum systems. For a classical everyday system the total probability for an event that can happen in multiple ways is calculated simply by adding the probabilities of each alternative. Thus the true value is approached from below, every alternative that is taken into account bringing one a little bit closer to the correct result. In quantum mechanics, on the other hand, the alternatives contribute probability amplitudes that have both direction and length. These are added end to end, and the final probability to measure an outcome is found as the square of the length of the total amplitude connecting the start and the end points, as shown in the following figure:

classical: 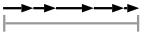 quantum: 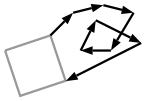 (1.15)

Thus while for a classical system calculating very unlikely processes may be unnecessary, at least one knows that they will bring you towards the correct result if only by a minimal amount. In quantum mechanics certain alternatives may end up forming loops in the sum and cancelling each other out. Calculating such loops makes no difference to the result, and if a loop is only partially included it may actually take you further away from the correct answer.

For an electron our scattering diagram corresponds to a probability amplitude. The length of this amplitude can be calculated by mirroring the diagram and gluing it to itself, in the same way that the self-energy diagrams are constructed. For example the probability to scatter via the process

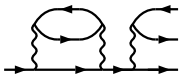 (1.16)

can be obtained by calculating

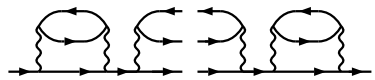

(1.17)

It follows that the scattering probability for an electron has the form of an amplitude for an interaction process (or a scattering from an initial state back to the same state), and therefore it can be calculated just from the knowledge of the self-energy without having to consider individual scattering processes. Indeed in practice the self-energy is the central quantity in such calculations, and different approximations for scattering processes are typically expressed in terms of approximations for the self-energy.

The connection between scattering processes and the self-energy has the added complication, that the same self-energy diagram can result from many different gluings of scattering diagrams. In such cases the self-energy diagram equals the sum of possible glued pairs; for example

$S =$ 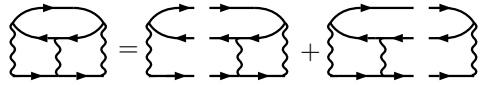

(1.18)

In this equation, however, the diagrams on the right-hand side have no clear physical meaning. Mirrored pairs such as in (1.17) represent scattering probabilities by the process depicted by the diagram being mirrored, however pairs of two different scattering processes have no such interpretation. To obtain a self-energy with clear physical content, we need to give it a form of a mirrored scattering amplitude, such as

$S' =$ 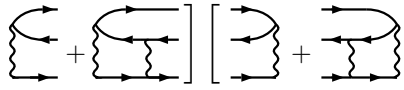

(1.19)

This now has the form of a scattering probability where the scattering can happen by two different processes. We note that this differs from (1.18) by inclusion of two additional terms

$S' = S +$ 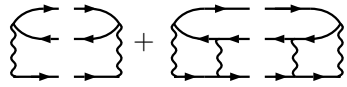

(1.20)

Here the first glued pair is equal to the two interaction self-energy diagram (first diagram in (1.12)) since there is only one possible gluing resulting in it. The second diagram however represents only a part of the four interaction self-energy diagram (third diagram in (1.12)).

This discussion raises the central point of this thesis. While the self-energy is a convenient object for calculations, one always has to keep in mind that the choice of the self-energy is in a sense a consequence of a more fundamental choice, i.e. that of which scattering processes are to be included. This is important since although every choice of scattering processes leads to a corresponding self-energy, not every self-energy follows from a set of scattering processes (for example (1.18)). Using

such a self-energy that does not correspond to a specific set of scattering processes can lead to unphysical results, such as negative probabilities and negative particle counts, which render the result incabable of being interpreted in any meaningful way. Furthermore when using the various diagram resummation schemes, a self-energy approximation not corresponding to a scattering approximation can cause the iteration to fail to converge even if the system under consideration is otherwise well behaved. These issues and how they can be avoided in practice when using diagrammatic quantum many-body theory are the main subject of this thesis. To get there we will first have to give the theory its true mathematical form.

Chapter 2

Quantum Mechanics: Brief Introduction

Before presenting the theory in its mathematically relatively simple but rather abstract form, we will try and give the reader some intuitive sense on how the states of a quantum system connect to those of a classical system. Consider therefore a classical many-body system consisting of N identical particles. The configuration of the system is determined by the N positions of the particles $\mathbf{x}_1, \ldots, \mathbf{x}_N$, and all such configurations form a $3N$ dimensional configuration space $\mathbb{R}^{3N}$. In order to solve the time-evolution of the system we need to further specify the velocities of the particles. For any set of positions and velocities we can then use the Newtonian equations of motion to find these values at any later (or earlier) time, and solve the time-evolution of the system which draws a path in the configuration space.

A state of the corresponding quantum many-body system is a complex valued function (known as the wave-function) over the classical configuration space $\Psi(\mathbf{x}_1, \ldots, \mathbf{x}_N)$, the time-evolution of which is determined by the Schrödinger equation (to be discussed later). Being complex valued it associates to each classical configuration an amplitude with a length and a phase. The length of the amplitude (or more precisely the square of the norm $|\Psi(\mathbf{x}_1, \ldots, \mathbf{x}_N)|^2$) for a particular configuration corresponds to the probability (or probability density if $\mathbf{x}$ are continuous) to find the system in that configuration when performing a measurement.

Information about the particle velocities is encoded in the phases of the wave-function, so that by Fourier transforming the wave-function

$$F\left[\Psi(\mathbf{x}_1, \ldots, \mathbf{x}_N)\right] = \Phi(\mathbf{p}_1, \ldots, \mathbf{p}_N) \tag{2.1}$$

we obtain a momentum wave-function. $|\Phi(\mathbf{p}_1, \ldots, \mathbf{p}_N)|^2$ gives the probability to find the particles with particular values of momenta in a measurement. This connection between the positions and momenta gives rise to the Heisenberg uncertainty principle, since the Fourier transform connects sharp features in the position space to broad features in the momentum space, and vice versa.

Arguably the most important difference to classical theory that follows, is that any sum of two wave-functions is also a complex valued function over the configurations space, and therefore also a possible state of the quantum system. For the probability interpretation to make sense we must of course require that

$$\int \mathrm{d}\mathbf{x}_1 \cdots \int \mathrm{d}\mathbf{x}_N |\Psi(\mathbf{x}_1, \ldots, \mathbf{x}_N)|^2 = 1 \tag{2.2}$$

so that we are certain to find the system in some state upon measurement. Given that we take care to maintain this normalization, we can add quantum states together to obtain new valid physical states as in

$$c_1\Psi_1 + c_2\Psi_2 = \Psi_3, \tag{2.3}$$

where c_1 and c_2 are complex numbers chosen so that Ψ_3 fulfills (2.2). (2.3) is the important superposition principle, from which much of the unique properties of quantum theories arise. Moreover, (2.3) tells us that the state-space of a quantum system is a vector space. This is the crucial fact that makes the mathematical form of quantum theory on the other hand very elegant, and on the other hand very different from that of classical physics.

Finally we note that the wave-functions is (anti)-symmetric with respect to exchanging two particles with each other, i.e.

$$\Psi(\mathbf{x}_1, \ldots, \mathbf{x}_i, \ldots, \mathbf{x}_j, \ldots, \mathbf{x}_N) = \pm\Psi(\mathbf{x}_1, \ldots, \mathbf{x}_j, \ldots, \mathbf{x}_i, \ldots, \mathbf{x}_N). \tag{2.4}$$

Particles with a symmetric wave-function are called Bosons, and those with anti-symmetric wave-function are called Fermions. Electrons, which we will in this work concern ourselves with, are Fermions. One consequence of this is that the probability to find two electrons in the same state is always zero. This is known as the Pauli exclusion principle. It is of fundamental importance to all chemistry, since by preventing the electrons from all condensing into the lowest energy state it leads for example to shell structure in atoms and consequently to band structure in materials. It follows that maintaining the anti-symmetry is an important concern for building approximations for electron systems.

2.1 States and Measurements

The states of a quantum system form a Hilbert space, i.e. a vector space with an inner product. We denote a vector in this space by $|\Psi\rangle$. Let $|\phi_1\rangle, |\phi_2\rangle, |\phi_3\rangle$ etc. form an orthonormal basis in this space. Any state vector can then be expressed as

$$|\Psi\rangle = \sum_i c_i |\phi_i\rangle \tag{2.5}$$

where c_i are complex numbers. The corresponding dual vector is given by

$$\langle\Psi| = \sum_i c_i^* \langle\phi_i|. \tag{2.6}$$

The inner product is defined by

$$\begin{aligned} \langle\Psi_1|\Psi_2\rangle &= \left[\sum_{i_1} c_{i_1}^* \langle\phi_{i_1}|\right] \left[\sum_{i_2} c_{i_2} |\phi_{i_2}\rangle\right] \\ &= \sum_{i_1 i_2} c_{i_1}^* c_{i_2} \langle\phi_{i_1}|\phi_{i_2}\rangle = \sum_{i_1} |c_{i_1}|^2, \end{aligned} \tag{2.7}$$

where we have used

$$\langle\phi_{i_1}|\phi_{i_2}\rangle = \delta_{i_1 i_2} \tag{2.8}$$

which holds since $|\phi_i\rangle$ were taken to be orthonormal. For a system in state $|\Psi\rangle$ the probability to find the system to be in state $|\phi_j\rangle$ when performing a measurement is given by

$$|\langle\phi_j|\Psi\rangle|^2 = \sum_i |c_i\langle\phi_j|\phi_i\rangle|^2 = |c_j|^2. \tag{2.9}$$

The numbers c_j are called probability amplitudes to distinguish them from the standard real valued probability $|c_j|^2$.

From experience we know that a measurement of any observable O from a quantum system always gives a consistent result on repeated experiments. We know therefore that for any measurement result O_i there must exist a state that the quantum system can be on so that measurements on that state give O_i with certainty. This is true for any possible result of the measurement. For a certain set of possible results $O_\mathcal{I} = \{O_1, \ldots, O_N\}$ we therefore have a corresponding set of states $\Psi_\mathcal{I}$. These states must be orthogonal whenever they correspond to distinct measurement results, since otherwise (2.9) would give a non-zero change to measure the other result from either state. Furthermore since a measurement always gives some result the states $|\Psi_\mathcal{I}\rangle$ must form a complete basis to the Hilbert space. Using these sets we can define an operator corresponding to the measurement of a specific observable O through

$$\hat{O}|\Psi_i\rangle = O_i|\Psi_i\rangle. \tag{2.10}$$

Since $|\Psi_\mathcal{I}\rangle$ form a complete basis, this defines the operation of $\hat{O}$ on any state of the system, giving

$$\hat{O}|\Phi\rangle = \hat{O}\sum_i c_i|\Psi_i\rangle = \sum_i c_i O_i|\Psi_i\rangle. \tag{2.11}$$

We then find that the expression

$$\begin{aligned}\langle\Phi|\hat{O}|\Phi\rangle &= \left[\sum_i c_i^*\langle\Psi_i|\right]\hat{O}\left[\sum_j c_j|\Psi_j\rangle\right] \\ &= \sum_{ij} c_i^* c_j O_j\langle\Psi_i||\Psi_j\rangle \\ &= \sum_{ij} c_i^* c_j O_j\delta_{ij} = \sum_i |c_i|^2 O_i\end{aligned} \tag{2.12}$$

gives the expectation value for the observable O when measured from a system in state $|\Phi\rangle$.

Thus to any observable O there corresponds an operator $\hat{O}$, which is Hermitian since its eigenvalues are measurement outcomes and therefore real valued, and in practice we find ourselves evaluating expressions of the form

$$\langle\Phi|\hat{O}|\Phi\rangle \tag{2.13}$$

in order to calculate results of experiments.

Particle positions are one possible observable to measure, and to them corresponds a basis consisting of states with definite particle positions $|\mathbf{x}_1, \ldots, \mathbf{x}_N\rangle$. Here we take $\mathbf{x}$ to be a composite variable containing a position and

a spin, i.e. $\mathbf{x}_i = \mathbf{r}_i\sigma_i$, σ_i being the spin of the particle i. This is a basis defined by continuous arguments, and thus we expand a state vector in this basis as

$$|\Psi\rangle = \int \mathrm{d}\mathbf{x}_1 \cdots \mathrm{d}\mathbf{x}_N \Psi(\mathbf{x}_1, \ldots, \mathbf{x}_N)|\mathbf{x}_1, \ldots, \mathbf{x}_N\rangle, \tag{2.14}$$

where $\int \mathrm{d}\mathbf{x}_i = \int \mathrm{d}\mathbf{r}_i \sum_{\sigma_i}$ is a shorthand for integral over position and sum over spin. Here $\Psi(\mathbf{x}_1, \ldots, \mathbf{x}_N)$ is the wave-function discussed in the previous section.

2.2 Time

To incorporate time into our calculations we define a time-evolution operator

$$|\Psi(t + \Delta t)\rangle = \hat{U}(t + \Delta t, t)|\Psi(t)\rangle, \tag{2.15}$$

that takes a state at time t and transforms it to the state at time $t + \Delta t$. For any quantum system there exist a set of states, called stationary states, with the property that their time-evolution consists simply of the phase rotating at a specific rate E_i, so that

$$|\psi_{E_i}(t + \Delta t)\rangle = e^{-iE_i\Delta t}|\psi_{E_i}(t)\rangle. \tag{2.16}$$

These are the states that correspond to specific values of the total energy E, and they form a basis to the Hilbert space. Thus any possible state of the system can be expressed as a linear combination of stationary states. Such a linear combination, e.g.

$$|\Psi(t)\rangle = \sum_n c_n|\psi_{E_n}(t)\rangle, \tag{2.17}$$

then follows the equation

$$|\Psi(t + \Delta t)\rangle = \sum_n e^{-iE_n\Delta t}c_n|\psi_{E_n}(t)\rangle. \tag{2.18}$$

The time-evolution of the state as a whole is thus generated by the changing interference pattern created by phases oscillating at different speeds corresponding to their energies. Note that a shift of all energies by a constant introduces only an overall phase factor, which does not affect the result of any measurement, since it cancels out in (2.13).

The stationary states thus define the energy operator

$$\hat{H}|\Psi_{E_n}(t)\rangle = E_n|\Psi_{E_n}(t)\rangle, \tag{2.19}$$

which is known as the Hamiltonian. We obtain

$$|\Psi(t + \Delta t)\rangle = \sum_n e^{-iE_n\Delta t}c_n|\psi_{E_n}(t)\rangle = e^{-i\hat{H}\Delta t}\sum_n c_n|\psi_{E_n}(t)\rangle = e^{-i\hat{H}\Delta t}|\Psi(t)\rangle, \tag{2.20}$$

showing that the time-evolution operator has the form

$$\hat{U}(t + \Delta t, t) = e^{-i\hat{H}\Delta t}. \tag{2.21}$$

We can then find the equation of motion by expanding $\hat{U}$ as

$$e^{-i\hat{H}\Delta t} = 1 - i\hat{H}\Delta t + \frac{(i\hat{H}\Delta t)^2}{2!} + \dots \tag{2.22}$$

from which it follows that

$$\frac{|\Psi(t+\Delta t)\rangle - |\Psi(t)\rangle}{\Delta t} = \left[-i\hat{H} + \frac{(i\hat{H})^2\Delta t}{2!} + \dots\right]|\Psi(t)\rangle. \tag{2.23}$$

Now taking the limit $\Delta t \to 0$ we obtain the equation of motion for the state-vector

$$\begin{aligned}\lim_{\Delta t\to 0}\frac{|\Psi(t+\Delta t)\rangle - |\Psi(t)\rangle}{\Delta t} &= \lim_{\Delta t\to 0}\left[-i\hat{H} + \frac{(i\hat{H})^2\Delta t}{2!} + \dots\right]|\Psi(t)\rangle \\ \Rightarrow \frac{\delta}{\delta t}|\Psi(t)\rangle &= -i\hat{H}|\Psi(t)\rangle,\end{aligned} \tag{2.24}$$

i.e. the Schrödinger equation.

So far we have made the tacit assumption that the Hamiltonian itself is time-independent. If the system has time-dependent elements, such as an oscillating electromagnetic field created by incoming light in a photoemission experiment, the Hamiltonian will be time-dependent and the energy eigenbasis will vary in time. Therefore the time-evolution operator also changes in time. To find an expression for this operator we first note that the time-evolution operator must certainly have the property

$$\hat{U}(t_3, t_2)\hat{U}(t_2, t_1) = \hat{U}(t_3, t_1). \tag{2.25}$$

We use this to write the evolution from t to $t + \Delta t$ as a series of n small time-steps $\delta t = \Delta t/n$. Assuming the time-evolution of the Hamiltonian is smooth (in a suitable sense) we can for large n take $\hat{H}$ to be constant during each sub-step and write

$$|\Psi(t+\Delta t)\rangle = \lim_{n\to\infty} e^{-i\hat{H}(t+n\delta t)\delta t}\cdots e^{-i\hat{H}(t+\delta t)\delta t}e^{-i\hat{H}(t)\delta t}|\Psi(t)\rangle. \tag{2.26}$$

We are now sorely tempted to use the multiplication property of exponential function $e^A e^B = e^{A+B}$. This, however, only holds when A and B commute, which may not be the case for the Hamiltonians at different time-points. This obstacle can be circumvented by introducing a time-ordering operation $\mathcal{T}\{\cdots\}$, which is defined by the rule that the objects inside it are to be ordered such that larger time arguments go to the left. For example

$$\mathcal{T}\{O(t_1)O(t_2)O(t_3\} = O(t_3)O(t_1)O(t_2), \qquad \text{when } t_3 > t_1 > t_2. \tag{2.27}$$

It follows that inside the time-ordering the objects commute. In the case of (2.26), since the exponentials are already time-ordered, we can write

$$\begin{aligned}|\Psi(t+\Delta t)\rangle &= \lim_{n\to\infty}\mathcal{T}\{e^{-i\hat{H}(t+n\delta t)\delta t}\cdots e^{-i\hat{H}(t+\delta t)\delta t}e^{-i\hat{H}(t)\delta t}\}|\Psi(t)\rangle \\ &= \lim_{n\to\infty}\mathcal{T}\{e^{-i(\hat{H}(t+n\delta t)+\ldots+\hat{H}(t+\delta t)+\hat{H}(t))\delta t}\}|\Psi(t)\rangle \\ &= \mathcal{T}\{e^{-i\int_t^{t+\Delta t}\hat{H}(\bar{t})d\bar{t}}\}|\Psi(t)\rangle.\end{aligned} \tag{2.28}$$

The time-evolution operator for time-dependant Hamiltonians can therefore be written as

$$\hat{U}(t_2,t_1) = \begin{cases} \mathcal{T}\{e^{-i\int_{t_1}^{t_2}\hat{H}(\bar{t})d\bar{t}}\}, & t_2 > t_1 \\ \bar{\mathcal{T}}\{e^{i\int_{t_2}^{t_1}\hat{H}(\bar{t})d\bar{t}}\}, & t_1 > t_2 \end{cases} \tag{2.29}$$

where the $t_1 > t_2$ form can be obtained in a similar way by defining the anti-time-ordering operation $\bar{\mathcal{T}}\{\cdots\}$ that orders larger times to the right.

Note that

$$\hat{U}^\dagger(t,t_0) = \mathrm{e}^{\mathrm{i}\int_{t_0}^{t}\mathrm{d}\bar{t}\,\hat{H}^\dagger(\bar{t})} = \mathrm{e}^{-\mathrm{i}\int_{t}^{t_0}\mathrm{d}\bar{t}\,\hat{H}(\bar{t})} = \hat{U}(t_0,t). \tag{2.30}$$

Thus the expectation value of an observable O at time t is given by

$$O(t) = \langle\Psi(t)|\hat{O}|\Psi(t)\rangle = \langle\Psi_0|\hat{U}(t_0,t)\hat{O}\hat{U}(t,t_0)|\Psi_0\rangle = \langle\Psi_0|\hat{O}_H(t)|\Psi_0\rangle, \tag{2.31}$$

where $\hat{O}_H(t) = \hat{U}(t_0,t)\hat{O}\hat{U}(t,t_0)$ is so-called Heisenberg form of the operator $\hat{O}$ and $|\Psi_0\rangle = |\Psi(t_0)\rangle$ is the state of the system at an initial time t_0. Thus the above expression describes a measurement performed by preparing the system in state Ψ_0 at time t_0 and then measuring the observable O at time t.

From this we can find the equation of motion for the Heisenberg operator $\hat{O}_H(t)$. We have from the chain rule

$$\frac{\mathrm{d}}{\mathrm{d}t}\hat{O}_H(t) = \frac{\mathrm{d}\hat{U}(t_0,t)}{\mathrm{d}t}\hat{O}\hat{U}(t,t_0) + \hat{U}(t_0,t)\frac{\mathrm{d}\hat{O}(t)}{\mathrm{d}t}\hat{U}(t,t_0) + \hat{U}(t_0,t)\hat{O}\frac{\mathrm{d}\hat{U}(t,t_0)}{\mathrm{d}t}. \tag{2.32}$$

On the other hand

$$\begin{aligned} \frac{d\hat{U}(t_0,t)}{dt} &= \frac{\mathrm{d}}{\mathrm{d}t}\bar{\mathcal{T}}\{e^{i\int_{t}^{t_0}\hat{H}(\bar{t})d\bar{t}}\} = -\mathrm{i}\hat{U}(t_0,t)\hat{H}(t) \\ \frac{d\hat{U}(t,t_0)}{dt} &= \frac{\mathrm{d}}{\mathrm{d}t}\mathcal{T}\{e^{-i\int_{t_0}^{t}\hat{H}(\bar{t})d\bar{t}}\} = \mathrm{i}\hat{H}(t)\hat{U}(t,t_0), \end{aligned} \tag{2.33}$$

and therefore

$$\frac{\mathrm{d}}{\mathrm{d}t}\hat{O}_H(t) = -i\hat{U}(t_0,t)\hat{H}(t)\hat{O}\hat{U}(t,t_0) + \left[\frac{\mathrm{d}\hat{O}(t)}{\mathrm{d}t}\right]_H + i\hat{U}(t_0,t)\hat{O}\hat{H}(t)\hat{U}(t,t_0). \tag{2.34}$$

Placing $\hat{U}(t,t_0)\hat{U}(t_0,t) = \hat{1}$ between $\hat{O}$ and $\hat{H}$ then leads to

$$i\frac{\mathrm{d}}{\mathrm{d}t}\hat{O}_H(t) = [\hat{H}_H(t),\hat{O}_H(t)] + i\left[\frac{\mathrm{d}\hat{O}(t)}{\mathrm{d}t}\right]_H, \tag{2.35}$$

where $[A,B] = AB - BA$ is the commutator.

2.3 Temperature

To consider a system at finite temperature one can apply the methods of classical statistical mechanics. One considers an ensemble of systems which are in states

distributed according to the Bolztmann distribution, so that a random system in the ensemble will be on state of energy E with probability $\frac{e^{-\beta E}}{Z}$ where $\beta = \frac{1}{T}$ is the inverse temperature (using the natural units so that the Boltzmann factor $k_B = 1$) and $Z = \sum_n e^{-\beta E_n}$ is the partition function. Now each system in the ensemble is a quantum system, and we can write the expectation value for the ensemble as

$$\begin{aligned} O(t) &= \sum_E \frac{e^{-\beta(E-\mu)}}{Z} \langle \Psi_E | \hat{O}_H(t) | \Psi_E \rangle \\ &= \sum_E \langle \Psi_E | \frac{e^{-\beta(\hat{H}(t_0)-\mu)}}{Z} \hat{O}_H(t) | \Psi_E \rangle = \text{tr}\left[\hat{\rho}\, \hat{O}_H(t)\right], \end{aligned} \tag{2.36}$$

where energies are given with respect to the chemical potential μ and we have defined the density operator

$$\hat{\rho} = \frac{e^{-\beta(\hat{H}(t_0)-\mu)}}{Z}. \tag{2.37}$$

The sum over E is now a trace, and is therefore basis independent.

For the thermodynamic ensemble (a macrocanonical ensemble) the $\hat{H}$ in (2.37) is the Hamiltonian of the system at the initial time, but (2.37) applies generally as well, since a positive semi-definite operator can always be written in this form (and $\hat{\rho}$ is PSD since its diagonal elements are probabilities). The density matrix is useful since it can be used to represent both an expectation value for a quantum mechanical superposition $|\Psi\rangle = \sum_i c_i |\psi_i\rangle$ by writing

$$\begin{aligned} \left[\sum_i c_i^* \langle \psi_i |\right] \hat{O}_H(t) \left[\sum_j c_j |\psi_j\rangle\right] &= \sum_n \langle \psi_n | \sum_{ij} c_i^* c_j |\psi_i\rangle \langle \psi_j | \hat{O}_H(t) | \psi_n \rangle \\ &= \text{tr}\left[\hat{\rho}\, \hat{O}_H(t)\right] \end{aligned} \tag{2.38}$$

as well as a classical probability distribution as in (2.36) at the same time. This makes it very convenient for treating ensembles of quantum states.

Chapter 3

Many-Body Quantum Theory

3.1 Creation and Annihilation Operators

To construct a perturbation theory based on adding up scattering processes we need a convenient way to modify a many-body quantum state by moving particles between single-particle orbitals to generate excited states from a ground state. To this end we define operators that add/remove particles to/from a many-body state.

Let us first consider a system with one particle, and denote by $|i\rangle$ the states in some orthogonal basis for this single-particle system. We take the quantum number i to be discrete, but all results here apply to continuous quantum numbers as well with the appropriate modifications (i.e. Kronecker deltas become delta-functions and sums become integrals). We introduce a set of operators defined by

$$\hat{d}_i^\dagger|0\rangle = |i\rangle, \qquad \hat{d}_i|j\rangle = \delta_{ij}|0\rangle. \tag{3.1}$$

The fact that these operators are related by conjugation follows from noting that

$$\langle j|\hat{d}_i^\dagger|0\rangle = \delta_{ij} = \langle 0|\hat{d}_i|j\rangle. \tag{3.2}$$

We then construct a basis for the many particle state-space (so called Fock-space) by defining the N-particle state in which the single-particle orbitals $\{i_1, \ldots, i_N\}$ are occupied as

$$|i_1 \cdots i_N\rangle = \hat{d}_{i_1}^\dagger \cdots \hat{d}_{i_N}^\dagger|0\rangle. \tag{3.3}$$

The corresponding dual state-vector can then be written as

$$\langle i_1 \cdots i_N| = [\hat{d}_{i_1}^\dagger \cdots \hat{d}_{i_N}^\dagger|0\rangle]^\dagger = \langle 0|\hat{d}_{i_N} \cdots \hat{d}_{i_1}. \tag{3.4}$$

It follows that these operators operate on many-particle states following

$$\hat{d}_j^\dagger|i_1 \cdots i_N\rangle = |i_j i_1 \cdots i_N\rangle, \qquad \langle i_1 \cdots i_N|\hat{d}_j = \langle i_j i_1 \cdots i_N|. \tag{3.5}$$

The requirement that the state should be anti-symmetric with respect to particle exchange for Fermionic particles then follows automatically if we define the operators to anti-commute, i.e. that

$$[\hat{d}_{i_1}^\dagger, \hat{d}_{i_2}^\dagger]_+ = 0, \qquad [\hat{d}_{i_1}, \hat{d}_{i_2}]_+ = 0 \tag{3.6}$$

where $[A, B]_+ = AB + BA$ is the anti-commutator. For Bosonic particles the anti-commutator is replaced by a commutator.

For the anti-commutator between creation and annihilation operators on the other hand we find

$$\begin{aligned}\langle i|[\hat{d}_j^\dagger, \hat{d}_k]_+|l\rangle &= \langle i|\hat{d}_j^\dagger \hat{d}_k|l\rangle + \langle i|\hat{d}_k \hat{d}_j^\dagger|l\rangle \\ &= \delta_{kl}\langle i|j\rangle - \langle ki|jl\rangle \\ &= \delta_{kl}\delta_{ij} + \delta_{kj}\delta_{il} - \delta_{kl}\delta_{ij} \\ &= \langle i|\delta_{jk}|l\rangle.\end{aligned} \tag{3.7}$$

Taking therefore

$$[\hat{d}_j^\dagger, \hat{d}_k]_+ = \delta_{jk} \tag{3.8}$$

to hold generally we find that the annihilation operator operates to the right as

$$\begin{aligned}\hat{d}_j|i_1 \cdots i_N\rangle &= \hat{d}_j \hat{d}_{i_1}^\dagger \cdots \hat{d}_{i_N}^\dagger|0\rangle \\ &= [\delta_{ji_1} - \hat{d}_{i_1}^\dagger \hat{d}_j]\hat{d}_{i_2}^\dagger \cdots \hat{d}_{i_N}^\dagger|0\rangle \\ &= [\delta_{ji_1}\hat{d}_{i_2}^\dagger - \hat{d}_{i_1}^\dagger \delta_{ji_2} + \hat{d}_{i_1}^\dagger \hat{d}_{i_2}^\dagger \hat{d}_j]\hat{d}_{i_3}^\dagger \cdots \hat{d}_{i_N}^\dagger|0\rangle \\ &= \sum_{n=1}^{N}(-1)^{n+1}\delta_{ji_n}|i_1 \cdots \overline{i_n} \cdots i_N\rangle,\end{aligned} \tag{3.9}$$

where $\overline{i_n}$ denotes that the index i_n is removed from the list of occupied single-particle states.

Using the anti-commutation relations the operation of any product of creation and annihilation operators on any many-body state can be calculated. For example, the combination of operators

$$\hat{n}_j = \hat{d}_j^\dagger \hat{d}_j \tag{3.10}$$

operators according to

$$\hat{n}_j|i_1 \cdots i_n\rangle = \sum_k \delta_{i_j i_k}|i_1 \cdots i_n\rangle = n_j|i_1, \ldots, i_n\rangle \tag{3.11}$$

and is therefore called the number operator since its eigenvalue n_j is one if the single-particle orbital j is occupied and zero otherwise (this can be generalized for Bosons in which case n_j can take larger values).

Any transition between the many-body basis states in the single-particle orbital basis can now be expressed as a string of creation and annihilation operators. A general many-body operator in this basis can then be expressed as

$$\hat{O}|i_\mathcal{N}\rangle = \sum_{\mathcal{K}\mathcal{M}} \hat{d}_\mathcal{K}^\dagger O_{\mathcal{K}\mathcal{M}} \hat{d}_\mathcal{M}|i_\mathcal{N}\rangle, \tag{3.12}$$

where $\mathcal{N} = \{i_1, \ldots, i_N\}$ etc. represent sets of single-particle orbital indices. This is a convenient form to express operators for purposes of calculations. We express the Hamiltonian in particular as

$$\hat{H}(t) = \sum_i \hat{d}_i^\dagger h_i(t)\hat{d}_i + \frac{1}{2}\sum_{ij}\hat{d}_i^\dagger \hat{d}_j^\dagger v_{ij}\hat{d}_j\hat{d}_i, \tag{3.13}$$

where $h_i(t)$ corresponds to the part of the energy that only depends on particle density at a single point (i.e. kinetic energy and potential energy of a particle in external potentials) and v_{ij} is the part of the energy that depends on correlations of particle density at two points (i.e. energy due to interactions). The factor $\frac{1}{2}$ for the interaction cancels double counting due to the symmetric sum including interaction in both directions for each particle pair. The fact that the $i = j$ case is also halved is not an issue for fermions, since two fermions never occupy the same single-particle state. For bosons this needs to be corrected for.

Using this form of the Hamiltonian the equations of motion for the Heisenberg forms of creation and annihilation operators are easy to derive from the general Heisenberg equation of motion (2.35). We have

$$i\frac{\mathrm{d}}{\mathrm{d}t}\hat{d}^\dagger_{k,H}(t) = [\hat{d}^\dagger_{k,H}(t), \hat{H}] = [\hat{d}^\dagger_k, \hat{H}]_H. \tag{3.14}$$

Using the commutation relations given above we obtain

$$\begin{aligned} \hat{d}^\dagger_k \hat{H} &= \hat{d}^\dagger_k \left[\sum_i \hat{d}^\dagger_i h_i(t) \hat{d}_i + \frac{1}{2} \sum_{ij} \hat{d}^\dagger_i \hat{d}^\dagger_j v_{ij} \hat{d}_j \hat{d}_i \right] \\ &= \hat{H} \hat{d}^\dagger_k - \hat{d}^\dagger_k h_k(t) - \sum_i \hat{d}^\dagger_k v_{ik} \hat{n}_i \end{aligned} \tag{3.15}$$

which leads to the unsurprising relation

$$\hat{H} \hat{d}^\dagger_k = \hat{d}^\dagger_k (\hat{H} + h_k(t) + \sum_i v_{ik} \hat{n}_i). \tag{3.16}$$

Therefore

$$-i\frac{\mathrm{d}}{\mathrm{d}t}\hat{d}^\dagger_{k,H}(t) = \hat{d}^\dagger_{k,H}(t) \left(h_k(t) + \sum_i v_{ik} \hat{n}_{i,H}(t) \right). \tag{3.17}$$

By conjugating this equation one then obtains for the annihilation operator

$$i\frac{\mathrm{d}}{\mathrm{d}t}\hat{d}_{k,H}(t) = \hat{d}_{k,H}(t) \left(h_k(t) + \sum_i v_{ik} \hat{n}_{i,H}(t) \right) \tag{3.18}$$

3.2 Response Functions

Now we have the tools necessary to consider the response of a system to a change in an external potential in a perturbative manner. We take a Hamiltonian of the general form

$$\hat{H}(t) = \sum_i \hat{d}^\dagger_i h_i(t) \hat{d}_i + \frac{1}{2} \sum_{ij} \hat{d}^\dagger_i \hat{d}^\dagger_j v_{ij} \hat{d}_j \hat{d}_i, \tag{3.19}$$

where the single particle part $h_i(t) = h_{0,i} + u_i(t)$ contains a time-dependent external potential.

We take the expectation value $O(1) = \langle \hat{O}(1) \rangle = \langle \hat{O}_{i_1}(t_1) \rangle$ (using the shorthand $n = i_n t_n$ for the arguments) of some observable O and expand it in terms of the potential u as

$$O(1) = O(1)_{u=0} + \int \mathrm{d}2\, R(1,2) u(2) + \frac{1}{2} \int \mathrm{d}2\mathrm{d}3\, R(1,2,3) u(2) u(3) + \dots \tag{3.20}$$

where $\int \mathrm{d}n = \int_{t_0}^{\infty} \mathrm{d}t_n \sum_{i_n}$. Here $R(1,2) = \frac{\delta O(1)}{\delta u(2)}_{u=0}$ is the first order response function, $R(1,2,3) = \frac{\delta^2 O(1)}{\delta u(2)\delta u(3)}_{u=0}$ the second order response function, and so on.

We can now work out expressions for the response functions as expectation values of operators. For the first order response we have using the Hellmann-Feynman theorem

$$\frac{\delta O(1)}{\delta u(2)} = \mathrm{tr}\left[\hat{\rho}\,\frac{\delta \hat{O}_H(1)}{\delta u(2)}\right] \tag{3.21}$$

where

$$\frac{\delta \hat{O}_H(1)}{\delta u(2)} = \frac{\delta \hat{U}(t_0,t_1)}{\delta u(2)}\hat{O}\hat{U}(t_1,t_0) + \hat{U}(t_0,t_1)\hat{O}\frac{\delta \hat{U}(t_1,t_0)}{\delta u(2)}. \tag{3.22}$$

Using the definition of the time-evolution operator (2.29) we get

$$\begin{aligned}
\frac{\delta \hat{U}(t_0,t_1)}{\delta u(2)} &= \frac{\delta}{\delta u(2)}\bar{\mathcal{T}}\{e^{i\int_{t_1}^{t_0}\hat{H}(\bar{t})\mathrm{d}\bar{t}}\} \\
&= \bar{\mathcal{T}}\left\{\left[i\int_{t_1}^{t_0}\frac{\delta \hat{H}(\bar{t})}{\delta u(2)}\mathrm{d}\bar{t}\right]e^{i\int_{t_1}^{t_0}\hat{H}(\bar{t})\mathrm{d}\bar{t}}\right\} \\
&= \bar{\mathcal{T}}\{e^{i\int_{t_2}^{t_0}\hat{H}(\bar{t})\mathrm{d}\bar{t}}\}\left[i\int_{t_1}^{t_0}\frac{\delta \hat{H}(\bar{t})}{\delta u(2)}\mathrm{d}\bar{t}\right]\bar{\mathcal{T}}\{e^{i\int_{t_1}^{t_2}\hat{H}(\bar{t})\mathrm{d}\bar{t}}\} \\
&= \hat{U}(t_0,t_2)\left[i\int_{t_1}^{t_0}\frac{\delta \hat{H}(\bar{t})}{\delta u(2)}\mathrm{d}\bar{t}\right]\hat{U}(t_2,t_1)
\end{aligned} \tag{3.23}$$

and since

$$\frac{\delta \hat{H}(\bar{t})}{\delta u(2)} = \frac{\delta}{\delta u(2)}\sum_i \hat{d}_i^\dagger u_i(\bar{t})\hat{d}_i = \delta(\bar{t}-t_2)\hat{d}_{i_2}^\dagger\hat{d}_{i_2} = \delta(\bar{t}-t_2)\hat{n}_{i_2} \tag{3.24}$$

we obtain using $\hat{U}(t_1,t_2)\hat{U}(t_2,t_3) = \hat{U}(t_1,t_3)$ and $\hat{U}(t,t) = \hat{1}$ that

$$\begin{aligned}
\frac{\delta \hat{U}(t_0,t_1)}{\delta u(2)} &= i\theta(t_1,t_2)\hat{U}(t_0,t_2)\hat{n}_{i_2}\hat{U}(t_2,t_1) \\
&= i\theta(t_1,t_2)\hat{U}(t_0,t_2)\hat{n}_{i_2}\hat{U}(t_2,t_1)\hat{U}(t_1,t_0)\hat{U}(t_0,t_1) \\
&= i\theta(t_1,t_2)\hat{n}(2)\hat{U}(t_0,t_1),
\end{aligned} \tag{3.25}$$

where $\hat{n}(2) = \hat{n}_{i_2,H}(t_2)$ is the Heisenberg form of the number operator. By analogous calculation we find

$$\frac{\delta \hat{U}(t_1,t_0)}{\delta u(2)} = -i\theta(t_1,t_2)\hat{U}(t_1,t_0)\hat{n}(2), \tag{3.26}$$

and substituting these into (3.22) obtain

$$\frac{\delta \hat{O}_H(1)}{\delta u(2)} = -i\theta(t_1,t_2)[\hat{O}_H(1),\hat{n}(2)]. \tag{3.27}$$

Thus the first order response function is given by

$$R(1,2) = -i\theta(t_1,t_2)\langle[\hat{O}_H(1),\hat{n}(2)]\rangle_0, \tag{3.28}$$

where $\langle\cdots\rangle_0 = \mathrm{tr}\{\hat{\rho}\cdots\}_{u=0}$. Note that $R(1,2) = 0$ for $t_2 > t_1$, and therefore R contains only the response to perturbations occurring in the past, in other words the retarded (or causal) response.

The higher order response functions can now be worked out inductively. Let us consider first the second order response given by

$$\begin{aligned}\frac{\delta^2 O(1)}{\delta u(2)\delta u(3)} = \frac{\delta}{\delta u(3)}\left[\frac{\delta O(1)}{\delta u(2)}\right] &= \frac{\delta}{\delta u(3)}\left[-i\int_{t_0}^{t_1}\mathrm{d}2\,\langle[\hat{O}_H(1),\hat{n}(2)]\rangle_0\right] \\ &= -i\int_{t_0}^{t_1}\mathrm{d}2\,\left[\langle\frac{\delta}{\delta u(3)}[\hat{O}_H(1),\hat{n}(2)]\rangle_0\right].\end{aligned} \tag{3.29}$$

We can write the operator commutator above as

$$[\hat{O}_H(1),\hat{n}(2)] = \hat{U}(t_0,t_2)[\hat{U}(t_2,t_1)\hat{O}\hat{U}(t_1,t_2),\hat{n}_{i_2}]\hat{U}(t_2,t_0). \tag{3.30}$$

Now if we take $t_2 > t_3$ the commutator on the right hand-side of (3.30) does not depend on $u(3)$. We can therefore follow the derivation for the first order response given above with $\hat{O}$ replaced by $[\hat{U}(t_2,t_1)\hat{O}\hat{U}(t_1,t_2),\hat{n}_{i_2}]$ and obtain

$$\frac{\delta^2 O(1)}{\delta u(2)\delta u(3)} = (-i)^2\int \mathrm{d}2\mathrm{d}3\,\theta(t_1,t_2)\langle[[\hat{O}_H(1),\hat{n}(2)],\hat{n}(3)]\rangle_0, \quad t_2 > t_3. \tag{3.31}$$

If on the other hand we take $t_3 > t_2$ we can simply apply the derivatives with respect to $u(2)$ and $u(3)$ in the opposite order, and obtain (3.31) with 2 and 3 exchanged. We therefore have in total

$$\begin{aligned}R(1,2,3) = \frac{\delta^2 O(1)}{\delta u(2)\delta u(3)}_{u=0} = (-i)^2\Big(&\theta(t_1,t_2,t_3)\langle[[\hat{O}_H(1),\hat{n}(2)],\hat{n}(3)] \\ &+\theta(t_1,t_3,t_2)\langle[[\hat{O}_H(1),\hat{n}(3)],\hat{n}(2)]\rangle\Big).\end{aligned} \tag{3.32}$$

Continuing this way one can derive for the $(n-1)$:th order response function the expression

$$\begin{aligned}&R(1,\ldots,n) \\ &= \frac{1}{i^{n-1}}\sum_P \theta(t_1,t_{P(2)},\ldots,t_{P(n)})\langle[\hat{O}_H(1),\hat{n}(P(2)),\ldots,\hat{n}(P(n))]\rangle,\end{aligned} \tag{3.33}$$

where the sum is over all permutations of $2,\ldots,n$ and

$$[O_1,\ldots,O_n] = [\cdots[[O_1,O_2],O_3],\ldots,O_n] \tag{3.34}$$

is a nested commutator.

In particular if we take the $\hat{O}(1) = \hat{n}(1)$ we obtain the so-called density response function

$$\begin{aligned}&\chi_n(1,\ldots,n) \\ &= \frac{1}{i^{n-1}}\sum_P \theta(t_1,t_{P(2)},\ldots,t_{P(n)})\langle[\hat{n}(1),\hat{n}(P(2)),\ldots,\hat{n}(P(n))]\rangle.\end{aligned} \tag{3.35}$$

3.3 Contour Formalism

In this section we will introduce a mathematical formalism that will make working with density response functions, and other similar objects, significantly simpler and our results more general. It turns out we can avoid the nested commutator structure appearing in the response functions, and go back to integrals over time-ordered products, if we interpret the time as a contour variable on a back-and-forth contour.

Consider first an integral over the first order response function

$$\int \mathrm{d}t_2\, \chi_2(t_1, t_2) = \frac{1}{i} \int \mathrm{d}t_2\, \theta(t_1, t_2) \langle [\hat{n}(t_1), \hat{n}(t_2)] \rangle, \tag{3.36}$$

where we have suppressed the quantum numbers i. Expanding the commutator, we have two integrals over two different orderings of the operators

$$\int \mathrm{d}t_2\, \theta(t_1, t_2) \langle [\hat{n}(t_1), \hat{n}(t_2)] \rangle = \int_{t_0}^{t_1} \mathrm{d}t_2\, \langle \hat{n}(t_1)\hat{n}(t_2) \rangle - \int_{t_0}^{t_1} \mathrm{d}t_2\, \langle \hat{n}(t_2)\hat{n}(t_1) \rangle. \tag{3.37}$$

In the first integral we need t_2 to be ordered before t_1 and in the second integral after t_1. We therefore define a contour γ_1 that starts from t_0, goes along the real-axis to t_1 and then returns back along the real-axis to t_0. We denote times on the forward branch γ_{1-} by t_-, and times on the returning backward branch γ_{1+} by t_+ (see left figure in Figure 1). Furthermore we define operators on the contour as

$$O(t_{1+}) = O(t_{1-}) = O(t_1). \tag{3.38}$$

This now allow us to write (3.37) as

$$\begin{aligned} &\int \mathrm{d}t_2\, \theta(t_1, t_2) \langle [\hat{n}(t_1), \hat{n}(t_2)] \rangle \\ &= \int_{t_{0-}}^{t_{1-}} \mathrm{d}t_{2-}\, \langle \mathcal{T}_{\gamma_1} \{ \hat{n}(t_{1-}) \hat{n}(t_{2-}) \} \rangle - \int_{t_{0+}}^{t_{1+}} \mathrm{d}t_{2+}\, \langle \mathcal{T}_{\gamma_1} \{ \hat{n}(t_{2+}) \hat{n}(t_{1+}) \} \rangle, \end{aligned} \tag{3.39}$$

where $\mathcal{T}_{\gamma_1}$ is a contour ordering operation ordering times further along the contour to the left. Times on the backward (t_+) branch are always later on the contour than those on the forward branch (t_-). For times on the forward branch larger real-time values are later on the contour, while for the times on the backward branch smaller real-time values are later on the contour.

Now let us denote times along the contour by z and use $z_1 > z_2$ to mean that z_1 is further along the contour than z_2. We then write the integrals over contour times as

$$\int_{t_{0-}}^{t_{1-}} \mathrm{d}t_- = \int_{\gamma_{1-}} dz \tag{3.40}$$

$$\int_{t_{0+}}^{t_{1+}} \mathrm{d}t_+ = -\int_{t_{1+}}^{t_{0+}} \mathrm{d}t_+ = \int_{\gamma_{1+}} dz, \tag{3.41}$$

where the integral over the backward branch is in the reverse direction so that the

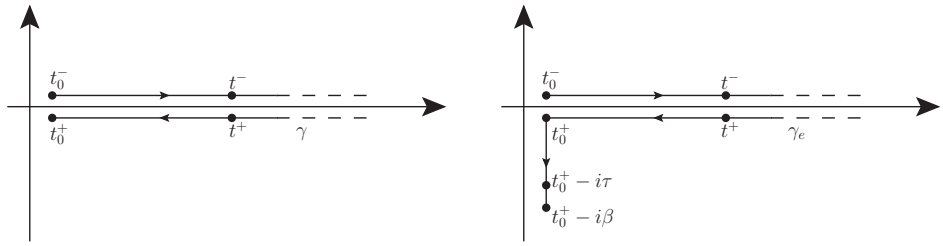

FIGURE 1: The two different contours used. (Left) The Keldysh contour γ, consisting of a forward branch γ^- and a backward branch γ^+. The contour is ordered, meaning that $t^+ > t^-$, while to both t^+ and t^- corresponds the same real-time value t (horizontal distance from $t_0^\pm$ to $t^\pm$). (Right) The extended contour γ', with an added vertical branch γ^M. Note that the horizontal branches are shifted from the real axis for illustrative purposes only; the times $t^\pm$ are real.

contour $\gamma_1 = \gamma_{1-} \bigoplus \gamma_{1+}$ is continuous. We can then write (3.39) as

$$\begin{aligned}
&\int \mathrm{d}t_2\, \theta(t_1, t_2) \langle [\hat{n}(t_1), \hat{n}(t_2)] \rangle \\
&= \int_{\gamma_{1-}} \mathrm{d}z_2\, \langle \mathcal{T}_{\gamma_1} \{ \hat{n}(z_1) \hat{n}(z_2) \} \rangle + \int_{\gamma_{1+}} \mathrm{d}z_2\, \langle \mathcal{T}_{\gamma_1} \{ \hat{n}(z_1) \hat{n}(z_2) \} \rangle \\
&= \int_{\gamma_1} \mathrm{d}z_2\, \langle \mathcal{T}_{\gamma_1} \{ \hat{n}(z_1) \hat{n}(z_2) \} \rangle.
\end{aligned} \tag{3.42}$$

Now we can also replace the contour γ_1 with contour γ that goes from t_0 to $+\infty$ and back, since the forward and backward parts for $t > t_1$ will cancel each other out. We then have the contour equation

$$\int_\gamma \mathrm{d}z_2\, \chi(z_1, z_2) = \frac{1}{i} \int_\gamma \mathrm{d}z_2\, \langle \mathcal{T}_\gamma \{ \hat{n}(z_1) \hat{n}(z_2) \} \rangle, \tag{3.43}$$

where $\chi(z_1, z_2)$ is a contour-ordered response function which can be expanded as

$$\chi(z_1, z_2) = \theta(z_1, z_2) \frac{1}{i} \langle \hat{n}(t_1) \hat{n}(t_2) \rangle + \theta(z_2, z_1) \frac{1}{i} \langle \hat{n}(t_2) \hat{n}(t_1) \rangle. \tag{3.44}$$

Note that for the expectation values above we can here use the real-time arguments since the branch the time argument is on only affects the ordering of the operators, and therefore the branch indices can be dropped whenever operators occur outside a contour-ordering operation. The contour step-function $\theta(z_1, z_2)$ is defined to be one when $z_1 > z_2$ and zero otherwise. Thus the contour formulation has allowed us to replace the commutator by a contour-ordering operation, which is very useful for manipulations of equations since operators under the ordering always commute. Note that for fermionic operators we define the orderings to anti-commute. Here $\hat{n}$ acts like a bosonic operator, being a product of an even number of fermionic operators.

The contour time-ordered expression is especially useful for perturbative expansions. To see this we note that if we define time-evolution operators on the contour through

$$\hat{U}(t_{1\pm}, t_{2\pm}) = \hat{U}(t_1, t_2), \tag{3.45}$$

we can express a Heisenberg operator as

$$\begin{aligned}\hat{O}_H(t_1) = \hat{U}(t_0,t_1)\hat{O}(t_1)\hat{U}(t_1,t_0) &= \mathcal{T}_{\gamma_1}\{\hat{U}(t_{0+},t_{1+})\hat{O}(z_1)\hat{U}(t_{1-},t_{0-})\} \\ &= \mathcal{T}_{\gamma_1}\{\hat{U}(t_{0+},t_{1+})\hat{U}(t_{1-},t_{0-})\hat{O}(z_1)\},\end{aligned} \tag{3.46}$$

where we have used the commutativity of bosonic operators under the ordering (the Hamiltonian is bosonic, and therefore so is $\hat{U}$). Note that we retain the time-argument in $\hat{O}(z_1)$ to keep track of its place in the contour ordering. Here

$$\begin{aligned}\hat{U}(t_{0+},t_{1+})\hat{U}(t_{1-},t_{0-}) &= \hat{U}(t_0,t_1)\hat{U}(t_1,t_0) \\ &= \bar{\mathcal{T}}\{e^{-i\int_{t_1}^{t_0} d\bar{t}\hat{H}(\bar{t})}\}\mathcal{T}\{e^{-i\int_{t_0}^{t_1} d\bar{t}\hat{H}(\bar{t})}\} \\ &= \mathcal{T}_{\gamma_1}\{e^{-i\int_{\gamma_1} d\bar{z}\hat{H}(\bar{z})}\},\end{aligned} \tag{3.47}$$

and therefore

$$\hat{O}_H(t_1) = \mathcal{T}_{\gamma_1}\{e^{-i\int_{\gamma_1} d\bar{z}\hat{H}(\bar{z})}\hat{O}(z_1)\}. \tag{3.48}$$

Thus the contour formulation allows one to express all the time-evolution operators as a single exponential, which makes differentiation with respect to parts of the Hamiltonian convenient since one avoids the multiplication of terms by the chain rule, as happened in (3.22).

For a product of operators

$$\hat{O}_{1,H}(t_1)\cdots\hat{O}_{n,H}(t_n) \tag{3.49}$$

we can replace each with (3.48) to obtain

$$\begin{aligned}&\mathcal{T}_{\gamma_1}\{e^{-i\int_{\gamma_1} d\bar{z}_1\hat{H}(\bar{z}_1)}\hat{O}_1(z_1)\}\cdots\mathcal{T}_{\gamma_n}\{e^{-i\int_{\gamma_n} d\bar{z}_n\hat{H}(\bar{z}_n)}\hat{O}_n(z_n)\} \\ &= \mathcal{T}_{\gamma_{1\cdots n}}\{e^{-i\int_{\gamma_{1\cdots n}} d\bar{z}\hat{H}(\bar{z})}\hat{O}_1(z_1)\cdots\hat{O}_n(z_n)\},\end{aligned} \tag{3.50}$$

where now $\gamma_{1\cdots n} = \gamma_1 \bigoplus \ldots \bigoplus \gamma_n$ is a contour consisting of the n loop-contours joined end to end. Now since $\hat{U}(z_1,z_2)\hat{U}(z_2,z_3) = \hat{U}(z_1,z_3)$ holds for the contour time-evolution operators, we can deform the contour by removing any parts where the contour goes back-and-forth without encountering any of the contour-times $z_1,\ldots,z_n$. Thus for example for

$$\hat{O}_1(z_1)\hat{O}_2(z_2)\hat{O}_3(z_3) \tag{3.51}$$

the replacement

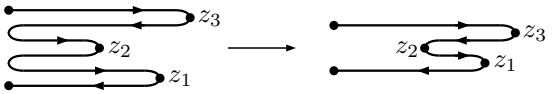

(3.52)

leaves integrals over this contour unchanged. The possible deformations depend on the real-time values of the time-arguments. For response functions in particular, we see from (3.33) that the ordering is always such that the real-time values first

increase and then decrease over the contour ordering, and therefore the contour can always be truncated to a single loop. For example

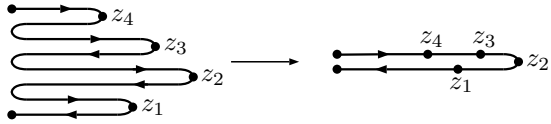

(3.53)

If we furthermore extend the contour to $+\infty$ we can use the same single-loop contour γ that goes from t_0 to ∞ and back for all response functions, and we have

$$\int \mathrm{d}t_2 \cdots \mathrm{d}t_n \, \chi_n(t_1, \ldots, t_n) = \int_\gamma \mathrm{d}z_2 \cdots \mathrm{d}z_n \, \chi_n(z_1, \ldots, z_n) \tag{3.54}$$

where the contour response function is given by

$$\begin{aligned} \chi_n(z_1, \ldots, z_n) &= \frac{1}{i^{n-1}} \langle \mathcal{T}_\gamma \{ n_H(z_1) \cdots n_H(z_n) \} \rangle \\ &= \frac{1}{i^{n-1}} \langle \mathcal{T}_\gamma \{ e^{-i \int_\gamma d\bar{z} \hat{H}(\bar{z})} n(z_1) \cdots n(z_n) \} \rangle \end{aligned} \tag{3.55}$$

Thus we have converted the expansion of the density in terms retarded response functions (suppressing sums over quantum numbers)

$$n(t_1) = \sum_n \frac{1}{n!} \int \mathrm{d}t_2 \cdots \mathrm{d}t_n \, \chi_n(t_1, \ldots, t_n) u(t_2) \cdots u(t_n), \tag{3.56}$$

where $\chi_1(t_1) = n(1)_{u=0}$, into an equation on the contour in terms of contour ordered response functions

$$n(t_1) = \sum_n \frac{1}{n!} \int_\gamma \mathrm{d}z_2 \cdots \mathrm{d}z_n \, \chi_n(z_1, \ldots, z_n) u(z_2) \cdots u(z_n). \tag{3.57}$$

3.3.1 Initial States and the Matsubara contour

The idea of the contour has a further use; we can express the density matrix as an integral over an imaginary branch of a contour, thus obtaining for the expectation value a simpler expression of a trace over a contour-ordered operator product. Consider the forward time-propagator for a constant Hamiltonian, which can be written simply as (see Section 2.2)

$$\hat{U}(t_1, t_0) = \mathrm{e}^{-i\hat{H}(t_1 - t_0)}. \tag{3.58}$$

Evaluating this for imaginary times gives

$$\hat{U}(-it_1, -it_0) = \mathrm{e}^{-\hat{H}(t_1 - t_0)}, \tag{3.59}$$

which evolves a general state according to

$$\hat{U}(-it_1, -it_0) |\Psi(t_0)\rangle = \sum_n \mathrm{e}^{-E_n(t_1 - t_0)} |\Psi_{E_n}(t_0)\rangle. \tag{3.60}$$

This obviously does not retain normalization, but it reduces the weight of each state relative to its energy, so that the higher energy states are more quickly suppressed. This is why imaginary time propagation can be used to find the ground-state starting from any state with finite overlap with the ground-state. However, if we propagate just the right amount, that is from t_0 to $t_0 - i\beta$, where $\beta = 1/(k_B T)$ is the inverse temperature, and then normalize the resulting state, we obtain

$$\sum_n \frac{\mathrm{e}^{-\beta E_n}}{\sum_m e^{-\beta E_m}} |\Psi_{E_n}(t_0)\rangle = \frac{\mathrm{e}^{-\beta \hat{H}_n}}{Z} |\Psi(t_0)\rangle \tag{3.61}$$

where the states are weighted by Boltzmann factors with Z being the partition function. Indeed $\frac{\mathrm{e}^{-\beta \hat{H}_n}}{Z}$ is just the density matrix operator (2.37) corresponding to the grand canonical ensemble for $\mu = 0$.

Therefore for systems initially in a finite temperature equilibrium one can express the density matrix operator as

$$\hat{\rho} = \frac{\mathrm{e}^{-\beta \hat{H}_M}}{Z} = \frac{1}{Z} \mathrm{e}^{-i \int_{t_0}^{t_0 - i\beta} \mathrm{d}\bar{t}\, \hat{H}_M(\bar{t})} = \frac{1}{Z} \mathcal{T}_{\gamma_M} \{ \mathrm{e}^{-i \int_{\gamma_M} \mathrm{d}\bar{z}\, \hat{H}_M(\bar{z})} \}, \tag{3.62}$$

where γ_M is a contour going from t_0 to $t_0 - i\beta$ and $\hat{H}_M$ is the so-called Matsubara Hamiltonian. The energy in Boltzmann factors is given with respect to the chemical potential μ, and therefore the Matsubara Hamiltonian is related to the Hamiltonian of the system by $\hat{H}_M = \hat{H} - \mu \hat{N}$. The value of the chemical potential fixes the number of particles in the many-body ground-state. Substituting (3.62) into an expectation value then leads to

$$\begin{aligned} \langle \hat{O}_H(t) \rangle &= \mathrm{tr} \left[\hat{\rho}\, \mathcal{T}_\gamma \{ \mathrm{e}^{-i \int_\gamma d\bar{z} \hat{H}(\bar{z})} \hat{O}(z) \} \right] \\ &= \frac{1}{Z} \mathrm{tr} \left[\mathcal{T}_{\gamma_M} \{ \mathrm{e}^{-i \int_{\gamma_M} \mathrm{d}\bar{z}\, \hat{H}_M(\bar{z})} \} \mathcal{T}_\gamma \{ \mathrm{e}^{-i \int_\gamma d\bar{z} \hat{H}(\bar{z})} \hat{O}(z) \} \right] \\ &= \frac{1}{Z} \mathrm{tr} \left[\mathcal{T}_{\gamma'} \{ \mathrm{e}^{-i \int_{\gamma'} d\bar{z} \hat{H}'(\bar{z})} \hat{O}(z) \} \right] \end{aligned} \tag{3.63}$$

where on the last line we have defined an extended contour γ' consisting of the Matsubara contour γ_M attached to the end of the loop contour γ, and a modified Hamiltonian

$$\hat{H}'(z) = \begin{cases} \hat{H}(t) & z \in \gamma \\ \hat{H}_M & z \in \gamma_M \end{cases} \tag{3.64}$$

Below we will continue to denote the contour by γ and the Hamiltonian by $\hat{H}$, with the understanding that they may be defined in multiple ways to obtain different forms of the theory.

Note that this formulation is in fact very general, since the density matrix is positive semi-definite, and therefore expression in the form of (3.62) is always possible. In the general case, however, the Matsubara Hamiltonian will not be related to the Hamiltonian of the system but is merely an alternative way to encode information about the initial state.

Finally we write the partition function in the form

$$\begin{aligned} Z &= \sum_m \mathrm{e}^{-\beta E_m} = \sum_m \langle \Psi_{E_m} | \mathrm{e}^{-\beta \hat{H}_M} | \Psi_{E_m} \rangle = \mathrm{tr}\left[\mathrm{e}^{-\beta \hat{H}_M} \right] \\ &= \mathrm{tr}\left[\mathcal{T}_{\gamma_M} \{ \mathrm{e}^{-i \int_{\gamma_M} \mathrm{d}\bar{z}\, \hat{H}_M(\bar{z})} \} \right] = \mathrm{tr}\left[\mathcal{T}_{\gamma'} \{ \mathrm{e}^{-i \int_{\gamma'} \mathrm{d}\bar{z}\, \hat{H}'(\bar{z})} \} \right], \end{aligned} \tag{3.65}$$

where in the end we have replaced the Matsubara contour with the full contour γ', since the loop part integrates to zero. Thus we obtain for an expectation value the expression

$$\langle \hat{O}(t) \rangle = \frac{\mathrm{tr}\left[\mathcal{T}_{\gamma'} \{ \mathrm{e}^{-i \int_{\gamma'} \mathrm{d}\bar{z} \hat{H}'(\bar{z})} \hat{O}(z_1) \} \right]}{\mathrm{tr}\left[\mathcal{T}_{\gamma'} \{ \mathrm{e}^{-i \int_{\gamma'} \mathrm{d}\bar{z}\, \hat{H}'(\bar{z})} \} \right]}. \tag{3.66}$$

3.4 Green's Functions

Previously we have introduced density response functions given by

$$\chi_n(z_1, \ldots, z_n) = \frac{1}{i^{n-1}} \langle \mathcal{T}_\gamma \{ n_H(z_1) \cdots n_H(z_n) \} \rangle. \tag{3.67}$$

It turns out to be useful to generalize these objects by splitting the number operators into two-time objects: $\hat{n}(1) = \hat{d}^\dagger_{i_1}(t_1)\hat{d}_{i_1}(t_1) \to \hat{d}^\dagger_{i_1}(t_1)\hat{d}_{i_2}(t_2)$. This leads to expectation values of equal numbers of creation and annihilation operators, of the form

$$G_n(1, \ldots, n; 1', \ldots, n') = \frac{1}{i^n} \langle \mathcal{T}_\gamma \{ \hat{d}_1 \cdots \hat{d}_n \hat{d}^\dagger_{n'} \cdots \hat{d}^\dagger_{1'} \} \rangle. \tag{3.68}$$

These objects are known as Green's functions. The main reason for introducing them is that using the equations of motion for the creation and annihilation operators ((3.17) and (3.18)) one can derive a hierarchy of equations of motion for the Green's function themselves, that links every G_n to G_{n+1} and G_{n-1}. This hierarchy is known as the Martin-Schwinger hierarchy and, importantly, it has a known solution by which any G_n can be expressed in terms of G_1. This result is the basis for the diagrammatic expansion. A corresponding hierarchy for the density response functions themselves can be derived (it is known as the BBGKY-hierarchy), but no general way to express higher order density response functions in terms of the lower order ones is currently known [3].

The simplest Green's function is the single-particle Green's function

$$G(z_1, z_2) = \frac{1}{i} \langle \mathcal{T}_\gamma \{ \hat{d}(z_1) \hat{d}^\dagger(z_2) \} \rangle. \tag{3.69}$$

Using the equations of motion for the creation and annihilation operators ((3.17)

and (3.18)) with the shorthand notation $\partial_1 = \frac{\partial}{\partial t_1}$, we find that

$$\begin{aligned} i\partial_1 G(1,2) &= \partial_1 \langle \mathcal{T}_\gamma \{ \hat{d}_1 \hat{d}_2^\dagger \} \rangle \\ &= \langle \mathcal{T}_\gamma \{ \hat{d}_1 (h_1 + \sum_i v_{i1} \hat{n}_i) \hat{d}_2^\dagger \} \rangle \\ &= h_1 G(1,2) + \sum_i v_{i1} \langle \mathcal{T}_\gamma \{ \hat{d}_1 \hat{d}_i^\dagger \hat{d}_i \hat{d}_2^\dagger \} \rangle \\ &= h_1 G(1,2) - \sum_i v_{i1} \langle \mathcal{T}_\gamma \{ \hat{d}_1 \hat{d}_i \hat{d}_i^\dagger \hat{d}_2^\dagger \} \rangle \\ &= h_1 G(1,2) + \sum_i v_{i1} G_2(1,i,2,i), \end{aligned} \tag{3.70}$$

where we have the two-particle Green's function

$$G_2(1,2,1',2') = \frac{1}{i^2} \langle \mathcal{T}_\gamma \{ \hat{d}_1 \hat{d}_2 \hat{d}_{2'}^\dagger \hat{d}_{1'}^\dagger \} \rangle. \tag{3.71}$$

Likewise we have

$$iG(1,2) \overleftarrow{\partial}_2 = h_2 G(1,2) + \sum_i v_{i2} G_2(1,i,2,i), \tag{3.72}$$

where $\overleftarrow{\partial}_2$ is a differential operator acting left.

In a similar manner one can then derive the equation of motion for the two-particle Green's function, finding that it depends in turn on the three particle Green's function, and so on. This forms the Martin-Schwinger hierarchy connecting each n-particle Green's function to the $n+1$ and $n-1$ particle Green's functions. These equation are given by

$$\begin{aligned} &[i\partial_k - h_k]\, G_n(1,\ldots,n;1',\ldots,n') \\ &= \pm i \int \mathrm{d}j\, v_{kj} G_{n+1}(1,\ldots,n,j;1',\ldots,n',j^+) \\ &+ \sum_{l=1}^{n} (\pm)^{k+l} \delta_{lk} G_{n-1}(1,\ldots,\overset{\sqcap}{k},\ldots,n;1',\ldots,\overset{\sqcap}{l'},\ldots,n') \end{aligned} \tag{3.73}$$

$$\begin{aligned} &G_n(1,\ldots,n;1',\ldots,n') \left[-i \overleftarrow{\partial}_k - h_k \right] \\ &= \pm i \int \mathrm{d}j\, v_{kj} G_{n+1}(1,\ldots,n,j^-;1',\ldots,n',j) \\ &+ \sum_{l=1}^{n} (\pm)^{k+l} \delta_{lk} G_{n-1}(1,\ldots,\overset{\sqcap}{l},\ldots,n;1',\ldots,\overset{\sqcap}{k'},\ldots,n'), \end{aligned} \tag{3.74}$$

where $\overset{\sqcap}{n}$ means that argument n is removed from the argument list, and $\pm$ means $+$ for bosons and $-$ for fermions. As might be expected from an interacting system, the propagation of n-particle excitations couples to the propagation of $n+1$-particle excitations with strength relative to the interaction strength, and so on, since the interactions ultimately connect all the particles in the system.

The Green's functions as defined above are solutions to the Martin-Schwinger hierarchy that fulfill the so-called KMS boundary conditions, i.e. they are symmetric/anti-symmetric for bosons/fermions over the contour:

$$G_n(\ldots,z_i,\ldots) = \pm G_n(\ldots,z_f,\ldots) \tag{3.75}$$

with z_i and z_f being the initial and final points of the contour respectively. These symmetry relations are straightforward to derive from (3.68) using the commutativity of objects under the contour-ordering along with the cyclic property of trace.

Let us first discuss the case of the non-interacting limit, around which we will later expand with respect to the interaction strength. It can be shown that for $v = 0$ the Martin-Schwinger hierarchy with KMS boundary conditions is solved by

$$g_n(1,\dots,n;1',\dots,n') = \begin{vmatrix} g(1;1') & \cdots & g(1;n') \\ \vdots & & \vdots \\ g(n;1') & \cdots & g(n;n') \end{vmatrix}_{\pm}, \tag{3.76}$$

where $\pm$ denotes that this is a determinant for fermions and for bosons a so called permanent, i.e. a determinant with all plus signs. This result is known as the Wick theorem, and it forms the basis for diagrammatic perturbation theory. Note that if $g(1;1')$ describes propagation of particle from $1'$ to 1, then g_n describes propagation of n particles from $1',\dots,n'$ to $1,\dots,n$ with a sum being taken over all the ways the particles can be reordered during the propagation. This reordering of particles gives for fermions a minus sign for every exchange according to their anti-symmetry property.

Now we take the interacting Green's function in the form

$$\begin{aligned} &G_n(1,\dots,n;1',\dots,n') \\ &= \frac{1}{i^n}\langle \mathcal{T}_\gamma\{\mathrm{e}^{-i\int_\gamma \mathrm{d}\bar{z}\,\hat{H}(\bar{z})}\hat{d}_1\cdots\hat{d}_n\hat{d}^\dagger_{n'}\cdots\hat{d}^\dagger_{1'}\}\rangle \\ &= \frac{1}{i^n}\langle \mathcal{T}_\gamma\{\mathrm{e}^{-i\int_\gamma \mathrm{d}\bar{z}\,\hat{h}(\bar{z})}\mathrm{e}^{-i\int_{\gamma'} \mathrm{d}\bar{z}\,\hat{H}_{int}(\bar{z})}\hat{d}_1\cdots\hat{d}_n\hat{d}^\dagger_{n'}\cdots\hat{d}^\dagger_{1'}\}\rangle \end{aligned} \tag{3.77}$$

where we have used the commutativity of bosonic operators under the contour-ordering to split the exponential. Expanding the exponentials in terms of the interaction as

$$\begin{aligned} \mathrm{e}^{-i\int_{\gamma'} \mathrm{d}\bar{z}\,\hat{H}_{int}(\bar{z})} &= \sum_n \frac{(-i)^n}{n!}\prod_{m=1}^n \int_\gamma \mathrm{d}z_m\,\hat{H}_{int}(z_m) \\ &= \sum_n \frac{(-i)^n}{2^n n!}\prod_{m=1}^n \int_\gamma \mathrm{d}m\,\hat{d}^\dagger_{i_m}\hat{d}^\dagger_{j_m} v_{i_m j_m}(z_m)\hat{d}_{j_m}\hat{d}_{i_m}, \end{aligned} \tag{3.78}$$

where $\int_\gamma \mathrm{d}m = \sum_{i_m j_m}\int_\gamma \mathrm{d}z_m$, allows one to take out of the expectation value everything but the creation and annihilation operators. These come in equal numbers, and thus one obtains an expression in terms of non-interacting Green's functions integrated against products of v. Specifically using the short-hand notation $G_n(1,\dots,n;1',\dots,n') = G_n(\mathcal{N};\mathcal{N}')$ with $\mathcal{N} = \{1,\dots,n\}$ an ordered set of argument labels, we have

$$G_n(\mathcal{N};\mathcal{N}') = \frac{1}{Z}\sum_{\mathcal{I}}\frac{1}{I!}\left(\frac{-i}{2}\right)^I\left[\prod_{i\in\mathcal{I}}\int \mathrm{d}i\,v(i,i')\right] g_{n+2I}(\mathcal{N},\mathcal{I},\mathcal{I}';\mathcal{N}',\mathcal{I}^+,\mathcal{I}'^+) \tag{3.79}$$

where $\mathcal{I} = \{i_1, \ldots, i_I\}$ is another ordered set of argument labels representing the arguments of the interactions v, and $\mathcal{I}^+$ represents the arguments $\mathcal{I}$ with each contour time infinitesimally larger, so that they get ordered to the left of the arguments in $\mathcal{I}$. The structure of this equation will be made more clear below when we express it diagrammatically. Note that the partition function expressed as in (3.65) is also given by the above expression when $n = 0$, and therefore

$$Z = \frac{1}{Z} \sum_{\mathcal{I}} \frac{1}{I!} \left(\frac{-i}{2} \right)^I \left[\prod_{i \in \mathcal{I}} \int \mathrm{d}i \, v(i, i') \right] g_{2I}(\mathcal{I}, \mathcal{I}'; \mathcal{I}^+, \mathcal{I}'^+). \tag{3.80}$$

3.4.1 Physical content of Green's functions

Multi-particle Green's functions on the contour are connected to the density-response functions through

$$\chi(1, \ldots, n) = iG_n(1, \ldots, n; 1^+, \ldots, n^+), \tag{3.81}$$

where argument $1^+ = i_1 z_1^+$ has a contour-time infinitesimally later than t_1, so that it is ordered by the contour-ordering to the left of argument 1. But Green's functions also contain additional useful information about transitions between many-body states in the system that can not be extracted from response functions.

The single-particle Green's function on the contour can be written as

$$G(1, 2) = \theta(z_1, z_2) G^{>}_{i_1 i_2}(t_1, t_2) + \theta(z_2, z_1) G^{<}_{i_1 i_2}(t_1, t_2), \tag{3.82}$$

where $G^>$ and $G^<$ are real-time functions given by

$$G^{>}_{i_1 i_2}(t_1, t_2) = -i \langle \hat{d}_{i_1}(t_1) \hat{d}^\dagger_{i_2}(t_2) \rangle, \qquad G^{<}_{i_1 i_2}(t_1, t_2) = i \langle \hat{d}^\dagger_{i_2}(t_2) \hat{d}_{i_1}(t_1) \rangle \tag{3.83}$$

that are called the greater component and the lesser component respectively (the operators here are Heisenberg operators).

The greater and the lesser Green's functions reduce to particle and hole density operators on the time-diagonal, but the off-diagonal components involve a time-evolution operator appearing between the operators when written in Schrödinger picture

$$G^{>}_{i_1 i_2}(t_1, t_2) = -i \langle \hat{U}(t_0, t_1) \hat{d}_{i_1} \hat{U}(t_1, t_2) \hat{d}^\dagger_{i_2} \hat{U}(t_2, t_0) \rangle, \tag{3.84}$$

which evolves the system in a $N + 1$ particle state (or $N - 1$ particle for the lesser propagator). For this reason the greater and lesser components are sometimes called particle and hole propagators respectively. It is important to keep in mind, however, that put precisely they are transition probability amplitudes between many-body states with an added particle/hole at a specific point, and it is misleading to think about a particular particle propagating since there is fundamentally no way to connect the particle that is added to the right hand side with the particle added to the left hand side since fundamental particles are indistinguishable. The greater Green's function $G^>(t_1 \mathbf{x}_1, t_2 \mathbf{x}_2)$ is the probability amplitude that a many-body state created by adding a particle at time t_2 to the single-particle orbital i_2 will after time-propagation from t_2 to t_1 be the many-body state that would have been created by adding a particle at time t_1 to the single-particle orbital i_1. Alternatively one

can say that $G^>(t_1 i_1, t_2 i_2)$ gives the amplitude that, if a particle is added at $(t_2 i_2)$ and after propagation until t_1 a particle is removed from $(t_1 i_1)$, one reaches the same many-body state that would have been reached without the particle addition and removal. The lesser Green's function represents the same amplitudes for holes instead of particles.

Let us consider now a system of N particles in equilibrium at finite temperature. The greater Green's function, for example, can then be expressed using an energy eigenbasis as

$$\begin{aligned} G^>_{i_1 i_2}(t_1, t_2) &= -i\langle \hat{U}(t_0, t_1)\hat{d}_{i_1}\hat{U}(t_1, t_2)\hat{d}^\dagger_{i_2}\hat{U}(t_2, t_0)\rangle \\ &= -i\sum_n \langle\psi_n|\hat{\rho}\, \mathrm{e}^{i\hat{H}(t_0-t_1)}\hat{d}_{i_1}\mathrm{e}^{i\hat{H}(t_1-t_2)}\hat{d}^\dagger_{i_2}\mathrm{e}^{i\hat{H}(t_2-t_0)}|\psi_n\rangle \\ &= -i\sum_n \rho_n \langle\psi_n|\hat{d}_{i_1}\mathrm{e}^{i(\hat{H}-E^N_n)(t_1-t_2)}\hat{d}^\dagger_{i_2}|\psi_n\rangle. \end{aligned} \tag{3.85}$$

Expanding the excited state in the energy eigenbasis as

$$\hat{d}^\dagger_i|\psi_n\rangle = \sum_m |\psi_m\rangle\langle\psi_m|\hat{d}^\dagger_i|\psi_n\rangle \tag{3.86}$$

we have

$$G^>_{i_1 i_2}(t_1, t_2) = -i\sum_{nm}\rho_n\langle\psi_n|\hat{d}_{i_1}|\psi_m\rangle\langle\psi_m|\hat{d}^\dagger_{i_2}|\psi_n\rangle\mathrm{e}^{i(E^{N+1}_m - E^N_n)(t_1-t_2)}. \tag{3.87}$$

For the diagonal elements in terms of quantum numbers, i.e. when $i_1 = i_2$, the two transition amplitudes turn into a probability

$$G^>_{i_1 i_1}(t_1, t_2) = -i\sum_{nm}\rho_n|\langle\psi_m|\hat{d}^\dagger_{i_1}|\psi_n\rangle|^2\mathrm{e}^{i(E^{N+1}_m - E^N_n)(t_1-t_2)}. \tag{3.88}$$

We see therefore that the Green's function only depends on the time difference $t_1 - t_2$ (as expected in equilibrium where we have time translational invariance) and that the Fourier transform with respect to the time difference gives the spectrum of the excitation energies $E^{N+1}_m - E^N_n$ from N particle states to $N+1$ particle states. Similarly the lesser Green's function gives the spectrum for transitions from N to $N-1$ particle states. The so called particle and hole spectral functions are defined by

$$\begin{aligned} A^>(\omega) &= iG^>(\omega) = i\int d(t_1 - t_2)\mathrm{e}^{i\omega(t_1-t_2)}G^>(t_1, t_2) \\ A^<(\omega) &= -iG^<(\omega) = -i\int d(t_1 - t_2)\mathrm{e}^{i\omega(t_1-t_2)}G^<(t_1, t_2). \end{aligned} \tag{3.89}$$

The spectrum of a two-particle Green's function, on the other hand, has peaks corresponding to transitions from N to $N+2$ and $N-2$ particle states, as well as transitions among N and $N+1$ particle states containing particle-hole excitations. We will discuss spectral representations of multi-particle Green's functions further in Section 5.3 below.

3.5 Diagrammatic Expansion

Consider first the single particle Green's function as given by (3.79)

$$G(1;1') = g(1;1') + \frac{1}{Z}\frac{-i}{2}\int \mathrm{d}2\mathrm{d}3\, v(2,3) g_3(1,2,3;1',2^+,3^+) + \dots \tag{3.90}$$

The first term here is simply the single-particle Green's function for the non-interacting Hamiltonian $\hat{h}$, which we denote diagrammatically by

$$g(1;1') = \quad 1 \bullet\!\longleftarrow\!\bullet\ 1' \tag{3.91}$$

In the first order correction, on the other hand, we have the non-interacting third-order Green's function, given according to the Wick theorem (3.76) by

$$g_3(1,2,3;1',2',3') = \begin{vmatrix} g(1;1') & g(1;2') & g(1;3') \\ g(2;1') & g(2;2') & g(2;3') \\ g(3;1') & g(3;2') & g(3;3') \end{vmatrix}_{\pm}. \tag{3.92}$$

We express a product of g-lines diagrammatically by

$$-g(1;1')g(2;3')g(3;2') = \begin{array}{ccc} 1 & \longleftarrow & 1' \\ 2 & \searrow\!\nearrow & 2' \\ 3 & \longleftarrow & 3' \end{array} \tag{3.93}$$

where we have also introduced a sign-rule stating that the sign of a diagram is given by $(-1)^{n_c}$ where n_c is the number of crossings of g-lines in the diagram. Note that from this sign-rule it follows that exchanging two vertices in the diagram, which always changes the number of crossings be an odd number, changes the sign of the diagram. This is consistent with the anti-symmetry of the Green's function with respect to exchanges of the primed or unprimed arguments among themselves, which follows from (3.68) and the anti-commutativity of the Fermionic creation/annihilation operators. Note that if the system also includes Bosonic particles, these creation/annihilation operators would commute, and likewise when applying the sign-rule for diagrams one should only take into account crossings of two Fermionic lines.

The sign-rule allows one to express for example the third order Green's function diagrammatically as a simple sum that has the same form for both Bosonic and Fermionic particles

$$g_3(1,2,3;1',2',3') = \begin{array}{ccc} 1 & \longleftarrow & 1' \\ 2 & \longleftarrow & 2' \\ 3 & \longleftarrow & 3' \end{array} + \begin{array}{ccc} 1 & \longleftarrow & 1' \\ 2 & \searrow\!\nearrow & 2' \\ 3 & \longleftarrow & 3' \end{array} + \begin{array}{ccc} 1 & \searrow\!\nearrow & 1' \\ 2 & \longleftarrow & 2' \\ 3 & \longleftarrow & 3' \end{array} + \begin{array}{ccc} 1 & \searrow\!\nearrow & 1' \\ 2 & \searrow\!\nearrow & 2' \\ 3 & \longleftarrow & 3' \end{array} + \begin{array}{ccc} 1 & \searrow\!\nearrow & 1' \\ 2 & \searrow\!\nearrow & 2' \\ 3 & \longleftarrow & 3' \end{array} + \begin{array}{ccc} 1 & \searrow\!\nearrow & 1' \\ 2 & \searrow\!\nearrow & 2' \\ 3 & \searrow\!\nearrow & 3' \end{array} \tag{3.94}$$

In the first order correction term in (3.90) we have the second and third primed/unprimed argument pairs of g_3 equal, and an interaction $v(2,3)$ connecting the pairs. We draw the interaction, including an i factor with it, as a wiggly line

$$iv(1;1') = \quad 1 \sim\!\sim\!\sim\ 1' \tag{3.95}$$

and would like to connect any lines sharing the same argument in a single point. However, moving the vertices might change the number of crossed lines. We therefore replace the crossed lines rule with an equivalent rule that does not depend on the positions of the vertices. This is based on the observation that if we imagine the primed/unprimed pairs of a Green's function to be connected pairwise by lines, as in

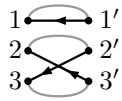

(3.96)

then every exchange of two vertices that changes the number of crossings by an odd number, also changes the number of closed loops created by the lines by an odd number. Given that for the case with no crossings the number of loops created is n, it follows that

$$(-1)^{n_c} = (-1)^{n_l+n}, \tag{3.97}$$

where n_l is the number of loops created when each vertex i is imagined to be connected to the vertex i'. This rule does not depend on how the diagram is drawn, and the value of a diagram therefore will depend only on its topology, i.e. on how its vertices are connected.

Substituting (3.94) into the first order correction term in (3.90) now leads to

$$\frac{1}{Z}\frac{-i}{2}\int \mathrm{d2d3}\, v(2,3) g_3(1,2,3;1',2^+,3^+) = \frac{1}{2Z}$$

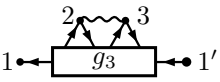

$$= \frac{1}{2Z}\Bigg[$$

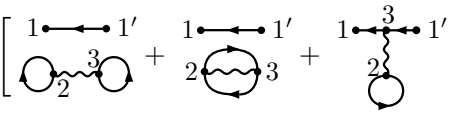

(3.98)

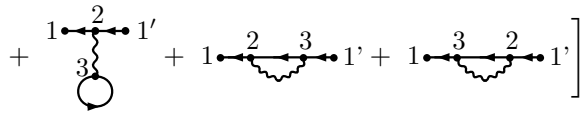

$$\Bigg]$$

where we have introduced another rule stating that internal vertices, i.e. those with all lines connected to them drawn, are to be integrated over the contour and summed over all quantum numbers. In these diagrams some of the external vertices of g_3 are connected, creating loops. These loops should be included in n_l when calculating the sign for these diagrams from (3.97).

The types of vertices that appear in these diagrams are determined by the terms of the Hamiltonian. Here the interaction term

$$\hat{H}_i = \frac{1}{2}\sum_{ij} \hat{d}_i^\dagger \hat{d}_j^\dagger v_{ij} \hat{d}_j \hat{d}_i \tag{3.99}$$

generates a three-point vertex connecting a v-line and two g-lines. The fact that we only have a single type of creation/annihilation operator means we only have one type of g-line, which we assume to be Fermionic (corresponding for example to electrons).

Note that since in (3.98) the arguments 2 and 3 are integrated over, the diagrams are symmetric with respect to exchanging them. Therefore two of the diagrams come in equal pairs, the doubles being conveniently cancelled by the factor $\frac{1}{2}$ in front. Thus we can express (3.98) more compactly as

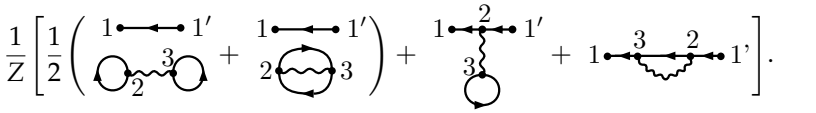

(3.100)

This cancellation is not a coincidence of course, since the factor $\frac{1}{2}$ is in (3.99) precisely because the sum over i and j includes v_{ij} and v_{ji} separately.

We will find that the two first diagrams in (3.100) are in fact cancelled by the partition function, however to see this we need to consider the full expansion of the interacting single-particle Green's function $G(1,1')$. The n-th order term in the expansion of $G(1,1')$ has the form

$$\frac{1}{Z}\frac{(-i)^n}{2^n n!}\int \mathrm{d}2\cdots\mathrm{d}(2n+1)\, v_{2,3}\cdots v_{2n,2n+1} \times g_{2n+1}(1,2,\ldots,2n+1;2,1',2^+,\ldots,(2n+1)^+), \tag{3.101}$$

which can be expressed diagrammatically by drawing n interaction lines and two external vertices and connecting them with g-lines in every possible topologically distinct way. Among the diagrams belonging to the second order correction to $G(1,1')$ are for example

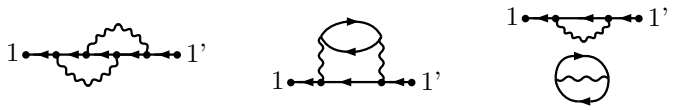

(3.102)

Among these are diagrams consisting of a connected diagram from the first order correction along with a disconnected piece. These disconnected pieces are sometimes called vacuum diagrams, since in relativistic quantum field theories they represent spontaneous particle/anti-particle pair generation from the vacuum. Likewise the third order correction term will contain connected diagrams from the second order correction along with a vacuum diagram, and connected diagrams from the first order correction along with a vacuum diagrams with two interaction lines in them (or two copies of the single interaction diagram). This pattern continues infinitely, and when all correction terms are included there will be for each connected diagram a set of diagrams consisting of that connected piece along with any arbitrary collection of vacuum diagrams. It follows that we can factorize the expansion into

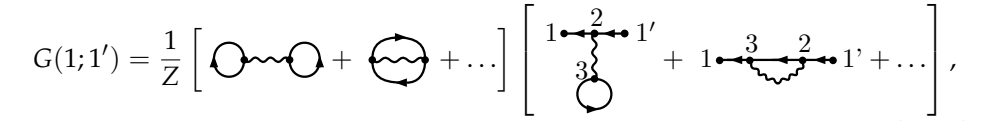

(3.103)

where the first sum goes over every possible vacuum diagram (including diagrams consisting of multiple disconnected vacuum diagrams) and the second sum every

possible connected diagram. The sum over the vacuum diagrams, however, is exactly the diagrammatic expansion of the partition function, as obtained from (3.80). Thus the partition function cancels out all disconnected diagrams from the expansion of $G(1;1')$.

The diagrammatic expansion of an n-particle Green's function can be found in an analogous way by simply adding another pair of external vertices for each additional particle. Thus for example the first order correction to the two-particle Green's function is

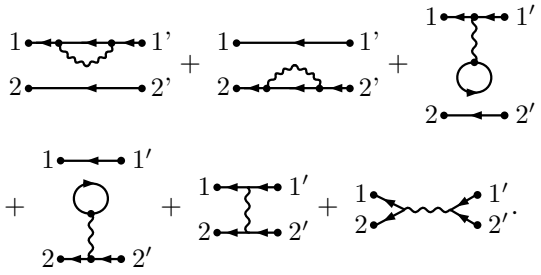

(3.104)

The vacuum diagrams not connected to any of the external vertices are cancelled from the expansion of any G_n just as for $G(1;1')$.

Since the response functions have representations in terms of multi-particle Green's functions, their diagrammatic forms follow directly. As has been seen, the first order response function can be expressed in terms of the two-particle Green's function as

$$\chi(z_1,z_2)=\frac{1}{i}\langle\mathcal{T}_\gamma\{\hat{n}(z_1)\hat{n}(z_2)\}\rangle=iG_2(1,2;1^+,2^+), \tag{3.105}$$

which gives it a diagrammatic representation as

$$-i\chi(z_1,z_2)=$$ 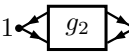

(3.106)

Likewise higher order response functions have representations in terms of higher order Green's functions as

$$-i\chi_n(z_1,\ldots,z_n)=$$ 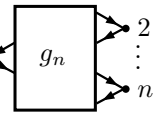

(3.107)

The change in single-particle density due to an external potential u can therefore be expanded as

$$\begin{aligned}\Delta\hat{n}(1)=\hat{n}(1)-\hat{n}(1)_{u=0}&=\sum_{n=2}^{\infty}\int d2\cdots dn\,\chi_n(1,\ldots,n)u(2)\cdots u(n)\\&=\sum_{n=2}^{\infty}\end{aligned}$$ 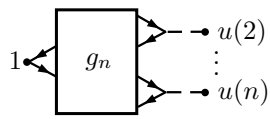

(3.108)

Note that the Green's function here is that for the Hamiltonian with $u=0$.

We finish this chapter by giving the rules for the reverse process, i.e. for associating with an arbitrary Green's function diagram the corresponding mathematical expression. These rules are known as Feynman rules, and can be stated as follows: for a diagram belonging to $G_n(1,\ldots,n;1',\ldots,n')$

1. label each vertex of the diagram
2. multiply together $g(i,j)$ for each g-line going from vertex j to vertex i and a v(i,j) for each interaction line connecting vertices i and j.
3. integrate each internal time-argument z_i over the contour and sum over all internal quantum numbers q_i.
4. multiply the result by $i^{n_v}(-1)^{n_l+n}$ where n_v is the number of interaction lines and n_l the total number of loops formed by g-lines in the diagram when the external vertices are imagined to be joined together from i to i'.

3.6 Self-Energy

The diagrams discussed above are seen to often contain repetitions of the same type of sub-diagrams. We will discuss on this chapter how by defining sums of such sub-diagram insertions we can resum repetitive diagrams and thus include certain classes of diagrams to infinite order while at the same time reducing the number of distinct diagrams we need to deal with.

The single-particle Green's function in particular is readily seen to be a sum of diagrams of the form

(3.109)

where pieces containing interactions are connected by singular g-lines into chains. By defining an object of the form

$\Sigma =$ 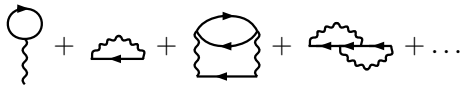 $+\ldots$

(3.110)

we can express G using a recursive equation known as the Dyson equation

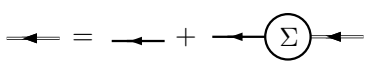

(3.111)

which can be solved iteratively by starting from

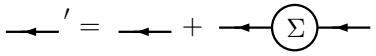

(3.112)

and then substituting G' to the right-hand side to obtain G'' and so on until convergence is reached. The object Σ is known as the self-energy. The reason for this name is made clear by an alternative derivation, which also gives us an expression for Σ in terms of G_2, making its diagrammatic representation precise.

The equation of motion for the single-particle Green's function can be written as

$$\left[i\frac{\mathrm{d}}{\mathrm{d}z_1} - h(1)\right] G(1;1') = \delta(1;1') \pm i \int d2v(1;2)G_2(1,2;1',2^+). \tag{3.113}$$

The self-energy Σ can be defined through the equation

$$\pm i \int \mathrm{d}2v(1;2)G_2(1,3;2,3^+) = \int \mathrm{d}3\Sigma(1;3)G(3;2), \tag{3.114}$$

which allows the equation of motion to be written as

$$\left[i\frac{\mathrm{d}}{\mathrm{d}z_1} - h(1)\right] G(1;1') = \delta(1;2) + \int \mathrm{d}3\Sigma(1;3)G(3;2). \tag{3.115}$$

This truncates the hierarchy, and allows the evolution of G to be solved as long as an approximation for Σ can be found. (3.115) can be written in an integral form (assuming the boundary condition (3.75)) as

$$G(1;2) = g(1;2) + \int \mathrm{d}3\mathrm{d}4\, g(1;3)\Sigma(3;4)G(4;2), \tag{3.116}$$

where $g(1;2)$ is the solution for $v = 0$, i.e. the non-interacting limit. This is exactly the Dyson equation given diagrammatically in (3.111).

Note that (3.115) can also be written in the alternative form

$$\int \mathrm{d}3 \left[i\frac{\mathrm{d}}{\mathrm{d}z_1}\delta(1,3) - \Big(h(1)\delta(1,3) + \Sigma(1;3)\Big)\right] G(3;2) = \delta(1;2), \tag{3.117}$$

which shows that the self-energy can be seen as a correction to the Hamiltonian that is integrated over past times and thus depends on the history of the system. The self-energy therefore represents a correction to the single-particle energies due to interactions with other particles, i.e. self-interaction of the system. This correction introduces memory, since the interaction causes the appearance of excitations with finite life-time. These excitations are represented by the diagrams in the expansion of the self-energy.

From (3.117) we also see that it is convenient to split the self-energy into time-local and analytic parts as

$$\Sigma(1,2) = \delta(z_1, z_2)\Sigma_{HF}(1,2) + \Sigma_c(1,2), \tag{3.118}$$

where $\Sigma_{HF}(1,2)$ is the so called Hartree-Fock self-energy given diagrammatically by

$\Sigma_{HF} =$ 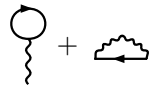 (3.119)

This is time-local, and can therefore be absorbed into h by defining

$$h_{HF} = h + \Sigma_{HF} \tag{3.120}$$

leading to (3.117) taking the form

$$\int \mathrm{d}3 \left[i\frac{\mathrm{d}}{\mathrm{d}z_1}\delta(1,3) - \Big(h_{HF}(1)\delta(1,3) + \Sigma(1;3)_c\Big)\right] G(3;2) = \delta(1;2). \tag{3.121}$$

Since (3.121) is of the same form as the original equation for g (3.117), the diagrammatic expansion can be performed using g_{HF} in the exact same way, the only difference being that the g-lines in the diagrams are now g_{HF} lines containing arbitrary numbers of Σ_{HF} insertions. We therefore need to only consider diagrams that do not have such insertions. Indeed including such diagrams in this expansion would lead to double-counting. This reduces the number of diagrams we need to deal with and includes interaction effects at the level of mean-field approximation into the non-interacting Green's functions (the content of this approximation is discussed in the following chapter). Furthermore it allows us to work with an analytic function Σ_c instead of Σ which contains delta-functions.

The correlation self-energy provides a convenient starting point for considering different approximations. Any approximation for the self-energy generates through the Dyson equation an approximation for the Green's function, which includes an arbitrary number of interaction processes, and is therefore essentially partially summed to infinite order in the interaction strength. This can make it possible to deal with stronger interactions as long as the Dyson equation still converges. Of course only certain classes of diagrams are summed, and therefore the result is still approximate. In the following chapter we will discuss further how the choices of self-energy diagrams affect the physical content of the resulting approximation.

3.7 Scattering Amplitudes

As has been mentioned, probabilities in quantum mechanics come in the form of probability amplitudes c represented by complex numbers, which are squared and averaged over the ensemble as in

$$p = \sum_n \rho_n c_n^* c_n \tag{3.122}$$

to obtain a real valued classical probability p, discarding in the process the phase information contained in the complex numbers. When trying to approximate a number representing a probability, we generally want to construct an approximation for the amplitude rather than the probability directly, as this will be more closely connected to the underlying theory and have a more clear physical interpretation as a result.

The contour formalism introduced in the preceding sections is very efficient in that it includes a large number of different physical processes into a minimal number of diagrams. It, however, gives us the diagonal elements of greater and lesser Green's functions/self-energies directly, and therefore makes their interpretation as probabilities difficult, since it is not obvious from which probability amplitudes these probabilities derive from. This can make the physical content of the resulting approximations less obvious, and even lead one to consider approximations that have no clear physical interpretation at all.

It is therefore expedient to obtain for quantities such as the single-particle Green's functions, self-energies and response functions expressions explicitly in terms of amplitudes. These are not necessarily optimal for purposes of deriving results or performing numerical calculations, but they are very useful as starting

points for building approximations. Importantly we want to obtain these expressions in diagrammatic form which allows us to connect the amplitudes directly to scattering processes represented by diagrams, and thus to build approximations to the various correlators starting from a set of scattering processes. This has the added advantage of building in certain positivity properties of the exact system so that they can be shown to be retained in the resulting approximations (see Pub. [III]).

At zero temperature the greater and lesser components of a single-particle Green's function are trivially expressed as squares of amplitudes since the expectation value becomes simply (using the lesser component as an example)

$$G^<(1,2) = i\langle \hat{d}^\dagger(1)\hat{d}(2)\rangle = i\langle\psi_0|\hat{d}^\dagger(1)\hat{d}(2)|\psi_0\rangle. \tag{3.123}$$

Placing a sum over states between the $\hat{d}$ operators gives

$$-iG^<(1,2) = \sum_n \langle\psi_0|\hat{d}^\dagger(1)|\psi_n\rangle\langle\psi_n|\hat{d}(2)|\psi_0\rangle = \sum_n A_n^\dagger(1)A_n(2), \tag{3.124}$$

with the amplitude

$$A_n(1) = \langle\psi_n|\hat{d}(1)|\psi_0\rangle. \tag{3.125}$$

This gives each term $A_n^\dagger(1)A_n(1)$ interpretation as the probability for removal of a particle on orbital 1 from the many-body ground-state ψ_0 to cause the system to transition to the excited state ψ_n. The diagonal element of $-iG^<$ is therefore the probability for the system to transition to any state, which is equal to the probability that there is a particle to be removed on orbital 1 at the ground state.

One could now construct the excited states ψ_n from the ground-state by applying creation and annihilation operators, obtaining expressions of the form

$$|\psi_n\rangle = \hat{d}^\dagger\cdots\hat{d}^\dagger\hat{d}\cdots\hat{d}|\psi_0\rangle. \tag{3.126}$$

Substituting this into (3.125) gives an amplitude that can be interpreted as scattering to a specific set of particle/hole excitations relative to the ground-state. It also gives the amplitude a form of a zero-temperature multi-particle Green's function, allowing for diagrammatic expansion wherein each diagram represents a particular way for the scattering process to occur.

At zero-temperature this process is also straightforward to follow for the self-energy, as has been done in [1] for the equilibrium case and in Pub. [II] for the steady-state limit, and for the polarizability (i.e. the irreducible part of the first order response function), as has been done in [2].

At finite temperature this approach runs into complications due to the fact that the finite temperature expectation value is a trace and therefore does not split neatly into a product of expectation values of the same form, as would be required for the diagrammatic expansion of each half to be performed. Nevertheless an approach along these line is possible, and is presented here in Appendix B as it offers some physical insight by separating the finite-temperature corrections into distinct diagrams.

For derivations it turns out to be more convenient to approach the problem from another angle, and start by performing the diagrammatic expansion and then

introducing a cutting procedure by which the diagrams are split into half-diagrams and then collected into products. This approach was taken in Pub. [III], and will be here briefly summarized.

The cutting procedure used in Pub. [III] proceeds by two steps. We first argue that by extending the contour to distant past we can under very broad conditions get rid of diagrams containing integrals over the Matsubara branch. This reduces the contour to a single loop, which we can then deform into two loops, as in

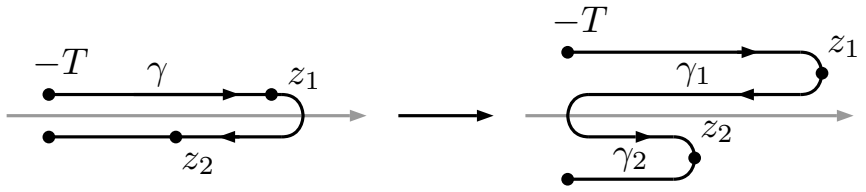

(3.127)

and by factorizing the g-lines passing between the two loops cut the diagrams into two half-diagrams, both on a single loop contour, that represent scattering amplitudes. We can then express the self-energy in terms of specific scattering processes, giving it a clear physical interpretation.

The removal of Matsubara diagrams can be argued for as follows (See Pub. [III] section 3.3. for more detail). We assume that our system is initially in a finite temperature equilibrium state up to some time t_0 when possible time-dependent perturbations are applied. We can then extend the contour to infinite past, since this merely corresponds to waiting for longer before applying the perturbation, which makes no physical difference in a system in equilibrium. The Matsubara branch is thus moved to infinitely remote past $t = -T \to -\infty$, after which every diagram containing Matsubara integrals involves Green's function lines between finite times and the time $-T$. The time-evolution operators in such Green's functions then involve phase-factors of the form

$$e^{-i\epsilon_i(t+T)}, \tag{3.128}$$

where ϵ_i is the energy of some single-particle orbital. These energies are summed over in the diagram, and if the spectrum of energies is continuous, these sums will become integrals. The integrals over the phase-factor will then vanish due to the Riemann-Lebesque theorem which states that

$$0 = \lim_{T\to\pm\infty} \int \mathrm{d}\epsilon\, F(\epsilon)\, \mathrm{e}^{\mathrm{i}\epsilon T} \tag{3.129}$$

when $F(\epsilon)$ is integrable. In Pub. [III] we further show that the assumption of continuous spectrum does not need to be made when the system is always in equilibrium. We therefore conclude that if the contour is extended to an infinite time in the past the Matsubara diagrams do not contribute and can be discarded, provided that the system is either always in equilibrium, or is initially in equilibrium and has a continuous single-particle energy spectrum.

We thus assume that we are now dealing with a diagrammatic expansion of the self-energy on the horizontal contour that extends to distant past with the

g-lines in the diagrams being finite temperature non-interacting Green's functions. Next we will deform the contour into two loops with the two external times of the self-energy in the two end-points of the loops, as depicted in (3.127).

Each integral over the double-loop contour is then split into integrals over the individual loops

$$\int_\gamma = \int_{\gamma_1} + \int_{\gamma_2} \tag{3.130}$$

and thus every diagram is split into a sum over diagrams with the internal vertices integrated over the two different contours in every possible combination. For example

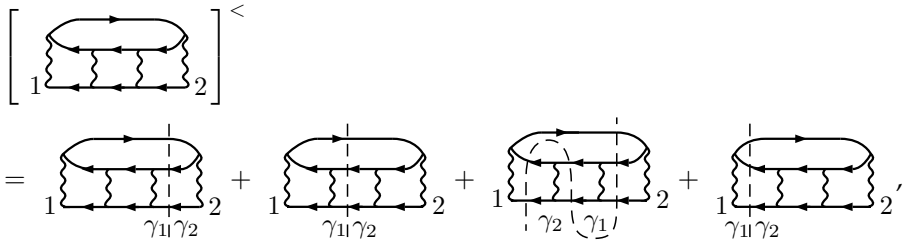

(3.131)

where the dashed line separates the regions integrated over γ_1 and γ_2. Here, since we have a lesser component, z_2 is later on the contour than z_1, and therefore γ_2 is after γ_1 on the deformed contour. Consequently every Green's function line going from a vertex in γ_1 to vertex in γ_2 is a greater component (as follows from (3.82)). Likewise lines going in the other direction are lesser components.

Thus the γ_1 and γ_2 parts of the diagram can be separated to a product by factorizing the greater and lesser components connecting them using the relation

$$g^{\lessgtr}(t,t') = g^R(t,t_0)g^{\lessgtr}(t_0,t_0)g^A(t_0,t'), \tag{3.132}$$

where g's are understood as matrices with respect to the quantum numbers. The equal time Green's functions are directly related to the single-particle density $\rho(t_0) = \rho_0$ at the initial time t_0 through

$$g^<(t_0,t_0) = \mathrm{i}\rho_0, \qquad g^>(t_0,t_0) = -\mathrm{i}(1-\rho_0) = -\mathrm{i}\bar{\rho}_0, \tag{3.133}$$

where $\bar{\rho}_0$ is the hole-density. Both ρ and $\bar{\rho}$ are positive matrices with respect to the quantum numbers, and therefore we have

$$-\mathrm{i}g^<(t,t') = [g^R(t,t_0)\rho_0^{\frac{1}{2}}][g^R(t',t_0)\rho_0^{\frac{1}{2}}]^\dagger \tag{3.134}$$

$$\mathrm{i}g^>(t,t') = [g^R(t,t_0)\bar{\rho}_0^{\frac{1}{2}}][g^R(t',t_0)\bar{\rho}_0^{\frac{1}{2}}]^\dagger. \tag{3.135}$$

We can write these relations in terms of contour Green's functions by defining the initial particle and hole densities on the contour to be

$$\begin{aligned}\rho_0^{\frac{1}{2}}(z) &= \big(\delta(z,t_{0-}) - \delta(z,t_{0+})\big)\rho_0^{\frac{1}{2}} \\ \bar{\rho}_0^{\frac{1}{2}}(z) &= \big(\delta(z,t_{0-}) - \delta(z,t_{0+})\big)\bar{\rho}_0^{\frac{1}{2}}\end{aligned} \tag{3.136}$$

so that we have

$$-\mathrm{i}g^{<}(t,t') = \left[\int_\gamma d\bar{z}\, g(z,\bar{z})\rho_0^{\frac{1}{2}}(\bar{z})\right]\left[\int_\gamma d\bar{z}'\, \rho_0^{\frac{1}{2}}(\bar{z}')g(\bar{z}',z')\right] \tag{3.137}$$

$$\mathrm{i}g^{>}(t,t') = \left[\int_\gamma d\bar{z}\, g(z,\bar{z})\bar{\rho}_0^{\frac{1}{2}}(\bar{z})\right]\left[\int_\gamma d\bar{z}'\, \bar{\rho}_0^{\frac{1}{2}}(\bar{z}')g(\bar{z}',z')\right]. \tag{3.138}$$

This splits every diagram into two halves, with the cut $g^{<}/g^{>}$-lines having extra $\rho_0^{1/2}/\bar{\rho}_0^{1/2}$ factors at the end of them. Crucially the half-diagrams are otherwise exactly the types of diagrams that appear in an expansion of a many-particle Green's function. Indeed if we sum over all cuts of all self-energy diagrams we obtain for the self-energy the expression

$$-\mathrm{i}\Sigma_c^{<}(1,2) = \sum_{N=1}^{\infty}\frac{(-1)^{N+1}}{N!(N+1)!}\sum_L$$

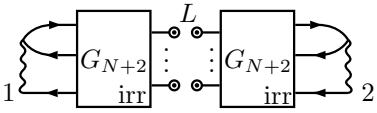

(3.139)

where the Green's functions are irreducible in the sense that diagrams in which the left side can be disconnected from the right side by removing a single g-line are not included. Sum over L represents the sum over all quantum numbers for the cut g-lines, and N represents the number of particle-hole pairs cut. Starting the N-sum from 1 leaves out diagrams that are reducible at the cut. The Green's functions here are contour ordered on a loop contour that starts from $-\infty$ and integrated over the contour for all vertices but 1 and 2. The circles on the end of the cut lines denote the $\rho_0^{1/2}/\bar{\rho}_0^{1/2}$ factors (for left-going and right-going g-lines respectively).

(3.139) is derived in Pub. [III] Section 3.1. starting from the Lehmann representation at zero-temperature. After removal of the Matsubara diagrams the finite temperature expansion contains the exact same diagrams as the zero-temperature one, but with internal g-lines at finite temperature, and therefore the same expression holds also at finite temperature with only the difference that the cut g-lines contain the $\rho_0^{1/2}/\bar{\rho}_0^{1/2}$ factors. In the following chapter we will further discuss how this expression can be used to generate approximations.

3.7.1 Response Functions in terms of Scattering Amplitudes

Like the self-energy, density response can also be expressed in terms of scattering amplitudes, giving it a clear physical interpretation. The single-particle density is given by

$$n(t) = -iG^{<}(t,t). \tag{3.140}$$

If we go through the derivation discussed in the previous section for the Green's function instead of the self-energy we obtain

$$-\mathrm{i}G^{<}(1,2) = \sum_{N=0}^{\infty}\frac{(-1)^{N+1}}{N!(N+1)!}\sum_L$$

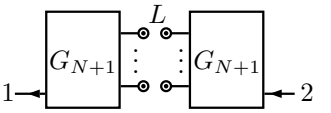

(3.141)

which gives the single-particle density the diagrammatic representation

$$n(1) = \sum_{N=0}^{\infty} \frac{(-1)^{N+1}}{N!(N+1)!} \sum_{L}$$

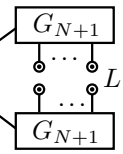

(3.142)

Diagrammatic representations for the response functions can now be found by expanding (3.142) with respect to the external potential u. The derivative of a Green's function with respect to u is given by

$$\begin{aligned}
&\frac{\delta}{\delta u(m)} G_n(1,\ldots,n;1',\ldots,n') \\
&= \frac{1}{i^n Z} \frac{\delta}{\delta u(m)} \operatorname{tr} \mathcal{T}_\gamma \{ \mathrm{e}^{-i\int_\gamma \mathrm{d}\bar{z} \hat{H}'(\bar{z})} \hat{d}_1 \cdots \hat{d}_n \hat{d}^\dagger_{n'} \cdots \hat{d}^\dagger_{1'} \} \\
&= \frac{1}{i^{n+1} Z} \operatorname{tr} \mathcal{T}_\gamma \{ \hat{d}^\dagger_m \hat{d}_m \mathrm{e}^{-i\int_\gamma \mathrm{d}\bar{z} \hat{H}'(\bar{z})} \hat{d}_1 \cdots \hat{d}_n \hat{d}^\dagger_{n'} \cdots \hat{d}^\dagger_{1'} \} \\
&= \frac{-1}{i^{n+1} Z} \operatorname{tr} \mathcal{T}_\gamma \{ \mathrm{e}^{-i\int_\gamma \mathrm{d}\bar{z} \hat{H}'(\bar{z})} \hat{d}_1 \cdots \hat{d}_n \hat{d}_m \hat{d}^\dagger_m \hat{d}^\dagger_{n'} \cdots \hat{d}^\dagger_{1'} \} \\
&= -G_{n+1}(1,\ldots,n,m;1',\ldots,n',m^+),
\end{aligned} \tag{3.143}$$

which can be expressed diagrammatically as

$$\frac{\delta}{\delta u(m)}$$

$$= -$$

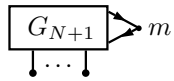

(3.144)

Using this for example the first order response can be expressed as

$$\chi(1,m) = \frac{\delta n(1)}{\delta u(m)}$$

$$= \sum_{N=0}^{\infty} \frac{(-1)^{N+2}}{N!(N+1)!} \sum_{L}$$

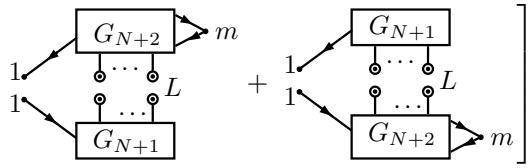

(3.145)

where now the Green's functions are those of the unperturbed system ($u = 0$).

Continuing in this way we find the M:th order response function to be

$$\chi_{M+1}(1,m_1,\ldots,m_M) = \frac{\delta n(1)}{\delta u(m_1)\cdots\delta u(m_M)}$$

$$= \sum_{N=0}^{\infty} \frac{(-1)^{N+M+1}}{N!(N+1)!} \sum_{l=0}^{M} \binom{M}{l}$$

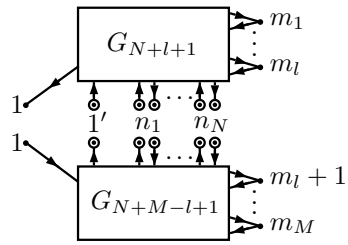

(3.146)

and thus the expansion of the density in terms of the response functions can be expressed as

$$n(1) = \sum_{M=0}^{\infty} \frac{1}{M!} \int_{\gamma} \mathrm{d}m_1 \cdots \mathrm{d}m_M \, \chi_{M+1}(1, m_1, \ldots, m_M) u(m_1) \cdots u(m_M)$$

$$= \sum_{N,M=0}^{\infty} \frac{(-1)^{N+M+1}}{N!(N+1)!} \sum_{l=0}^{M} \frac{1}{l!(M-l)!}$$

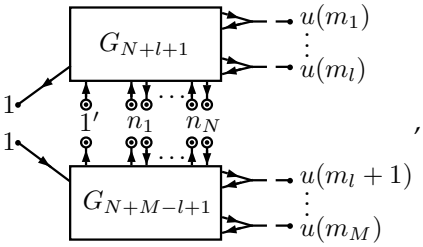

, (3.147)

where $\chi_1(1) = n(1)_{u=0}$. In the following chapter we will make use of this expansion to generate approximations for the response functions.

Chapter 4

Diagrammatic Approximations

Diagrammatic expansions are an useful tool for constructing approximations with tailored properties for modeling specific systems. They can also be used to derive various techniques for extending approximations by chaining or nesting diagrams recursively to effectively sum certain classes of diagrams up to infinite order. In this chapter we will discuss the different ways diagrammatic approximations can be constructed and how the choices made affect the physical content and properties of the approximation. As examples we will exhibit several commonly used approximations.

Consider first the single-particle Green's function, that can be expressed diagrammatically as

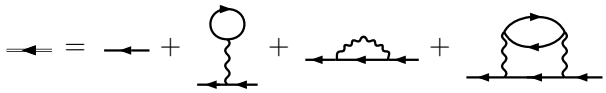

(4.1)

The simplest way to approximate this is to simply cut the series at certain order, obtaining for example to the first order the Hartree-Fock approximation

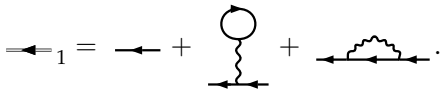

(4.2)

Here the second diagram gives by applying the Feynman rules (given at the end of Section 3.5)

$$\begin{aligned} &= -i \int \mathrm{d3d4}\, g(1,3) g(3,2) v(3,4) g(4,4^+) \\ &= \int \mathrm{d3d4}\, g(1,3) g(3,2) v(3,4) n(4), \end{aligned} \tag{4.3}$$

where one integrates over the particle density of the unperturbed system $n(4)$. Note that the equal time Green's function becoming $g(4,4^+)$, and thus relating to the particle density, follows from (3.79), and ultimately from the fact that the interaction term in our Hamiltonian contains particle densities. The Hartree diagram can thus be seen to represent interaction with the particles of the unperturbed initial state.

The last diagram in (4.2) is the corresponding exchange diagram (obtained for example by exchanging the g-lines going into the interaction line). It corresponds to the expression

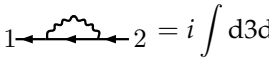

$$= i \int \mathrm{d}3\mathrm{d}4\, g(1,3)g(3,4)g(4,2)v(3,4). \tag{4.4}$$

If the interaction is time-local (4.4) reduces to

$$i \int \mathrm{d}3\, g(1,3)g(3,2)g(3,3^+)v(3,3), \tag{4.5}$$

since the equal time Green's function is diagonal with respect to the quantum numbers. Thus (4.4) cancels the interaction of the particle with itself from (4.3).

Dealing with the Green's function directly, however, is not very effective. Usually one starts instead from the Dyson equation

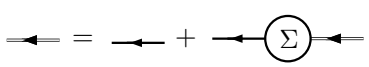

(4.6)

which after choosing a diagrammatic approximation for the self-energy Σ is solved self-consistently to effectively generate diagrams to infinite order. The self-energy is usually separated into $\Sigma = \Sigma_{HF} + \Sigma_c$ where

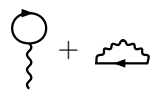

(4.7)

is the time-local Hartree-Fock part that is first order in the interaction, and the remaining time-non-local second-order or higher correlation self-energy Σ_c. As discussed below (3.118), being time-local the Hartree-Fock part of the self-energy enters the equations as a potential, which we can include into the single-particle Hamiltonian. This leads to a diagrammatic expansion where the g-lines in the diagrams are Hartree-Fock Green's functions, which is obtained from the Dyson equation (4.6) when $\Sigma = \Sigma_{HF}$. We then do not include any diagrams containing Σ_{HF} insertions, as these are already included to arbitrary order, and thus the correlation self-energy to second order has only two diagrams

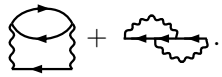

(4.8)

As opposed to the Hartree-Fock self-energy, which describes interaction with the unperturbed initial state, the correlation self-energy describes excitations due to the interaction. The first diagram in (4.8) is the simplest such process, wherein a single particle-hole excitation is created and then decays depositing its energy back to the propagating particle. The second diagram is again the exchange diagram corresponding to the first one, which is made more clear by drawing it as

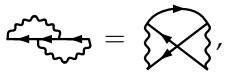

(4.9)

and describes a process in which the original particle combines with the hole of the excitation, and the excited particle continues propagating. Note that although we discuss particle propagation for the sake of specificity, any g-line in these diagrams can be either a particle or a hole propagator depending on the ordering on the contour of its end points, with particles going forward on the contour and holes backward. Thus each self-energy diagram involves multiple different physical processes.

To higher orders the number of self-energy diagrams quickly increases. Computing the self-energy order by order therefore quickly becomes quite complicated. However, the idea of the Dyson equation, that is solving a set of diagrammatic equations self-consistently, can be applied in multiple ways to the self-energy in turn. This allows one to effectively include certain sets of diagrams to infinite order.

The simplest self-consistency cycle that can be utilized is based on the fact that the self-energy expressed diagrammatically depends on the single-particle Green's function, which in turn depends on the self-energy via the Dyson equation. This makes a closed system of equations, so that after choosing a self-energy approximation and using that to find a Green's function from

$$G^{(1)} = g + g \cdot \Sigma[g] \cdot G^{(1)}, \tag{4.10}$$

(here $a \cdot b = \int \mathrm{d}2\, a(1;2)b(2;3)$) one can then solve the self-energy again using $G^{(1)}$ and find

$$G^{(2)} = g + g \cdot \Sigma[G^{(1)}] \cdot G^{(2)}. \tag{4.11}$$

Continuing this cycle until convergence leads to a G that fulfills

$$G = g + g \cdot \Sigma[G] \cdot G. \tag{4.12}$$

Diagrammatically this process nests self-energy insertions on themselves, so that for example for the self-energy

$$\Sigma_c[g] = \tag{4.13}$$

one obtains after the first cycle

$$\Sigma_c[G_1] = \tag{4.14}$$

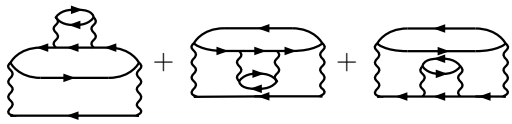

and further all diagrams with arbitrary numbers of repeated insertions on any g-line. The next cycle nests insertions inside these insertions, and so on, so that at convergence one includes effectively infinitely nested interaction processes. Note that although an effectively infinite amount of diagrams is included in this way, this is still a vanishingly small subset of all diagrams in the exact expansion, since no new fundamental scattering processes are included, but merely those included in the original self-energy are repeated in differing orders. This is the nature of all such resummation schemes, as the full complexity of the many-body scatterings

cannot be captured by any cycling of simple equations. Note that it is not even guaranteed that a self-consistent solution of the Green's function will provide a better physical description. For example in finite systems self-consistency can introduce spurious damping effects, as seen in [4]. This can happen, since the resummation can introduce diagrams that in the full expansion would be cancelled by some other set of diagrams that the resummation misses.

The self-energy approximation used in this type of scheme should not include any diagrams that can be built by placing other self-energy diagrams as insertions into each other, as this would lead to double-counting during the self-consistency cycle. The exact self-energy expressed in terms of G then contains only diagrams with no self-energy insertions of any type (an insertion being any part of the diagram that can be detached from the rest of the diagram by cutting two g-lines). Such diagrams are called G-skeletonic. This significantly reduces the number of diagrams in Σ to any given order.

An alternative way to set up a resummation scheme is to express the self-energy in terms of a higher-order kernel that can be chained via a Dyson-like equation. As was discussed around (3.114), the self-energy can be related to the two-particle Green's function through

$\Sigma \cdot g =$ 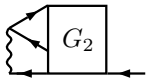 (4.15)

which on the other hand can be obtained from the Bethe-Salpeter equation for G_2

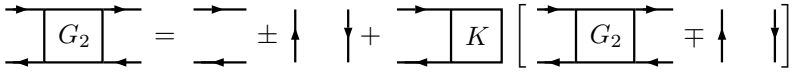 (4.16)

where the Bethe-Salpeter kernel $K(1,2;3,4)$ now plays a role similar to the self-energy in the Dyson equation. Choosing for example

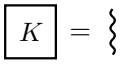 (4.17)

gives the two-particle Green's function

 (4.18)

which leads to the self-energy approximation

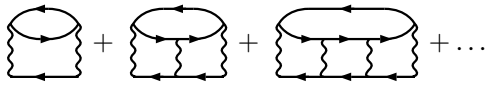 (4.19)

that includes a single particle-hole excitation and an arbitrary number of interactions between the propagating particle and the hole of the excitation. (4.19) is known as the particle-hole T-matrix approximation. It is useful for example for modeling of excitons, which are bound states of electrons and holes. There is also a particle-particle (or hole-hole) T-matrix approximation, where the interactions are between g-lines going in the same direction. This can be derived from an

alternative form of the Bethe-Salpeter equation (Dyson type equations for higher order functions come in multiple channels). Exchange diagrams can also be added to both of these variants (see for example Pub. [III] Chapter 4.).

On the other hand taking

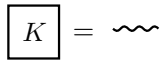

(4.20)

leads to the two-particle Green's function

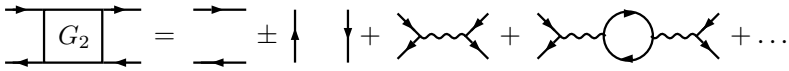

(4.21)

and the self-energy approximation

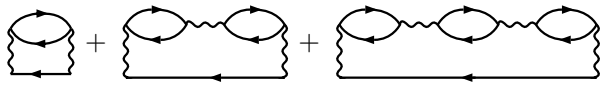

(4.22)

known as the *GW*-approximation. The physical content of this approximation is made more clear by noting that a single bubble

(4.23)

has the form of a non-interacting first order response function (see (3.106)). It can thus be seen as describing response of the particle density to internal excitations of the system, as opposed to an external potential. The *GW*-approximation chains these responses together, thus introducing contributions from large scale density fluctuations involving large numbers of particles. This is exemplified by the fact that self-consistent *GW*-spectrum will include a plasmon peak coming from collective oscillation of the electrons.

The name *GW* is based on the convention of denoting by *W* the so called screened interaction

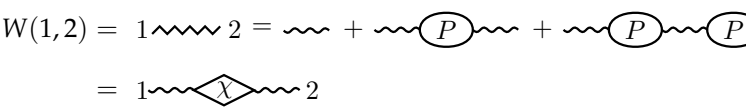

(4.24)

where *P* is the polarizability

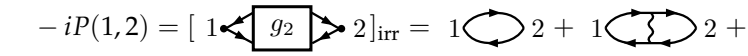

(4.25)

that is irreducible in the sense that the one cannot disconnect 1 and 2 by removing a single interaction line. In other words *P* is the irreducible part of the interacting first order density response function $\chi(1,2)$, which can be obtained from the polarizability via a Dyson-like equation

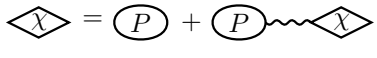

(4.26)

Expressing diagrammatic approximations in terms of W is useful particularly since it incorporates screening effects and is therefore often much shorter range than the bare Coulomb interaction v. Shorter range interactions can lead to easier numerical integration and better convergence properties, while also giving a better physical description of the system. Of course there are additional equations to solve, but these form a closed system that can be solved self-consistently, since G depends on Σ, which depends on W, which depends on χ, which depends on P, which depends on G again.

4.1 Scattering Diagrams and Positive Approximations

Taking the self-energy as a starting point for generating approximations has the advantage of generating a large number of Green's function diagrams based on a small number of relatively simple self-energy diagrams. We can, however, take a step further and generate the self-energy from an even smaller set of diagrams representing scattering processes. This has the additional benefit of making the physical content of the approximation more clear. Furthermore it allows one to show that certain positivity properties of the exact system are retained by approximations arrived at in this way. We will here give a brief overview of these topics, that are discussed in detail in Pub. [III].

The scattering amplitude representation of a self-energy approximation can be obtained by applying so-called cutting rules to factorize the self-energy diagrams and writing them as products of amplitudes. This is achieved by applying the contour-deformation used in 3.7 to individual diagrams.

Take for example the diagram

$$D^<(1,2) = \Big[$$ 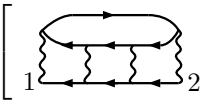 $$\Big]^<$$ (4.27)

from the T-matrix approximation. Deforming the contour into two loops containing the two external vertices (see (3.127)), and splitting each internal contour time-integral into a sum over the two loops, leads to a sum of diagrams corresponding to every distribution of the internal times between the two loops. Denoting by γ_1 and γ_2 the two loops we have

$D^<(1,2)$

$=$ 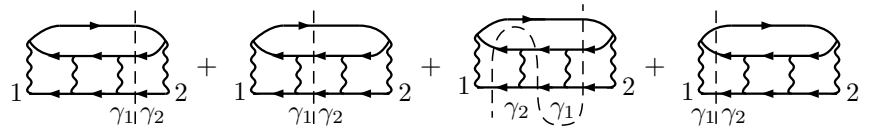

(4.28)

Since we are considering the lesser component of the self-energy the loop γ_2 comes after the loop γ_1 in the contour. Any g-line connecting the two-loops thus reduces

to either a greater of a lesser component, and we have

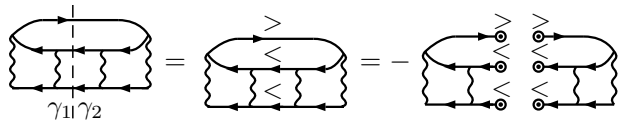

(4.29)

where we have used (3.137) to factorize the lesser/greater g-lines. Here the minus sign comes from the difference in prefactors when we consider the Feynman rules for the self-energy diagram and the Feynman rules for the two half-diagrams interpreted as diagrams belonging to expansion of G_2 (see Pub. [III] Appendix B). From the fact that $g^*(1,2) = -g(2,1)$ for the contour Green's function (and that the prefactor for the right half-diagram has i^2 for the two interaction lines) it then follows that the diagonal elements of the self-energy have the form

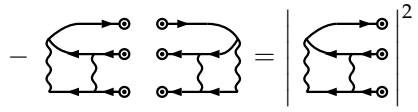

(4.30)

and can thus be interpreted as probabilities to scatter by the process depicted by the half-diagram. The off-diagonal elements on the other hand can be seen as transition amplitudes between many-body states created by the two different scattering processes.

Note that not every self-energy approximation can be expressed in this form. For example if we take the first two lowest order terms of the GW-approximation

(4.31)

and apply the cutting rules, we obtain

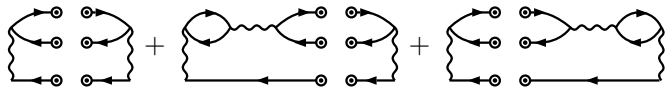

(4.32)

This cannot be written as a product of mirrored diagrams, and therefore does not admit interpretation in terms of a well-defined set of scattering processes. Instead if we take the two scattering processes appearing here and build a symmetric product out of them we obtain

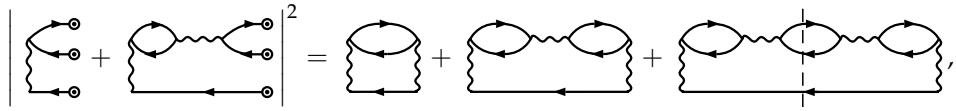

(4.33)

Interpreting the right-hand side here as a two-point function then gives a self-energy approximation containing these two scattering processes. The last diagram here represent a partial integral of the fourth order diagram over a double loop contour, which cannot be converted into a diagram integrated over a single loop unless all parts of the double loop integral can be summed. In this way starting

from a set of scattering processes often generates pieces of contour diagrams along with the simple contour diagrams.

Adding the next higher order scattering diagram to the left hand side in (4.33) would lead to all contributions to the fourth order GW self-energy diagram being generated. However, this would also introduce partial integrals of the fifth and sixth order self-energy diagrams. This process continues in higher orders, and all the partial integrals can be fully summed only on the limit of infinite order.

This exemplifies the important point that the contour diagram representation of the self-energy, while very efficient, can be misleading in that an approximation consisting of a set of diagrams integrated fully over the contour does not necessarily correspond to any well-defined set of scattering processes.

More generally we can add terms including higher order scattering processes, such as

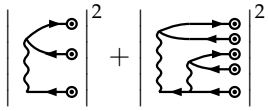

(4.34)

Note that sometimes a single contour self-energy diagram will include contributions from multiple orders of scattering processes, such as in

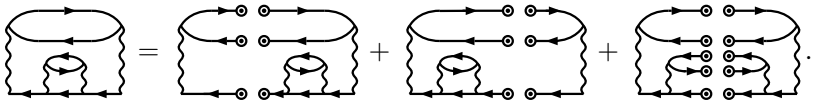

(4.35)

If we consider approximations that contain exchange terms, such as the 2B-approximation, that can be expressed as

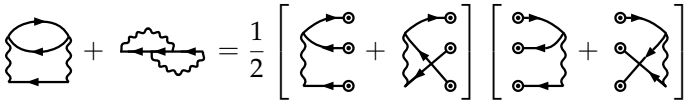

(4.36)

we find that evaluating the bare product leads to duplicates of diagrams and therefore an additional prefactor is needed to avoid double-counting. This happens since the direct and exchange half-diagrams are related by permutation of the labels of the cut lines, and thus two exchange half-diagrams combine to create a direct diagram, the permutations cancelling each other out. Such expressions can be simplified if the sum over permutations of the labels is over a subgroup of their full permutation group. In such case the combinations of two permutations end up generating the permutations of the same subgroup, and we sum over only a single set of permutations. This generates no duplicate diagrams and requires no prefactor to cancel them. For example for the 2B-approximation we could write

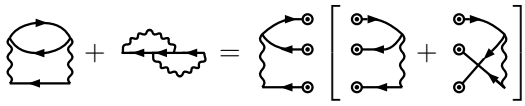

(4.37)

These cutting rules can also be applied to dressed diagrams. Since from the Dyson equation one can derive (see A for a derivation including also the Matsubara

contour)

$$G^{\lessgtr}(t_1,t_2) = G^R(t_1,t_0)g^<(t_0,t_0)G^A(t_0,t_2) + \int_{t_0}^{\infty} \mathrm{d}t_3\mathrm{d}t_4\, G^R(t_1,t_3)\Sigma[g]^<(t_3,t_4)G^A(t_4,t_2), \tag{4.38}$$

it follows that if $\Sigma[g]$ is factorizable, then $G^{\lessgtr}$ is factorizable as well. Furthermore if $G^{\lessgtr}$ and $\Sigma[g]$ are factorizable, so is $\Sigma[G]$. Thus the positivity property is retained by the self-consistency cycle for dressing G, and any positive $\Sigma[g]$ approximation will be positive for dressed G-lines as well. Note however that, as seen in (4.35), certain products of scattering diagrams may come from cutting of non-skeletonic contour diagrams. Therefore including a specific scattering process in a self-energy approximation expressed fully in terms of dressed contour diagrams may not be straightforward.

If one also wishes to dress the interaction lines, it is important to note that W is not time local, and therefore can pass between different loops of the deformed contour. Therefore diagrams expressed in terms off W generate additional cut diagrams, that require factorization relations for W to cut them. These can be derived using

$$W^{\lessgtr}(t_1,t_2) = \int_{t_0}^{\infty} \mathrm{d}t_3\mathrm{d}t_4\, W^R(t_1,t_3)P[g]^<(t_3,t_4)W^A(t_4,t_2), \tag{4.39}$$

and applying the cutting rules discussed above to the polarization diagrams (this has been done at zero-temperature in [2]).

In [1] it was shown that diagrammatic approximations constructed from scattering processes as discussed above have certain positivity properties. These results are generalized to finite temperature in Pub. [III]. These properties guarantee in particular that both the spectral function of the self-energy and that of the Green's function will be positive semi-definite. This is important since the spectral functions represent probabilities that are directly linked to observations such as those obtained from photo-emission spectroscopy experiments. If these functions take negative values their interpretation as probabilities breaks down.

4.2 Conserving Approximations

In addition to the positivity of probabilities, another important physical constraint one would wish to preserve in approximations is the upholding of various conservation laws. In this section we will briefly discuss how one can choose approximations in such a way as to guarantee these laws.

Baym and Kadanoff showed [5] that if the single-particle Green's function fulfills the equations of motion

$$\begin{aligned} i\partial_1 G(1,2) &= h_1 G(1,2) + \sum_i v_{i1} G_2(1,i,2,i) \\ iG(1,2)\overleftarrow{\partial}_2 &= h_2 G(1,2) + \sum_i v_{i2} G_2(1,i,2,i) \end{aligned} \tag{4.40}$$

with a two-particle Green's function that has the symmetry

$$G(1,2;1^+,2^+) = G(2,1;2^+,1^+), \tag{4.41}$$

then the particle density and current obtained from $G(1,2)$ will fulfill the continuity equation locally, and the total momentum change of the system will equal the total force applied by external fields. If G_2 furthermore fulfills the same boundary conditions as the exact G_2, it follows that the total energy change equals the total power applied by external fields.

Baym also introduced [6] a convenient way to generate self-energy approximations that do not break these conservation laws. If a self-energy is obtained from a functional $\Phi[G]$ through

$$\Sigma(1;2) = \frac{\delta\Phi[G]}{\delta G(2,1^+)}, \tag{4.42}$$

then if $\Phi[G]$ is invariant under gauge transformation, time translations, space translations, and rotations the resulting approximation will conserve particle number, energy, momentum, and angular momentum respectively. Note that this so-called Φ-derivability is a stricter condition than those given above for G_2. Every Φ-derivable self-energy is conserving, but the reverse need not be true.

Suitable $\Phi[G]$ functionals can be constructed through a diagrammatic procedure by summing over vacuum diagrams. These diagrams should be two particle irreducible, i.e. not breakable into disconnected pieces by removing two g-lines, as such diagrams would generate reducible self-energy diagrams. Resummations of these vacuum diagrams can be performed by dressing the Green's functions and interaction lines either fully or partially in each vacuum diagram [7]. For practical purposes one can interpret the functional derivative in (4.42) as a diagrammatic rule that removes from Φ each G-line in turn. For example

$\frac{\delta}{\delta G(2,1^+)}$ 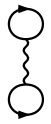 $= 2 \times$  , $\frac{\delta}{\delta G(2,1^+)}$  $= 2 \times$  , (4.43)

which shows that the Hartree and Fock diagrams are both conserving individually. The second diagram in (4.43) for a dressed interaction gives the GW self-energy, which is therefore conserving. Likewise the two diagrams in the Second Born self-energy can be obtained through

$\frac{\delta}{\delta G(2,1^+)}$ 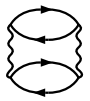 $= 4 \times$  $\frac{\delta}{\delta G(2,1^+)}$  $= 4 \times$ 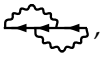 , (4.44)

and are therefore conserving. From higher order bubbles one can obtain linear combinations of self-energy diagrams, in which case all diagrams need to be included in the self-energy with correct relative weights to maintain the conservation properties.

Note that any self-energy obtained from a Φ-functional consisting of full contour diagrams will be made up of full contour diagrams as well. However, as

was seen above, when building the self-energy approximation from scattering processes in order to guarantee positivity properties, the resulting approximation is often not of this form, but contains also partial contour diagrams. While most commonly used approximations, such as Second-Born, and various *GW* and *T*-matrix approximations are both conserving and positive, this is seen to result mainly from the simplicity of the diagrams involved. It appears that going beyond these simplest approximations while retaining both conservation laws and positivity is not possible, and that sacrificing one or the other is going to be inevitable. Still, even if the presence of certain properties cannot be guaranteed, this does not mean that they can not hold in practice, at least to the precision required for the particular calculation in question. When going beyond the standard approximations it therefore becomes important to be able to determine not only whether a particular approximation breaks conservation rules or positivity, but to what extent they are broken.

4.3 Approximations to Response Functions

We can obtain diagrammatic approximations for the response functions by substituting approximations for the multi-particle Green's functions into (3.107).

For example the density shift in the linear response approximation is given by

$$\Delta n(1) = n(1) - n(1)_{u=0} = \int d2\, G_2(1,2;1^+,2^+)u(2), \tag{4.45}$$

into which we can now substitute an approximation for the two-particle Green's function. On the non-interacting limit this is

$$g_2(1,2;1',2') = g(1;1')g(2;2') \pm g(1;2')g(2;1') \tag{4.46}$$

leading to

$$\Delta n(1;1^+) = \int d2 \left[g(1;1^+)g(2;2^+) \pm g(1;2)g(2;1)\right] u(2). \tag{4.47}$$

Here the second term vanishes since $\int d2\, g(2,2^+)u(2)$ integrates to zero over the loop contour and we are assuming that $u = 0$ on the Matsubara branch (with no loss of generality, since we can always split the potential into initial value plus correction and expand with respect to the correction). The density shift in the linear response can therefore be expressed diagrammatically as

$\Delta n(1) =$ 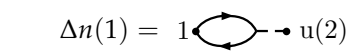

(4.48)

on the non-interacting limit. The first order correction due to interaction can be obtained simply by including the first order correction to G_2 (3.104) which results in

$\Delta n(1) =$ 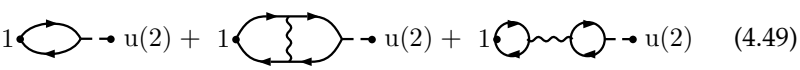

(4.49)

where we take the arrows to denote Hartree-Fock Green's functions and have therefore removed the diagrams with first order self-energy insertions.

The first diagram in (4.49) can be interpreted as the probability for the external potential u (describing for example a laser beam) to cause a particle to propagate into the detector at point 1, while the second diagram includes the effect of interaction between the excited particle and the hole left behind to the first order. The last diagram describes a process in which the excited particle transfers its energy to another particle and sends it into the detector, which can be seen as the exchange process corresponding to the second diagram (and indeed it has an opposite sign due to an additional loop).

In the second order approximation we have the additional diagrams

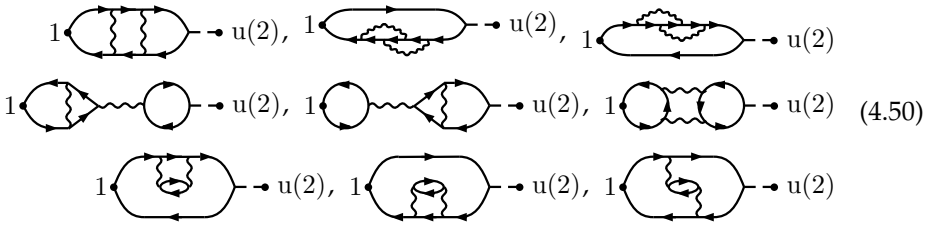

(4.50)

that include time-non-local second order self-energy insertions. Considering an expansion in terms of G-lines dressed with the Second-Born self-energy

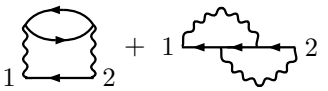

(4.51)

would then allow us to remove diagrams containing these insertions and express the first order response to second order in terms of G-skeletonic diagrams as

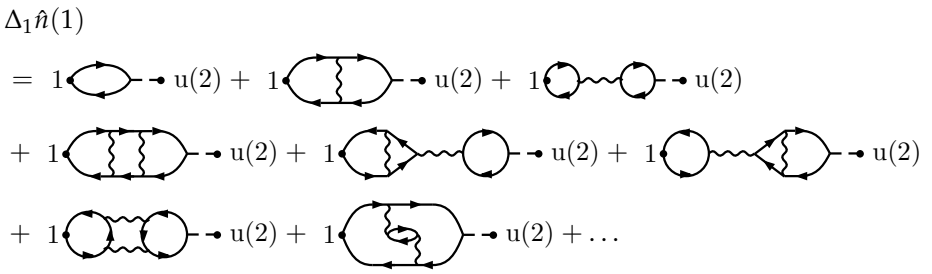

(4.52)

Given that the first order response depends on the two-particle Green's function, one can also make use of the Bethe-Salpeter equation (4.16) to resum first order response diagrams to infinite order. For example solving the Bethe-Salpeter equation with the kernel

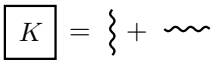

(4.53)

and substituting into (4.45) will generate all but the last two diagrams in (4.52), along with an infinite series of others.

Like for the self-energy, these approximations are not always positive. To construct positive approximations we can start from the scattering diagram expansion of the density response (3.147). This will also show that most of the diagrams in

(4.52) actually give zero contribution if vertex 1 is outside the sample material, as in a photo-emission experiment. To the first order in u (3.147) gives on the non-interacting limit

$$-in(1) = \quad + \quad + \quad + \quad . \tag{4.54}$$

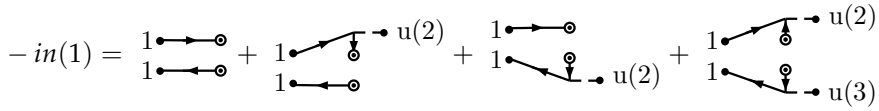

Gluing these diagrams using (3.137) thus gives

$$-i\Delta n(1) = \quad + \quad + \quad \tag{4.55}$$

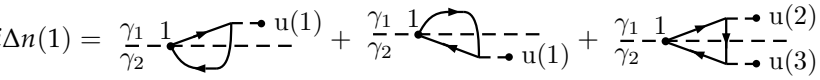

since the first diagram in (4.54) simply becomes $iG^{<}_{u=0}(1;1^{+}) = n(1)_{u=0}$. Now if vertex 1 is outside of the material, the three first diagrams in (4.54) include non-interacting Green's functions describing particle propagation from inside the material to the detector. These vanish assuming that electrons are not escaping the material without receiving energy from the external field. Thus the lowest order contribution to the photo-emission current comes from the diagram second-order in u in (4.55). Furthermore, this is the only second-order diagram that contributes, since the other two cuts of the second order contour response function

$$\quad , \qquad \tag{4.56}$$

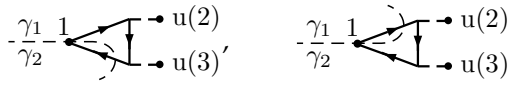

also vanish by the argument used previously. Due to these diagrams vanishing, the second order density response outside of the material can be expressed simply as

$$-i\Delta n(1) = \quad \tag{4.57}$$

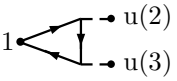

where 2 and 3 are integrated over γ. This is, furthermore, a positive approximation, since it equals (4.54).

The next higher order positive approximation is obtained by adding the second order u scattering diagram

$$\quad \tag{4.58}$$

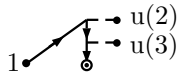

which leads to

$$-i\Delta n(1) = \quad + \quad + \quad . \tag{4.59}$$

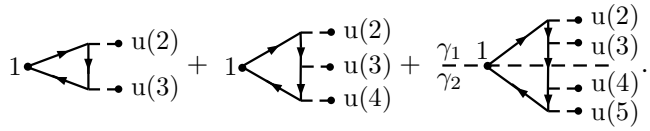

We see that analogously to what happens with the self-energy, going beyond the very simplest positive approximation we no longer have an expression in terms of full contour diagrams only.

Let us now briefly consider adding interactions to the second order response given in (4.57). To begin with we will make the so-called 'sudden approximation', which assumes that after an electron has been kicked by the external potential it has sufficient energy that it no longer significantly feels interactions with the other electrons as it leaves the material. Diagrammatically this means leaving out any diagrams that connect the three Green's function lines in (4.57) to each other. It follows that only scattering diagrams of the form

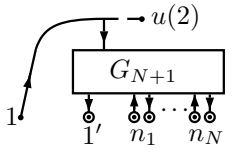

(4.60)

appear. Substituting this into (3.147) we obtain

$$-in(1) = \sum_{N=0}^{\infty} \frac{(-1)^{N+1}}{N!(N+1)!}$$

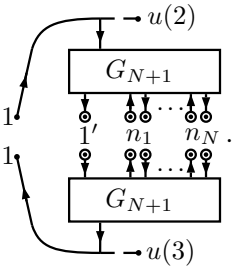

(4.61)

But here between the two connections to the external potential we have simply the dressed Green's function (3.141), and thus gluing the cut lines we obtain in the sudden approximation

$$-in(1) =$$

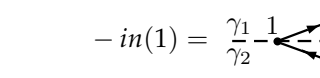

(4.62)

This depends on the interaction v only through the dressed Green's function between points 2 and 3, both of which are inside the sample. This Green's function can be taken to be the Green's function of the bulk material, assuming the electron is extracted from deep enough in the sample. The Green's functions connected to the point 1 outside the sample depend only on the mean-field of the electrons along with the background potential describing the nucleai and the core electrons.

To improve on the sudden approximation while retaining the positivity of the approximation, one can add scattering diagrams that couple to the leaving particle. For example

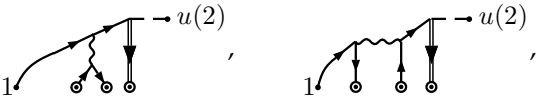

(4.63)

where the left diagram describes a process in which the leaving particle creates an excitation on its way (or alternatively receives energy from a decaying excitation), and the right diagram describes a process in which the leaving particle deposits its energy to another particle, sending it out of the sample to the detector. For further discussion see for example [8].

Chapter 5

Multi-Point Contour Functions

In the preceding chapters we have dealt with diagrammatic expressions on a contour, which are mapped by the Feynman rules to contour integrals over multi-point functions defined in terms of contour-ordered products. In this chapter we will discuss the structure of such expressions in terms of real-time functions, and give tools to evaluate them in practice. We will emphasize clarity and refer to the attached publications for derivations of many of the results.

The types of functions we are dealing with are products of (possibly real-time dependant) operators inside a contour ordering operation, of the form

$$O(z_1, \ldots, z_N) = \langle \mathcal{T}_\gamma \{ \hat{O}_1(z_1) \cdots \hat{O}_N(z_N) \} \rangle, \tag{5.1}$$

where the contour γ is a single loop starting from some initial time $t_0 < t_\mathcal{N}$ and turning back at some later time $T > t_\mathcal{N}$. Specifically any unintegrated contour diagram is of this form up to a prefactor. For our purposes here it is convenient to expand the contour ordering as

$$O(z_1, \ldots, z_N) = \sum_P \theta(z_{P(1)}, \ldots, z_{P(N)}) (-1)^{|P|} \langle \hat{O}_{P(1)}(t_{P(1)}) \cdots \hat{O}_{P(N)}(t_{P(N)}) \rangle \tag{5.2}$$

where the sum is over all permutations of the indices 1 to N. We define a set $\mathcal{N} = \{1, \ldots, N\}$ of the indices 1 to N and write (5.2) in the shorthand form

$$O(z_\mathcal{N}) = \sum_P \theta(z_{P(\mathcal{N})}) O^{P(\mathcal{N})}(t_\mathcal{N}), \tag{5.3}$$

where $O^{P(\mathcal{N})} = (-1)^{|P|} \langle \hat{O}_{P(1)} \cdots \hat{O}_{P(N)} \rangle$. The important point here is that $O(z_\mathcal{N})$ depends on the branch indices of the contour times only through step-functions, i.e. only so far as the branch indices affect the ordering of the times on the contour. Functions with this property are discussed in Pub. [I] where they are called Keldysh functions. Here we will briefly outline the results.

First we note that (5.3) is in fact more general than (5.1). For example the correlation self-energy has the form

$$\Sigma_c(z_1, z_2) = \theta(z_1, z_2) \Sigma^>(t_1, t_2) + \theta(z_2, z_1) \Sigma^<(t_1, t_2) \tag{5.4}$$

although it can not be written as (5.1). This can be seen for example from the fact that the self-energy has a diagrammatic representation, and each diagram is

a Keldysh function. As shown in Pub. [I], the integrated form of a diagram is also a Keldysh function, as is a sum of Keldysh functions. Another immediate consequence of (5.3) is that $O(z_{\mathcal{N}})$ is symmetric with respect to the branch index of the argument with the highest real-time value, i.e.

$$O(\ldots, t_{i-}, \ldots) = O(\ldots, t_{i+}, \ldots), \qquad t_i > t_{\mathcal{N}\setminus i}. \tag{5.5}$$

5.1 Multi-Retarded Functions

The retarded component of a two-time Keldysh-function was defined earlier to have the form

$$O^R(t_1, t_2) = \theta(t_1, t_2)[O^>(t_1, t_2) - O^<(t_1, t_2)], \tag{5.6}$$

where O was for example the single-particle Green's function or the self-energy. This can be derived by considering a contour integral over z_2

$$\int_\gamma \mathrm{d}z_2\, O(z_1, z_2) = \int_\gamma \mathrm{d}z_2\, \theta(t_1, t_2) O(z_1, z_2), \tag{5.7}$$

where we are allowed to place a step-function that effectively truncates the contour at t_1, since the part of the contour after that is simply a back and forth integration of the same function, that gives zero. Splitting the integral over contour into the forward and backward parts then gives

$$\begin{aligned} \int_\gamma \mathrm{d}z_2\, O(z_1, z_2) &= \int_{\gamma_-} \mathrm{d}t_{2-}\, \theta(t_1, t_2) O(z_1, z_2) + \int_{\gamma_+} \mathrm{d}t_{2+}\, \theta(t_1, t_2) O(z_1, z_2) \\ &= \int_{t_0}^{\infty} \mathrm{d}t_2\, \theta(t_1, t_2) O(z_1, t_{2-}) + \int_{\infty}^{t_0} \mathrm{d}t_2\, \theta(t_1, t_2) O(z_1, t_{2+}). \end{aligned} \tag{5.8}$$

Here since

$$O(z_1, z_2) = \theta(z_1, z_2) O^{12}(t_1, t_2) + \theta(z_2, z_1) O^{21}(t_1, t_2) \tag{5.9}$$

we have

$$O(z_1, t_{2-}) = O^{12}(t_1, t_2), \qquad O(z_1, t_{2+}) = O^{21}(t_1, t_2) \tag{5.10}$$

and thus

$$\begin{aligned} \int_\gamma \mathrm{d}z_2 O(z_1, z_2) &= \int_{t_0}^{\infty} \mathrm{d}t_2 \theta(t_1, t_2) [O^{12}(t_1, t_2) - O^{21}(t_1, t_2)] \\ &= \int \mathrm{d}t_2 O^{R(1,2)}(t_1, t_2), \end{aligned} \tag{5.11}$$

where $O^{12} = O^>$, $O^{21} = O^<$ and $O^{R(1,2)} = O^R$. We can take the retarded component to be defined by the requirement that the real-time integration over the retarded component equals the contour integration over the original contour function. From this follows the structure of the retarded component. The step function essentially truncates the contour integral so that it turns back at z_1, and therefore causes the contour ordering between 1 and 2 to switch when the integral turns back. This turns the forward and backward contour integrals into integrals over

ordered components, which are independent of the branch-indices, allowing the integrals to be converted into real-time integrals, with a minus sign introduced when the backward contour integration is reversed.

One can then introduce the higher order retarded components simply by considering more complicated integrals over Keldysh functions. First off, we add another integrated time and consider

$$\int_\gamma \mathrm{d}z_2 \mathrm{d}z_3 \, O(z_1, z_2, z_3). \tag{5.12}$$

Splitting the contour integrals into forward and backward parts now generates four integrals

$$\begin{aligned}&\int_\gamma \mathrm{d}z_2 dz_3 \\ &= \int_{\gamma_-} \mathrm{d}t_{2-}\mathrm{d}t_{3-} + \int_{\gamma_-} \mathrm{d}t_{2-} \int_{\gamma_+} \mathrm{d}t_{3+} + \int_{\gamma_+} \mathrm{d}t_{2+} \int_{\gamma_-} \mathrm{d}t_{3-} + \int_{\gamma_+} \mathrm{d}t_{2+}\mathrm{d}t_{3+}.\end{aligned} \tag{5.13}$$

As before we restrict the integrals below t_1, and obtain (using shorthand $\theta(t_i, t_j) = \theta_{ij}$)

$$\begin{aligned}&\int_\gamma \mathrm{d}z_2 \mathrm{d}z_3 \, O(z_1, z_2, z_3) \\ &= \int_{\gamma_-} \mathrm{d}t_{2-}\mathrm{d}t_{3-} \, \theta_{12}\theta_{13} O(z_1, t_{2-}, t_{3-}) + \int_{\gamma_-} \mathrm{d}t_{2-} \int_{\gamma_+} \mathrm{d}t_{3+} \, \theta_{12}\theta_{13} O(z_1, t_{2-}, t_{3+}) \\ &+ \int_{\gamma_+} \mathrm{d}t_{2+} \int_{\gamma_-} \mathrm{d}t_{3-} \, \theta_{12}\theta_{13} O(z_1, t_{2+}, t_{3-}) + \int_{\gamma_+} \mathrm{d}t_{2+}\mathrm{d}t_{3+} \, \theta_{12}\theta_{13} O(z_1, t_{2+}, t_{3+}).\end{aligned} \tag{5.14}$$

Here since z_1 is at the end point of the contour

$$O(z_1, t_{2-}, t_{3+}) = O^{312}(t_1, t_2, t_3), \qquad O(z_1, t_{2+}, t_{3-}) = O^{213}(t_1, t_2, t_3). \tag{5.15}$$

However, when both of the times are on the same branch the contour ordering is not unambiguous. Therefore we further subdivide the terms by writing $\theta_{12}\theta_{13} = \theta_{12}\theta_{13}(\theta_{23} + \theta_{32}) = \theta_{123} + \theta_{132}$. This reduces all the contour functions to real-time ordered components, and allows all contour integrals to be converted to real-time integrals (with a minus sign for each integral on the backward branch) giving

$$\begin{aligned}&\int_\gamma \mathrm{d}z_2 \mathrm{d}z_3 \, O(z_1, z_2, z_3) \\ &= \int \mathrm{d}t_2 \mathrm{d}t_3 \Big[\theta_{123} \left(O^{123} - O^{213} - O^{312} + O^{321} \right) \\ &\qquad + \theta_{132} \left(O^{132} - O^{213} - O^{312} + O^{231} \right) \Big].\end{aligned} \tag{5.16}$$

Now we can use the shorthand notation

$$O^{123} - O^{213} - O^{321} + O^{321} = O^{123-213-312+321} = O^{[[1,2],3]} = O^{[1,2,3]}, \tag{5.17}$$

to express the sums over ordered components as nested commutators. Therefore we find that

$$\int_\gamma \mathrm{d}z_2 \mathrm{d}z_3\, O(z_1, z_2, z_3) = \int \mathrm{d}t_2 \mathrm{d}t_3\, O^{R(1,23)}(t_1, t_2, t_3), \tag{5.18}$$

where we have defined the retarded component

$$O^{R(1,23)}(t_1, t_2, t_3) = \theta(t_1, t_2, t_3) O^{[1,2,3]}(t_1, t_2, t_3) + \theta(t_1, t_3, t_2) O^{[1,3,2]}(t_1, t_2, t_3). \tag{5.19}$$

Thus by this derivation we reach exactly the structure we have met before in the second order response function.

By an analogous derivation we find that

$$\int_\gamma \mathrm{d}z_2 \cdots \mathrm{d}z_N\, O(z_1, \ldots, z_N) = \int \mathrm{d}t_2 \cdots \mathrm{d}t_N\, O^{R(1,2\cdots N)}(t_1, \ldots, t_N), \tag{5.20}$$

holds for

$$O^{R(1,2\cdots N)}(t_1, \ldots, t_N) = \sum_P \theta(t_1, t_{P(2)}, \ldots, t_{P(N)}) O^{[1,P(2),\ldots,P(N)]}(t_1, \ldots, t_N). \tag{5.21}$$

Using the set notation we write this in a more compact form as

$$O^{R(e,\mathcal{I})}(t_\mathcal{N}) = \sum_P \theta(t_e, t_{P(\mathcal{I})}) O^{[e,P(\mathcal{I})]}(t_\mathcal{N}). \tag{5.22}$$

where $\mathcal{I} = \mathcal{N} \setminus e$.

These retarded components correspond to the case of a single external time, so that every time argument except one is integrated over. This occurs for example for the response functions or for individual half-diagrams obtained from cutting a self-energy diagram. The definition can also be generalized for diagrams with multiple external vertices. As the simplest example we may take

$$\int_\gamma \mathrm{d}z_3\, O(z_1, z_2, z_3). \tag{5.23}$$

We will treat separately the two contour orderings of z_1 and z_2, and start by assuming that $z_2 > z_1$. In this case we can deform the contour such that it returns to t_0 between z_1 and z_2 and therefore has two loops. Since z_1 and z_2 are in different loops of contour both loops can be truncated to the corresponding external time to obtain:

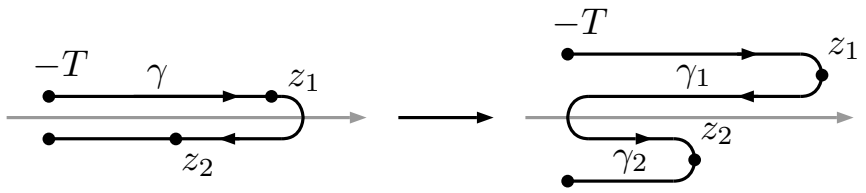

(5.24)

We denote this truncated contour by $\gamma' = \gamma_1 + \gamma_2$. The integral over z_3 then breaks down to four branches

$$\int_{\gamma'} \mathrm{d}z_3 = \int_{\gamma_{1-}} \mathrm{d}t_{3,1-} + \int_{\gamma_{1+}} \mathrm{d}t_{3,1+} + \int_{\gamma_{2-}} \mathrm{d}t_{3,2-} + \int_{\gamma_{2+}} \mathrm{d}t_{3,2+}. \tag{5.25}$$

The first two integrals here give

$$\begin{aligned}
&\int_{\gamma_{1-}} \mathrm{d}t_{3,1-}\, \theta_{13} O(z_1, z_2, z_{3,1-}) + \int_{\gamma_{1+}} \mathrm{d}t_{3,1+}\, \theta_{13} O(z_1, z_2, z_{3,1+}) \\
&= \int_{\gamma_{1-}} \mathrm{d}t_{3,1-}\, \theta_{13} O^{213}(t_1, t_2, t_3) + \int_{\gamma_{1+}} \mathrm{d}t_{3,1+}\, \theta_{13} O^{231}(t_1, t_2, t_3) \\
&= \int \mathrm{d}t_3\, \theta_{13} [O^{213}(t_1, t_2, t_3) - O^{231}(t_1, t_2, t_3)].
\end{aligned} \tag{5.26}$$

where the contour orderings are fully determined, since z_2 comes always after anything on γ_1, and on γ_1 anything on the forward/backward branch is before/after z_1. We write the last line above as

$$\int \mathrm{d}t_3\, \theta_{13} O^{2[1,3]}(t_1, t_2, t_3) = \int \mathrm{d}t_3\, O^{2R(1,3)}(t_1, t_2, t_3), \tag{5.27}$$

using a partially retarded component. After an analogous calculation for the integral over γ_2 we have

$$\begin{aligned}
&\int_\gamma \mathrm{d}z_3\, \theta(z_2, z_1) O(z_1, z_2, z_3) \\
&= \int \mathrm{d}t_3\, O^{2R(1,3)}(t_1, t_2, t_3) + \int \mathrm{d}t_3\, O^{R(2,3)1}(t_1, t_2, t_3).
\end{aligned} \tag{5.28}$$

For the other ordering we would obtain

$$\begin{aligned}
&\int_\gamma \mathrm{d}z_3\, \theta(z_1, z_2) O(z_1, z_2, z_3) \\
&= \int \mathrm{d}t_3\, O^{R(1,3)2}(t_1, t_2, t_3) + \int \mathrm{d}t_3\, O^{1R(2,3)}(t_1, t_2, t_3),
\end{aligned} \tag{5.29}$$

and thus defining

$$O^{R(1,3)}(t_1, t_2, t_3) = \theta(z_1, z_2) O^{R(1,3)2}(t_1, t_2, t_3) + \theta(z_2, z_1) O^{2R(1,3)}(t_1, t_2, t_3) \tag{5.30}$$

etc. we can write

$$\int_\gamma \mathrm{d}z_3\, O(z_1, z_2, z_3) = \int \mathrm{d}t_3 \left[O^{R(1,3)}(t_1, t_2, t_3) + O^{R(2,3)}(t_1, t_2, t_3) \right]. \tag{5.31}$$

By a similar calculation we would obtain for example

$$\begin{aligned}
&\int \mathrm{d}z_3 \mathrm{d}z_4\, \theta(z_1, z_2) O(z_1, z_2, z_3, z_4) \\
&= \int \mathrm{d}t_3 \mathrm{d}t_4 \left[O^{R(1,34)2} + O^{R(1,3)R(2,4)} + O^{R(1,4)R(2,3)} + O^{1R(2,34)} \right],
\end{aligned} \tag{5.32}$$

where

$$\begin{aligned}
O^{R(1,34)2} &= \theta_{134} O^{[1,3],4]2} + \theta_{143} O^{[1,4],3]2} \\
O^{R(1,3)R(2,4)} &= \theta_{13} \theta_{24} O^{[1,3][2,4]} \\
O^{R(1,4)R(2,3)} &= \theta_{14} \theta_{23} O^{[1,4][2,3]} \\
O^{1R(2,34)} &= \theta_{234} O^{1[2,3],4]} + \theta_{243} O^{1[2,4],3]}.
\end{aligned} \tag{5.33}$$

The general case follows this same pattern, and is derived in detail in Pub. [I]. For a multi-loop contour with E loops corresponding to E external arguments $\mathcal{E} = \{e_1, \ldots, e_E\}$ in this order, we have

$$\int_\gamma \mathrm{d}z_{\mathcal{N}\setminus\mathcal{E}}\, O(z_{\mathcal{N}}) = \sum_{\mathcal{N}_1 \cdots \mathcal{N}_E} \int \mathrm{d}t_{\mathcal{N}_1} \cdots \mathrm{d}t_{\mathcal{N}_E}\, O^{R(e_1,\mathcal{N}_1)\cdots R(e_E,\mathcal{N}_E)}(t_{\mathcal{N}}), \tag{5.34}$$

where the sum is over all ways to divide the argument labels in set $\mathcal{N} \setminus \mathcal{E}$ into the non-overlapping sets $\mathcal{N}_1, \ldots, \mathcal{N}_E$ (with no sum over permutations) and the multi-retarded component in which arguments $\mathcal{N}_i$ are retarded with respect to e_i for each i, is given by

$$\begin{aligned} &O^{R(e_1,\mathcal{N}_1)\cdots R(e_E,\mathcal{N}_E)}(t_{\mathcal{N}}) \\ &= \sum_{P_1 \cdots P_E} \left[\prod_i \theta(t_{e_i}, t_{P_i(\mathcal{N}_i)}) \right] O^{[e_1,P_1(\mathcal{N}_1)]\cdots[e_E,P_E(\mathcal{N}_E)]}(t_{\mathcal{N}}). \end{aligned} \tag{5.35}$$

5.2 Langreth Rules

By Langreth rules we mean rules by which one may obtain from an equation given in terms of contour diagrams equations relating diagrams given in terms of real-time propagators. For example, the time-ordered cutting rules presented in Pub. [III] Section 3.3. constitute Langreth rules in this sense, since after either a $+$ or $-$ has been assigned to each vertex, every Green's function reduces to one of four real-time functions:

$$G^{+-} = G^{>}, \qquad G^{-+} = G^{<}, \qquad G^{--} = G^{T}, \qquad G^{++} = G^{\bar{T}}. \tag{5.36}$$

Thus for any contour diagram equation, any choice of plusses and minuses for the external vertices produces an equation in terms of real-time Green's functions only.

On the other hand, the retarded cutting rules given in Pub. [III] Section 3.4. do not lead directly to Langreth rules. One would hope to be able to write a retarded diagram in terms of greater, lesser and retarded single particle Green's functions, like a time-ordered diagram can be written in terms of greater, lesser and time-ordered Green's functions, however, the more complex structure of the retarded diagram complicates such a derivation. Such retarded Langreth rules have been discussed in Pub. [I], where several useful general results are derived and used to derive Langreth rules for certain diagrams, but these derivations are done in per diagram basis and it is not clear if they are possible for an arbitrary diagram.

Here we will discuss the original Langreth rules [9] applicable to convolutions of two-point functions on a contour that possibly includes a Matsubara branch, and present some generalizations of these rules for more complicated diagrammatic structures.

As an example on how to deal with contour equations, we consider first a chain of three two-point functions convoluted over the Keldysh contour:

$$A(z_1, z_2) = \int_\gamma \mathrm{d}z_3 \mathrm{d}z_4\, B(z_1, z_3) C(z_3, z_4) D(z_4, z_2). \tag{5.37}$$

A straightforward approach to convert (5.37) into real-time convolutions is to simply integrate the branches separately by substituting

$$\int_\gamma \mathrm{d}z = \int_{t_0}^{\infty} \mathrm{d}t_- + \int_{\infty}^{t_0} \mathrm{d}t_+. \tag{5.38}$$

Corresponding to the different branch indices one can define four real-time components

$$\begin{aligned} A^{--}(t_1,t_2) &= A(t_{1-},t_{2-}), \qquad & A^{-+}(t_1,t_2) &= A(t_{1-},t_{2+}), \\ A^{+-}(t_1,t_2) &= A(t_{1+},t_{2-}), \qquad & A^{++}(t_1,t_2) &= A(t_{1+},t_{2+}), \end{aligned} \tag{5.39}$$

which together map the domain of definition of the contour-function. Substituting (5.38) into (5.37) then generates for example

$$\begin{aligned} A^{--}(t_1,t_2) = B^{--}\cdot C^{--}\cdot D^{--}(t_1,t_2) \;-\; B^{-+}\cdot C^{+-}\cdot D^{--}(t_1,t_2) \\ -\, B^{--}\cdot C^{-+}\cdot D^{+-}(t_1,t_2) \;+\; B^{-+}\cdot C^{++}\cdot D^{+-}(t_1,t_2), \end{aligned} \tag{5.40}$$

using the shorthand notation

$$A\cdot B(t_1,t_2) \doteq \int_{t_0}^{\infty} \mathrm{d}t_3\, A(t_1,t_3)B(t_3,t_2). \tag{5.41}$$

Similar equation exists for each component of A. This approach is straightforward to apply to any diagram, and in general results in 2^N equations, each being a sum of 2^N real-time diagrams, when N is the number of internal vertices.

For functions, such as the singe particle Green's function, that can be written as a contour-ordered product of real-time operators

$$B(z_1,z_2) = \langle \mathcal{T}_\gamma \Big\{ \hat{O}_1(z_1)\hat{O}_2(z_2) \Big\} \rangle, \qquad \hat{O}_n(t_{n+}) = \hat{O}_n(t_{n-}) = \hat{O}_n(t_n), \tag{5.42}$$

the branch-index components are not independent. They are symmetric with respect to the branch-index of the component with the highest value, so that for example $\theta(t_1,t_2)O^{--}(t_1,t_2) = \theta(t_1,t_2)O^{+-}(t_1,t_2)$. Thus for a two-point function only two of the components need to be solved.

For functions like (5.42) an alternative approach was introduced by Langreth [9]. Writing the contour-ordering explicitly in (5.42) leads to

$$B(z_1,z_2) = \theta(z_1,z_2)B^{>}(t_1,t_2) + \theta(z_2,z_1)B^{<}(t_1,t_2) \tag{5.43}$$

where the greater and lesser components

$$B^{>}(t_1,t_2) = \langle \hat{O}_1(t_1)\hat{O}_2(t_2)\rangle, \qquad B^{<}(z_1,z_2) = \pm\langle \hat{O}_2(t_2)\hat{O}_1(t_1)\rangle, \tag{5.44}$$

are correlators of specific order, that are functions of real parameters only, since the operators are the same on both branches. The lesser component gets a minus sign from the permutation if $\hat{O}_1$ and $\hat{O}_2$ are fermionic.

Now starting from a chain of two functions

$$E(z_1,z_2) = F\cdot G(z_1,z_2) \tag{5.45}$$

and assuming that F and G can be written as in (5.43), one can write the right hand side as

$$\begin{aligned} E(z_1, z_2) = \theta(z_1, z_2) \int_{t_0}^{\infty} \mathrm{d}t_3 \left[F^R(t_1, t_3) G^>(t_3, t_4) + F^>(t_1, t_3) G^A(t_3, t_4) \right] \\ + \theta(z_2, z_1) \int_{t_0}^{\infty} \mathrm{d}t_3 \left[F^R(t_1, t_3) G^<(t_3, t_4) + F^<(t_1, t_3) G^A(t_3, t_4) \right], \end{aligned} \tag{5.46}$$

where

$$F^R(t_1, t_2) = \theta(t_1 - t_2) \left[F^>(t_1, t_2) - F^<(t_1, t_2) \right] \tag{5.47}$$

$$F^A(t_1, t_2) = -\theta(t_2 - t_1) \left[F^>(t_1, t_2) - F^<(t_1, t_2) \right] \tag{5.48}$$

are the retarded and advanced components. This reveals that E also has a representation in terms of real-time components in the form (5.43) with the greater and lesser components given by

$$E^> = F^R \cdot G^> + F^> \cdot G^A, \qquad E^< = F^R \cdot G^< + F^< \cdot G^A. \tag{5.49}$$

For the retarded and advanced components themselves one can derive

$$E^R = F^R \cdot G^R, \qquad E^A = F^A \cdot G^A. \tag{5.50}$$

Equations (5.49) and (5.50) are known as Langreth rules (along with others given in table 5.1). They can be applied repeatedly to work out longer convolution chains. For example for a chain of three functions one obtains the rules

$$A^{\lessgtr} = B^R \cdot C^R \cdot D^{\lessgtr} + B^R \cdot C^{\lessgtr} \cdot D^A + B^{\lessgtr} \cdot C^A \cdot D^A. \tag{5.51}$$

$$A^{R/A} = B^{R/A} \cdot C^{R/A} \cdot D^{R/A}. \tag{5.52}$$

One notices that working with retarded and advanced components leads to rules with three terms as opposed to the four terms in (5.40). Furthermore the rules for the retarded and advanced components are especially simple. This advantage grows larger for longer chains. Looking at (5.51) one can already notice a pattern starting to emerge, which shows that for a chain with N internal vertices the sum will contain $N + 1$ terms, in contrast to the 2^N terms in the rules obtained by fixing the branch indices. The chain convolution, however, turns out to be an optimal case. For more complicated diagrams the cancellations are not always as drastic.

Another advantage to the use of ordered components, as opposed to the branch-index components, is their more directly physical nature. For two-point Green's function for example, the greater component corresponds to particle propagation while the lesser component corresponds to hole propagation (as discussed in 3.4.1). The retarded and advanced components correspond to forward and backward propagation respectively, and are closely related to the spectral function. The ordered components of higher order Green's function can likewise be connected to different types of multi-particle/hole excitations. While in the case of a single particle Green's function the different components are closely connected, through $G^{+-} = G^>$ and $G^{-+} = G^<$, this direct connection breaks down for higher order functions.

$D(z_1,z_2)=\int_\gamma \mathrm{d}z_3\, A(z_1,z_3)B(z_3,z_2)$	$D(z_1,z_2)=A(z_1,z_2)B(z_2,z_1)$
$D^> = A^R\cdot B^> + A^>\cdot B^A + A^\rceil\cdot B^\lceil$	$D^> = A^>B^<$
$D^< = A^R\cdot B^< + A^<\cdot B^A + A^\rceil\cdot B^\lceil$	$D^< = A^<B^>$
$D^R = A^R\cdot B^R$	$D^R = \begin{cases} A^RB^< + A^<B^A \\ A^RB^> + A^>B^A \end{cases}$
$D^A = A^A\cdot B^A$	$D^A = \begin{cases} A^AB^< + A^<B^R \\ A^AB^> + A^>B^R \end{cases}$
$D^\rceil = A^\rceil\star B^M + A^R\cdot B^\rceil$	$D^\rceil = A^\rceil B^\lceil$
$D^\lceil = A^\lceil\cdot B^A + A^M\star B^\lceil$	$D^\lceil = A^\lceil B^\rceil$
$D^M = A^M\star B^M$	$D^M = A^MB^M$

Table 5.1: The Langreth rules for convolutions (left) and products (right) given using (5.41) and (5.56). The time-arguments for the real-time functions have been suppressed.

Let us now consider extension of the above discussion to a contour that includes the Matsubara branch. Branch index approach generalises trivially, one merely adds an additional possible value for the branch index. We denote the vertical branch by a vertical line $|$. There are now nine components in total, in addition to A^{--}, A^{-+}, A^{+-} and A^{++} we have

$$\begin{aligned} A^{|-}(\tau_1,t_2) &= A(t_0-i\tau_1,t_{2-}) \qquad & A^{-|}(t_1,\tau_2) &= A(t_{1-},t_0-i\tau_2) \\ A^{|+}(\tau_1,t_2) &= A(t_0-i\tau_1,t_{2+}) \qquad & A^{+|}(t_1,\tau_2) &= A(t_{1+},t_0-i\tau_2) \\ A^{||}(\tau_1,\tau_2) &= A(t_0-i\tau_1,t_0-i\tau_2). \end{aligned} \tag{5.53}$$

For a two-point function of the form (5.42) these components are connected through $A^{|-}=A^{|+}$ and $A^{-|}=A^{+|}$, leaving a total of five independent components. Because there are now three possible branch indices, the number of real-time diagrams in each equation rises to 3^N for N internal vertices.

For the retarded Langreth rules the generalization is less obvious, as even if the contour-order is specified there remains a difference between operators on the horizontal and on the vertical branch. One solution for this is to mix methods, and start by using the branch-index approach to separate the horizontal and vertical branches, before continuing with Langreth's approach on the horizontal branch. This is achieved by including the left-, right- and Matsubara components

$$\begin{aligned} A^\lceil(\tau_1,t_2) &= A^{|\pm}(\tau_1,t_2) \qquad & A^\rceil(\tau_1,t_2) &= A^{\pm|}(\tau_1,t_2) \\ A^M(\tau_1,\tau_2) &= A^{||}(\tau_1,\tau_2), \end{aligned} \tag{5.54}$$

and using the greater and lesser components only when both parameters are on the horizontal branches.

Starting then from a chain of two functions and separating the integrals between Matsubara and horizontal branches $\left(\int_\gamma = \int_{\gamma_M}+\int_{\gamma_K}\right)$, one can derive for the greater and lesser components the Langreth rules

$$E^> = F^R\cdot G^> + F^>\cdot G^A + F^\rceil\star G^\lceil, \qquad E^< = F^R\cdot G^< + F^<\cdot G^A + F^\rceil\star G^\lceil, \tag{5.55}$$

where

$$A \star B(t_1, t_2) \doteq -i \int_0^\beta \mathrm{d}\tau_3 \, A(t_1, \tau_3) B(\tau_3, t_2). \tag{5.56}$$

These integrals over the Matsubara branch take into account the effect of initial state correlations on the propagation amplitude. The corrections for particle and hole propagation are identical, and thus for the retarded/advanced component these are cancelled and one obtains:

$$E^{R/A} = F^{R/A} \cdot G^{R/A}. \tag{5.57}$$

The rules for all the components are given in 5.1).

Repeated application of these rules again leads to expressions for example for the three function chain:

$$\begin{aligned} A^{\lessgtr} = {} & B^R \cdot C^R \cdot D^{\lessgtr} + B^R \cdot C^{\lessgtr} \cdot D^A + B^{\lessgtr} \cdot C^A \cdot D^A \\ & + B^R \cdot C^\rceil \star D^\lceil + B^\rceil \star C^\lceil \cdot D^A + B^\rceil \star C^M \star D^\lceil. \end{aligned} \tag{5.58}$$

$$A^{R/A} = B^{R/A} \cdot C^{R/A} \cdot D^{R/A}. \tag{5.59}$$

In this case the mixed approach results in 6 real-time diagrams for each of the five components, in contrast to the $3^2 = 9$ diagrams from the branch index method.

These Langreth rules can also be seen to follow from the cutting rules discussed previously in 3.7 and with more detail, including effect of the Matsubara branch, in Pub. [I]. For chain convolutions the retarded half-diagrams reduce to chains of retarded or advanced single-particle Green's functions following (5.57), giving for example the three terms in (5.51) from the three possible cuts. See Appendix A for an example of applying these rules to the interacting single-particle Green's function.

As mentioned, we do not know how to repeat this process for a general half-diagram. We can, however, give some general results that help in reducing retarded components into smaller pieces. In particular we can generalize the rules for chains given above in several ways. Note first that performing some of the real-time integrals over a retarded component leads to a retarded component of the corresponding integrated diagram. This follows simply from

$$\begin{aligned} \int \mathrm{d}t_{\mathcal{N}_1} \mathrm{d}\, t_{\mathcal{N}_2} \, D^{R(1,\mathcal{N}_1,\mathcal{N}_2)}(t_1, t_{\mathcal{N}_1}, t_{\mathcal{N}_2}) &= \int_\gamma \mathrm{d}\, z_{\mathcal{N}_1} dz_{\mathcal{N}_2} \, D(z_1, z_{\mathcal{N}_1}, z_{\mathcal{N}_2}) \\ &= \int_\gamma \mathrm{d}\, z_{\mathcal{N}_1} \, \bar{D}(z_1, z_{\mathcal{N}_1}) = \int \mathrm{d}\, t_{\mathcal{N}_1} \, \bar{D}^{R(1,\mathcal{N}_1)}(t_1, t_{\mathcal{N}_1}), \end{aligned} \tag{5.60}$$

where $\bar{D}(z_1, z_{\mathcal{N}_1}) = \int_\gamma dz_{\mathcal{N}_2} D(z_1, z_{\mathcal{N}_1}, z_{\mathcal{N}_2})$. Thus supposed we have a retarded component of some diagram that has a structure that consists of multiple sub-diagrams connected by singular links

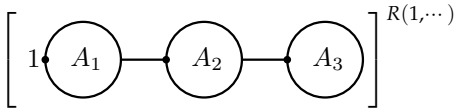

(5.61)

One can then first integrate all internal time-arguments from the sub-diagrams to reduce the diagram to a chain of two-point functions, and use the Langreth

rules for a chain to obtain a simple chain of two-point functions. Expanding the sub-diagrams again then leads to

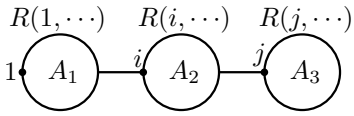

(5.62)

Furthermore, diagrams that can be represented as forked chains such as

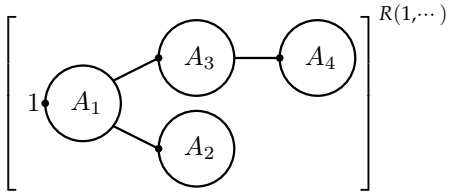

(5.63)

can also be reduced to simple chains by for example taking in the above diagram A_1 and A_2 to form a single sub-diagram A_1', in which case the situation reduces to the previous one. The resulting retarded component of A_1' is then just another chain of sub-diagrams, and thus one obtains

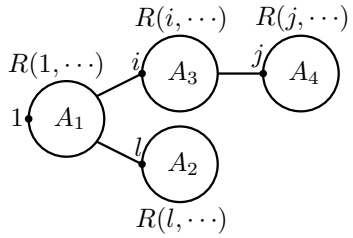

(5.64)

One practical result of this is that for retarded components of diagrams with external legs, the external legs can be extracted as G^R and G^A lines, for example

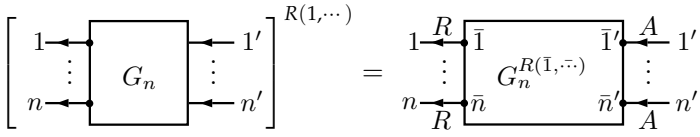

(5.65)

and therefore retarded components of Green's functions diagrams, for example, can be immediately reduced to retarded components of kernel diagrams.

5.3 Spectral Representations

In this section we will briefly discuss how to obtain spectral representations for multi-retarded objects, such as retarded half-diagrams. Like the spectra of greater and lesser Green's functions defined in (3.89) are peaked at particle addition/removal energies, so the spectra obtained from scattering diagrams are peaked at energies related to more complicated excitations involving particle/hole pairs.

We will demonstrate the steps of the general derivation given in Appendix D of Pub. [III] by finding the spectral representation for the retarded single-particle Green's function. First we find the Fourier transform

$$\begin{aligned} g^R(\omega_1,\omega_2) &= \int \mathrm{d}t_1\mathrm{d}t_2\, \mathrm{e}^{\mathrm{i}\omega_1 t_1+\mathrm{i}\omega_2 t_2} g^R(t_1,t_2) \\ &= \int \mathrm{d}t_1\mathrm{d}t_2\, \mathrm{e}^{\mathrm{i}\omega_1 t_1+\mathrm{i}\omega_2 t_2}\theta(t_1-t_2)\Big(g^>(t_1,t_2)-g^<(t_1,t_2)\Big). \end{aligned} \tag{5.66}$$

Substituting

$$g^{\lessgtr}(t_1,t_2) = \int \frac{\mathrm{d}\nu}{2\pi} g^{\lessgtr}(\nu)\mathrm{e}^{-\mathrm{i}\nu(t_1-t_2)} \tag{5.67}$$

for the lesser and greater Green's functions (assuming equilibrium so that there is dependence only on the time difference) we obtain

$$g^R(\omega_1,\omega_2) = \int \frac{\mathrm{d}\nu}{2\pi}\int \mathrm{d}t_1\mathrm{d}t_2\,\theta(t_1-t_2)\mathrm{e}^{\mathrm{i}(\omega_1-\nu)t_1+\mathrm{i}(\omega_2+\nu)t_2}\Big(g^>(\nu)-g^<(\nu)\Big). \tag{5.68}$$

The time integral here can be evaluated by expressing the step-function as

$$\theta(t_1-t_2) = -\frac{1}{2\pi\mathrm{i}}\int_{-\infty}^{\infty}\mathrm{d}\xi\,\frac{\mathrm{e}^{-\mathrm{i}\xi(t_1-t_2)}}{\xi+\mathrm{i}\eta}, \tag{5.69}$$

where η is an infinitesimal positive number. This leads to

$$\begin{aligned} &\int \mathrm{d}t_1\mathrm{d}t_2\,\theta(t_1-t_2)\mathrm{e}^{\mathrm{i}(\omega_1-\nu)t_1+\mathrm{i}(\omega_2+\nu)t_2} \\ &= -\frac{1}{2\pi\mathrm{i}}\int \mathrm{d}\xi\,\frac{1}{\xi+\mathrm{i}\eta}\int \mathrm{d}t_1\,\mathrm{e}^{\mathrm{i}(\omega_1-\nu-\xi)t_1}\int \mathrm{d}t_2\,\mathrm{e}^{\mathrm{i}(\omega_2+\nu+\xi)t_2} \\ &= 2\pi\mathrm{i}\int \mathrm{d}\xi\,\frac{1}{\xi+\mathrm{i}\eta}\delta(\omega_1-\nu-\xi)\delta(\omega_2+\nu+\xi) \\ &= 2\pi\mathrm{i}\delta(\omega_1+\omega_2)\frac{1}{\omega_1-\nu+\mathrm{i}\eta}. \end{aligned} \tag{5.70}$$

Thus we have

$$g^R(\omega_1,\omega_2) = 2\pi\delta(\omega_1+\omega_2)g^R(\omega_1), \tag{5.71}$$

with

$$g^R(\omega) = \int \frac{\mathrm{d}\nu}{2\pi}\frac{A(\nu)}{\omega-\nu+\mathrm{i}\eta} \tag{5.72}$$

being the commonly used retarded Green's function in frequency domain (i.e. the Fourier transform of $g^R(t_1,t_2)$ with respect to t_1-t_2) and

$$A(\nu) = A^>(\nu)+A^<(\nu) = \mathrm{i}g^>(\nu)-\mathrm{i}g^<(\nu) \tag{5.73}$$

the associated spectral function that has peaks at both particle addition and removal energies.

We note that the Matsubara Green's function in frequency domain is given by

$$g^M(\omega) = \int \frac{\mathrm{d}\nu}{2\pi}\frac{A(\nu)}{\omega-\nu+\mu}, \tag{5.74}$$

and is therefore related to the retarded Green's function (5.72) by

$$g^R(\omega) = g^M(\omega - \mu + i\eta). \tag{5.75}$$

In Appendix D. of Pub. [III] we generalize the derivation given above for a fully retarded function of the form

$$O^{R(e,\mathcal{I})}(t_{\mathcal{N}}) = \sum_P \theta(t_e, t_{P(\mathcal{I})}) O^{[e,P(\mathcal{I})]}(t_{\mathcal{N}}), \tag{5.76}$$

where $O(z_{\mathcal{N}})$ is an arbitrary Feynman diagram. This derivation gives for the Fourier transform of (5.76)

$$\mathcal{O}^{R(e,\mathcal{I})}(\omega_{\mathcal{N}}) = \int \mathrm{d}t_{\mathcal{N}}\, \mathrm{e}^{\mathrm{i}\omega_{\mathcal{N}}\cdot t_{\mathcal{N}}} D^{R(e,\mathcal{I})}(t_{\mathcal{N}}), \tag{5.77}$$

the expression

$$\mathcal{D}^{R(e,\mathcal{I})}(\omega_{\mathcal{N}}) = 2\pi\delta(\omega)\mathscr{D}^{R(e,\mathcal{I})}(\omega_{\mathcal{N}}) \tag{5.78}$$

where $\delta(\omega) = \delta(\omega_1 + \ldots + \omega_N)$ and the analytical part is given by

$$\begin{aligned}&\mathscr{D}^{R(e,\mathcal{I})}(\omega_{\mathcal{N}}) \\ &= \sum_P \int \frac{\mathrm{d}\nu_{\mathcal{L}}}{(2\pi)^{|L|}} \frac{(-1)^{N_+^P}(-\mathrm{i})^{N-1}}{\prod_{k=1}^{N_-^P}(\Omega_k^{\overline{P(\mathcal{N})}} - \mathrm{i}\eta_k)\prod_{l=1}^{N_+^P}(\Omega_l^{P(\mathcal{N})} - \mathrm{i}\eta_l)} \mathcal{D}^{P(\mathcal{N})}(\nu_{\mathcal{L}}).\end{aligned} \tag{5.79}$$

Here the sum is over all permutations of the ordered set $\mathcal{N} = \{1, \ldots, N\}$, and N_-^P/N_+^P is the number of elements of $\mathcal{N}$ ordered right/left of element e by permutation P (corresponding to time-arguments on the forward/backward branch). Furthermore Ω is given by

$$\Omega_l^{\mathcal{N}} = \sum_{i=1}^{l} \sigma_i, \qquad \Omega_l^{\bar{\mathcal{N}}} = \sum_{i=1}^{l} \sigma_{N+1-l}, \tag{5.80}$$

where σ_i is the total energy leaving the vertex/vertices at time t_j of the diagram O. Each Ω_k thus corresponds to the total energy leaving certain part of the full diagram, containing k of the first/last vertices in contour order. This expression will therefore have peaks whenever this total energy becomes zero, i.e. when that part of the diagram conserves energy. The function will be most strongly peaked when the subsequent interaction processes that occur during the scattering each conserve energy. The delta function in (5.78) enforces energy conservation over the whole diagram. See Appendix D of Pub. [III] for precise diagrammatic rules for calculating this expression for any diagram.

An analogous derivation for an arbitrary Matsubara diagram can also be performed ([10, 11]). Comparison of these results leads to a generalization of (5.75) to

$$\mathcal{O}^{R(e,\mathcal{I})}(\omega_{\mathcal{N}}) = \mathcal{O}^M(\omega_{\mathcal{N}} - \mu - \mathrm{i}\eta_{\mathcal{N}}), \tag{5.81}$$

where $\mathcal{O}^M$ is the Fourier transform of the Matsubara component of $O(z_{\mathcal{N}})$.

Chapter 6

Summary and Outlook

In diagrammatic many-body perturbation theory [12] behaviour of systems of many interacting quantum particles is modelled by breaking the effect of the interaction down into specific scattering processes. The individual processes can then be freely included or excluded from the model to create various approximations with differing accuracy and computational demand. These scattering processes are represented using diagrams, which makes them intuitive to manipulate and to interpret physically.

Due to the property of quantum mechanics, in which probabilities for events follow from lengths of probability amplitudes, there arises a potential disconnect between the structure of the theory and the results that are calculated from it, which does not exist for classical theories. The length of an amplitude represented as a complex number is given by the product of the amplitude with its conjugate. In the diagrammatic perturbation theory the two halves of the product can be conveniently combined into diagrams integrated over a looped contour [13] that goes first forward and then backward in time. In this form equations are greatly simplified and manipulations made more convenient. These manipulations on the level of classical probabilities can, however, end up obscuring the underlying probability amplitudes. And it is these amplitudes that have the clearest physical interpretation in terms of the fundamental theory, and are therefore the best guide to choosing appropriate approximations. Furthermore manipulations of the contour diagrams can lead to expressions for probabilities that have no unambiguous representation in terms of probability amplitudes at all. In addition to the resulting ambiguity when it comes to the physical content of the approximation, this can lead to uninterpretable results, such as negative probabilities, and to a loss of certain mathematical properties important for example for convergence of self-consistent calculations.

To solve these issues so called cutting rules have been developed, by which contour diagrams are again cut into products of half-diagrams that represent scattering amplitudes. In particular such an approach was applied [1, 2] to develop a recipe for building so called positive approximations with certain guaranteed positivity properties as well as a clear physical content in terms of scattering processes. This recipe is based on extending the loop contour to distant future and then cutting it into two halves at its end-point, leading to the contour diagram being

cut into half-diagrams with one on a forward time-contour and one on a backward time contour. This cut at the end-point of the contour necessitated assuming equilibrium conditions in order retain knowledge of the systems state in the distant future. Furthermore, this approach was restricted to the zero-temperature limit. Earlier attempts to develop cutting rules for finite temperature systems had ran into issues related to canceling out diagrams depicting thermal fluctuations (see introduction of Pub. [III] for an overview of the earlier developments).

In the publications making up this thesis we derive cutting rules that can be applied at finite temperature and to non-equilibrium systems, and use these rules to generalize the recipe for building positive approximations.

In Pub. [I] we derive results for converting arbitrary contour functions into real-time functions. These real-time functions have a structure that represents a generalization of so called retarded functions. These results are based on deforming the loop contour into multiple loops, and then cutting the contour between the loops at the initial time. This leads to an expression in terms of sub-functions expressed on the full loop contour, which can be represented as real-time retarded functions. We apply these results to diagrams, obtaining a cutting rule that cuts a contour diagram into retarded sub-diagrams. We further derive relations to convert the resulting generalized retarded diagrams into smaller real time pieces. These derivations generalize earlier results, especially those of Danielewicz [14] and Langreth [9], allowing them to be applied to more complicated diagrams and for finite temperature systems.

In Pub. [II] we apply the retarded cutting rule derived in Pub. [I] to express the self-energy in terms of products of two retarded scattering diagrams. This allows us to repeat the derivation of [1] while avoiding the equilibrium assumption, since the contour is now cut at the initial time and therefore the state of the system in the distant future does not enter the calculations. This generalizes the recipe for building positive approximations to non-equilibrium systems on a steady-state limit.

In Pub. [III] we develop finite temperature cutting rules based on the results of Pub. [I], and use them to generalize the recipe for positive approximations to finite temperature cases. We discuss the important positivity properties of correlators in general terms, and then proceed to show how the approach used in Pub. [II] does not neatly transform to finite temperature, but leads to proliferation of diagrams and a need for stronger assumptions. We then introduce an alternative diagrammatic derivation that avoids these issues, and leads to a scattering diagram representation of the self-energy at finite temperature that has an analogous structure to the zero-temperature expression, and thus allows the same recipe for building positive approximations to be applied. We show that certain commonly used approximations are positive at finite temperature. Finally we derive rules for obtaining spectral representations for general retarded diagrams, and show that an analytical continuation relation connects these diagrams to Matsubara diagrams used for finite temperature equilibrium calculations.

The results derived in this thesis are of rather general nature, and are potentially of use anywhere in the wide variety of contexts in which diagrammatic quantum many-body theory is applied. The recipe for determining the positivity of approxi-

mations is especially valuable when there is need to go beyond the commonly used approximations. Such cases also benefit from the cleaner physical picture provided by the scattering amplitude based approach to approximations made possible by existence of applicable cutting rules. Furthermore, to reach our final results we have presented many tools related to working with higher order propagators, such as multi-particle Green's functions. These tools are also of use for other pursuits that involve such objects.

Appendix A

Factorization of the Dressed G

In this appendix we will sketch out a diagrammatic derivation of (see 5.2 for the notation)

$$\begin{aligned} &G^{\lessgtr}(t_1,t_2) \\ &= G^R(t_1,t_0)G^{\lessgtr}(t_0,t_0)G^A(t_0,t_2) + G^R\cdot\left(\Sigma_c^{\lessgtr}+\Sigma_c^{\rceil}\star G^M\star\Sigma_c^{\lceil}\right)\cdot G^A(t_1,t_2) \\ &+ iG^R(t_1,t_0)[G^{\rceil}\star\Sigma_c^{\lceil}\cdot G^A](t_0,t_2) - i[G^R\cdot\Sigma_c^{\rceil}\star G^{\lceil}](t_1,t_0)G^A(t_0,t_2), \end{aligned} \tag{A.1}$$

where G and Σ are matrices with respect to the quantum numbers and

$$\begin{aligned} A\cdot B(t_1,t_2) &\doteq \int_{t_0}^{\infty} \mathrm{d}t_3\, A(t_1,t_3)B(t_3,t_2) \\ A\star B(t_1,t_2) &\doteq -i\int_0^{\beta} \mathrm{d}\tau_3\, A(t_1,\tau_3)B(\tau_3,t_2) \end{aligned} \tag{A.2}$$

are convolutions over the real and the imaginary branches of the contour respectively.

(A.1) can also be written as

$$G^{\lessgtr}(t_1,t_2) = G^R(t_1,t_0)G^{\lessgtr}(t_0,t_0)G^A(t_0,t_2) + G^R\cdot\tilde{\Sigma}_c[G]\cdot G^A(t_1,t_2), \tag{A.3}$$

with

$$\begin{aligned} \tilde{\Sigma}_c^{\lessgtr}(t_1,t_2) &= \Sigma_c^{\lessgtr}+\Sigma_c^{\rceil}\star G^M\star\Sigma_c^{\lceil} \\ &+ \delta(t_1,t_0)\left[G^{\rceil}\star\Sigma_r^M\star G^{\lceil}\right](t_1,t_2)\delta(t_2,t_0) \\ &+ i\delta(t_1,t_0)\left[G^{\rceil}\star\Sigma_c^{\lceil}\right](t_1,t_2) - i\left[\Sigma_c^{\rceil}\star G^{\lceil}\right](t_1,t_2)\delta(t_2,t_0). \end{aligned} \tag{A.4}$$

an alternative derivation can be found for example in [12] Section 9.7.

Starting from the Dyson equation

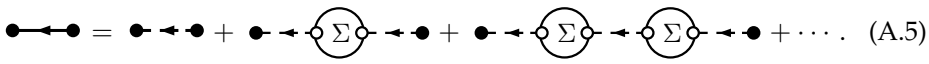

(A.5)

Using the Langreth rule (5.57) we obtain for the retarded and advanced components

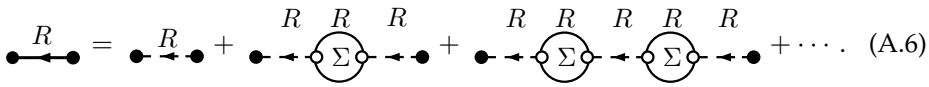

(A.6)

and

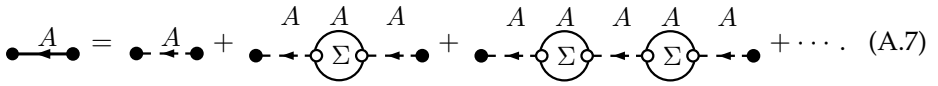

(A.7)

respectively. For the lesser and greater components we obtain a sum of every diagram for which each internal vertex is either retarded with respect to one of the external vertices, or else part of a Matsubara set, with the additional rule that retarded sets must be connected. In practice this leads to diagrams with a retarded set to the left and to the right and a possible Matsubara set in the middle. The diagrams fall into six different groups, depending on whether the edges between the various sets fall on a g-line or a Σ-line. We will consider these groups of diagrams one by one, taking as an example the lesser component.

1. Diagrams with no Matsubara set, where the edge of the retarded sets falls on a g-line, are of the form

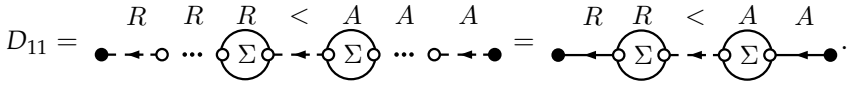

(A.8)

   Here the three dots denote a chain of alternating g's and Σ's of an arbitrary length, and as such they sum up to a dressed G-line by (4.6). Besides the diagrams in (A.8) there are the special cases for when one or other of the retarded sets is empty. If the left/right set is empty we are left with

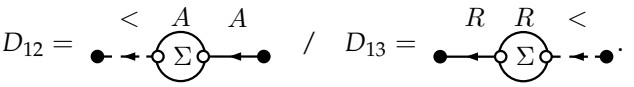

(A.9)

   Finally there is the single diagram for which both the retarded sets are empty

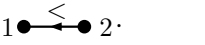

(A.10)

   Making use of (3.132), which diagrammatically can be expressed as

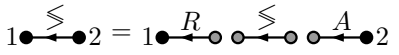

(A.11)

   as well as the rule for combination of retarded pieces derived in Pub. [I] we obtain

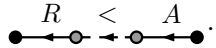

(A.12)

2. Diagrams with no Matsubara set, where the edge of the retarded sets falls on a Σ-line, are of the form

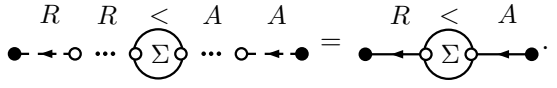

(A.13)

3. Diagrams containing a Matsubara set, where both the set edges fall on a g-line, are of the form

$D_{31} =$ 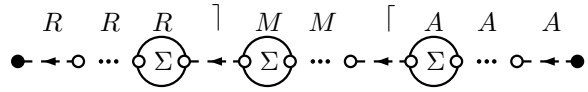

$=$ 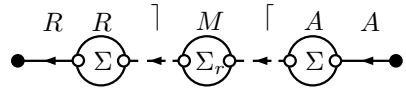

(A.14)

Note that here Σ_r is the reducible self-energy. again we must consider the special cases where one or both of the retarded sets are empty, given by

$D_{32} =$ 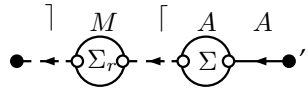

$D_{33} =$ 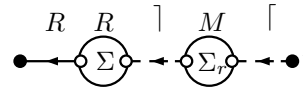

(A.15)

and

$D_{34} =$ 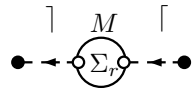

(A.16)

Using

$$g^{\rceil}(t_1,\tau) = ig^R(t_1,t_0)g^M(t_0,\tau), \quad g^{\lceil}(\tau,t_2) = -ig^M(\tau,t_0)g^A(t_0,t_2), \tag{A.17}$$

which can be expressed diagrammatically as

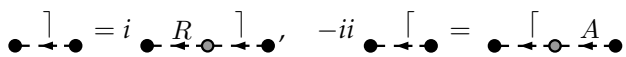

(A.18)

we obtain

$D_3 = D_{31} + D_{32} + D_{33} + D_{34} =$ 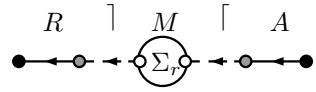

(A.19)

4. Diagrams containing a Matsubara set, where both the set edges fall on a Σ-line, are of the form

$D_4 =$ 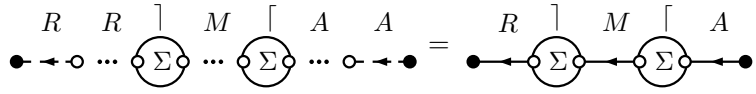

(A.20)

5. Diagrams containing a Matsubara set, where the left edge falls on a g-line and the right edge falls on a Σ-line, are of the form

$D_{51} =$ 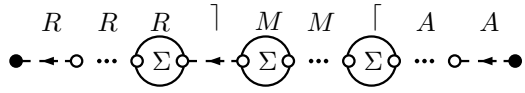

$=$ 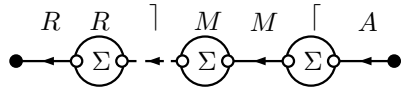

(A.21)

Here there are again three special cases. One with a Matsubara set of a single vertex, given by

$D_{52} =$ 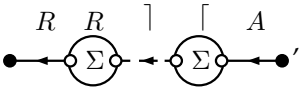

, (A.22)

one with the left retarded set being empty, given by

$D_{53} =$ 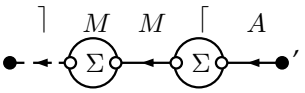

, (A.23)

and one with both of the above, given by

$D_{54} =$ 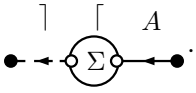

. (A.24)

Making use of (A.18) we obtain

$D_5 = D_{51} + D_{52} + D_{53} + D_{54} = i$ 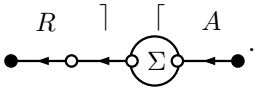

. (A.25)

6. Diagrams containing a Matsubara set, where the left edge falls on a Σ-line and the right edge falls on a g-line, are left-to-right mirrored counterparts to those of the previous category. Therefore we have

$D_6 = -i$ 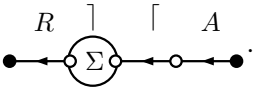

. (A.26)

We can further combine diagrams of the first and the third category to a single expression, since

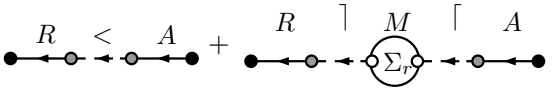

$$= G^R(t_1,t_0)G^<(t_0,t_0)G^A(t_0,t_2) + G^R(t_1,t_0)\left[G^\rceil \star \Sigma_r^M \star G^\lceil\right](t_0,t_0)G^A(t_0,t_2). \tag{A.27}$$

Using $G^<(t_0,t_0) = G^M(0,0^+)$, $G^\rceil(t_0,\tau) = G^M(0,\tau)$, $G^\lceil(\tau,t_0) = G^M(\tau,0)$ we have

$$\begin{aligned} &G^<(t_0,t_0) + \left[G^\rceil \star \Sigma_r^M \star G^\lceil\right](t_0,t_0) = \left[G^M + G^M \star \Sigma_r^M \star G^M\right](t_0,t_0^+) \\ &= G^M(t_0,t_0^+) = G^<(t_0,t_0), \end{aligned} \tag{A.28}$$

which when placed back into (A.27) leads to

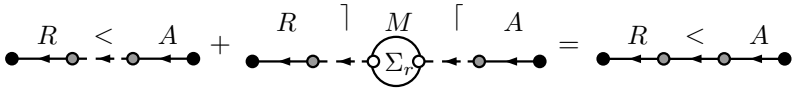

(A.29)

Collecting all the diagrams we obtain finally

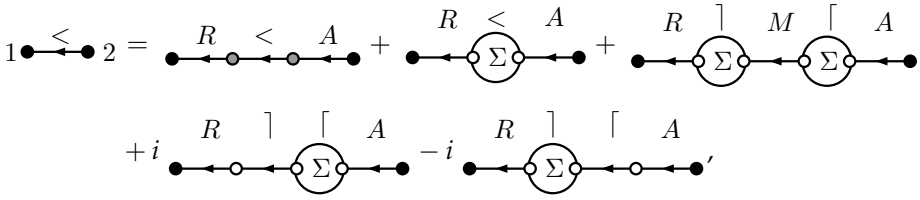

(A.30)

which is a diagrammatic representation of the original equation (A.1).

Appendix B

Finite Temperature Cutting Rules from the Lehmann Representation

In this appendix we will derive cutting rules for the Green's function

$$G(\mathbf{x}_1 z_1, \mathbf{x}_2 z_2) = -\mathrm{iTr}\left[\hat{\rho}\,\mathcal{T}_\gamma\left\{\hat{d}_H(\mathbf{x}_1 z_1)\hat{d}_H^\dagger(\mathbf{x}_2 z_2)\right\}\right] \tag{B.1}$$

at finite temperature, starting from the Lehmann representation. The derivation applies with small modifications to other two-particle correlators, for example the self-energy and the polarizatio function. Here the contour γ is a single loop containing the forward and backward real-time branches (see Figure 1) but we do not include the Matsubara branch but instead work directly with the density matrix $\hat{\rho}$.

We start by making the adiabatic assumption [13]

$$\hat{\rho} = \hat{U}_\eta(t_0, -T)\hat{\rho}_0\hat{U}_\eta(-T, t_0), \tag{B.2}$$

where ρ_0 is the density operator of a noninteracting system and $\hat{U}_\eta$ includes an adiabatic switch-on of the interactions from a distant time $-T$ in the past with η an adiabatic parameter. This is a much stronger assumption than the Gell-Mann-Low theorem used in the zero-temperature derivation [1], since in addition to requiring that the non-interacting ground-state evolves to the interacting ground-state during the switch-on, this must be assumed for all excited states as well. Note that this assumption is not required for the diagrammatic derivation of the finite temperature cutting rules presented in Pub. [III]. Under the adiabatic assumption the single-particle Green's function takes the form

$$\begin{aligned} G^<(1,2) &= -i\,\mathrm{tr}\,\hat{\rho}_0\mathcal{T}\{\hat{U}_\eta(-T,t_0)\hat{d}_H(1)\hat{d}_H^\dagger(2)\hat{U}_\eta(t_0,-T)\} \\ &= -i\,\mathrm{tr}\,\hat{\rho}_0\mathcal{T}_{\gamma'}\{\hat{d}_H(1)\hat{d}_H^\dagger(2)\}. \end{aligned} \tag{B.3}$$

where we used the short-hand notation $1 = \mathbf{x}_1 t_1$ and γ' is the loop contour extended backwards to $-T$.

We then introduce a complete set of non-interacting many-body eigenstates $|L\rangle$ of the form

$$|L\rangle = \hat{c}_{i'_1}\ldots\hat{c}_{i'_M}\hat{c}^\dagger_{i_N}\ldots\hat{c}^\dagger_{i_1}|\Phi_0\rangle \tag{B.4}$$

where $L = (I, I')$ is a multi-index with $I = (i_1, \ldots, i_N)$ and $I' = (i'_1, \ldots, i'_M)$. The states $|L\rangle$ satisfy the orthonormality relations

$$\langle L_1 | L_2 \rangle = \delta_{N_1,N_2} \delta_{M_1,M_2} \sum_P (-1)^{|P|} \delta_{L_1,P(L_2)} \tag{B.5}$$

where $P(L) = (P_1(I), P_2(I'))$ consists of all permutations P_1 and P_2 of the labels I and I' in L separately and $|P| = |P_1| + |P_2|$ is the overall sign of the permutation. There are $N!M!$ of such permutations and the completeness relation in the relevant Hilbert space for our states is therefore given by

$$\sum_{N,M=0}^{\infty} \sum_L \frac{1}{N!M!} |L\rangle\langle L| = 1 \tag{B.6}$$

where the summation index $L = (I, I')$ runs over all orderings of the indices in the multi-labels I and I'.

The states $|L\rangle$ are eigenstates of the non-interacting many-body Hamiltonian $\hat{H}_0$ with eigenvalues

$$E_L = E_0 + \sum_{i=1}^{N} \epsilon_i - \sum_{i'=1}^{M} \epsilon_{i'}. \tag{B.7}$$

Thus expressing the trace in terms of these states allows the density-matrix, expressed as $\hat{\rho}_0 = \frac{e^{-\beta(\hat{H}_0 - \mu\hat{N})}}{Z_0}$, to be brought outside the trace, leading to an expression for the Green's function of the form

$$G(1,2) = -i \sum_L \frac{\mathrm{e}^{-\beta(E_L - \mu N_L)}}{Z_0} \langle L | \hat{d}^\dagger_{H'}(2) \hat{d}_{H'}(1) | L \rangle. \tag{B.8}$$

In the zero-temperature derivations one places a sum over states between the $\hat{d}$-operators in order to reach a PSD expression. As will be seen below, for the finite temperature case this is not helpful, since the two factors will in any case be coupled by the summation over L. We therefore express the expectation value in (B.8) as a whole in terms of Green's functions as

$$\begin{aligned} &\langle L | \hat{d}^\dagger_{H'}(2) \hat{d}_{H'}(1) | L \rangle \\ &= \langle \Psi_0 | \hat{d}_{i_1} \cdots \hat{d}_{i_N} \hat{d}^\dagger_{i'_M} \cdots \hat{d}^\dagger_{i'_1} \hat{d}^\dagger_{H'}(2) \hat{d}_{H'}(1) \hat{d}_{j'_1} \ldots \hat{d}_{j'_M} \hat{d}^\dagger_{j_N} \ldots \hat{d}^\dagger_{j_1} | \Psi_0 \rangle \\ &= (-1)^M i^{N+M+1} G_{N+M+1}(1, i_1 \cdots i_N, i'_1 \cdots i'_M; 2, i_1, \cdots i_N, i'_1 \cdots i'_M), \end{aligned} \tag{B.9}$$

where the $(-1)^M$ factor comes rearranging the operators according to the definition of Green's function, with creation operators to the right and annihilation operators to the left.

Using (B.9) (B.8) can be expanded diagrammatically using the zero-temperature Wick-theorem as

$G^<(1,2)$

$$= \sum_{N,M=0}^{\infty} \frac{1}{N!M!} \sum_L \frac{\mathrm{e}^{-\beta \tilde{E}_L}}{Z_0} i^N (-i)^M$$

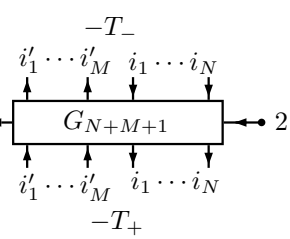

, (B.10)

where the sum over L sums over the quantum numbers $i_1, \ldots, i_N$ and $i'_1, \ldots, i'_M$.

It turns out that connecting the L vertices to each other generates, together with the Boltzmann factors, terms that can be interpreted as finite temperature corrections to the other g-lines. We therefore express a contour-ordered single-particle Green's function at finite temperature as

$$g_\lambda(z_1, z_2) = g_{0,\lambda}(z_1, z_2) + \delta g_\lambda(t_1, t_2), \tag{B.11}$$

where $g_{0,\lambda}$ is the zero-temperature Green's function (here $\bar{n}_\lambda = 1 - n_\lambda$)

$$\begin{aligned} g_{0,\lambda}(z_1, z_2) &= \theta(z_1, z_2) g^{>}_{0,\lambda}(t_1, t_2) + \theta(z_2, z_1) g^{<}_{0,\lambda}(t_1, t_2) \\ &= \theta(z_1, z_2)(-i)\bar{n}_\lambda \mathrm{e}^{-i\epsilon_\lambda(t_1 - t_2)} + \theta(z_2, z_1) i n_\lambda \mathrm{e}^{-i\epsilon_\lambda(t_1 - t_2)}, \end{aligned} \tag{B.12}$$

and δg_λ is a correction term given by

$$\delta g_\lambda(t_1, t_2) = i(f_\lambda - n_\lambda)\mathrm{e}^{-i\epsilon_\lambda(t_1 - t_2)} = i\left[\bar{n}_\lambda f_\lambda - n_\lambda \bar{f}_\lambda\right] \mathrm{e}^{-i\epsilon_\lambda(t_1 - t_2)}, \tag{B.13}$$

where $f_\lambda = f(\bar{\epsilon}_\lambda)$ and $\bar{f}_\lambda = 1 - f_\lambda$. The density matrix element in (B.10), on the other hand, can be expressed as

$$\frac{\mathrm{e}^{-\beta \bar{E}_L}}{Z_0} = \frac{\mathrm{e}^{-\beta \sum_\lambda n^{(L)}_\lambda \bar{\epsilon}_\lambda}}{\prod_\lambda (1 + \mathrm{e}^{-\beta \bar{\epsilon}_\lambda})} = \prod_\lambda \frac{\mathrm{e}^{-\beta n^{(L)}_\lambda \bar{\epsilon}_\lambda}}{1 + \mathrm{e}^{-\beta \bar{\epsilon}_\lambda}} = \prod_\lambda \left[n^{(L)}_\lambda f_\lambda + \bar{n}^{(L)}_\lambda \bar{f}_\lambda \right]. \tag{B.14}$$

The L vertices are all either the start or the end point of the contour, and therefore any g-lines connecting to them reduce to either a greater component (the unprimed vertices) or a lesser component (the primed vertices). Therefore unless the pair of vertices i are directly connected without interactions (a case that will be handled later) the L sum will glue the external legs together according to the relation

$$\begin{aligned} g^{>}_{0,\lambda}(t_1, \pm T) g^{>}_{0,\lambda}(\pm T, t_2) &= -i g^{>}_{0,\lambda}(t_1, t_2) \\ g^{<}_{0,\lambda}(t_1, \pm T) g^{<}_{0,\lambda}(\pm T, t_2) &= i g^{<}_{0,\lambda}(t_1, t_2). \end{aligned} \tag{B.15}$$

Whenever an L vertex corresponding to orbital λ is glued, we pick from (B.14) the corresponding factor $n^{(L)}_\lambda f_\lambda + \bar{n}^{(L)}_\lambda \bar{f}_\lambda$. If we are gluing an unprimed i vertex the Green's functions are greater, i.e. particle propagators, and therefore $n^{(L)}_{\lambda'} = 1$. We then have

$$f_{\lambda'}\, g^{>}_{0,\lambda'}(t_1, T) g^{>}_{0,\lambda'}(T, t_2) = -\bar{n}_{\lambda'} f_{\lambda'}\, \mathrm{e}^{-i\epsilon_\lambda(t_1 - t_2)}. \tag{B.16}$$

Likewise if we are gluing a primed i' vertex, the Green's functions are lesser, i.e. hole propagators, and therefore $n^{(I)}_{\lambda'} = 0$. We then have

$$\bar{f}_{\lambda'}\, g^{<}_{0,\lambda'}(t_1, T) g^{<}_{0,\lambda'}(T, t_2) = -n_{\lambda'} \bar{f}_{\lambda'}\, \mathrm{e}^{-i\epsilon_\lambda(t_1 - t_2)}. \tag{B.17}$$

These terms sum up to create the finite temperature correction δg_λ ((B.13)) provided we add an extra $-i$ factor for each of the N greater g-lines glued and an extra i for each of the M lesser g-lines glued. This absorbs the $i^N(-i)^M$ prefactor in (B.10).

The diagrams with $N, M \neq 0$ can thus can be interpreted as finite temperature corrections to the base zero-temperature Green's function diagrams ($N, M = 0$). For example for the diagram

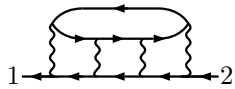

(B.18)

one of the finite temperature corrections is generated by the diagram

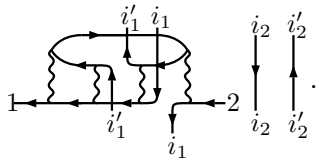

(B.19)

In particular the above diagram contributes the greater part of the correction, (B.16), for the split g-line connected to i_1 and the lesser part of the correction, (B.17), for the split g-line connected to i_1'. Adding this diagram with the versions where the splits are connected up-down or down-up in different ways (four diagrams in total) to the zero-temperature diagram generates a diagram with the two split g-lines replaced by finite temperature g-lines. Summing over every possible way to split and connect the g-lines in (B.18) generates the full finite-temperature version of (B.18). This can be done for every zero-temperature diagram, and thus the complete finite-temperature expansion of the self-energy is generated (including vacuum bubbles containing interactions).

The correction diagrams can also include an arbitrary number of disconnected g-lines, such as the lines labeled i_2 and i_2' in (B.19). These generate non-interacting vacuum diagrams which are cancelled by the remaining parts of the Boltzmann factors. These g-lines have the form (again taking $-i$ and i factor from the prefactor in (B.10))

$$\begin{aligned} -if_\lambda\, g^{>}_{0,\lambda}(-T,-T) &= -\bar{n}_\lambda f_\lambda \\ i\bar{f}_\lambda\, g^{<}_{0,\lambda}(-T,T) &= -n_\lambda \bar{f}_\lambda. \end{aligned} \tag{B.20}$$

For a specific state in the L sum in (B.10), the remaining Boltzmann factors after the gluing are those corresponding to particles remaining below the Fermi level, and holes remaining above the Fermi level, in the state $|L\rangle$. Thus for each $\lambda \neq i_1', \ldots, i_{N_1}', i_1, \ldots, i_{N_2}$ there is a prefactor

$$n_\lambda f_\lambda + \bar{n}_\lambda \bar{f}_\lambda. \tag{B.21}$$

For each such state λ there exists an equivalent diagram with a loop as in (B.20) for λ, which is a $g^>$ loop if above the Fermi energy, and a $g^<$ loop if below it. Thus we

have for example (taking the λ-part of the Boltzmann factor and the L-sum)

$$
\begin{aligned}
&[n_\lambda f_\lambda + \bar{n}_\lambda \bar{f}_\lambda] \quad 1 \;\bigcirc\!\!\!\!\!\!\bigcirc\; 2 \;+\; 1 \;\bigcirc\!\!\!\!\!\!\bigcirc\; 2 \;\overset{\lambda}{\underset{\lambda}{\uparrow}}\; + \; 1 \;\bigcirc\!\!\!\!\!\!\bigcirc\; 2 \;\overset{\lambda}{\underset{\lambda}{\downarrow}} \\
&= [n_\lambda f_\lambda + \bar{n}_\lambda \bar{f}_\lambda] \quad 1 \;\bigcirc\!\!\!\!\!\!\bigcirc\; 2 \;+ n_\lambda \bar{f}_\lambda \; 1 \;\bigcirc\!\!\!\!\!\!\bigcirc\; 2 \;+ \bar{n}_\lambda f_\lambda \; 1 \;\bigcirc\!\!\!\!\!\!\bigcirc\; 2 \qquad \text{(B.22)} \\
&= [n_\lambda f_\lambda + \bar{n}_\lambda \bar{f}_\lambda + n_\lambda \bar{f}_\lambda + \bar{n}_\lambda f_\lambda] \; 1 \;\bigcirc\!\!\!\!\!\!\bigcirc\; 2 \;= \; 1 \;\bigcirc\!\!\!\!\!\!\bigcirc\; 2
\end{aligned}
$$

In this way every remaining Boltzmann factor for all diagrams is cancelled by the simple vacuum bubbles.

The result of this gluing procedure is a diagrammatic expansion for the self-energy containing the same diagrams as the zero-temperature expansion, but with all g-lines replaced by finite temperature g-lines.

References

[1] G. Stefanucci, Y Pavlyukh, A.-M. Uimonen and R. van Leeuwen, Diagrammatic expansion for positive spectral functions beyond GW: Application to vertex corrections in the electron gas, Phys. Rev. B **90** 115134 (2014).

[2] A.-M. Uimonen, G. Stefanucci, Y. Pavlyukh and R. van Leeuwen, Diagrammatic expansion for positive density-response spectra: Application to the electron gas, Phys. Rev. B **91** 115104 (2015).

[3] A. Akbari, M. J. Hashemi, A. Rubio, R. M. Nieminen and R. van Leeuwen, Challenges in truncating the hierarchy of time-dependent reduced density matrices equations, Phys. Rev. B **85** 235121 (2012).

[4] M. Puig von Friesen, C. Verdozzi and C.-O. Almbladh, Artificial damping in the Kadanoff-Baym dynamics of small Hubbard chains, J. Phys. Conf. Ser. **220** 012016 (2010).

[5] G. Baym and L. Kadanoff, Conservation laws and correlation functions, Phys. Rev. **124** 287–299 (1961).

[6] G. Baym, Self-consistent approximations in many-body systems, Phys. Rev. **127** 1391–1401 (1962).

[7] D. Karlsson and R. van Leeuwen, Partial self-consistency and analyticity in many-body perturbation theory: Particle number conservation and a generalized sum rule, Phys. Rev. B **94** 125124 (2016).

[8] C.-O. Almbladh, Photoemission beyond the sudden approximation, J. Phys. Conf. Ser. **35** 127–144 (2006).

[9] D. C. Langreth, Linear and Nonlinear Response Theory with Applications, *Linear nonlinear electron transp. solids*, edited by J. T. Devreese and V. E. Doren (Springer US, Boston, MA, 1976).

[10] R. Balian and C. De Dominicis, Sur la fonction de green à une particule en mécanique statistique quantique, Nuclear Physics **16** 502–517 (1960).

[11] G. Baym and A. M. Sessler, Perturbation-theory rules for computing the self-energy operator in quantum statistical mechanics, (1962) `10.2172/4749105`.

[12] G. Stefanucci and R. van Leeuwen, *Nonequilibrium Many-Body Theory of Quantum Systems: A Modern Introduction* (Cambridge University Press, Cambridge, July 2013).

[13] L. V. Keldysh, Diagram technique for nonequilibrium processes, Sov. Phys. JETP **20** 1018–1026 (1965).

[14] P. Danielewicz, Quantum theory of nonequilibrium processes, I, Ann. Phys. (N. Y). **152** 239–304 (1984).

ORIGINAL PAPERS

I

CONTOUR CALCULUS FOR MANY-PARTICLE FUNCTIONS

by

M. Hyrkäs, D. Karlsson and R. van Leeuwen 2019

Journal of Physics A: Mathematical and Theoretical **52** 215303

DOI:10.1088/1751-8121/ab165d

6 May 2019

Contour calculus for many-particle functions

M. J. Hyrkäs, D. Karlsson, and R. van Leeuwen

Department of Physics, Nanoscience Center P.O.Box 35 FI-40014 University of Jyväskylä, Finland

E-mail: markku.hyrkas@jyu.fi

Abstract. In non-equilibrium many-body perturbation theory, Langreth rules are an efficient way to extract real-time equations from contour ones. However, the standard rules are not applicable in cases that do not reduce to simple convolutions and multiplications. We introduce a procedure for extracting real-time equations from general multi-argument contour functions with an arbitrary number of arguments. This is done for both the standard Keldysh contour, as well as the extended contour with a vertical track that allows for general initial states. This amounts to the generalization of the standard Langreth rules to much more general situations. These rules involve multi-argument retarded functions as key ingredients, for which we derive intuitive graphical rules. We apply our diagrammatic recipe to derive Langreth rules for the so-called double triangle structure and the general vertex function, relevant for the study of vertex corrections beyond the GW approximation.

Submitted to: *J. Phys. A: Math. Theor.*

1. Introduction

Many-body perturbation theory (MBPT) is an invaluable asset when studying complex multi-particle phenomena out of equilibrium and at finite temperatures. A crucial step in the development of modern MBPT was its formulation in the language of non-equilibrium Green's functions [1, 2]. Within this formulation, quantities are defined on a directed time contour which allows one to derive diagrammatic perturbation theory at finite temperature and out of equilibrium in precisely the same way as for the traditional zero-temperature case [3]. Within the contour formalism, traditional formalisms such as the zero-temperature or the Matsubara formalism, follow from choosing the contour in specific ways and attaching specific time dependencies to the interactions [2].

The contour formalism, however, introduces an additional complexity by the replacement of real-time integrals with contour integrals. This makes objects, such as Green's functions and self-energies, more cumbersome to calculate numerically. An efficient tool was developed by Langreth and Wilkins [4, 5], who derived rules for obtaining real-time objects from contour objects. These rules are now commonly referred to as the Langreth rules [1, 2].

The Langreth rules, however, are not applicable when the structure of a contour equation does not reduce to convolutions and products. This situation occurs, for example, when including vertex corrections to the commonly used GW approximation [6]. Furthermore, the Langreth rules are not applicable if the equation contains three-point or higher-order objects, such as the vertex function and the Bethe-Salpeter kernel in the Hedin equations [7].

In such cases, a direct evaluation of the contour integrals, by splitting the integrals over the various branches, results in an unwieldy amount of terms, many of which add up to yield zero contribution. Moreover, the objects involved often have no physical interpretation. This problem was studied by Danielewicz [8] who introduced a way to obtain real-time components in terms of explicitly retarded or advanced objects which have a physical interpretation. Moreover, he derived rules that allow some of the vanishing terms to be discarded from the outset.

The purpose of the present paper is twofold. First, we extend the analysis of Danielewicz [8] to the realm of non-equilibrium systems with general initial states, by considering the addition of an vertical time branch to the contour. Furthermore, we present alternative proofs of known results. Second, we extend the Langreth rules to general contour equations, to cover all cases of interest. An important new addition to the original Langreth rules are those for the so-called double triangle graph, appearing in the lowest order vertex corrections beyond the GW approximation. These rules already found an important application in the construction of positive semi-definite spectral functions in non-equilibrium systems [9].

The paper is structured as follows. In Section 2 we discuss the structure of commonly encountered contour equations, and briefly review the Langreth rules. In Section 3 we discuss general properties of contour objects. In Section 4 we give

an alternative derivation of results of Danielewicz [8], providing rules to extract the real-time part of n-point functions. We also provide a different graphical recipe to intuitively obtain the end results. In Section 5 we extend the discussion of Section 4 for contours including the Matsubara branch, thereby generalizing the results by Danielewicz and extending our graphical recipe correspondingly. In Section 6 we derive extended Langreth rules for general diagrams, and in Section 7 we apply our formalism to derive Langreth rules for selected diagrams of common interest, that cannot be handled using the standard rules. We conclude in Section 8.

2. Theoretical Background and Motivation

2.1. Time-dependent ensemble averages

The time-dependent ensemble average $O(t)$ of an operator $\hat{O}(t)$ is given by [2]

$$O(t) = \mathrm{Tr}\left[\hat{\rho}\,\hat{U}(t_0,t)\hat{O}(t)\hat{U}(t,t_0)\right], \tag{1}$$

where $\hat{U}(t,t_0)$ is the time-evolution operator, t_0 the initial time, and $\hat{\rho}$ is the density matrix. The ensemble average can be written in a form convenient for perturbation theory by introducing a directed time contour γ_t [10, 11, 2], that runs from the initial time t_0 to t, and then back to t_0 again. For manipulations, it is convenient to extend the contour to $t=\infty$, which leaves the result unchanged since $\hat{U}(t,t')\hat{U}(t',t)=1$. We denote this contour by γ, which is often referred to as the Keldysh contour [10] (see Figure 1, left figure. Note, however, that in the original work by Keldysh, the contour starts at $t_0=-\infty$). The ensemble average of Eq. (1) can then be expressed as [2]

$$O(z) = \mathrm{Tr}\left[\hat{\rho}\,\mathcal{T}_\gamma\left\{\mathrm{e}^{-i\int_\gamma \mathrm{d}\bar{z}\,\hat{H}(\bar{z})}\hat{O}(z)\right\}\right]. \tag{2}$$

The contour time z is a parameter on the contour γ. The first part of the contour, from t_0 to ∞, we call the forward branch γ_-, and denote times on it by t_-. The returning branch we call the backward branch γ_+ with times t_+. The contour-ordering operator $\mathcal{T}_\gamma\{\ldots\}$ orders operators according to the order of their contour-time arguments, with the convention that later contour times (as measured along the contour) are ordered to the left, and that for equal times the existing order is retained [2]. The Hamiltonian on the contour is defined through $\hat{H}(t_\pm)=\hat{H}(t)$, and likewise for the operators $\hat{O}$. Consequently, the ensemble average is independent of the branch index, so that $O(t)=O(t_\pm)$.

Since the density matrix $\hat{\rho}$ is a positive semi-definite operator, it can always be written as [12, 13, 2, 14]

$$\hat{\rho} = \frac{\mathrm{e}^{-\hat{H}_M}}{Z} = \frac{\mathrm{e}^{-i\int_{t_0}^{t_0-i}\mathrm{d}\bar{z}\,\hat{H}_M(\bar{z})}}{Z}, \tag{3}$$

where $\hat{H}_M(\bar{z})=\hat{H}_M$ is time-independent and $Z=\mathrm{Tr}\left[\mathrm{e}^{-\hat{H}_M}\right]$. In general, the operator $\hat{H}_M$ is an n-body operator unrelated to $\hat{H}$, but in the special case where $\hat{\rho}$ represents

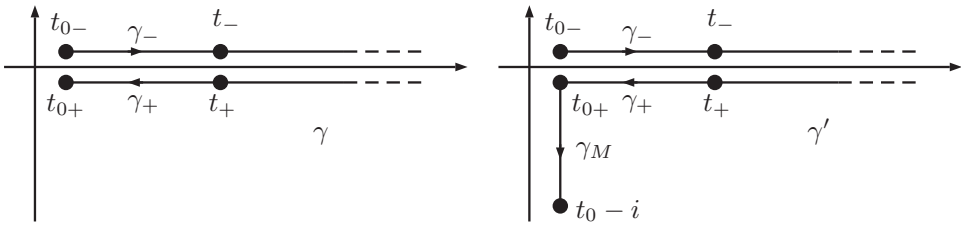

Figure 1. The two different contours used in this work. (Left) The Keldysh contour γ, consisting of a forward branch γ_- and a backward branch γ_+. $t_-(t_+)$ denotes a contour time on the forward (backward) branch at distance t from t_0. The contour is ordered such that t_+ is later than t_-. (Right) The extended contour γ', with an added vertical branch γ_M. Note that the horizontal branches are shifted vertically for illustrative purposes only; both branches are on the real axis.

the grand canonical ensemble, it is given by $\hat{H}_M = \beta(\hat{H} - \mu\hat{N})$, where μ is the chemical potential and $\hat{N}$ the particle number operator [12, 13, 2]. Eq. (3) allows for writing the ensemble average Eq. (2) as

$$O(z) = \frac{\mathrm{Tr}\left[\mathcal{T}_{\gamma'}\left\{\mathrm{e}^{-i\int_{\gamma'}\mathrm{d}\bar{z}\,\hat{H}(\bar{z})}\hat{O}(z)\right\}\right]}{Z} \tag{4}$$

using an extended contour [15, 1, 14] γ' with an vertical Matsubara branch γ_M going from t_0 to $t_0 - i$ attached to the end and a corresponding extended definition of $\hat{H}(z)$ given by $\hat{H}(z \in \gamma_M) = \hat{H}_M$ (see Figure 1).

Using the extended contour, initial correlations can be treated perturbatively [12]. The expansion is performed by expanding all n-body terms higher than one in $\hat{H}(z)$, which allows Wick's theorem to be applied. In our following discussion, we will make use of both contours (see Figure 1).

2.2. Contour-time structure of diagrammatic expansions

To discuss the types of structures that arise in many-body perturbation theory, we here focus on the diagrammatic expansion of the single-particle Green's function G when the interaction $\hat{V}$ is of two-body type. The discussion pertains to both the Keldysh contour and the extended contour.

The simplest structure that appears is the convolution:

$$C(z_1, z_2) = \int_\gamma \mathrm{d}\bar{z}_1\, A(z_1, \bar{z}_1)B(\bar{z}_1, z_2), \tag{5}$$

which appears, for example, in the Dyson equation. The expressions generally involve also relevant quantum numbers. For clarity, we will suppress arguments other than time arguments.

The Langreth rules use the fact that the functions involved can be expressed as

$$A(z_1, z_2) = \theta(z_1, z_2)A^>(t_1, t_2) + \theta(z_2, z_1)A^<(t_1, t_2), \tag{6}$$

using real-time greater ($A^>$) and lesser ($A^<$) components for contour orders $z_1 > z_2$ and $z_2 > z_1$ respectively. The Langreth rules for a convolution yield, for the extended contour,

$$A^{\lessgtr} = B^R \cdot C^{\lessgtr} + B^{\lessgtr} \cdot C^A + B^{\rceil} \star C^{\lceil}. \tag{7}$$

In Eq. (7), we have defined the short-hand notation for real-time convolutions as

$$[B \cdot C](t_1, t_2) = \int_{t_0}^{\infty} \mathrm{d}t_3 \, B(t_1, t_3) C(t_3, t_2), \tag{8}$$

and the star represents the imaginary-time convolution

$$[B^{\rceil} \star C^{\lceil}](t_1, t_2) \doteq -i \int_0^1 \mathrm{d}t_3 \, B^{\rceil}(t_1, t_3) C^{\lceil}(t_3, t_2). \tag{9}$$

The retarded (A^R) and advanced (A^A) compositions are defined as

$$A^R(t_1, t_2) = \Theta(t_1 - t_2)\big[A^>(t_1, t_2) - A^<(t_1, t_2)\big] \tag{10}$$

$$A^A(t_1, t_2) = -\Theta(t_2 - t_1)\big[A^>(t_1, t_2) - A^<(t_1, t_2)\big]. \tag{11}$$

Here, $\Theta(t)$ is 1 for $t > 0$, and zero otherwise. We use $\Theta(t_1 - t_2)$ to denote the real-time step function, which is to be distinguished from the contour step function $\theta(z_1, z_2)$. The relations between these functions are given by $\theta(t_{1-}, t_{2-}) = \Theta(t_1 - t_2)$, $\theta(t_{1+}, t_{2+}) = \Theta(t_2 - t_1)$, $\theta(t_{1-}, t_{2+}) = 0$ and $\theta(t_{1+}, t_{2-}) = 1$. The retarded and advanced compositions can also be immediately obtained from another Langreth rule:

$$A^{R/A} = B^{R/A} \cdot C^{R/A}. \tag{12}$$

All Langreth rules for convolutions are shown in Table 1. The Langreth rules for the Keldysh contour can be obtained simply by taking the terms from the extended contour and putting all imaginary-time convolutions to zero [2]. Another structure that appears often in many-body perturbation theory is a product:

$$C(z_1, z_2) = A(z_1, z_2) B(z_2, z_1). \tag{13}$$

Notable examples come from the GW approximation [7]. Here, the exchange-correlation self-energy $\Sigma_{xc}(z_1, z_2) = iG(z_1, z_2)W(z_2, z_1)$ is of product form, where W is the screened interaction and G is the Green's function. Another example is the polarization $P(z_1, z_2) = -iG(z_1, z_2)G(z_2, z_1)$ (see Figure 2). These structures can also be treated by Langreth rules, shown in Table 1.

When considering higher-order diagrams, however, structures emerge that are not reducible to these basic types. For example, the diagrams in Figure 2, second order in W for Σ, and first order for P, are not of the chain convolution or product type. These diagrams are examples of a structure which we call the double-triangle,

$$F(z_1, z_2) = \int_\gamma \mathrm{d}\bar{z}_3 \mathrm{d}\bar{z}_4 \, A(z_1, \bar{z}_3) B(\bar{z}_3, z_2) C(\bar{z}_3, \bar{z}_4) D(z_1, \bar{z}_4) E(\bar{z}_4, z_2), \tag{14}$$

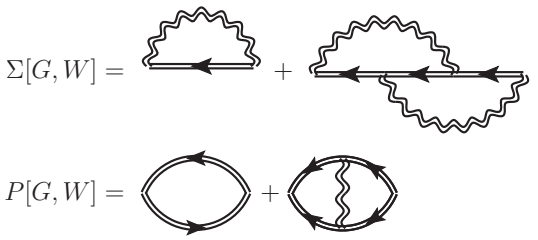

Figure 2. The self-energy to second order in the screened interaction (upper) and the polarization up to first order (lower). The *GW* approximation amounts to keeping the first diagram in each row. The second diagrams are of the double-triangle structure.

which can be diagrammatically expressed as

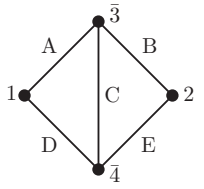

(15)

Higher-order diagrams will yield increasingly complex structures. For these types of diagrams, the original Langreth rules are not enough, and need to be generalized.

Another example for which the Langreth rules cannot be applied directly is the case in which we have integrals over general n-point functions. An example is one of the Hedin equations, which has the structure

$$H(z_1, z_2) = \int_\gamma \mathrm{d}\bar{z}_3 \mathrm{d}\bar{z}_4 \, A(z_1, \bar{z}_3) B(z_1, \bar{z}_4) C(\bar{z}_4, z_2, \bar{z}_3) \tag{16}$$

in which the three-point function C appears. This equation is the Hedin equation for the exact exchange-correlation self-energy $\Sigma_{xc} = H$ if we identify $A = W$ and $B = G$, and $C = i\Lambda$ is the so-called vertex function [7]. It can be diagrammatically expressed as

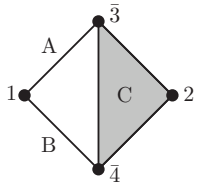

(17)

In this case the problem arises of expressing the three-point function C on the contour in terms of its real-time components [16]. We also mention the Bethe-Salpeter equation for the two-particle Green's function as another important equation to which the Langreth rules cannot be directly applied.

These considerations motivate the generalization of the Langreth rules for more complex expressions than convolutions and products, as well as the consideration of general n-point functions. These issues will be discussed in the following sections.

3. Properties of Contour Functions

To generalize the Langreth rules, we introduce general real-time components that encode the information contained in a contour function. Specifically, we are interested in contour functions that have a diagrammatic representation in terms of Green's functions. In this section, we consider the case of the Keldysh contour, while the extended contour will be treated in Section 5.

For dealing with functions with an arbitrary number of arguments, we will introduce a convenient notation. We start by defining an ordered set of labels $\mathcal{N} = \{n_1, \ldots, n_N\}$. By ordered set we mean that different orderings of the elements are considered to be different sets, for example $\{a, b, c\} \neq \{b, a, c\}$. A collection of contour or real times corresponding to the labels $\mathcal{N}$ is denoted by $z_\mathcal{N} = \{z_{n_1}, \ldots, z_{n_N}\}$ and similarly for real times $t_\mathcal{N}$. We stress that the contour times z are also real-time numbers, but carry an additional branch index to indicate which branch they are on. The collection of real times $t_\mathcal{N}$ is the collection $z_\mathcal{N}$ with the branch indices removed. We define the contour step function $\theta(z_\mathcal{N}) = 1$ if $z_{n_1} > z_{n_2} > \cdots > z_{n_N}$ on the contour, and zero otherwise. For zero and one argument sets $\mathcal{N}$, we define $\theta(z_\mathcal{N}) = 1$. Permutations of ordered sets are denoted by

$$P(\mathcal{N}) = \{P(n_1), \ldots, P(n_N)\}. \tag{18}$$

We often sum over all $N!$ permutations belonging to the symmetric group S_N of order N, which we denote by $\sum_{P \in S_N}$. With these definitions, we can conveniently define a *Keldysh function* $\mathscr{O}(z_\mathcal{N})$, denoted by a cursive letter, as a function of N contour variables that can be expressed as

$$\mathscr{O}(z_\mathcal{N}) = \sum_{P \in S_N} \theta(z_{P(\mathcal{N})}) O^{P(\check{\mathcal{N}})}(t_\mathcal{N}), \tag{19}$$

with some set of real-time functions $O^{P(\check{\mathcal{N}})}(t_\mathcal{N})$. The háček ($\check{}$) above an argument index denotes the position of that argument in the argument list of the relevant function. For example,

$$O^{\check{b}\check{c}\check{a}}(t_a, t_b, t_c) = O^{231}(t_a, t_b, t_c). \tag{20}$$

Therefore, the háček is a mapping from labels to integers, which will make the components independent of the labeling of their arguments. The value of this notation will become clear later. The real-time functions $O^{P(\check{\mathcal{N}})}(t_\mathcal{N})$ are referred to as the *Keldysh components* of $\mathscr{O}(z_\mathcal{N})$. We call Eq. (19) a *Keldysh sum* representation. The concept of a Keldysh function is a useful one, since both Green's functions themselves, as well as diagrams built out of Green's functions, are Keldysh functions. For future use, we define a short-hand notation. We define the formal sum $L = \sum_j \sigma_j l_j$ as a sum over

signs $\sigma_j = \pm$ and integer strings l_j of equal length. Correspondingly, we define a linear combination of Keldysh components

$$O^L = \sum_j \sigma_j O^{l_j}. \tag{21}$$

For example,

$$O^{123-231} = O^{123} - O^{231}. \tag{22}$$

This notation will be especially useful when we encounter nested commutators.

Keldysh functions depend on branch indices of their arguments only so far as they affect the ordering of the arguments on the contour. The domain of definition of a Keldysh function on the contour can be divided into sub-domains of constant contour order, such that in each sub-domain the function can be described by a real-time function. The Keldysh components are assumed to be defined in all of $\mathbb{R}^N$, although only the values of $O^{P(\check{\mathcal{N}})}$ for which the multiplying step-function yields 1 contribute to $\mathscr{O}$ through the Keldysh sum. As a special case, a Keldysh function with a single contour argument, $\mathscr{O}(z_{n_1})$ has a single Keldysh component $O^1(t_{n_1}) = \mathscr{O}(t_{n_1\pm})$.

As an example, a two-point Keldysh function $\mathscr{A}(z_a, z_b)$ has the representation

$$\mathscr{A}(z_a, z_b) = \theta(z_a, z_b) A^{\check{a}\check{b}}(t_a, t_b) + \theta(z_b, z_a) A^{\check{b}\check{a}}(t_a, t_b), \tag{23}$$

where, as before, $A^{\check{a}\check{b}} = A^{12}$ and $A^{\check{b}\check{a}} = A^{21}$. Eq. (23) is identical to Eq. (6), with $A^{>} = A^{12}$ and $A^{<} = A^{21}$. Thus, Keldysh components are a generalization of greater and lesser components to more variables, where each Keldysh component corresponds to a particular contour-order of the arguments.

We now examine two important properties of Keldysh functions. The first is that products of Keldysh functions are Keldysh functions. This can be seen by multiplying two Keldysh functions, and re-expressing the products of step functions in terms of sums of single step functions of varying argument lists, see, e.g., Eq. (A.2) in Appendix A. For example, multiplying two two-point functions $\mathscr{C}(z_a, z_b)\mathscr{D}(z_b, z_c)$ involves multiplications of, for example,

$$\theta(z_a, z_b)\theta(z_c, z_b) = \theta(z_c, z_a, z_b) + \theta(z_a, z_c, z_b). \tag{24}$$

The terms on the right-hand side appear in the expansion of a new Keldysh function $\mathscr{E}(z_a, z_b, z_c)$. In general, an N-point Keldysh function multiplied with an M-point Keldysh function yields an L-point Keldysh function with $L \leq M + N$.

The second property that we will use is that integrating time arguments of a Keldysh function over the contour yields another Keldysh function. This can be seen by directly integrating a Keldysh sum. Let us consider the unit permutation in an N-point Keldysh sum, and integrate the variable z_i:

$$\int_\gamma \mathrm{d}z_i\, \theta(z_\mathcal{N}) O^\mathcal{N}(t_\mathcal{N}) = \theta(z_{\mathcal{N}\setminus i}) \int_{z_{i+1}}^{z_{i-1}} \mathrm{d}z_i\, O^\mathcal{N}(t_\mathcal{N}). \tag{25}$$

Here, $\mathcal{N} \setminus i$ is the set $\mathcal{N}$ with the element i removed. By considering different branches for z_{i-1} and z_{i+1}, and taking into account that the Keldysh component $O^\mathcal{N}(t_\mathcal{N})$ is

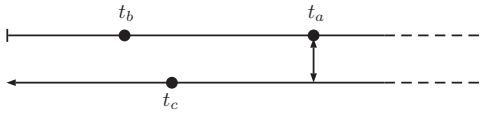

Figure 3. If z_a is the argument with the highest real-time value t_a, the contour ordering is *cab*, independently on whether z_a is on the forward or the backward branch.

independent of the branch indices, we can readily see that the integral on the right-hand side is independent of the branch indices as well, and is thus an $(N-1)$–point Keldysh component. In particular, it follows that integrating N arguments from an N-point Keldysh function yields zero,

$$\int_\gamma \mathrm{d}z_\mathcal{N}\, \bar{\mathscr{O}}(z_\mathcal{N}) = 0. \tag{26}$$

An arbitrary integrand in a Feynman diagram is a polynomial in Keldysh functions, and hence a Keldysh function. Thus, any Feynman diagram is a Keldysh function. As a small remark, a perturbation expansion also includes time-local interactions. For example, the two-point interaction has the form

$$V(z_1, z_2) = v(z_1)\delta(z_1, z_2). \tag{27}$$

If these interaction lines connect internal vertices of a diagram, the delta-functions are integrated out and only a multiplication by the coupling constant $v(z_1)$ remains. Since a multiplication by a real-time function trivially leaves a Keldysh function a Keldysh function, any diagram with only internal interaction lines is a Keldysh function. External interaction lines, i.e. interaction lines that connect to an external vertex, can be dealt with by expressing the function as a sum of singular and regular parts.

Finally, we point out a symmetry property of Keldysh functions that will be useful. A Keldysh function $\mathscr{O}(z_\mathcal{N})$ is symmetric with respect to the branch index of the parameter with the highest real-time value, i.e.

$$\mathscr{O}(\ldots, t_{a+}, \ldots) = \mathscr{O}(\ldots, t_{a-}, \ldots), \qquad \text{if } t_a > t_{\mathcal{N}\setminus a}, \tag{28}$$

since the contour order is identical with either t_{a+} or t_{a-} (see figure 3).

4. Integrals over Keldysh Functions

In the previous section we discussed how Keldysh functions can be expressed in terms of real-time Keldysh components. We will make use of this decomposition to transform an integral involving Keldysh functions to equations between the corresponding Keldysh components. The equations we are interested in have the general form

$$\mathscr{O}(z_\mathcal{E}) = \int_\gamma \mathrm{d}z_\mathcal{I}\, \bar{\mathscr{O}}(z_\mathcal{N}), \tag{29}$$

in which a Keldysh function $\bar{\mathscr{O}}(z_{\mathcal{N}})$ has some of its arguments integrated over the Keldysh contour. We will typically denote integrands by barred symbols. We call $\mathcal{E} = \{e_1, \ldots, e_E\} \subset \mathcal{N}$ the external arguments and $\mathcal{I} = \{i_1, \ldots, i_I\} = \mathcal{N} \setminus \mathcal{E}$ the internal arguments. The function $\bar{\mathscr{O}}$ may have a diagrammatic structure, but in this section we only assume that it is a Keldysh function. The fact that $\mathscr{O}(z_{\mathcal{E}})$ is a Keldysh function was derived in the last section.

The question is then how to obtain the Keldysh components of $\mathscr{O}$ directly in terms of the Keldysh components of $\bar{\mathscr{O}}$. An elegant result accomplishing this, in case of the Keldysh contour, was derived by Danielewicz [8] using an expansion in terms of retarded compositions of Keldysh components. In this section we will provide an alternative derivation, and generalize it to the extended contour in the subsequent section.

4.1. Deforming the Contour

We use the fact that the contour can be truncated, so that it turns back at $t = t_M$, with t_M the largest real-time value of an external argument:

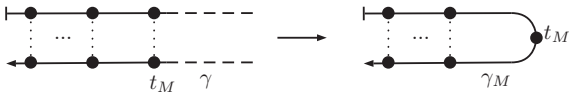

(30)

This follows from Eq. (26), since we can consider a contour that starts at t_M, goes to infinity and returns to t_M, for which the integral over all internal variables vanishes. We denote the truncated contour by γ_M, and we have

$$\int_{\gamma} \mathrm{d}z_{\mathcal{I}}\, \bar{\mathscr{O}}(z_{\mathcal{N}}) = \int_{\gamma_M} \mathrm{d}z_{\mathcal{I}}\, \bar{\mathscr{O}}(z_{\mathcal{N}}), \qquad t_M \geq t_{\mathcal{E}}. \tag{31}$$

The same idea can be used to deform the contour γ_M into several loops. In an integral back and forth on the real-axis, components with the same order will appear in both branches, cancelling each other out. Consider, for example, the contour γ_{ab}, consisting of two loops γ_a and γ_b:

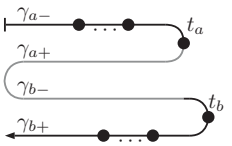

(32)

where two new branches, going from t_a to t_0 and back along the real-axis, have been added between the arguments a and b. In other words:

$$\int_{\gamma} \mathrm{d}z_{\mathcal{I}}\, \bar{\mathscr{O}}(z_{\mathcal{N}}) = \int_{\gamma_{ab}} \mathrm{d}z_{\mathcal{I}}\, \bar{\mathscr{O}}(z_{\mathcal{N}}). \tag{33}$$

It follows that additional back-and-forth loops can be freely added to the contour without changing the value of the integral. This idea will be used in the subsequent sections.

4.2. A Single External Argument

The situation in which all but one argument of a Keldysh function $\bar{\mathscr{O}}(z_e, z_{\mathcal{I}}) = \bar{\mathscr{O}}(z_e, z_{i_1}, \ldots, z_{i_I})$ are integrated over, provides a useful stepping stone to the general result. We therefore consider

$$\mathscr{O}(z_e) = O^1(t_e) = \int_{\gamma_e} \mathrm{d}z_{\mathcal{I}}\ \bar{\mathscr{O}}(z_e, z_{\mathcal{I}}), \tag{34}$$

where the contour γ_e has been truncated to turn back at t_e. Note that, as was seen in the previous section, a Keldysh function of a single argument is equal to its only Keldysh component. Therefore the right-hand side of Eq. (34) can not depend on the branch index of z_e either. We consider the Keldysh sum

$$\bar{\mathscr{O}}(z_e, z_{\mathcal{I}}) = \sum_{P\in S_{I+1}} \theta_{P(ei_1\cdots i_I)} \bar{O}^{P(\check{e}\check{i}_1\cdots\check{i}_I)}(t_e, t_{\mathcal{I}}), \tag{35}$$

over permutations of the $I+1$ arguments, where we have introduced the short-hand notation for contour step functions $\theta(z_{n_1}, \ldots, z_{n_N}) = \theta_{n_1\cdots n_N}$. We remark that although we denote z_e to be the first in the argument list in Eq. (35), the equation holds for any location of z_e in the list, illustrating the usefulness of the háček notation. Our strategy to obtain a real-time expression from Eq. (34) will be to split the I contour integrals into separate contributions from the forward branch γ_- and the backward branch γ_+. For this purpose, it will be convenient to write the sum in Eq. (35) as a sum over permutations of the I internal arguments, and an additional sum over the position (j) of the external argument:

$$\bar{\mathscr{O}}(z_e, z_{\mathcal{I}}) = \sum_{j=0}^{I} \sum_{P\in S_I} \theta_{(P,j)} \bar{O}^{(\check{P},j)}(t_e, \bar{t}), \tag{36}$$

where we have defined

$$(P, j) = P(i_1 \cdots i_j) e P(i_{j+1} \cdots i_I). \tag{37}$$

For example, $(P, 0) = eP(i_1 \cdots i_I)$, $(P, 2) = P(i_1 i_2) e P(i_3 \cdots i_I)$. As such, j is also the number of arguments to the left of e, while we have $I - j$ arguments to the right of e. This means that the arguments $z_{P(i_1)}, \ldots, z_{P(i_j)}$ are on the backward branch, while $z_{P(i_{j+1})}, \ldots, z_{P(i_I)}$ are on the forward branch. We illustrate the situation in the figure below.

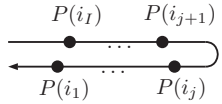

(38)

When Eq. (36) is inserted into Eq. (34), each integral is restricted to either the forward or the backward branch. For $j = 0$, there are no arguments later than z_e, which means that all I integrals are over the forward branch. For $j = 1$, one integral is over

the backward branch, and $I-1$ over the forward branch. Eq. (34) can then be written as

$$O^1(t_e) = \sum_{j=0}^{I} \sum_{P\in S_I} \int_{\gamma_e^+} \mathrm{d}z_{P(i_1\cdots i_j)} \int_{\gamma_e^-} \mathrm{d}z_{P(i_{j+1}\cdots i_I)} \underbrace{\theta_{P(i_1\cdots i_j)}}_{\text{backward branch}} \underbrace{\theta_{P(i_j)e}}_{=1} \underbrace{\theta_{eP(i_{j+1})}}_{=1} \underbrace{\theta_{P(i_{j+1}\cdots i_I)}}_{\text{forward branch}} \bar{O}^{(\check{P},j)}(t_e, t_{\mathcal{I}}). \tag{39}$$

The two step-functions in the middle always equal one, since the integral domains only extend to t_e. We also define, that step-functions with one or zero arguments always yield unity, which ensures that Eq. (39) is well defined for all values of j.

For integrals over the forward branch, the contour integrals can be converted into real-time integrals via the replacement $\int_{\gamma_e} \mathrm{d}z \to \int_{t_0}^{t_e} \mathrm{d}t$, and the contour step functions can be converted into real-time step functions, using $\theta(t_{1-}, t_{2-}) = \Theta(t_1 - t_2)$. For the backward branch, the replacement $\int_{\gamma_e} \mathrm{d}z \to -\int_{t_0}^{t_e} \mathrm{d}t$ yields an additional minus sign due to the reversal of the integration direction, yielding an extra factor of $(-1)^j$ from the backward-branch integrations. The conversion of contour step functions to real-time step functions is reversed as compared to the forward branch, since $\theta(t_{1+}, t_{2+}) = \Theta(t_2 - t_1)$. We now use the short-hand notation $\Theta(t_{n_1}, \ldots, t_{n_N}) = \Theta_{n_1\cdots n_N}$, allowing Eq. (39) to be written in the form

$$O^1(t_e) = \sum_{j=0}^{I} \sum_{P\in S_I} \int_{t_0}^{\infty} \mathrm{d}t_{\mathcal{I}} (-1)^j \Theta_{eP(i_j\cdots i_1)} \Theta_{eP(i_{j+1}\cdots i_I)} \bar{O}^{(\check{P},j)}(t_e, t_{\mathcal{I}}), \tag{40}$$

where we have placed t_e back into the step-functions, and extended the integral to infinity.

To elucidate the structure of Eq. (40) we give examples for one ($I = 1$) and two ($I = 2$) integrations.

For $I = 1$, the sum over permutations in Eq. (40) yields one term, and the j-sum yields two terms:

$$O^1(t_e) = \int_{t_0}^{\infty} \mathrm{d}t_{i_1} \left(\Theta_{ei_1} \bar{O}^{\check{e}\check{i}_1}(t_e, t_{i_1}) - \Theta_{ei_1} \bar{O}^{\check{i}_1\check{e}}(t_e, t_{i_1}) \right) = \int_{t_0}^{\infty} \mathrm{d}t_{i_1} \Theta_{ei_1} \bar{O}^{[\check{e},\check{i}_1]}(t_e, t_{i_1}), \tag{41}$$

where we have defined the commutator $[\check{e}, \check{i}_1] = \check{e}\check{i}_1 - \check{i}_1\check{e}$ and used the short-hand notation introduced in Eq. (21). Defining the retarded composition of two arguments as

$$\bar{O}^{R(\check{e},\check{i}_1)}(t_e, t_{i_1}) = \Theta_{ei_1} \bar{O}^{[\check{e},\check{i}_1]}(t_e, t_{i_1}). \tag{42}$$

we obtain the compact expression

$$O^1(t_e) = \int_{t_0}^{\infty} \mathrm{d}t_{i_1} \bar{O}^{R(\check{e},\check{i}_1)}(t_e, t_{i_1}). \tag{43}$$

Let us now consider $I = 2$, and the equation

$$\mathscr{O}(z_e) = \int_{\gamma_e} \mathrm{d}z_{i_1} \mathrm{d}z_{i_2} \bar{\mathscr{O}}(z_e, z_{i_1}, z_{i_2}), \tag{44}$$

Eq. (40) gives after writing out the j sum:

$$O^1(t_e) = \int_{t_0}^{\infty} \mathrm{d}t_{i_1}\mathrm{d}t_{i_2} \sum_{P\in S_2} \times \big[\underbrace{\Theta_{eP(i_1i_2)}\bar{O}^{\check{e}P(\check{i}_1)P(\check{i}_2)}}_{j=0} - \underbrace{\Theta_{eP(i_1)}\Theta_{eP(i_2)}\bar{O}^{P(\check{i}_1)\check{e}P(\check{i}_2)}}_{j=1} + \underbrace{\Theta_{eP(i_2i_1)}\bar{O}^{P(\check{i}_1)P(\check{i}_2)\check{e}}}_{j=2}\big]. \tag{45}$$

We will break the derivation from this point into three steps, so that it can be easily compared with the derivation of the general result, that follows the same steps.

(i) First the step-functions in the $j = 1$ term in Eq. (45) are written in the form $\Theta_{eP(i_1)}\Theta_{eP(i_2)} = \Theta_{eP(i_1i_2)} + \Theta_{eP(i_2i_1)}$.

(ii) Next we relabel permutations in the two terms containing $\Theta_{eP(i_2i_1)}$, so that $P(i_1)$ and $P(i_2)$ are swapped. We can then factor out the step function $\Theta_{eP(i_1i_2)}$ to obtain

$$O^1(t_e) = \int_{t_0}^{\infty} \mathrm{d}t_{i_1}\mathrm{d}t_{i_2} \sum_{P\in S_2} \times \Theta_{eP(i_1i_2)}\big[\bar{O}^{\check{e}P(\check{i}_1)P(\check{i}_2)} - \bar{O}^{P(\check{i}_1)\check{e}P(\check{i}_2)} - \bar{O}^{P(\check{i}_2)\check{e}P(\check{i}_1)} + \bar{O}^{P(\check{i}_2)P(\check{i}_1)\check{e}}\big]. \tag{46}$$

(iii) Finally we observe that the sum of terms in the square brackets in Eq. (46) can be written as

$$\bar{O}^{\check{e}P(\check{i}_1)P(\check{i}_2)} - \bar{O}^{P(\check{i}_1)\check{e}P(\check{i}_2)} - \bar{O}^{P(\check{i}_2)\check{e}P(\check{i}_1)} + \bar{O}^{P(\check{i}_2)P(\check{i}_1)\check{e}} = \bar{O}^{[\check{e},P(\check{i}_1),P(\check{i}_2)]}, \tag{47}$$

where $[a,b,c] = [[a,b],c]$ is a nested commutator (see Appendix B for a discussion on properties of nested commutators). Defining a generalized retarded composition as

$$\bar{O}^{R(\check{e},\check{i}_1\check{i}_2)}(t_e,t_{i_1},t_{i_2}) = \sum_{P\in S_2}\Theta_{eP(i_1i_2)}\bar{O}^{[\check{e},P(\check{i}_1),P(\check{i}_2)]}, \tag{48}$$

then leads to the compact result

$$O^1(t_e) = \int_{t_0}^{\infty}\mathrm{d}t_{i_1}\mathrm{d}t_{i_2}\bar{O}^{R(\check{e},\check{i}_1\check{i}_2)}(t_e,t_{i_1},t_{i_2}). \tag{49}$$

We now show that the general case of $I = N$ can be rewritten in terms of generalized retarded compositions. The proof proceeds by the same three steps as used above for the $I = 2$ case.

(i) The product of step functions in Eq. (40) is written as a sum of step-functions as

$$\Theta_{eP(i_j\cdots i_1)}\Theta_{eP(i_{j+1}\cdots i_I)} = \sum_{T\in\mathcal{T}_{I,j}}\Theta_{eT(P(i_1))T(P(i_2))\cdots T(P(i_I)))} = \sum_{T\in\mathcal{T}_{I,j}}\Theta_{eT\circ P(\mathcal{I})}. \tag{50}$$

Here the set $\mathcal{T}_{I,j}$ contains every permutation of the arguments $\mathcal{I}$ for which the subsets $\{i_j,\ldots,i_1\}$ and $\{i_{j+1},\ldots,i_I\}$ remain in the same relative order as given by the step-functions on the left-hand side. Graphically this corresponds to every

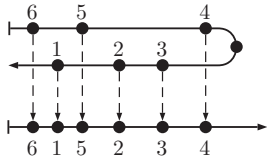

Figure 4. An example of a permutation belonging to the set $\mathcal{T}_{6,3}$, permuting 123456 to 432516. Note that the relative order of 456 is retained, while the order of 123 is inverted. Moving the arguments on the upper contour without changing their order generates all the permutations in $\mathcal{T}_{6,3}$.

permutation that can result from projecting the forward and backward branches vertically to the same axis (see figure 4).
The structure of these permutations is derived in detail in Appendix A. Eq. (40) now takes the form

$$O^1(t_e) = \sum_{j=0}^{I} \sum_{P\in S_I} \sum_{T\in\mathcal{T}_{I,j}} \int_{t_0}^{\infty} \mathrm{d}t_{\mathcal{I}}\ (-1)^j \Theta_{e\,T\circ P(\mathcal{I})} \bar{O}^{(\check{P},j)}(t_e, t_{\mathcal{I}}). \tag{51}$$

(ii) Since we sum over all permutations P in the group S_I, we can equivalently sum over all permutations $U = T \circ P$, where $U \in S_I$. Inserting this relation into Eq. (51), and reordering, yields

$$O^1(t_e) = \sum_{U\in S_I} \int_{t_0}^{\infty} \mathrm{d}t_{\mathcal{I}}\ \Theta_{e\,U(\mathcal{I})} \sum_{j=0}^{I} \sum_{T\in\mathcal{T}_{I,j}} (-1)^j \bar{O}^{(\check{T^{-1}}\circ U,j)}(t_e, t_{\mathcal{I}}). \tag{52}$$

(iii) Finally we will show that the sum over components of $\bar{O}$ in Eq. (52) corresponds to a nested commutator:

$$\sum_{j=0}^{I} \sum_{T\in\mathcal{T}_{I,j}} (-1)^j \bar{O}^{(\check{T^{-1}}\circ U,j)}(t_e, t_{\mathcal{I}}) = \bar{O}^{[\check{e},U(\check{i}_1),U(\check{i}_2),\cdots,U(\check{i}_I)]}(t_e, t_{\mathcal{I}}). \tag{53}$$

It is sufficient to consider Eq. (53) for the identity permutation $U(i_1 \cdots i_I) = i_1 \cdots i_I$, as the general case simply follows from relabeling. Let us also focus on a specific j term. Using the definition of (T^{-1}, j), Eq. (37), we have

$$\sum_{T\in\mathcal{T}_{I,j}} (-1)^j (T^{-1}, j) = \sum_{T\in\mathcal{T}_{I,j}} (-1)^j T^{-1}(i_1 \cdots i_j)\, e\, T^{-1}(i_{j+1} \cdots i_I). \tag{54}$$

The permutations T^{-1} are the inverse of those considered in step (i), and can thus be represented by inverting the arrows in figure 4, see figure 5. Thus permutation T^{-1}, when $T \in \mathcal{T}_{I,j}$, permutes $1 \cdots I$ in such a way that the first j arguments are in decreasing order and the remaining $I - j$ arguments are in increasing order. These are exactly the permutations generated by $[e, 1, 2, \ldots, I]_j$, i.e. the part of the nested commutator with j elements to the left of e (see the discussion in Appendix B).

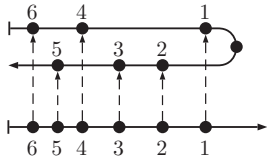

Figure 5. An example of an inverse of a permutation belonging to the set $\mathcal{T}_{6,3}$, permuting 123456 to 532146. Since $j = 3$, three arguments are moved to the backward branch. Inverses of all the permutations in $\mathcal{T}_{6,3}$ are generated by all the possible ways to place three arguments on the backward branch, and three on the forward branch. Thus there are 6!/3! permutations in $\mathcal{T}_{6,3}$.

Furthermore, since a nested commutator generates a minus sign for each element to left of e, it has the sign $(-1)^j$, matching that in Eq. (54). We thus have

$$\sum_{T\in\mathcal{T}_{I,j}} (-1)^j T^{-1}(i_1\cdots i_j)\, e\, T^{-1}(i_{j+1}\cdots i_I) = [e, i_1, \cdots, i_I]_j. \tag{55}$$

A more rigorous derivation of Eq. (55) is found by comparing the definitions of the permutations $T^{-1}(i_1\cdots i_I)$, found in Eq. (A.8), to the permutations Q given in Eq. (B.7). The definitions are identical, and thus (55) follows directly from Eq. (B.4).

The full nested commutator is given by $[e, i_1, \cdots, i_I] = \sum_j [e, i_1, \cdots, i_I]_j$. Summing over j in Eq. (53) thus yields the total nested commutator $[e, i_1, \cdots, i_I]$, which proves Eq. (53) for the identity permutation. The proof for other permutations follows in the same way from an initial relabeling.

Having proven Eq. (53), we now insert it into Eq. (52). By defining the retarded composition as

$$\bar{O}^{R(\check{e},\check{\mathcal{I}})}(t_e, t_{\mathcal{I}}) = \sum_{P\in S_I} \Theta_{eP(i_1 i_2\cdots i_I)} \bar{O}^{[\check{e},P(\check{i}_1),P(\check{i}_2),\cdots,P(\check{i}_I)]}(t_e, t_{\mathcal{I}}), \tag{56}$$

we obtain the final result

$$O^1(t_e) = \int_{t_0}^{\infty} \mathrm{d}t_{\mathcal{I}}\, \bar{O}^{R(\check{e},\check{\mathcal{I}})}(t_e, t_{\mathcal{I}}). \tag{57}$$

The function $\bar{O}^{R(\check{e},\check{\mathcal{I}})}$ is called a retarded composition of Keldysh components.

We call the ordered union $\{\check{e},\check{\mathcal{I}}\}$ a retarded set. Its first argument $\check{e}$ we call the top argument, and the arguments in $\check{\mathcal{I}}$ the retarded arguments. The retarded composition is non-zero only when the top argument has a higher real-time value than any of the retarded arguments. It follows from its definition in Eq. (56) that the retarded composition is symmetric with respect to permutations of the retarded arguments, so that:

$$\bar{O}^{R(\check{e},P(\check{\mathcal{I}}))}(t_e, t_{\mathcal{I}}) = \bar{O}^{R(\check{e},\check{\mathcal{I}})}(t_e, t_{\mathcal{I}}), \tag{58}$$

for any permutation $P \in S_I$. Note also that Eq. (56) is not unique in satisfying Eq. (57). In particular one could, if desired, symmetrize Eq. (56) with respect to the internal times without changing the integral in Eq. (57). We use the definition in Eq. (56) for its simplicity.

4.3. Multiple External and Internal Arguments

We now have all the pieces required to lay out the proof for the case with an arbitrary number of both internal I and external E arguments. Let us return to the equation

$$O(z_{\mathcal{E}}) = \int_{\gamma} \mathrm{d}z_{\mathcal{I}}\, \bar{O}(z_{\mathcal{N}}), \tag{59}$$

Let us take as an example the Keldysh component $O^{1\cdots E}$. We deform the contour γ into E loops, obtaining

$$\int_{\gamma} \mathrm{d}z = \Big(\int_{\gamma_{e_1}} + \ldots + \int_{\gamma_{e_E}} \Big) \mathrm{d}z. \tag{60}$$

For example for two external arguments we have two loops

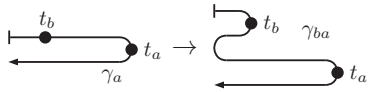

(61)

Substituting Eq. (60) for each integral in Eq. (59) results in a sum containing each possible distribution of the internal arguments among the loops. We write this as

$$\int_{\gamma} \mathrm{d}z_{\mathcal{I}} = \sum_{\mathcal{I}} \int_{\gamma_{e_1}} \mathrm{d}z_{\mathcal{I}_{e_1}} \ldots \int_{\gamma_{e_E}} \mathrm{d}z_{\mathcal{I}_{e_E}}, \tag{62}$$

where the sum is over every possible way to split the set $\mathcal{I}$ into the subsets $\mathcal{I}_{e_1}, \ldots, \mathcal{I}_{e_E}$, while retaining the relative order of the indices within each subset. $\int_{\gamma_{e_i}} \mathrm{d}z_{\mathcal{I}_{e_i}}$ denotes integrating the arguments $z_{\mathcal{I}_{e_i}}$ over the loop γ_{e_i}.

In each term of the $\mathcal{I}$ sum, we can handle the integral over each loop γ_{e_i} separately, because the arguments on the other loops are always earlier or later in contour time. Performing the integral over γ_{e_i}, we obtain a composition in which $t_{\mathcal{I}_{e_i}}$ are retarded with respect to t_{e_i}, leading to

$$O^{\check{e}_1 \cdots \check{e}_E}(t_{\mathcal{E}}) = \sum_{\mathcal{I}} \int_{t_0}^{\infty} \mathrm{d}t_{\mathcal{I}}\, \bar{O}^{R(\check{e}_1, \check{\mathcal{I}}_1) \cdots R(\check{e}_E, \check{\mathcal{I}}_E)}(t_{\mathcal{N}}). \tag{63}$$

We note that since $z_{\mathcal{E}}$ is ordered as $(e_1, \cdots, e_E)$, it follows that $\check{e}_1 \cdots \check{e}_E = 1 \cdots E$. All other Keldysh components can be obtained from Eq. (63) by permuting $1, \ldots, E$ on both sides. The integrand in Eq. (63) is a general type of multi-retarded composition defined as

$$\bar{O}^{R(\check{e}_1, \check{\mathcal{I}}_1) \cdots R(\check{e}_E, \check{\mathcal{I}}_E)}(t_{\mathcal{N}}) = \sum_{P_1 \in S_{I_1}} \Theta_{e_1 P_1(\mathcal{I}_1)} \cdots \sum_{P_E \in S_{I_E}} \Theta_{e_E P_E(\mathcal{I}_E)} \bar{O}^{[\check{e}_1, P_1(\mathcal{I}_1)] \cdots [\check{e}_E, P_E(\mathcal{I}_E)]}(t_{\mathcal{N}}), \tag{64}$$

where I_k is the number of elements in the set $\mathcal{I}_k$, and we define $\Theta_{eP(\mathcal{I})} = \Theta_{eP(i_1)\cdots P(i_I)}$ for $\mathcal{I} = \{i_1, \ldots, i_I\}$. We furthermore define the nested commutator

$$[e, P(\mathcal{I})] = [e, P(i_1), \ldots, P(i_I)], \tag{65}$$

see Appendix B for further details. Note that in Eq. (64) some of the sets $\mathcal{I}_i$ can be empty, in which case one substitutes $R(\check{e}_i, \emptyset) \to \check{e}_i$, and correspondingly $[\check{e}_i, \emptyset] \to \check{e}_i$. For example for one internal argument all the sets are empty except one, and Eq. (63) reduces to

$$O^{\check{e}_1\cdots\check{e}_E}(t_{\mathcal{E}}) = \int_{t_0}^{\infty} \mathrm{d}t_i \sum_{k=1}^{E} \bar{O}^{\check{e}_1\cdots R(\check{e}_k,\check{i})\cdots\check{e}_E}(t_{\mathcal{N}}). \tag{66}$$

The definition of a multi-retarded composition subsumes both the completely retarded compositions defined in Eq. (56) (when $E = 1$) and the Keldysh components (when $E = N$ and thus all $\mathcal{I}_i$ are empty).

Let us now illustrate Eq. (63) with an example. We apply the equation to a four-point function when we integrate two arguments:

$$\mathscr{D}(z_a, z_d) = \int_\gamma \mathrm{d}z_b \mathrm{d}z_c\, \bar{\mathscr{D}}(z_a, z_b, z_c, z_d). \tag{67}$$

In Eq. (67), the internal arguments constitute the set $\mathcal{I} = \{b, c\}$, and the external arguments are in $\mathcal{E} = \{a, d\}$. The four possible divisions of $\mathcal{I}$ into two subsets are $\{\mathcal{I}_1, \mathcal{I}_2\} = \{\{b, c\}, \emptyset\}$, and $\{\{b\}, \{c\}\}$, and $\{\{c\}, \{b\}\}$, and $\{\emptyset, \{b, c\}\}$.

The component D^{12}_{ad} is given by Eq. (63):

$$\begin{aligned} D^{12}_{ad} &= \int \bar{D}^{R(\check{a},\check{b}\check{c})\check{d}}_{a\bar{b}\bar{c}d} + \int \bar{D}^{R(\check{a},\check{b})R(\check{d},\check{c})}_{a\bar{b}\bar{c}d} + \int \bar{D}^{R(\check{a},\check{c})R(\check{d},\check{b})}_{a\bar{b}\bar{c}d} + \int \bar{D}^{\check{a}R(\check{d},\check{b}\check{c})}_{a\bar{b}\bar{c}d} \\ &= \int \bar{D}^{R(1,23)4}_{a\bar{b}\bar{c}d} + \int \bar{D}^{R(1,2)R(4,3)}_{a\bar{b}\bar{c}d} + \int \bar{D}^{R(1,3)R(4,2)}_{a\bar{b}\bar{c}d} + \int \bar{D}^{1R(4,23)}_{a\bar{b}\bar{c}d}, \end{aligned} \tag{68}$$

where the integrals are over the barred arguments (real-time integrals are from t_0 to ∞ unless otherwise stated). This equation illustrates the usefulness of the háček notation, as for example the argument z_d denotes the second argument of D but the fourth argument of the integrand $\bar{D}$. The other component D^{21}_{ad} is obtained by reordering the retarded sets so that d comes after a in the contour order:

$$D^{21}_{ad} = \int \bar{D}^{4R(1,23)}_{a\bar{b}\bar{c}d} + \int \bar{D}^{R(4,3)R(1,2)}_{a\bar{b}\bar{c}d} + \int \bar{D}^{R(4,2)R(1,3)}_{a\bar{b}\bar{c}d} + \int \bar{D}^{R(4,23)1}_{a\bar{b}\bar{c}d}. \tag{69}$$

The retarded compositions appearing in the real-time integrals can be calculated from the Keldysh components using the equation for multi-retarded compositions, Eq. (64):

$$\bar{O}^{R(1,23)4}_{abcd} = \Theta_{abc}\bar{O}^{[[1,2],3]4}_{abcd} + \Theta_{acb}\bar{O}^{[[1,3],2]4}_{abcd} \tag{70}$$

$$\bar{O}^{R(1,2)R(4,3)}_{abcd} = \Theta_{ab}\Theta_{dc}\bar{O}^{[1,2][4,3]}_{abcd}. \tag{71}$$

4.4. The Diagrammatic Representation

The previous discussion of obtaining different real-time components was mostly algebraical. In this section we describe a diagrammatic recipe for obtaining the components. The recipe includes four steps.

(i) Write the initial contour equation in diagrammatic form.

(ii) Choose a Keldysh component.

(iii) Represent the various terms using diagrammatic rules.

(iv) Convert the result into a real-time expression.

We will use as an example the equation

$$\mathscr{D}(z_a, z_d) = \int_\gamma \mathrm{d}z_b \mathrm{d}z_c \, \bar{\mathscr{D}}(z_a, z_b, z_c, z_d). \tag{72}$$

The steps are performed as follows.

(i) The contour functions are depicted by collections of vertices representing their arguments. We use filled circles for external arguments and empty circles for internal arguments. For Eq. (72) we draw

$\mathscr{D}_{ad} = \int \bar{\mathscr{D}}_{a\bar{b}\bar{c}d}$ → 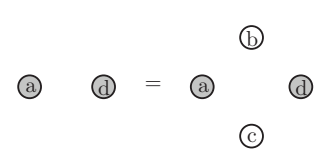 (73)

(ii) We choose the Keldysh component by drawing a contour through the external vertices to determine their ordering:

 : z_a comes after z_b on the contour. (74)

The contour must be drawn in the same way on both sides of the equation. Choosing the component $D^{21}_{ad} = D^{\check{d}\check{a}}_{ad}$ we obtain from Eq. (73)

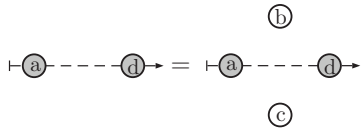 (75)

(iii) Each internal vertex is assigned to a retarded set with an external vertex, marked by a double circle, as the top argument. We denote a retarded set diagrammatically by circling the vertices in it:

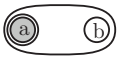 : $R(\check{a}, \check{b})$ (t_b is retarded with respect to t_a) (76)

If assigning the internal vertices to retarded sets can be done in multiple ways, each option generates a separate diagram. Thus the right hand side of Eq. (75) becomes

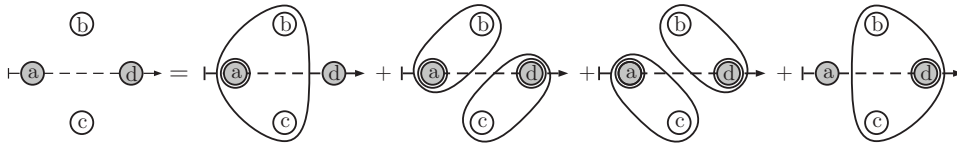

(77)

(iv) Each diagram is converted to a single retarded composition using two rules:

(a) For every circled set of vertices, one obtains a retarded set:

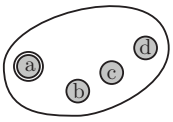

$$\rightarrow \quad R(\check{a}, \check{b}\check{c}\check{d}) \tag{78}$$

(b) The retarded sets are ordered according to their order on the contour in the diagram.

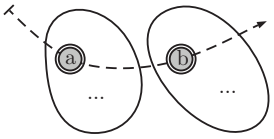

$$\rightarrow \quad R(\check{b}, \cdots)R(\check{a}, \cdots) \quad (z_b > z_a) \tag{79}$$

For the example case we then obtain

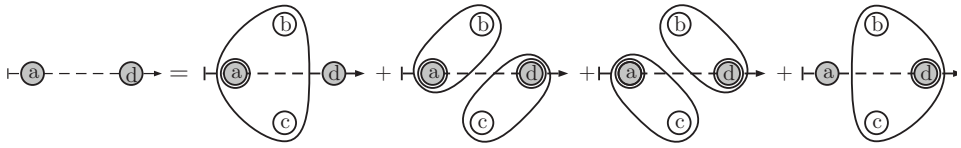

$$D^{\check{d}\check{a}}_{ad} \quad = \quad \bar{D}^{\check{d}R(\check{a},\check{b}\check{c})}_{a\bar{b}\bar{c}d} \quad + \quad \bar{D}^{R(\check{d},\check{c})R(\check{a},\check{b})}_{a\bar{b}\bar{c}d} \quad + \quad \bar{D}^{R(\check{d},\check{b})R(\check{a},\check{c})}_{a\bar{b}\bar{c}d} \quad + \quad \bar{D}^{R(\check{d},\check{b}\check{c})\check{a}}_{a\bar{b}\bar{c}d}, \tag{80}$$

where we integrate over all barred arguments. Writing the argument positions explicitly we obtain the result we obtained algebraically in Eq. (69).

The diagrammatic procedure described above can be applied to obtain any Keldysh components of a general n-point Keldysh function.

4.5. Obtaining Retarded Compositions

In the previous section we discussed a diagrammatic recipe for obtaining real-time Keldysh components, the result being expressed in terms of retarded compositions. It is possible to generalize the recipe to directly obtain these retarded compositions [8].

Diagrammatically, this fits elegantly with what has been presented so far. Here we introduce the diagrammatic recipe, and refer to Appendix D for a derivation.

As an example, we consider a case with five external variables and two internal ones:

$$\mathscr{E}(z_a, z_b, z_c, z_d, z_e) = \int_\gamma \mathrm{d}z_f \mathrm{d}z_g \, \bar{\mathscr{E}}(z_a, z_b, z_c, z_d, z_e, z_f, z_g), \tag{81}$$

and calculate the retarded composition $E^{R(1,2)R(3,45)} = E^{R(\check{a},\check{b})R(\check{c},\check{d}\check{e})}$. We perform the same four steps as for Keldysh components:

(i) The diagrammatic equation for Eq. (81) is

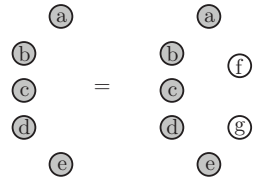

(82)

(ii) To choose the desired composition $E^{R(\check{a},\check{b})R(\check{c},\check{d}\check{e})}$ we encircle the retarded sets $R(\check{a},\check{b})$ and $R(\check{c},\check{d}\check{e})$ separately, and order the sets by drawing a contour through a and c:

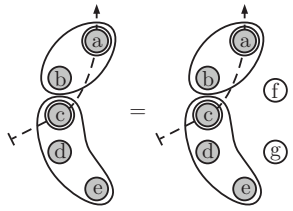

(83)

(iii) The internal vertices are now assigned to retarded sets. If an external vertex is already within a retarded set, the internal vertices are simply added to the pre-existing set. Each different possibility generates a diagram, and we obtain

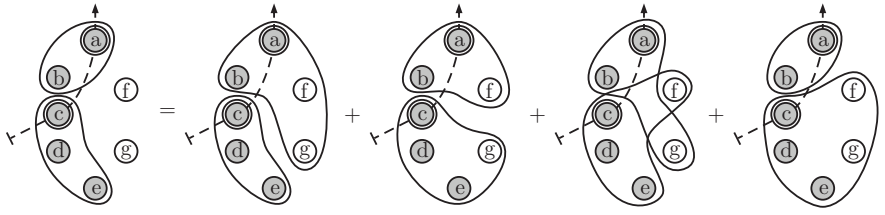

(84)

(iv) We can then directly read off the retarded representation

$$\begin{aligned} &E^{R(\check{a},\check{b})R(\check{c},\check{d}\check{e})}_{abcde} \\ &= \int \bar{E}^{R(\check{a},\check{b}\check{f}\check{g})R(\check{c},\check{d}\check{e})}_{abcde\bar{f}\bar{g}} + \int \bar{E}^{R(\check{a},\check{b}\check{f})R(\check{c},\check{d}\check{e}\check{g})}_{abcde\bar{f}\bar{g}} + \int \bar{E}^{R(\check{a},\check{b}\check{g})R(\check{c},\check{d}\check{e}\check{f})}_{abcde\bar{f}\bar{g}} + \int \bar{E}^{R(\check{a},\check{b})R(\check{c},\check{d}\check{e}\check{f}\check{g})}_{abcde\bar{f}\bar{g}}. \end{aligned} \tag{85}$$

As seen in the example studied above, a retarded composition is obtained by summing over all different distributions of the internal vertices into retarded sets. In general, if

$$\mathscr{O}(z_{\mathcal{E}}) = \int_{\gamma} \mathrm{d}z_{\mathcal{I}}\, \bar{\mathscr{O}}(z_{\mathcal{N}}), \tag{86}$$

then a general multi-retarded composition with H retarded sets, as defined in Eq. (64), will be given by

$$O^{R(\check{h}_1,\check{\mathcal{H}}_1)\cdots R(\check{h}_H,\check{\mathcal{H}}_H)}(t_{\mathcal{E}}) = \sum_{\mathcal{I}} \int \mathrm{d}t_{\mathcal{I}}\, \bar{O}^{R(\check{h}_1,\check{\mathcal{H}}_1\cup\check{\mathcal{I}}_1)\cdots R(\check{h}_H,\check{\mathcal{H}}_H\cup\check{\mathcal{I}}_H)}(t_{\mathcal{N}}), \tag{87}$$

where $\{h_1,\ldots,h_H\}$ and $\mathcal{H}_0,\ldots,\mathcal{H}_H$ constitute a non-overlapping cover of $\mathcal{E}$. A proof of Eq. (87) is presented in Appendix D (Eq. (87) is equivalent to Eq (4.18) in Danielewicz [8]). In our example Eq. (85), $E^{R(\check{a},\check{b})R(\check{c},\check{d}\check{e})}_{abcde}$ corresponds to $h_1 = a, \mathcal{H}_1 = \{b\}$, and $h_2 = c$, $\mathcal{H}_2 = \{d,e\}$. The possible internal sets $\mathcal{I}$ that are summed over are $\{\mathcal{I}_1,\mathcal{I}_2\} = \{\{f,g\},\emptyset\}$, and $\{\{f\},\{g\}\}$, and $\{\{g\},\{f\}\}$, and $\{\emptyset,\{f,g\}\}$. Note that when the left-hand side of Eq. (87) is a Keldysh component, $\mathcal{H}_i = \emptyset$, the equation reduces to Eq. (63).

5. The Extended Contour

5.1. Matsubara-Restricted Keldysh Functions

We now generalize the discussion of the previous two sections to the case of the extended contour. For a Keldysh function on the extended contour, $\mathscr{O}(z_{\mathcal{N}})$ the arguments can take values on the Matsubara branch ($z = t_0 - it$) as well as on the horizontal Keldysh branches ($z = t_\pm$). Out of the total set of arguments $\mathcal{N}$, we can select a set $\mathcal{M}$ of arguments on the Matsubara branch γ_M, and $\mathcal{K}$ arguments on the Keldysh branch. Naturally, $\mathcal{N} = \mathcal{K}\cup\mathcal{M}$. Selecting a time $z_m = t_0 - it_m$ on the Matsubara branch yields a real-time function of t_m. For the remaining arguments on the Keldysh contour, the function is still a Keldysh function. Any such function in which we restrict the domain we refer to as an *Matsubara-restricted Keldysh function* (MK-function) $\mathscr{O}^{M(\check{\mathcal{M}})}(t_{\mathcal{M}}\cup z_{\mathcal{K}})$, defined by

$$\mathscr{O}^{M(\check{\mathcal{M}})}(t_{\mathcal{M}}\cup z_{\mathcal{K}}) = \sum_{Q\in S_M} \Theta(t_{Q(\mathcal{M})}) \sum_{P\in S_K} \theta(z_{P(\mathcal{K})}) O^{M(Q(\check{\mathcal{M}}))P(\check{\mathcal{K}})}(t_{\mathcal{N}}). \tag{88}$$

Note that the union set designation $t_{\mathcal{M}}\cup z_{\mathcal{K}}$ is just for convenience of notation and does not imply that the arguments t_M are earlier in the argument list. We have used the fact that all the Matsubara arguments are later in contour time than any of the arguments on the Keldysh contour. When no argument is on the Matsubara branch, $\mathcal{M} = \emptyset$, we obtain a Keldysh function of a type we considered previously $\mathscr{O}^{\mathcal{M}(\emptyset)}(z_{\mathcal{N}}) = \mathscr{O}(z_{\mathcal{N}})$. The equation above can be rewritten as

$$\mathscr{O}^{M(\check{\mathcal{M}})}(t_{\mathcal{M}}\cup z_{\mathcal{K}}) = \sum_{P\in S_K} \theta(z_{P(\mathcal{K})}) O_S^{M(\check{\mathcal{M}})P(\check{\mathcal{K}})}(t_{\mathcal{N}}), \tag{89}$$

where we have defined the symmetrized Matsubara function

$$O_S^{M(\check{\mathcal{M}})P(\check{K})}(t_{\mathcal{N}}) = \sum_{Q\in S_M} \Theta(t_{Q(\mathcal{M})}) O^{M(Q(\check{\mathcal{M}}))P(\check{K})}(t_{\mathcal{N}}). \tag{90}$$

The symmetrized functions are symmetric under exchanging the order of the Matsubara labels in the super index.

For example, for a four-point Keldysh function $\mathscr{C}(z_a, z_b, z_c, z_d)$, if z_a, z_c are on the Matsubara branch and z_b, z_d on the Keldysh branch, the symmetrized Matsubara function is

$$O_S^{M(\check{a}\check{c})P(\check{b})P(\check{d})}(t_a, t_b, t_c, t_d) = \sum_{Q\in S_2} \Theta(t_{Q(a)} - t_{Q(c)}) O^{M(Q(\check{a})Q(\check{c}))P(\check{b})P(\check{d})}(t_a, t_b, t_c, t_d). \tag{91}$$

The MK function can be written according to Eq. (89) as

$$\mathscr{O}^{M(\check{a}\check{c})}(t_a, z_b, t_c, z_d) = \sum_{P\in S_2} \theta(z_{P(b)}, z_{P(d)}) O_S^{M(\check{a}\check{c})P(\check{b})P(\check{d})}(t_a, t_b, t_c, t_d). \tag{92}$$

In the following, we only work with the symmetrized functions, and will therefore drop the sub-index S from the general expansion Eq. (89). Each of the components in this expansion we will still call a Keldysh component.

Since MK functions are Keldysh functions, multiplications and convolutions between MK functions are again MK functions. Also, retarded compositions will appear naturally from integrations, as will be seen below. Retarded compositions of MK functions have the form

$$O^{M(\check{\mathcal{M}})R(\check{h}_1,\check{\mathcal{H}}_1)\cdots R(\check{h}_H,\check{\mathcal{H}}_H)}(t_{\mathcal{N}}), \tag{93}$$

where $\{h_1, \ldots, h_H\}, \mathcal{M}, \mathcal{H}_0, \ldots, \mathcal{H}_H$ constitute a non-overlapping cover of $\mathcal{N}$.

5.2. Integrals over the Extended Contour

Let us now consider an integral over the extended contour:

$$\mathscr{O}(z_{\mathcal{E}}) = \int_{\gamma'} \mathrm{d}z_{\mathcal{I}}\, \bar{\mathscr{O}}(z_{\mathcal{N}}). \tag{94}$$

Our basic strategy is to split the integrations as $\int_{\gamma'} = \int_{\gamma_M} + \int_{\gamma}$ and in each integral replace the integrand with a suitable MK function. This breaks the right-hand side of Eq. (94) into terms containing real-time integrals over the Matsubara branch and integrals over the Keldysh contour, for which results were derived previously.

Take for example the equation

$$\mathscr{D}_{ad} = \int_{\gamma'} \mathrm{d}z_b \mathrm{d}z_c\, \bar{\mathscr{D}}_{abcd} = \int_{\gamma'} \bar{\mathscr{D}}_{a\check{b}\check{c}d}, \tag{95}$$

where we introduced the notation that we integrate over barred variables. Suppose now that a and d are on the Keldysh branches. The substitution $\int_{\gamma'} = \int_{\gamma_M} + \int_{\gamma}$ generates four terms, in each of which we can replace $\bar{\mathscr{D}}$ by an MK function. We obtain

$$\mathscr{D}_{ad} = \int_{\gamma'} \bar{\mathscr{D}}_{a\bar{b}\bar{c}d} = \int \bar{\mathscr{D}}^{M(\check{b}\check{c})}_{a\bar{b}\bar{c}d} + \int \bar{\mathscr{D}}^{M(\check{b})}_{a\bar{b}\bar{c}d} + \int \bar{\mathscr{D}}^{M(\check{c})}_{a\bar{b}\bar{c}d} + \int \bar{\mathscr{D}}_{a\bar{b}\bar{c}d}, \quad a, d \in \mathcal{K}, \tag{96}$$

where the unspecified integrals are over the Matsubara branch if the barred argument is part of the Matsubara set, and over the Keldysh contour otherwise. Integrals over the Matsubara branch take the form

$$\int_{\gamma_M} \mathrm{d}z_i \, \mathscr{O}(z_i) = -i \int_0^1 \mathrm{d}t_i \, \mathscr{O}(t_0 - it_i) = -i \int_0^1 \mathrm{d}t_i \, O^{M(\check{\imath})}(t_i). \tag{97}$$

Thus the $\int$-sign in Eq. (96) contains an implicit factor $(-i)^M$, with M the number of arguments in the Matsubara set. Diagrammatically we denote Eq. (96) by

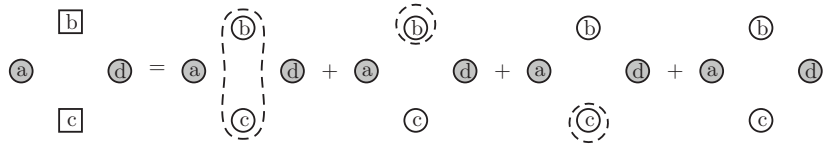

(98)

where internal vertices that we integrate over the extended contour γ' are denoted by squares, and vertex labels in a Matsubara set are circled by a dashed line. Once we choose the component, the retarded set representation can be obtained for each of these terms, by regarding the Matsubara vertices as spectators. This yields, for example for the component $D^{12}_{ad} = D^{\check{a}\check{d}}_{ad}$ and the second term in Eq. (96),

$$\int \bar{\mathscr{D}}^{M(\check{b})\check{a}\check{d}}_{a\bar{b}\bar{c}d} = \int \bar{D}^{M(\check{b})R(\check{a},\check{c})\check{d}}_{a\bar{b}\bar{c}d} + \int \bar{D}^{M(\check{b})\check{a}R(\check{d},\check{c})}_{a\bar{b}\bar{c}d}, \tag{99}$$

which we write diagrammatically as

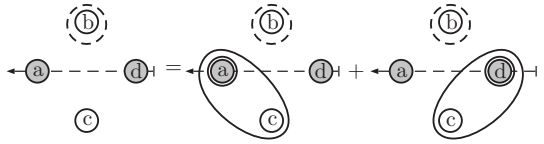

(100)

The diagrammatic recipe on the extended contour can be described using the same four steps as for the Keldysh contour, given in section 4.4. The only difference is, that in step iii) there are additional diagrams resulting from placing internal vertex labels in the Matsubara set.

Real-time components with one or more external arguments on the Matsubara branch can be obtained through the same steps. As an example, $D_{ab}^{M(\check{a})\check{d}}$ is

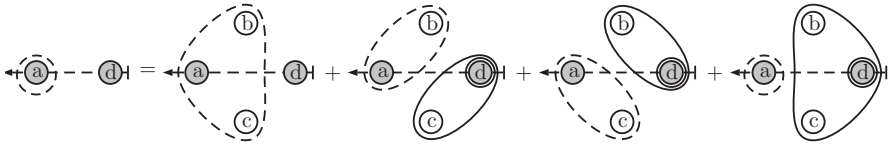

(101)

which corresponds to the equation

$$D_{ad}^{M(\check{a})\check{d}} = \int \bar{D}_{a\bar{b}\bar{c}d}^{M(\check{a}\check{b}\check{c})\check{d}} + \int \bar{D}_{a\bar{b}\bar{c}d}^{M(\check{a}\check{b})R(\check{d},\check{c})} + \int \bar{D}_{a\bar{b}\bar{c}d}^{M(\check{a}\check{c})R(\check{d},\check{b})} + \int \bar{D}_{a\bar{b}\bar{c}d}^{M(\check{a})R(\check{d},\check{b}\check{c})}. \tag{102}$$

The general equations on the extended contour are closely related to the equations derived above on the Keldysh contour. For a Keldysh component of an MK function with no arguments on the Matsubara branch we have

$$O^{\check{e}_1\cdots\check{e}_E}(t_{\mathcal{E}}) = \sum_{\mathcal{I}} \int \mathrm{d}t_{\mathcal{I}}\, \bar{O}^{M(\check{\mathcal{I}}_0)R(\check{e}_1,\check{\mathcal{I}}_1)\ldots R(\check{e}_E,\check{\mathcal{I}}_E)}(t_{\mathcal{N}}), \tag{103}$$

which is identical to the result on the Keldysh contour (Eq. (63)), except that the sum also covers the additional set $\mathcal{I}_0$, containing the internal arguments on the Matsubara branch. A general retarded composition is given by a similarly modified version of Eq. (87):

$$O^{M(\check{\mathcal{H}}_0)R(\check{h}_1,\check{\mathcal{H}}_1)\cdots R(\check{h}_H,\check{\mathcal{H}}_H)}(t_{\mathcal{E}}) = \sum_{\mathcal{I}} \int \mathrm{d}t_{\mathcal{I}}\, \bar{O}^{M(\check{\mathcal{H}}_0\cup\check{\mathcal{I}}_0)R(\check{h}_1,\check{\mathcal{H}}_1\cup\check{\mathcal{I}}_1)\cdots R(\check{h}_H,\check{\mathcal{H}}_H\cup\check{\mathcal{I}}_H)}(t_{\mathcal{N}}). \tag{104}$$

The above equation is the most general form of a multi-retarded composition we consider. The Eq. (104) reduces to Eq. (103) by setting $\mathcal{H}_i = \emptyset$ for $i = 0, \ldots, H$, and to Eq. (87) by setting $\mathcal{H}_0 = \mathcal{I}_0 = \emptyset$. Note that if all the external parameters in Eq. (104) are in the Matsubara set $\mathcal{I}_0$, meaning that only $\mathcal{H}_0$ is non-empty, then all integrals reduce to integrals over the set $\mathcal{I}_0$, i.e. all integrals are over the Matsubara branch.

6. Deriving Langreth Rules

In the previous section we discussed a general integral equation of the form

$$\mathscr{O}(z_{\mathcal{E}}) = \int_{\gamma'} \mathrm{d}z_{\mathcal{I}}\, \bar{\mathscr{O}}(z_{\mathcal{N}}), \tag{105}$$

and obtained expressions for the retarded compositions of $\mathscr{O}$ in terms of the retarded compositions of Keldysh components of $\bar{\mathscr{O}}$. In practice $\bar{\mathscr{O}}$ typically has some structure in

terms of functions of fewer arguments, being for example a product of Green's functions appearing in a perturbation expansion, so that it takes the form

$$\bar{\mathscr{O}}(z_{\mathcal{N}}) = \prod_i \bar{\mathscr{O}}_i(z_{\mathcal{N}_i}). \tag{106}$$

where $\mathcal{N}_i \subset \mathcal{N}$. We call $\bar{\mathscr{O}}_i$ the sub-functions of $\bar{\mathscr{O}}$. By a *Langreth rule* we mean an equation that expresses a retarded composition of $\mathscr{O}$ in terms of retarded compositions of the sub-functions $\bar{\mathscr{O}}_i$.

For example, let us take the convolution:

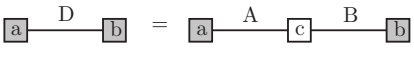

$$\mathscr{D}_{ab} = \int_{\gamma'} \mathscr{A}_{a\bar{c}}\mathscr{B}_{\bar{c}b}. \tag{107}$$

Suppose we are interested in the component D^{12}. The diagrammatic recipe gives

$$D^{\check{a}\check{b}}_{ab} = \int [\mathscr{A}_{a\bar{c}}\mathscr{B}_{\bar{c}b}]^{M(\bar{c})\check{a}\check{b}} + \int [\mathscr{A}_{a\bar{c}}\mathscr{B}_{\bar{c}b}]^{R(\check{a},\bar{c})\check{b}} + \int [\mathscr{A}_{a\bar{c}}\mathscr{B}_{\bar{c}b}]^{\check{a}R(\check{b},\bar{c})}, \tag{108}$$

where on the second line we have used the háček notation to avoid confusion between argument numbering in the sub-functions and the total function. The recipe, as laid out so far, thus leads to expressions containing retarded compositions of products of sub-functions. The issue faced in this section is how to evaluate such compositions directly in terms of the components of the sub-functions.

Before proceeding further, we will introduce some terminology:

- An n-point subfunction is diagrammatically represented by a polygon of n vertices representing the n arguments. For example, $n = 1$ is a dot, $n = 2$ is a line, and $n = 3$ is a triangle.
- Two subfunctions sharing the same argument correspond to a diagram in which two polygons share the same vertex.
  For example the expression $\mathscr{A}_{abcd}\mathscr{B}_{cdfgh}\mathscr{C}_{ijk}\mathscr{D}_{be}\mathscr{E}_{ef}$ converts to the diagram

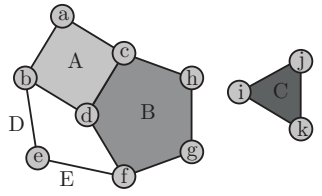

(109)

- Two vertices are *directly connected* if they belong to the same polygon, and therefore the corresponding arguments appear in the same sub-function.
- Two vertices are *connected* if there is a path consisting of polygon edges connecting them. Likewise the corresponding arguments of subfunctions are said to be connected.
- A set of vertices is *connected*, if each two vertices in the set are either directly connected or connected by an edge path that does not leave the set. If this is not the case, the set of vertices is *disconnected*. The same nomenclature is used for arguments.

6.1. Arguments on the Matsubara branch

The goal of this section is to express an MK function in terms of its sub-functions. Generally, an MK function $\mathscr{O}^{M(\check{\mathcal{M}})}(t_{\mathcal{M}} \cup z_{\mathcal{K}})$ for some $\mathcal{M} \subset \mathcal{N}$, can be worked out as follows. For sub-function $\bar{\mathscr{O}}_i$ we define $\mathcal{M}_i = \mathcal{M} \cap \mathcal{N}_i$ and $\mathcal{K}_i = \mathcal{N}_i \setminus \mathcal{M}_i$, one then has

$$\mathscr{O}^{M(\check{\mathcal{M}})}(t_{\mathcal{M}} \cup z_{\mathcal{K}}) = \prod_i \bar{\mathscr{O}}_i^{M(\check{\mathcal{M}}_i)}(t_{\mathcal{M}_i} \cup z_{\mathcal{K}_i}). \tag{110}$$

In practice one can simply move the Matsubara set superscript from the total function to each individual sub-function, as in

$$[\mathscr{A}_{a\bar{c}}\mathscr{B}_{\bar{c}b}]^{M(\check{c})} = \mathscr{A}_{a\bar{c}}^{M(\check{c})}\mathscr{B}_{\bar{c}b}^{M(\check{c})}, \tag{111}$$

while dropping from the Matsubara set any arguments that do not appear in the relevant sub-function. Note that since $\mathscr{A}^{M(\check{c})}(z_a, t_c)$ and $\mathscr{B}^{M(\check{c})}(t_c, z_b)$ are Keldysh functions of a single argument, they are equal to the MK-components $A^{M(\check{c})\check{a}}(t_a, t_c)$ and $B^{M(\check{c})\check{b}}(t_c, t_b)$ respectively. For example, if we take a product with vertex structure

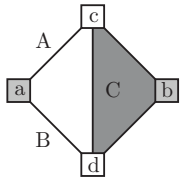

$$\int_{\gamma'} \mathscr{A}_{a\bar{c}}\mathscr{B}_{a\bar{d}}\mathscr{C}_{\bar{d}b\bar{c}}, \tag{112}$$

and calculate the MK function $[\cdots]^{M(\check{c})}$, the integrand is

$$[\mathscr{A}_{ac}\mathscr{B}_{ad}\mathscr{C}_{dbc}]^{M(\check{c})} = A_{ac}^{M(\check{c})\check{a}}\mathscr{B}_{ad}\mathscr{C}_{dbc}^{M(\check{c})}. \tag{113}$$

Diagrammatically the above equation corresponds to splitting the diagram into two separate pieces:

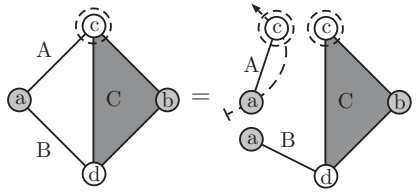

(114)

Thus any sub-function with some of its arguments in a Matsubara set, reduces to the corresponding MK function. If no more than one argument is outside a Matsubara set, the sub-function reduces immediately to a real-time MK component. The real-time components can then be separated from the diagram, leaving behind a simpler diagram on the Keldysh contour. For example, in Eq. (114), A can be separated in the integrand, and what remains is essentially a convolution between two-point functions, since $\mathscr{C}_{dbc}^{M(\check{c})}(z_a, z_b, t_c)$ is a two-point Keldysh function with an additional real-time argument. The problem on the extended contour is then essentially reduced to the problem on the Keldysh contour, which we will discuss in the next sections.

6.2. Arguments on the Keldysh branch

We take now all the arguments on the Keldysh contour, and consider Keldysh components of products. As an example we consider $C^{\check{a}\check{b}\check{c}}_{abc} = [\mathscr{A}_{ac}\mathscr{B}_{cb}]^{\check{a}\check{b}\check{c}}$, which is, by definition, given by the real-time function that describes the product $\mathscr{A}_{ac}\mathscr{B}_{cb}$ in the $z_a > z_b > z_c$ subspace. In this subspace the product takes the form

$$\mathscr{A}_{ac}\mathscr{B}_{cb} = [\underbrace{\theta_{ac}}_{=1} A^{\check{a}\check{c}}_{ac} + \underbrace{\theta_{ca}}_{=0} A^{\check{c}\check{a}}_{ac}][\underbrace{\theta_{cb}}_{=0} B^{\check{c}\check{b}}_{cb} + \underbrace{\theta_{bc}}_{=1} B^{\check{b}\check{c}}_{cb}] = A^{\check{a}\check{c}}_{ac} B^{\check{b}\check{c}}_{cb}, \tag{115}$$

and therefore

$$C^{\check{a}\check{b}\check{c}}_{abc} = A^{\check{a}\check{c}}_{ac} B^{\check{b}\check{c}}_{cb}. \tag{116}$$

The general case can be handled analogously. Writing the right-hand side of Eq. (106) as a Keldysh sum we obtain

$$\mathscr{O}(z_{\mathcal{N}}) = \prod_i \sum_{P_i \in S_{N_i}} \theta_{P_i(\mathcal{N}_i)} \bar{O}_i^{P_i(\check{\mathcal{N}}_i)}(t_{\mathcal{N}_i}). \tag{117}$$

Suppose we wish to obtain the Keldysh component $\mathscr{O}^{P(\check{\mathcal{N}})}(t_{\mathcal{N}})$. It can be obtained from the above equation by choosing $z_{P(n_1)} > z_{P(n_2)} > \ldots > z_{P(n_N)}$. The left hand side then reduces to the desired Keldysh component. On the right-hand side, most of the step-function vanish. The only step functions that remain, and attain the value 1, are those for which $P_i(\mathcal{N}_i) = P(\mathcal{N}) \setminus \mathcal{N}_i^c$, where we defined the complementary set $\mathcal{N}_i^c = \mathcal{N} \setminus \mathcal{N}_i$. The permutation P therefore picks out a unique permutation P_i for each set $\mathcal{N}_i$, and we have

$$\mathscr{O}^{P(\check{\mathcal{N}})}(t_{\mathcal{N}}) = \prod_i \bar{O}_i^{P_i(\check{\mathcal{N}}_i)}(t_{\mathcal{N}_i}), \quad P_i(\mathcal{N}_i) = P(\mathcal{N}) \setminus \mathcal{N}_i^c. \tag{118}$$

As an example, let us now take the term $C^{\check{b}\check{a}\check{c}}_{abc} = [\mathscr{A}_{ac}\mathscr{B}_{cb}]^{\check{b}\check{a}\check{c}}$. In this case, $P(\{a,b,c\}) = \{b,a,c\}$, $\mathcal{N}_1 = \{a,c\}$, $\mathcal{N}_1^c = \{b\}$, and $\mathcal{N}_2 = \{c,b\}$, $\mathcal{N}_2^c = \{a\}$. Therefore, $P_1(\mathcal{N}_1) = \{b,a,c\} \setminus \{b\} = \{a,c\}$, and likewise $P_2(\mathcal{N}_2) = \{b,c\}$. In this particular case, P_1 is the identity permutation and P_2 is the transposition. Equation (118) applied to our example yields

$$C^{\check{b}\check{a}\check{c}}_{abc} = A^{\check{a}\check{c}}_{ac} B^{\check{b}\check{c}}_{cb}. \tag{119}$$

In practice, only those components of the sub-functions remain, in which the argument labels are in the same relative order as they are for the full product function. Thus the correct result can be obtained simply by moving the full string of super indices to each subfunction, and then removing all the labels that are not part of the argument list of the particular subfunction.

Retarded compositions of products can be worked out by writing the compositions in terms of Keldysh components by using Eq. (64). For example, the integrand in the second term in Eq. (108) can be written as

$$\begin{aligned}
[\mathscr{A}_{ac}\mathscr{B}_{cb}]^{R(\check{a},\check{c})\check{b}} &= \Theta_{ac}\left([\mathscr{A}_{ac}\mathscr{B}_{cb}]^{\check{a}\check{c}\check{b}} - [\mathscr{A}_{ac}\mathscr{B}_{cb}]^{\check{c}\check{a}\check{b}}\right) \\
&= \Theta_{ac}\left(A^{\check{a}\check{c}}_{ac} - A^{\check{c}\check{a}}_{ac}\right) B^{\check{c}\check{b}}_{cb} \\
&= A^{R(\check{a},\check{c})}_{ac} B^{\check{c}\check{b}}_{cb}.
\end{aligned} \tag{120}$$

The third term in Eq. (108) can be handled likewise. We can then express the component D^{12}_{ab} in Eq. (108) as

$$\begin{aligned} D^{12}_{ab} &= \int [\mathscr{A}_{a\breve{c}}\mathscr{B}_{\breve{c}b}]^{M(\breve{c})\breve{a}\breve{b}} + \int [\mathscr{A}_{a\breve{c}}\mathscr{B}_{\breve{c}b}]^{R(\breve{a},\breve{c})\breve{b}} + \int [\mathscr{A}_{a\breve{c}}\mathscr{B}_{\breve{c}b}]^{\breve{a}R(\breve{b},\breve{c})} \\ &= \int A^{M(\breve{c})\breve{a}}_{a\breve{c}} B^{M(\breve{c})\breve{b}}_{\breve{c}b} + \int A^{R(\breve{a},\breve{c})}_{a\breve{c}} B^{\breve{c}\breve{b}}_{\breve{c}b} + \int A^{\breve{a}\breve{c}}_{a\breve{c}} B^{R(\breve{c},\breve{b})}_{\breve{c}b}. \end{aligned} \tag{121}$$

The above equation is an example of a known Langreth rule, Eq. (7). The procedure laid out above can in principle be used to derive Langreth rules from arbitrary equations. Below we will derive additional rules that make these calculations less cumbersome.

6.3. The Vanishing of Retarded Compositions on Disconnected Sets

Specifying the structure of a Keldysh function in terms of sub-functions typically introduces new symmetries on top of those of a general Keldysh function, since there are permutations of super indices that do not change the components of the subfunctions. It is an advantage of the retarded set representation that these symmetries can be employed to directly discard certain terms of the representation. As we will show, this feature is consequence of the definition of retarded compositions in terms of nested commutators. We will therefore begin by considering commutator expressions.

In the previous section we noted that for our example two different permutations $P(\mathcal{N})$ give the same result, see equations Eq. (119) and Eq. (116):

$$\begin{aligned} [\mathscr{A}_{ac}\mathscr{B}_{cb}]^{\breve{a}\breve{b}\breve{c}} &= A^{\breve{a}\breve{c}}_{ac} B^{\breve{b}\breve{c}}_{cb} \\ [\mathscr{A}_{ac}\mathscr{B}_{cb}]^{\breve{b}\breve{a}\breve{c}} &= A^{\breve{a}\breve{c}}_{ac} B^{\breve{b}\breve{c}}_{cb}. \end{aligned} \tag{122}$$

Other permutations of the superindices, like *acb* and *bca*, will not produce the same result. The situation can be illustrated by the following diagram, in which higher points on the vertical axis denote later contour times:

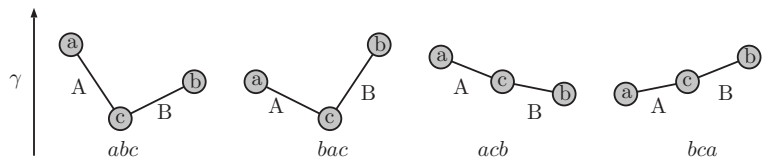

(123)

For the permutations *abc* and *bac*, the order within sub-functions A and B remains the same when the order of a and b is exchanged. On the other hand, exchanging a and b by going from *abc* to *bca* does change the internal order of A and B, as the ordering with respect to c is changed. Thus the symmetry appears only when a and b are neighbouring in the contour order. Furthermore, if there was a sub-function connecting a and b, its internal order would be reversed by any exchange of a and b, breaking the symmetry.

Generally, if for a function $\mathscr{O}(z_{\mathcal{N}})$ the arguments z_a and z_b are next to each other on the contour, exchanging their positions only changes their relative contour order.

Furthermore, if the vertices a and b are not directly connected, it follows that in Eq. (118) none of the sets $\mathcal{N}_i$ contains both a and b, and consequently changing their relative order does not change the order in any $\mathcal{N}_i$. We can therefore state a rule:

$$O^{\check{X}\check{a}\check{b}\check{Y}} = O^{\check{X}\check{b}\check{a}\check{Y}}, \quad \text{when } a \text{ and } b \text{ are not directly connected,} \tag{124}$$

where $\check{X}$ and $\check{Y}$ are strings of the remaining superindices. This rule can be used repeatedly, so that for example

$$O^{\check{X}\check{a}\check{c}\check{b}\check{Y}} = O^{\check{X}\check{c}\check{a}\check{b}\check{Y}} = O^{\check{X}\check{c}\check{b}\check{a}\check{Y}}, \quad \text{when } a \text{ is not directly connected to either } b \text{ or } c. \tag{125}$$

Note that b and c may be directly connected, since their relative order is not changed in Eq. (125). Continuing in this way, one arrives at a general rule for a string of arguments $a_1 \dots a_A$, or a linear combinations Z of such strings:

$$O^{\check{X}[\check{Z},\check{b}]\check{Y}} = O^{\check{X}\check{Z}\check{b}\check{Y}} - O^{\check{X}\check{b}\check{Z}\check{Y}} = 0, \quad \text{when } b \text{ is not directly connected to any } a_i. \tag{126}$$

If we choose Z to be the nested commutator $Z = [a_1, \dots, a_{A-1}]$ and we denote $b = a_A$, we obtain

$$O^{\check{X}[\check{a}_1,\dots,\check{a}_A]\check{Y}} = 0, \quad \text{when } a_A \text{ is not directly connected to any other } a_i \tag{127}$$

Furthermore, if we pick some argument a_k from the nested commutator, and write $O^{\check{X}[\check{a}_1,\dots,\check{a}_A]\check{Y}} = O^{\check{X}[[\check{a}_1,\dots,a_k],\dots,a_A]\check{Y}}$, when the outermost nested commutator is expanded, each of the resulting terms will vanish according to rule (127), unless a_k is directly connected to some argument a_l with $l < k$. This is true for any a_k, which allows us to state a more general rule:

$$\begin{aligned} \bar{O}^{\check{X}[\check{a}_1,\dots,\check{a}_A]\check{Y}} = 0, \quad & \text{unless every argument } a_k \text{ is directly connected} \\ & \text{to at least one argument to its left in the commutator.} \end{aligned} \tag{128}$$

Thus every argument in a nested commutator must be directly connected to an argument to its left, and this argument must in turn be directly connected to another, until the leftmost argument a_1 is reached. Therefore rule (128) requires that each argument is connected to the leftmost argument by a chain of direct connections that links to the left in the commutator.

We are now in position to work out the condition for a retarded composition to vanish. In the definition of a retarded composition

$$\bar{O}^{\check{X}R(\check{a}_1,\check{a}_2\cdots\check{a}_A)\check{Y}}(t_{\mathcal{N}}) = \sum_{P\in N_{A-1}} \Theta_{a_1 a_{P(2)}\cdots a_{P(A)}} \bar{O}^{\check{X}[\check{a}_1,\check{a}_{P(2)},\dots,\check{a}_{P(A)}]\check{Y}}(t_{\mathcal{N}}), \tag{129}$$

a sum is taken over every permutation of the arguments in the nested commutator, apart from the leftmost one. Therefore, if every argument is connected to the leftmost argument a_1 by some chain of direct connections, there will always be at least one term in the sum such that each argument is directly connected to an argument to its left.

The retarded composition vanishes, when there is at least one argument in the nested commutator that is not connected to a_1, i.e. when the retarded set $\mathcal{A} = \{\check{a}_1, \check{a}_2 \cdots \check{a}_A\}$ is disconnected. We therefore have the rule

A retarded composition vanishes, if it contains a disconnected retarded set. (130)

As an example, let us take a chain convolution of three functions

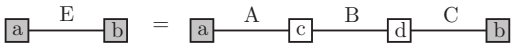

$$\mathscr{E}_{ab} = \int_{\gamma'} \bar{\mathscr{E}}_{ab\bar{c}\bar{d}} = \int_{\gamma'} \mathscr{A}_{a\bar{c}} \mathscr{B}_{\bar{c}\bar{d}} \mathscr{C}_{\bar{d}b}, \tag{131}$$

that appears for example in the Dyson equation. For the component $E^{R(\check{a},\check{b})}_{ab}$ we find the representation

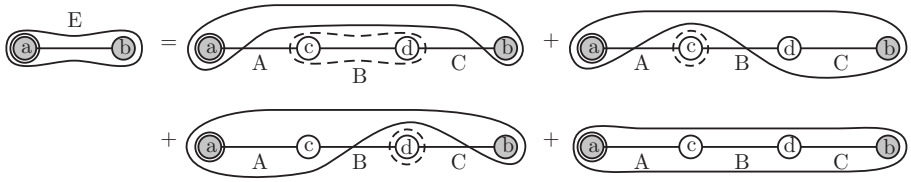

(132)

Here the first three terms vanish, since a and b are not connected inside the retarded set. Thus a retarded composition of a chain convolution, no matter the length, will never contain any MK components, as it is not possible to place any Matsubara sets without disconnecting the retarded set. From Eq. (132) we are then left with

$$E^{R(\check{a},\check{b})}_{ab} = \int [\mathscr{A}_{a\bar{c}} \mathscr{B}_{\bar{c}\bar{d}} \mathscr{C}_{\bar{d}b}]^{R(\check{a},\check{b}\check{c}\check{d})}. \tag{133}$$

Expanding the right-hand side of Eq. (133) using Eq. (129) sums over the six different permutations of b, c and d. However, out of the six resulting nested commutator expressions five are seen to give zero by applying the rule (128). Since the vertices are connected in a chain, there's only one permutation in which each vertex is directly connected to another to its left, that corresponding to the commutator $[\check{a}, \check{c}, \check{d}, \check{b}]$, and thus we obtain from Eq. (133) simply

$$E^{R(\check{a},\check{b})}_{ab} = \int \Theta_{acdb} [\mathscr{A}_{a\bar{c}} \mathscr{B}_{\bar{c}\bar{d}} \mathscr{C}_{\bar{d}b}]^{[\check{a},\check{c},\check{d},\check{b}]}. \tag{134}$$

This expression will be simplified further by rules that we will derive later.

6.4. Separating Retarded Sets

A diagram in a retarded set representation typically consists of sub-functions in multiple retarded sets that are connected via other sub-functions. Often these diagrams can be split into multiple pieces, so that each retarded set can be handled individually. This is

based on the fact that the retarded sets are ordered with respect to each other. If each of the vertices of a sub-function is in a different retarded set, the contour ordering of its vertices is determined, and it will reduce to a single MK component. For example we have

$$[\mathscr{A}_{abcd}\mathscr{B}_{ghi}\mathscr{C}_{dfg}\mathscr{D}_{ef}]^{R(\check{g},\check{h}\check{i})R(\check{c},\check{a}\check{b}\check{d})R(\check{e},\check{f})} = A^{R(\check{c},\check{a}\check{b}\check{d})}_{abcd}B^{R(\check{g},\check{h}\check{i})}_{ghi}C^{\check{g}\check{d}\check{f}}_{dfg}D^{R(\check{e},\check{f})}_{ef}. \tag{135}$$

which corresponds to the graph

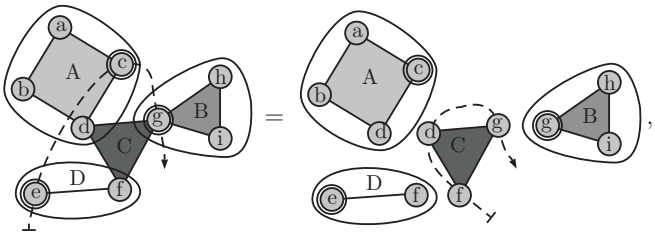

(136)

To consider this procedure in more detail, let us return to the chain convolution

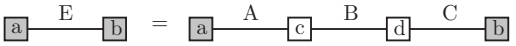

$$\mathscr{E}_{ab} = \int_{\gamma'} \bar{\mathscr{E}}_{ab\bar{c}\bar{d}} = \int_{\gamma'} \mathscr{A}_{a\bar{c}}\mathscr{B}_{\bar{c}\bar{d}}\mathscr{C}_{\bar{d}b}. \tag{137}$$

Choosing now to obtain the greater component E^{12}_{ab}, we get

$$E^{\check{a}\check{b}}_{ab} = \int \bar{E}^{R(\check{a},\check{c})R(\check{b},\check{d})}_{ab\bar{c}\bar{d}} + \int \bar{E}^{R(\check{a},\check{d})R(\check{b},\check{c})}_{ab\bar{c}\bar{d}} + \int \bar{E}^{R(\check{a},\check{c}\check{d})\check{b}}_{ab\bar{c}\bar{d}} + \int \bar{E}^{\check{a}R(\check{b},\check{c}\check{d})}_{ab\bar{c}\bar{d}}. \tag{138}$$

Let us start with the first term with superindex $R(\check{a},\check{c})R(\check{b},\check{d})$. If we expand the retarded sets in terms of commutators, we obtain terms in which the order between a and c, as well as b and d, varies term by term. However, in every term c is later than d in contour order. Consequently $\mathscr{B}_{cd}$ reduces to the same Keldysh-component $B^{\check{c}\check{d}}_{cd}$ in every term, and we can pull it out of the brackets as a common factor:

$$[\mathscr{A}_{ac}\mathscr{B}_{cd}\mathscr{C}_{db}]^{R(\check{a},\check{c})R(\check{b},\check{d})} = [\mathscr{A}_{ac}\mathscr{C}_{db}]^{R(\check{a},\check{c})R(\check{b},\check{d})}B^{\check{c}\check{d}}_{cd}. \tag{139}$$

The crucial point is that all the arguments of function B are in different retarded sets. If we expand the retarded set $R(\check{a},\check{c})$ we obtain

$$[\mathscr{A}_{ac}\mathscr{C}_{db}]^{R(\check{a},\check{c})R(\check{b},\check{d})} = \theta_{ac}\Big([\mathscr{A}_{ac}\mathscr{C}_{db}]^{\check{a}\check{c}R(\check{b},\check{d})} - [\mathscr{A}_{ac}\mathscr{C}_{db}]^{\check{c}\check{a}R(\check{b},\check{d})}\Big), \tag{140}$$

where in both of the terms the contour order of a and c is fixed. Therefore we can now place A in front of the brackets to obtain

$$\theta_{ac}\Big([\mathscr{A}_{ac}\mathscr{C}_{db}]^{\check{a}\check{c}R(\check{b},\check{d})} - [\mathscr{A}_{ac}\mathscr{C}_{db}]^{\check{c}\check{a}R(\check{b},\check{d})}\Big) = \theta_{ac}\Big(A^{\check{a}\check{c}}_{ac}C^{R(\check{b},\check{d})}_{db} - A^{\check{c}\check{a}}_{ac}C^{R(\check{b},\check{d})}_{db}\Big). \tag{141}$$

We can now factor out $C^{R(\check{b},\check{d})}_{db}$ and obtain

$$[\mathscr{A}_{ac}\mathscr{C}_{db}]^{R(\check{a},\check{c})R(\check{b},\check{d})} = A^{R(\check{a},\check{c})}_{ac}C^{R(\check{b},\check{d})}_{db}. \tag{142}$$

This result can be represented graphically as

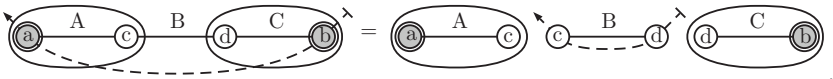

. (143)

This is a specific instance of a more general rule. As was discussed, if there is a connecting piece that has multiple vertices inside some retarded sets, it cannot be completely split from a diagram. However, if the connecting piece has a single vertex inside some other retarded sets, those sets can still be split off. For example we have the equation

$$[\mathscr{A}_{abcd}\mathscr{B}_{ghi}\mathscr{C}_{dfg}\mathscr{D}_{ef}]^{R(\check{c},\check{a}\check{b}\check{d})R(\check{e},\check{f}\check{g}\check{h}\check{i})} = A^{R(\check{c},\check{a}\check{b}\check{d})}_{abcd}[\mathscr{B}_{ghi}\mathscr{C}_{dfg}\mathscr{D}_{ef}]^{\check{d}R(\check{e},\check{f}\check{g}\check{h}\check{i})}, \tag{144}$$

which corresponds to the graph

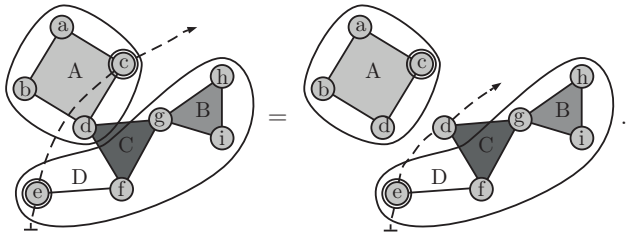

. (145)

Diagrammatically the above considerations can be condensed to the single statement, that one is allowed to split the diagram by splitting vertices through the process

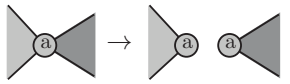

(146)

whenever this can be done without altering the retarded sets. Note that Matsubara sets can be split freely (this statement is merely a diagrammatic equivalent of Eq. (110)).

To demonstrate this rule, let us now return to Eq. (138), the right hand side of which can be written diagrammatically as

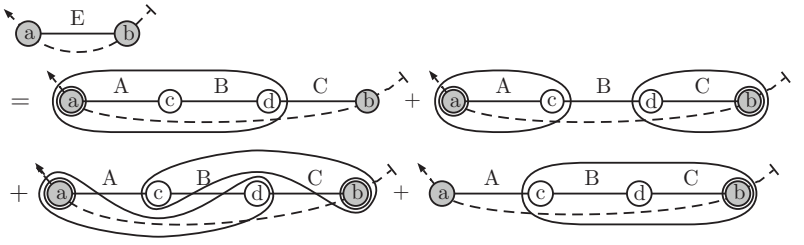

(147)

Note that the third diagram vanishes due to disconnected retarded sets, as per rule (130). After using Eq. (146) to split the vertices on the edges of retarded sets, we

obtain

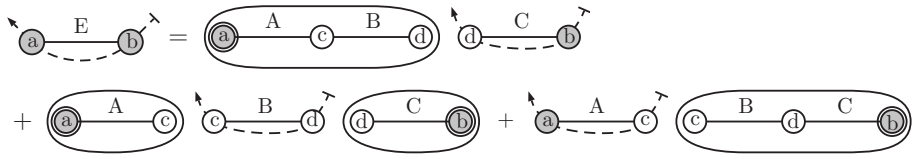

(148)

Converting Eq. (148) back into a mathematical expression now yields

$$E^{\check{a}\check{b}}_{ab} = \int [\mathscr{A}_{a\bar{c}}\mathscr{B}_{\bar{c}\bar{d}}]^{R(\check{a},\check{c}\check{d})} C^{\bar{d}\check{b}}_{\bar{d}b} + \int A^{R(\check{a},\check{c})}_{a\bar{c}} B^{\check{c}\bar{d}}_{\bar{c}\bar{d}} C^{R(\check{b},\check{d})}_{\bar{d}b} + \int A^{\check{a}\check{c}}_{a\bar{c}} [\mathscr{B}_{\bar{c}\bar{d}}\mathscr{C}_{\bar{d}\bar{b}}]^{R(\check{b},\check{c}\check{d})}. \tag{149}$$

However, the square bracketed expressions can not be split further, as cutting between A and B in the first term, for example, splits a retarded set. These terms will be considered more closely in the following sections.

6.5. Nested Retarded Compositions

After performing the possible separations of the product, we are generally still left with factors that contain retarded compositions of products of several sub-functions. If the factor is simple enough, one may now expand the retarded composition in terms of nested commutators using Eq. (129), and solve each of these one by one. Some of the terms may vanish as per the rule (128). This expansion can always be done, but it easily gets rather cumbersome. It is possible to define an alternative way to expand retarded sets, that opens up more options and thus in many cases allows for a cleaner derivation. Nested retarded compositions are defined by

$$\bar{O}^{\check{X}R(R(\check{\mathcal{H}}_1),R(\check{\mathcal{H}}_2)\cdots R(\check{\mathcal{H}}_r))\check{Y}}(t_{\mathcal{N}}) = \sum_{P\in S_{r-1}} \Theta_{h_1 h_{P(2)}\cdots h_{P(r)}} \bar{O}^{\check{X}[R(\check{\mathcal{H}}_1),R(\check{\mathcal{H}}_{P(2)}),\ldots,R(\check{\mathcal{H}}_{P(r)})]\check{Y}}(t_{\mathcal{N}}), \tag{150}$$

where $\mathcal{H}_i = h_i \cup \mathcal{I}_i$, in which h_i is the top element of $\mathcal{H}_i$, such that $R(\mathcal{H}_i) = R(h_i, \mathcal{I}_i)$. In the nested commutator the retarded sets $R(\mathcal{H}_i)$ are treated as single elements, so that for example $[R(\mathcal{H}_1), R(\mathcal{H}_2)] = R(\mathcal{H}_1)R(\mathcal{H}_2) - R(\mathcal{H}_2)R(\mathcal{H}_1)$, and for the super-indices we again make use of Eq. (21). The resulting multi-retarded compositions are defined as in Eq. (64). Let us, for example, take a look at the factor that appears in the first term of Eq. (149):

$$[\mathscr{A}_{ac}\mathscr{B}_{cd}]^{R(\check{a},\check{c}\check{d})} = \Theta_{acd}[\mathscr{A}_{ac}\mathscr{B}_{cd}]^{[\check{a},\check{c},\check{d}]} + \Theta_{adc}[\mathscr{A}_{ac}\mathscr{B}_{cd}]^{[\check{a},\check{d},\check{c}]}. \tag{151}$$

Because of the nested commutator structure we can make use of the Jacobi identity

$$[[A,B],C] + [[C,A],B] + [[B,C],A] = 0, \tag{152}$$

to derive

$$[\mathscr{A}_{ac}\mathscr{B}_{cd}]^{[\check{a},\check{c},\check{d}]} = [\mathscr{A}_{ac}\mathscr{B}_{cd}]^{[\check{a},\check{d},\check{c}]} + [\mathscr{A}_{ac}\mathscr{B}_{cd}]^{[\check{d},\check{c},\check{a}]}. \tag{153}$$

This allows us to obtain

$$\begin{aligned}[\mathscr{A}_{ac}\mathscr{B}_{cd}]^{R(\check{a},\check{c}\check{d})} &= \Theta_{acd}\left([\mathscr{A}_{ac}\mathscr{B}_{cd}]^{[\check{a},\check{d},\check{c}]} + [\mathscr{A}_{ac}\mathscr{B}_{cd}]^{[\check{d},\check{c},\check{a}]}\right) + \Theta_{adc}[\mathscr{A}_{ac}\mathscr{B}_{cd}]^{[\check{a},\check{d},\check{c}]} \\ &= \Theta_{ac}\Theta_{cd}[\mathscr{A}_{ac}\mathscr{B}_{cd}]^{[\check{a},[\check{c},\check{d}]]} + \Theta_{ad}\Theta_{ac}[\mathscr{A}_{ac}\mathscr{B}_{cd}]^{[[\check{a},\check{d}],\check{c}]} \\ &= [\mathscr{A}_{ac}\mathscr{B}_{cd}]^{R(\check{a},R(\check{c},\check{d}))} + [\mathscr{A}_{ac}\mathscr{B}_{cd}]^{R(R(\check{a},\check{d}),\check{c})},\end{aligned} \tag{154}$$

where we can express the result cleanly using nested retarded compositions.

Note that when expanding a retarded set containing nested sets, only the top arguments of the nested sets are included in the sum over permutations, so that for example

$$[\mathscr{A}_{ac}\mathscr{B}_{cd}]^{R(\check{a},R(\check{c},\check{d}))} = \Theta_{ac}[\mathscr{A}_{ac}\mathscr{B}_{cd}]^{[\check{a},R(\check{c},\check{d})]} = \Theta_{ac}\Theta_{cd}[\mathscr{A}_{ac}\mathscr{B}_{cd}]^{[\check{a},[\check{c},\check{d}]]}. \tag{155}$$

The vanishing rule (130) still holds, and the retarded composition vanishes if any of the nested sets are disconnected.

Diagrammatically we express the expansion in Eq. (154) as

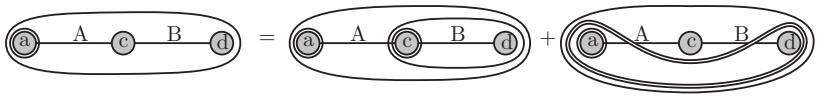

(156)

Note that a nested retarded set sharing the top argument with the outer retarded set is circled with a double line, to distinguish it from other nested sets on the same level. In figure 156 the second term vanishes, as the retarded set $\{a, d\}$ is disconnected.

One advantage of the expansion in nested retarded sets, is that since the expansion can be performed with respect to any of the retarded vertices, there is a number of alternative expansions for any retarded set. This allows one to choose the particular expansion that results in the largest number of terms vanishing due to disconnected retarded sets. The various expansions are related by the symmetry of retarded compositions with respect to permutations of the retarded arguments, see Eq. (58). For example, for the retarded composition in Eq. (151) one has the symmetry $[\cdots]^{R(\check{a},\check{c}\check{d})} = [\cdots]^{R(\check{a},\check{d}\check{c})}$, which allows one to immediately obtain from Eq. (154) the alternative expansion

$$[\mathscr{A}_{ac}\mathscr{B}_{cd}]^{R(\check{a},\check{c}\check{d})} = [\mathscr{A}_{ac}\mathscr{B}_{cd}]^{R(\check{a},R(\check{d},\check{c}))} + [\mathscr{A}_{ac}\mathscr{B}_{cd}]^{R(R(\check{a},\check{c}),\check{d})}. \tag{157}$$

which is expressed diagrammatically as

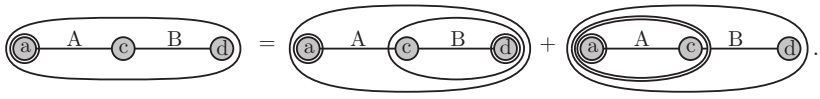

(158)

In this case, the expansion in Eq. (154) and Eq. (156) is the more expedient choice, since in Eq. (158) no terms vanish.

The result in Eq. (156) is independent of the sub-functions involved, and can be generalized to (see Eq. (C.2))

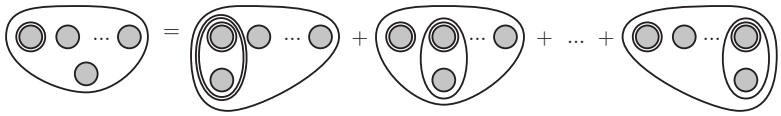

(159)

Here, the gray dots may represent single vertices or retarded sets. The top element in each retarded set, which may be a retarded set itself, is always designated with a double-lined closed curve. This graphical rule corresponds to Eq. (C.2), proven in Appendix C. As a further generalization, the outer retarded set in Eq. (159) may itself be inside larger retarded sets (see Eq. (C.10)).

For example, for a four-point function, expanding with respect to argument 4, we have

$$O^{R(1,234)} = O^{R(R(1,4),23)} + O^{R(1,R(2,4)3)} + O^{R(1,2R(3,4))}, \tag{160}$$

which we represented diagrammatically as

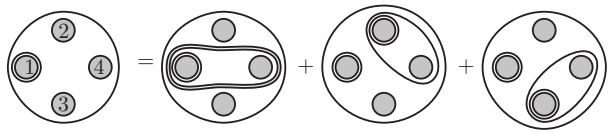

(161)

We can expand each term on the right-hand side of Eq. (161) again with respect to vertex 3 (or the retarded set containing 3). This leads to

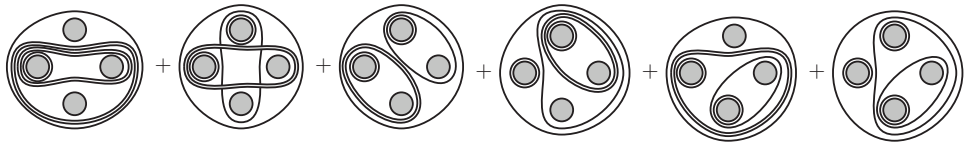

(162)

We can further apply Eq. (159) in reverse to combine the first and the fifth term, as well as the fourth and the sixth term, in Eq. (162) to obtain

(163)

This constitutes a diagrammatic proof of the relation

$$O^{R(1,234)} = O^{R(R(1,34),2)} + O^{R(R(1,4),R(2,3))} + O^{R(R(1,3),R(2,4))} + O^{R(1,R(2,34))}. \tag{164}$$

Another useful result relating nested retarded compositions can be derived by considering a retarded composition of the form $[\mathscr{A}_{ab}\mathscr{B}_{b\mathcal{N}}]^{R(\bar{a},R(\bar{b},L_{\mathcal{N}}))}$, where $L_{\mathcal{N}}$ is an

arbitrary string of retarded sets containing the labels $\mathcal{N} = \{n_1, \ldots, n_N\}$ (such as $L_\mathcal{N} = R(n_1, n_2 \cdots n_N)$, to take the simplest option). Expanding the outermost retarded set in terms of commutators, we obtain

$$\begin{aligned}
[\mathscr{A}_{ab}\mathscr{B}_{b\mathcal{N}}]^{R(\check{a},R(\check{b},L_\mathcal{N}))} &= \Theta_{ab}\Big([\mathscr{A}_{ab}\mathscr{B}_{b\mathcal{N}}]^{\check{a}R(\check{b},L_\mathcal{N})} - [\mathscr{A}_{ab}\mathscr{B}_{b\mathcal{N}}]^{R(\check{b},L_\mathcal{N})\check{a}}\Big) \\
&= \Theta_{ab}\Big(A^{\check{a}\check{b}}_{aj}B^{R(\check{j},L_\mathcal{N})}_{j\mathcal{N}} - A^{\check{b}\check{a}}_{ab}B^{R(\check{b},L_\mathcal{N})}_{b\mathcal{N}}\Big) \\
&= A^{R(\check{a},\check{b})}_{ab}B^{R(\check{b},L_\mathcal{N})}_{b\mathcal{N}}
\end{aligned} \tag{165}$$

Diagrammatically this result can be drawn as

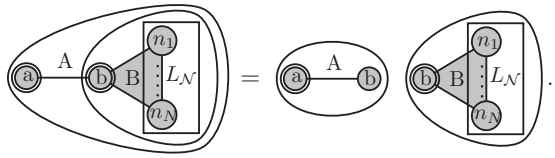

(166)

Applying Eq. (166) to the first term in Eq. (156) we have

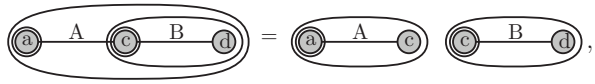

(167)

which corresponds to

$$[\mathscr{A}_{ac}\mathscr{B}_{cd}]^{R(\check{a},R(\check{c},\check{d}))} = A^{R(\check{a},\check{c})}_{ac}B^{R(\check{c},\check{d})}_{cd}. \tag{168}$$

Using Eq. (168), along with the analogous result for $[\mathscr{B}_{\check{c}\bar{d}}\mathscr{C}_{\bar{d}b}]^{R(\check{b},\check{c}\check{d})}$, we can now obtain from Eq. (149) the Langreth rule

$$E^{12}_{ab} = A^{R(\check{a},\check{c})}_{ac}B^{\check{c}\check{d}}_{cd}C^{R(\check{b},\check{d})}_{db} + A^{R(\check{a},\check{c})}_{ac}B^{R(\check{c},\check{d})}_{cd}C^{\check{d}\check{b}}_{db} + A^{\check{a}\check{c}}_{ac}B^{R(\check{c},\check{d})}_{cd}C^{R(\check{d},\check{b})}_{db}. \tag{169}$$

The diagrammatic representation of the above equation, including its diagrammatic derivation, is shown in figure 6.

We now have all the tools to derive the known and extended versions of the Langreth rules. In the following section we will demonstrate the rules laid out above, by going through the process of deriving Langreth rules for two important practical cases, namely the double-triangle graph and the vertex graph.

7. Langreth Rules for the Double-triangle and Vertex Structures

Let us now apply the extended Langreth rules to two important practical examples introduced in the beginning, that involve two external and two internal arguments:

$$\mathscr{D}_{ab} = \int_{\gamma'} \bar{\mathscr{D}}_{ab\bar{c}\bar{d}} \quad : \quad \boxed{\text{a}} \quad \boxed{\text{b}} = \boxed{\text{a}} \quad \begin{matrix}\boxed{\text{c}} \\ \boxed{\text{d}}\end{matrix} \quad \boxed{\text{b}} \tag{170}$$

We will consider the following two structures:

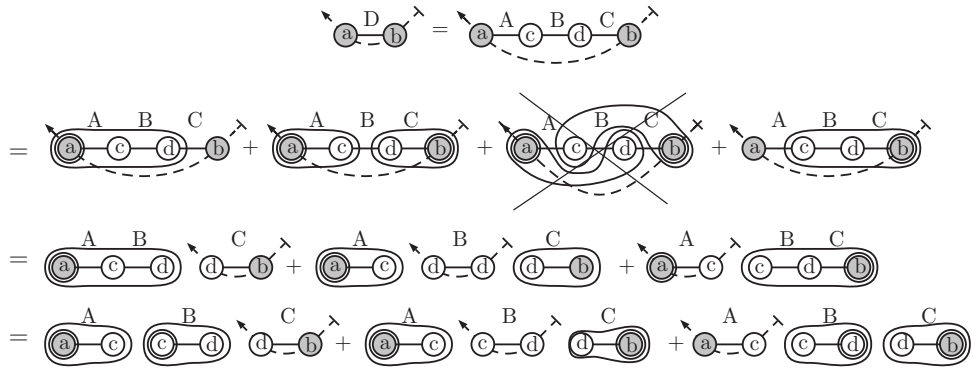

Figure 6. Diagrammatic derivation of the langreth rule Eq. (169) for a chain of two convolutions. We have used the separate results of Eq. (156) and Eq. (167) for the first and the last terms in the last step.

(i) The double-triangle structure $\bar{\mathscr{X}}_{abcd} = \mathscr{A}_{ac}\mathscr{B}_{cb}\mathscr{C}_{cd}\mathscr{D}_{ad}\mathscr{E}_{db}$

$$\mathscr{X}_{ab} = \int_{\gamma'} \bar{\mathscr{X}}_{ab\bar{c}\bar{d}} \quad : \quad$$

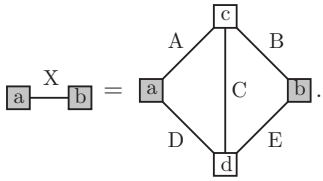

. (171)

(ii) The vertex structure $\bar{\mathscr{H}}_{abcd} = \mathscr{A}_{ac}\mathscr{B}_{ad}\mathscr{C}_{cdb}$

$$\mathscr{H}_{ab} = \int_{\gamma'} \bar{\mathscr{H}}_{ab\bar{c}\bar{d}} \quad : \quad$$

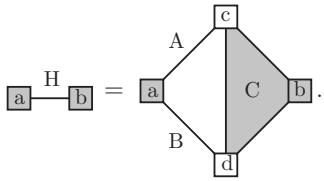

. (172)

All the Langreth rules for these structures are listed in Table 2 and Table 3. We will provide explicit derivations of a few of the rules.

7.1. The $D^{M(\check{a}\check{b})}$ component.

For the fully Matsubara restricted component, the retarded set representation is

$$D^{M(\check{a}\check{b})}_{ab} =$$

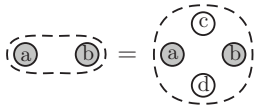

(173)

(i) Substituting the double-triangle structure into the above diagram results in:

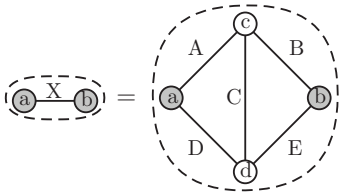

$$: \quad X_{ab}^{M(\check{a}\check{b})} = \int [\mathscr{A}_{a\bar{c}}\mathscr{B}_{\bar{c}b}\mathscr{C}_{\bar{c}\bar{d}}\mathscr{D}_{a\bar{d}}\mathscr{E}_{\bar{d}b}]^{M(\check{a}\check{b}\check{c}\check{d})} \quad (174)$$

Since Matsubara sets can be distributed over the sub-functions for the case when no arguments are on the Keldysh branch (see the discussion below Eq. (104)), we find

$$X_{ab}^{M(\check{a}\check{b})} = \int A_{a\bar{c}}^{M(\check{a}\check{c})} B_{\bar{c}b}^{M(\bar{c}\check{b})} C_{\bar{c}\bar{d}}^{M(\check{c}\check{d})} D_{a\bar{d}}^{M(\check{a}\check{d})} E_{\bar{d}b}^{M(\bar{d}\check{b})}. \quad (175)$$

(ii) For the vertex structure we likewise obtain

$$H_{ab}^{M(\check{a}\check{b})} = \int A_{a\bar{c}}^{M(\check{a}\check{c})} B_{a\bar{d}}^{M(\check{a}\check{d})} C_{\bar{c}\bar{d}b}^{M(\check{c}\bar{d}\check{b})} \quad (176)$$

7.2. The $D^{M(\check{a})\check{b}}$ component.

The retarded set representation is

$$D^{M(\check{a})\check{b}} =$$

(177)

(i) Substituting the double-triangle structure into the above diagram results in:

$X_{ab}^{M(1)2} =$ 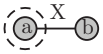

$=$ 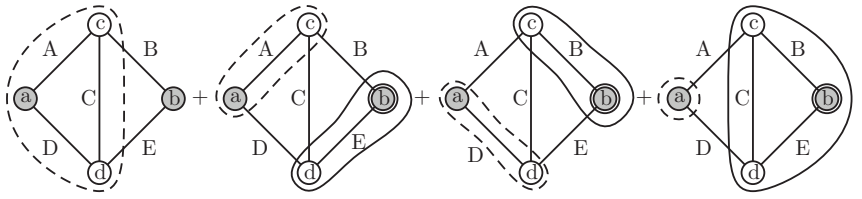

$=$ 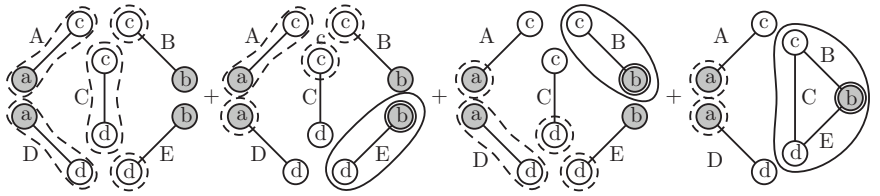

$$= \int A_{a\bar{c}}^{M(\check{a}\check{c})} C_{\bar{c}\bar{d}}^{M(\check{c}\check{d})} D_{a\bar{d}}^{M(\check{a}\check{d})} B_{\bar{c}b}^{M(\check{c})\check{b}} E_{\bar{d}b}^{M(\check{d})\check{b}} + \int A_{a\bar{c}}^{M(\check{a}\check{c})} B_{\bar{c}b}^{M(\check{c})\check{b}} C_{\bar{c}\bar{d}}^{M(\check{c})\check{d}} D_{a\bar{d}}^{M(\check{a})\check{d}} E_{\bar{d}b}^{R(\check{b},\check{d})}$$
$$+ \int B_{\bar{c}b}^{R(\check{b},\check{c})} A_{a\bar{c}}^{M(\check{a})\check{c}} C_{\bar{c}\bar{d}}^{M(\check{d})\check{c}} E_{\bar{d}b}^{M(\check{d})\check{b}} D_{a\bar{d}}^{M(\check{a}\check{d})} + \int A_{a\bar{c}}^{M(\check{a})\check{c}} D_{a\bar{d}}^{M(\check{a})\check{d}} [\mathscr{B}_{\bar{c}b}\mathscr{E}_{\bar{d}b}\mathscr{C}_{\bar{c}\bar{d}}]^{R(\check{b},\check{c}\check{d})} \tag{178}$$

Here we encounter a retarded composition of a triangle in the term $[\mathscr{B}_{\bar{c}b}\mathscr{E}_{\bar{d}b}\mathscr{C}_{\bar{c}\bar{d}}]^{R(\check{b},\check{c}\check{d})}$. Because every vertex connects to every other, there are no symmetries that could be leveraged. Through brute force expansion of the retarded set, either using nested commutators or nested retarded sets, we obtain two forms of a Langreth rule

$$\begin{aligned}[\mathscr{B}_{\bar{c}b}\mathscr{E}_{\bar{d}b}\mathscr{C}_{\bar{c}\bar{d}}]^{R(\check{b},\check{c}\check{d})} &= B_{\bar{c}b}^{R(\check{b},\check{c})} E_{\bar{d}b}^{\check{b}\check{d}} C_{\bar{c}\bar{d}}^{R(\check{c},\check{d})} + B_{\bar{c}b}^{\check{c}\check{b}} E_{\bar{d}b}^{R(\check{b},\check{d})} C_{\bar{c}\bar{d}}^{R(\check{d},\check{c})} + B_{\bar{c}b}^{R(\check{b},\check{c})} E_{\bar{d}b}^{R(\check{b},\check{d})} C_{\bar{c}\bar{d}}^{\check{d}\check{c}} \\ &= B_{\bar{c}b}^{R(\check{b},\check{c})} E_{\bar{d}b}^{\check{d}\check{b}} C_{\bar{c}\bar{d}}^{R(\check{c},\check{d})} + B_{\bar{c}b}^{\check{b}\check{c}} E_{\bar{d}b}^{R(\check{b},\check{d})} C_{\bar{c}\bar{d}}^{R(\check{d},\check{c})} + B_{\bar{c}b}^{R(\check{b},\check{c})} E_{\bar{d}b}^{R(\check{b},\check{d})} C_{\bar{c}\bar{d}}^{\check{c}\check{d}}.\end{aligned} \tag{179}$$

These two expressions only differ in the change of order of the Keldysh components.

(ii) Substituting the vertex structure into (177) leads to

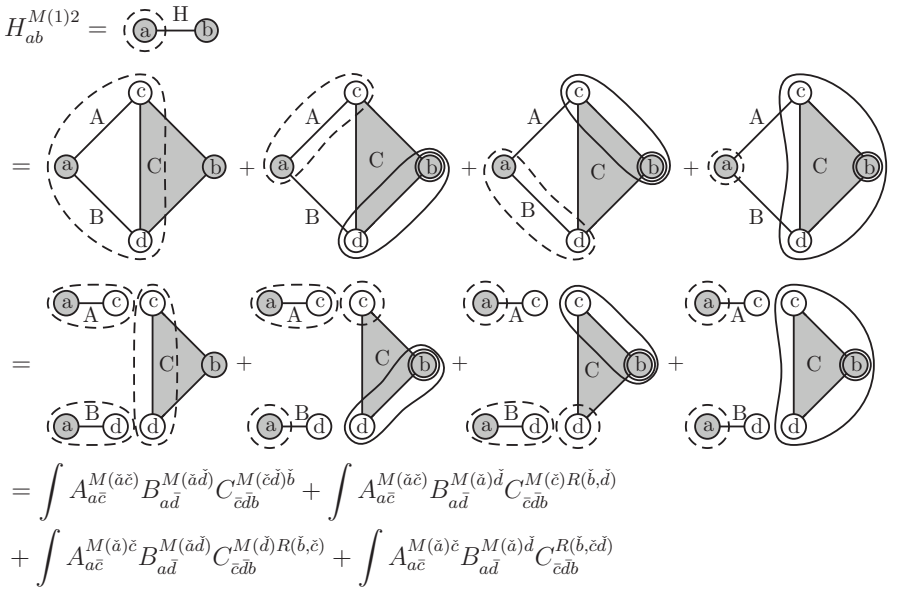

$$= \int A^{M(\check{a}\check{c})}_{a\bar{c}} B^{M(\check{a}\check{d})}_{a\bar{d}} C^{M(\check{c}\check{d})\check{b}}_{\bar{c}\bar{d}b} + \int A^{M(\check{a}\check{c})}_{a\bar{c}} B^{M(\check{a})\check{d}}_{a\bar{d}} C^{M(\check{c})R(\check{b},\check{d})}_{\bar{c}\bar{d}b}$$
$$+ \int A^{M(\check{a})\check{c}}_{a\bar{c}} B^{M(\check{a}\check{d})}_{a\bar{d}} C^{M(\check{d})R(\check{b},\check{c})}_{\bar{c}\bar{d}b} + \int A^{M(\check{a})\check{c}}_{a\bar{c}} B^{M(\check{a})\check{d}}_{a\bar{d}} C^{R(\check{b},\check{c}\check{d})}_{\bar{c}\bar{d}b}$$

(180)

7.3. The $D^{\check{a}\check{b}}$ component.

The retarded set representation is now

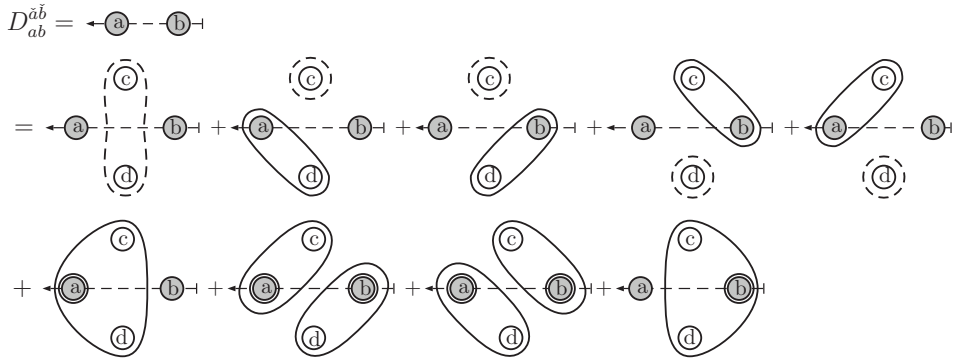

(181)

(i) After substituting the double-triangle structure we can cut every line in every term, except for the last two terms for which the rule in Eq. (179) is needed. The rule is the same for any ordering of the arguments, and therefore by substituting $B_{b\bar{c}} \to A_{a\bar{c}}$ and $E_{b\bar{d}} \to D_{a\bar{d}}$ on both sides of Eq. (179), we obtain the rule for $[\mathscr{A}_{a\bar{c}}\mathscr{D}_{a\bar{d}}\mathscr{C}_{\bar{c}\bar{d}}]^{R(\check{a},\check{b}\check{c})}$.

The second and third term in Eq. (181) sum up to

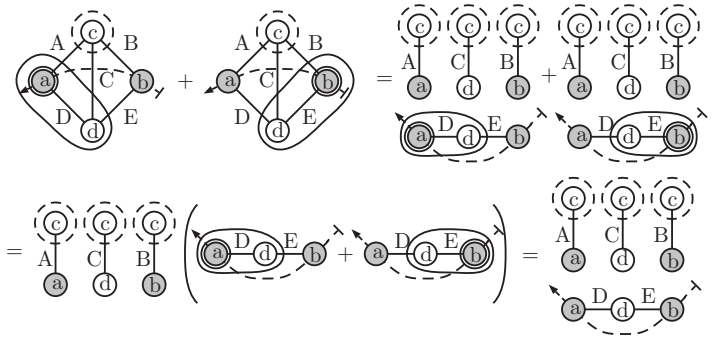

(182)

and therefore we can express these compactly using a chain-convolution. The same is true for the fourth and fifth terms in Eq. (181). We obtain

$$
\begin{aligned}
X^{\check{a}\check{b}}_{ab} = & \int A^{M(\check{c})\check{a}}_{a\bar{c}} B^{M(\check{c})\check{b}}_{\bar{c}b} C^{M(\check{c}\check{d})}_{\bar{c}\bar{d}} D^{M(\check{d})\check{a}}_{a\bar{d}} E^{M(\check{d})\check{b}}_{\bar{d}b} \\
& + \int [\mathscr{A}_{a\bar{c}} \mathscr{B}_{\bar{c}b}]^{\check{a}\check{b}} C^{M(\check{d})\check{c}}_{\bar{c}\bar{d}} D^{M(\check{d})\check{a}}_{a\bar{d}} E^{M(\check{d})\check{b}}_{\bar{d}b} + \int A^{M(\check{c})\check{a}}_{a\bar{c}} B^{M(\check{c})\check{b}}_{\bar{c}b} C^{M(\check{c})\check{d}}_{\bar{c}\bar{d}} [\mathscr{D}_{\check{a}\bar{d}} \mathscr{E}_{\bar{d}\bar{b}}]^{\check{a}\check{b}} \\
& + \int [\mathscr{A}_{\check{a}\bar{c}} \mathscr{D}_{\check{a}\bar{d}} \mathscr{C}_{\bar{c}\bar{d}}]^{R(\check{a},\check{c}\check{d})} B^{\check{c}\check{b}}_{\bar{c}\check{b}} E^{\bar{d}\bar{b}}_{\bar{d}\bar{b}} + \int A^{R(\check{a},\check{c})}_{\check{a}\bar{c}} B^{\check{c}\check{b}}_{\bar{c}\check{b}} C^{\check{c}\check{d}}_{\bar{c}\bar{d}} D^{\check{a}\check{d}}_{\check{a}\bar{d}} E^{R(\check{b},\check{d})}_{\bar{d}\bar{b}} \\
& + \int A^{\check{a}\check{c}}_{\check{a}\bar{c}} B^{R(\check{b},\check{c})}_{\bar{c}\check{b}} C^{\check{d}\check{c}}_{\bar{c}\bar{d}} D^{R(\check{a},\check{d})}_{\check{a}\bar{d}} E^{\bar{d}\bar{b}}_{\bar{d}\bar{b}} + \int A^{\check{a}\check{c}}_{\check{a}\bar{c}} E^{\check{a}\check{d}}_{\check{a}\bar{d}} [\mathscr{B}_{\bar{c}\check{b}} \mathscr{D}_{\bar{d}\bar{b}} \mathscr{C}_{\bar{c}\bar{d}}]^{R(\check{b},\check{c}\check{d})} .
\end{aligned}
\tag{183}
$$

After applying the rule in Eq. (179), this can be manipulated into a more compact form, shown in the table 2.

(ii) After substituting the vertex structure we obtain

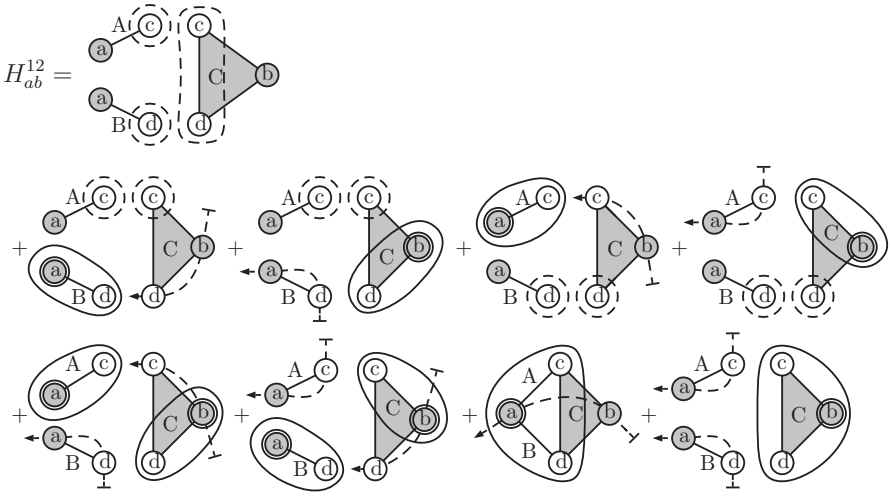

(184)

$$
\begin{aligned}
&= \int A^{M(\check{c})\check{a}}_{a\bar{c}} B^{M(\check{d})\check{a}}_{a\bar{d}} C^{M(\check{c}\check{d})\check{b}}_{\bar{c}\bar{d}b} \\
&+ \int A^{M(\check{c})\check{a}}_{a\bar{c}} B^{R(\check{a},\check{d})}_{a\bar{d}} C^{M(\check{c})\bar{d}\check{b}}_{\bar{c}\bar{d}b} + \int A^{M(\check{c})\check{a}}_{a\bar{c}} B^{\check{a}\check{d}}_{a\bar{d}} C^{M(\check{c})R(\check{b},\check{d})}_{\bar{c}\bar{d}b} \\
&+ \int A^{R(\check{a},\check{c})}_{a\bar{c}} B^{M(\check{d})\check{a}}_{a\bar{d}} C^{M(\check{d})\bar{d}\check{b}}_{\bar{c}\bar{d}b} + \int A^{\check{a}\check{c}}_{a\bar{c}} B^{M(\check{d})\check{a}}_{a\bar{d}} C^{M(\check{d})R(\check{b},\check{c})}_{\bar{c}\bar{d}b} \\
&+ \int A^{R(\check{a},\check{c})}_{a\bar{c}} B^{\check{a}\check{d}}_{a\bar{d}} C^{\check{c}R(\check{b},\check{d})}_{\bar{c}\bar{d}b} + \int A^{\check{a}\check{c}}_{a\bar{c}} B^{R(\check{a},\check{d})}_{a\bar{d}} C^{\check{d}R(\check{b},\check{c})}_{\bar{c}\bar{d}b} + \int [\mathscr{A}_{a\bar{c}} \mathscr{B}_{a\bar{d}} \mathscr{C}_{\bar{c}\bar{d}b}]^{R(\check{a},\check{c}\check{d})\check{b}} + \int A^{\check{a}\check{c}}_{a\bar{c}} B^{\check{a}\check{d}}_{a\bar{d}} C^{R(\check{b},\check{c}\check{d})}_{\bar{c}\bar{d}b}.
\end{aligned}
\tag{185}
$$

Here the second to last term can be handled using the rule Eq. (179), as b, being always first in contour order, does not interfere.

7.4. The $D^{R(\check{a},\check{b})}$ component.

Performing the retarded set expansion leads to

$D^{R(\check{a},\check{b})} =$ 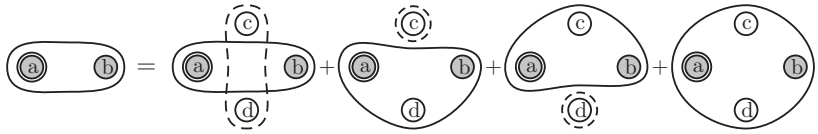

(186)

(i) After substituting the double-triangle structure the first term after the last equal sign vanishes, as a and b are not directly connected. In the second and third terms the sub-functions connecting to the Matsubara set can be separated, and the remaining piece is a retarded composition of a convolution (shown in Table 1). The final piece can be worked out by expanding the retarded set, in which the lack of direct connection between a and b leading to cancellations.

(ii) The vertex structure can be handled similarly. Starting from Eq. (186) the first term after the second equal sign vanishes because a and b are not directly connected. The second and third terms reduce to retarded compositions of convolutions, as the three-point sub-function reduces to an MK function of two contour arguments when one of its vertices is in the Matsubara set.

7.5. The Tables of Langreth Rules

We give in Table 1 the known Langreth rules for convolutions and products. The new Langreth rules for the double-triangle structure are shown in Table 2, and the new rules for the vertex structure are shown in Table 3. For clarity and to conform to common nomenclature, we have used the notation of Langreth for two-point functions:

$$
\begin{gathered}
O^{12} = O^{>}, \quad O^{21} = O^{<}, \quad O^{R(1,2)} = O^{R}, \quad O^{R(2,1)} = O^{A} \\
O^{M(1)2} = O^{\lceil}, \quad O^{M(2)1} = O^{\rceil}, \quad O^{M(12)} = O^{M}.
\end{gathered}
\tag{187}
$$

We also omit the sub-indices when writing the rules, as these can be read from the contour expression of the structure considered.

$\mathscr{D}_{ab} = \int_{\gamma'} \mathscr{A}_{a\bar{c}} \mathscr{B}_{\bar{c}b}$	$\mathscr{D}_{ab} = \mathscr{A}_{ab} \mathscr{B}_{ba}$
$D^{>} = \int A^R B^{>} + \int A^{>} B^A + \int A^{\rceil} B^{\lceil}$	$D^{>} = A^{>} B^{<}$
$D^{<} = \int A^R B^{<} + \int A^{<} B^A + \int A^{\rceil} B^{\lceil}$	$D^{<} = A^{<} B^{>}$
$D^R = \int A^R B^R$	$D^R = \begin{cases} A^R B^{<} + A^{<} B^A \\ A^R B^{>} + A^{>} B^A \end{cases}$
$D^A = \int A^A B^A$	$D^A = \begin{cases} A^A B^{<} + A^{<} B^R \\ A^A B^{>} + A^{>} B^R \end{cases}$
$D^{\rceil} = \int A^{\rceil} B^M + \int A^R B^{\rceil}$	$D^{\rceil} = A^{\rceil} B^{\lceil}$
$D^{\lceil} = \int A^{\lceil} B^A + \int A^M B^{\lceil}$	$D^{\lceil} = A^{\lceil} B^{\rceil}$
$D^M = \int A^M B^M$	$D^M = A^M B^M$

Table 1. The Langreth rules for convolutions (left) and products (right). See section 7.5 for explanation of the notation.

Note that in this notation the Langreth rules are specific to a particular ordering of arguments. For example, we have for the chain convolution in the form $\mathscr{C}_{ab} = \int_{\gamma'} \mathscr{A}_{a\bar{c}} \mathscr{B}_{\bar{c}b}$ the rule

$$C^R_{ab} = \int A^R_{a\bar{c}} B^R_{\bar{c}b}. \tag{188}$$

If we wish to obtain the rule for a different ordering of arguments, such as $\mathscr{C}_{ab} = \int_{\gamma'} \mathscr{A}_{a\bar{c}} \mathscr{B}_{b\bar{c}}$, we can write the rule above using explicit argument labels as

$$C^{R(\check{a},\check{b})}_{ab} = A^{R(\check{a},\check{c})}_{a\bar{c}} B^{R(\check{c},\check{b})}_{\bar{c}b}. \tag{189}$$

In this form the rule remains valid if the argument order is changed, which again indicates the convenience of the háček notation. We can then convert back to the earlier notation to obtain

$$C^{R(\check{a},\check{b})}_{ab} = A^{R(\check{a},\check{c})}_{a\bar{c}} B^{R(\check{c},\check{b})}_{b\bar{c}} \to C^R_{ab} = A^R_{a\bar{c}} B^A_{\bar{c}b}. \tag{190}$$

We have made use of the simpler Langreth rules to simplify the notation for the more complex ones. Thus there appears for example $[A_{a\bar{c}} B_{\bar{c}b} D_{a\bar{d}} E_{\bar{d}b}]^R_{ab}$, which is a product of two convolutions and can be worked out using the rules in Table 1 to give

$$\begin{aligned} [A_{a\bar{c}} B_{\bar{c}b} D_{a\bar{d}} E_{\bar{d}b}]^R_{ab} &= [A_{a\bar{c}} B_{\bar{c}b}]^R_{ab} \, [D_{a\bar{d}} E_{\bar{d}b}]^<_{ab} + [A_{a\bar{c}} B_{\bar{c}b}]^<_{ab} \, [D_{a\bar{d}} E_{\bar{d}b}]^A_{ab} \\ &= A^R_{a\bar{c}} B^R_{\bar{c}b} \left(D^R_{a\bar{d}} E^<_{\bar{d}b} + D^<_{a\bar{d}} E^A_{\bar{d}b} \right) + \left(A^R_{a\bar{c}} B^<_{\bar{c}b} + A^<_{a\bar{c}} B^A_{\bar{c}b} \right) D^A_{a\bar{d}} E^A_{\bar{d}b}. \end{aligned} \tag{191}$$

Likewise there are chains of three two-point sub-functions, such as

$$[D_{a\bar{d}} C_{\bar{c}\bar{d}} B_{\bar{c}b}]^R_{ab} = [D_{a\bar{d}} C_{\bar{c}\bar{d}}]^R_{a\bar{d}} B^R_{\bar{c}b} = D^R_{a\bar{d}} C^A_{\bar{c}\bar{d}} B^R_{\bar{c}b}. \tag{192}$$

$$\mathscr{G}_{ab} = \int_{\gamma'} \bar{\mathscr{G}}_{ab\bar{c}\bar{d}} = \int_{\gamma'} \mathscr{A}_{a\bar{c}} \mathscr{B}_{\bar{c}b} \mathscr{C}_{\bar{c}\bar{d}} \mathscr{D}_{a\bar{d}} \mathscr{E}_{\bar{d}b}$$

$$\begin{aligned}
G^{>} = {} & \int A^{\rceil} B^{\lceil} C^{M} D^{\rceil} E^{\lceil} + \int [AB]^{>} C^{\rceil} D^{\rceil} E^{\lceil} + \int A^{\rceil} B^{\lceil} C^{\lceil} [DE]^{>} \\
& + \int [AB]^{>} C^{>} [DE]^{>} + \int [AB]^{>} C^{R} (D^{<} - D^{A}) E^{>} + \int A^{>} (B^{<} + B^{R}) C^{A} [DE]^{>} \\
G^{<} = {} & \int A^{\rceil} B^{\lceil} C^{M} D^{\rceil} E^{\lceil} + \int [AB]^{<} C^{\rceil} D^{\rceil} E^{\lceil} + \int A^{\rceil} B^{\lceil} C^{\lceil} [DE]^{<} \\
& + \int [AB]^{<} C^{>} [DE]^{<} + \int [AB]^{<} C^{R} D^{<} (E^{>} - E^{R}) + \int (A^{>} + A^{A}) B^{<} C^{A} [DE]^{<} \\
G^{R} = {} & \int [AB]^{R} C^{\rceil} D^{\rceil} E^{\lceil} + \int A^{\rceil} B^{\lceil} C^{\lceil} [DE]^{R} \\
& + \int [ABDE]^{R} C^{>} + \int [AB]^{R} C^{R} D^{<} E^{>} + \int A^{>} B^{<} C^{A} [DE]^{R} \\
& + \int A^{>} [DCB]^{R} E^{>} + \int B^{<} [ACE]^{R} D^{<} \\
G^{A} = {} & \int [AB]^{A} C^{\rceil} D^{\rceil} E^{\lceil} + \int A^{\rceil} B^{\lceil} C^{\lceil} [DE]^{A} \\
& + \int [ABDE]^{A} C^{>} + \int [AB]^{A} C^{R} D^{<} E^{>} + \int A^{>} B^{<} C^{A} [DE]^{A} \\
& + \int A^{>} [DCB]^{A} E^{>} + \int B^{<} [ACE]^{A} D^{<}
\end{aligned}$$

$$G^{\rceil} = \int A^{\rceil} B^{M} C^{M} D^{\rceil} E^{M} + \int A^{\rceil} B^{M} C^{\lceil} D^{R} E^{\rceil} + \int A^{R} B^{\rceil} C^{\rceil} D^{\rceil} E^{M} + \int [ADC]^{1} B^{\rceil} E^{\rceil}$$

$$G^{\lceil} = \int A^{M} B^{\lceil} C^{M} D^{M} E^{\lceil} + \int A^{M} B^{\lceil} C^{\lceil} D^{\lceil} E^{A} + \int A^{\lceil} B^{A} C^{\rceil} D^{M} E^{\lceil} + \int A^{\lceil} D^{\lceil} [CBE]^{1}$$

$$G^{M} = \int A^{M} B^{M} C^{M} D^{M} E^{M}$$

$$\mathscr{F}_{a} = \int_{\gamma'} \bar{\mathscr{F}}_{a\bar{b}\bar{c}} = \int_{\gamma'} \mathscr{A}_{a\bar{b}} \mathscr{B}_{a\bar{c}} \mathscr{C}_{\bar{b}\bar{c}}$$

$$F^{1} = \int A^{\rceil} B^{\rceil} C^{M} + \int A^{\rceil} B^{R} C^{\lceil} + \int A^{R} B^{\rceil} C^{\rceil} + \int \bar{F}^{R(\check{a},\check{b}\check{c})}_{a\bar{b}\bar{c}}$$

$$\bar{F}^{R(\check{a},\check{b}\check{c})}_{abc} = \begin{cases} A^{R} B^{>} C^{R} + A^{<} B^{R} C^{A} + A^{R} B^{R} C^{<} \\ A^{R} B^{<} C^{R} + A^{>} B^{R} C^{A} + A^{R} B^{R} C^{>} \end{cases}$$

Table 2. Langreth rules for the double-triangle structure. See section 7.5 for explanation of the notation.

8. Conclusions

Non-equilibrium Green's function methods require a translation between contour quantities, well suited for representing the abstract theory, and real-time quantities, well suited for numerical calculations. In this paper we have provided general rules to perform this translation effectively.

We have constructed a diagrammatic recipe to straightforwardly obtain generalized Langreth rules for the important cases of the double-triangle structure and the vertex diagram. Our diagrammatic recipe can be applied to other structures of interest, such as the Hedin equation for the vertex function, and for the Bethe-Salpeter equation. The general rules laid out in this paper will make this possible.

Apart from deriving Langreth rules, the results derived in this paper are of use in other contexts. As an example, we recently showed that an expression for the self-energy, that yields a positive semi-definite spectral function, can be derived in non-equilibrium situations by making use of generalized retarded compositions of half-diagrams [9].

$\mathscr{H}_{ab} = \int_{\gamma'} \bar{\mathscr{H}}_{ab\bar{c}\bar{d}} = \int_{\gamma'} \mathscr{A}_{a\bar{c}} \mathscr{B}_{a\bar{d}} \mathscr{C}_{\bar{d}b\bar{c}}$

$$
\begin{aligned}
H^{>} = {} & \int A^{\rceil} B^{\rceil} C^{M(\check{c}\check{d})\check{b}} \\
& + \int A^{>} B^{\rceil} C^{M(\check{d})R(\check{b},\check{c})} + \int A^{R} B^{\rceil} C^{M(\check{d})\check{c}\check{b}} + \int A^{\rceil} B^{>} C^{M(\check{c})R(\check{b},\check{d})} + \int A^{\rceil} B^{R} C^{M(\check{c})\check{d}\check{b}} \\
& + \int A^{>} B^{R} C^{R(\check{d},\check{c})\check{b}} + \int A^{R} B^{<} C^{R(\check{c},\check{d})\check{b}} + \int A^{R} B^{>} C^{\check{c}R(\check{b},\check{d})} + \int A^{>} B^{R} C^{\check{d}R(\check{b},\check{c})} \\
& + \int A^{R} B^{R} C^{\check{c}\check{d}\check{b}} + \int A^{>} B^{>} C^{R(\check{b},\check{c}\check{d})}
\end{aligned}
$$

$$
\begin{aligned}
H^{<} = {} & \int A^{\rceil} B^{\rceil} C^{M(\check{c}\check{d})\check{b}} \\
& + \int A^{<} B^{\rceil} C^{M(\check{d})R(\check{b},\check{c})} + \int A^{R} B^{\rceil} C^{M(\check{d})\check{b}\check{c}} + \int A^{\rceil} B^{<} C^{M(\check{c})R(\check{b},\check{d})} + \int A^{\rceil} B^{R} C^{M(\check{c})\check{b}\check{d}} \\
& + \int A^{>} B^{R} C^{\check{b}R(\check{d},\check{c})} + \int A^{<} B^{R} C^{R(\check{b},\check{c})\check{d}} + \int A^{R} B^{<} C^{\check{b}R(\check{c},\check{d})} + \int A^{R} B^{<} C^{R(\check{b},\check{d})\check{c}} \\
& + \int A^{R} B^{R} C^{\check{b}\check{c}\check{d}} + \int A^{<} B^{<} C^{R(\check{b},\check{c}\check{d})}
\end{aligned}
$$

$$
\begin{aligned}
H^{R} = {} & \int A^{R} B^{\rceil} C^{M(\check{d})R(\check{c},\check{b})} + \int A^{\rceil} B^{R} C^{M(\check{c})R(\check{d},\check{b})} \\
& + \int A^{>} B^{R} C^{R(\check{d},\check{b}\check{c})} + \int A^{R} B^{<} C^{R(\check{c},\check{b}\check{d})} + \int A^{R} B^{R} \big(C^{\check{c}R(\check{d},\check{b})} + \int C^{R(\check{c},\check{b})\check{d}} \big)
\end{aligned}
$$

$$
\begin{aligned}
H^{A} = {} & \int A^{A} B^{\rceil} C^{M(\check{d})R(\check{b},\check{c})} + \int A^{\rceil} B^{A} C^{M(\check{c})R(\check{b},\check{d})} \\
& + \int \big(A^{>} B^{A} + A^{A} B^{<} \big) C^{R(\check{b},\check{c}\check{d})} + \int A^{R} B^{A} C^{\check{c}R(\check{b}\check{d})} + \int A^{A} B^{R} C^{R(\check{b},\check{c})\check{d}}
\end{aligned}
$$

$$
\begin{aligned}
H^{\rceil} = {} & \int A^{\rceil} B^{\rceil} C^{M(\check{b}\check{c}\check{d})} + \int A^{\rceil} B^{R} C^{M(\check{b}\check{c})\check{d}} + \int A^{R} B^{\rceil} C^{M(\check{b}\check{d})\check{c}} \\
& + \int A^{R} B^{<} C^{M(\check{b})R(\check{c},\check{d})} + \int A^{>} B^{R} C^{M(\check{b})R(\check{d},\check{c})} + \int A^{R} B^{R} C^{M(\check{b})\check{c}\check{d}}
\end{aligned}
$$

$$
H^{\lceil} = \int A^{M} B^{M} C^{M(\check{c}\check{d})\check{b}} + \int A^{M} B^{\lceil} C^{M(\check{c})R(\check{b},\check{d})} + \int A^{\lceil} B^{M} C^{M(\check{d})R(\check{b},\check{c})} + \int A^{\lceil} B^{\lceil} C^{R(\check{b},\check{c}\check{d})}
$$

$$
H^{M} = \int A^{M} B^{M} C^{M(\check{b}\check{c}\check{d})}
$$

Table 3. Langreth rules for the vertex structure. See section 7.5 for explanation of the notation.

Acknowledgments

D.K. acknowledges the Academy of Finland for funding under Project No. 308697. M.H. thanks the Finnish Cultural Foundation for support. R.v.L. acknowledges the Academy of Finland for funding under Project No. 317139.

Appendix A. Decomposition of Step Functions

In this section, we will show how to write products of two step functions as sums in terms of permutations of a single step function. This joining of step functions is useful when discussing the retarded composition. As an example, we consider the multiplication of two step functions containing two times:

$$
\begin{aligned}
\Theta(t_1,t_2)\Theta(t_3,t_4) = {} & \Theta(t_1,t_2,t_3,t_4) + \Theta(t_1,t_3,t_2,t_4) + \Theta(t_1,t_3,t_4,t_2) \\
& + \Theta(t_3,t_1,t_2,t_4) + \Theta(t_3,t_1,t_4,t_2) + \Theta(t_3,t_4,t_1,t_2).
\end{aligned}
\tag{A.1}
$$

The sum contains all six permutations for which t_1 is to the left of t_2, and t_3 to the left of t_4. This example can be generalized. Let us consider two sets of time variables, $t_1, t_2, \ldots, t_k$ and $t_{k+1}, t_{k+2}, \ldots, t_m$, and the product $\Theta(t_1, t_2, \ldots, t_k)\Theta(t_{k+1}, t_{k+2}, \ldots, t_m)$.

The multiplication can be written as a sum over permutations $R \in \mathcal{R}_{m,k}$ of the time arguments $t_1, \ldots, t_m$ in a single step function,

$$\Theta(t_1, t_2, \ldots, t_k)\Theta(t_{k+1}, t_{k+2}, \ldots, t_m) = \sum_{R \in \mathcal{R}_{m,k}} \Theta\left(t_{R(1)}, t_{R(2)}, \ldots, t_{R(m)}\right). \tag{A.2}$$

where we sum over all permutations $R \in \mathcal{R}_{m,k}$ that retain the relative ordering among $t_1, \ldots, t_k$ and $t_{k+1}, \ldots, t_m$, separately, as imposed by the original step functions on the left-hand side. That is, the permutation R orders the times such that the position of t_1 is to the left of t_2, and so on until t_k, and the same for the times $t_{k+1}, \ldots, t_m$. In case a step function contains only one or zero arguments, we define that step function to yield 1.

Equation (A.1) is a special case of Eq. (A.2) with $m = 4$ and $k = 2$, for which there are a six permutations that keep the original time ordering. We write these permutations as

$$\sum_{R \in \mathcal{R}_{4,2}} R(1234) = 1234 + 1324 + 1342 + 3124 + 3142 + 3412. \tag{A.3}$$

The set $\mathcal{R}_{m,k}$ is a subset of the symmetric group $\mathcal{S}_m$. The set $\mathcal{R}_{m,k}$ is, however, not a group itself, since inverse permutations are not always included. As an example, we can take $\mathcal{R}_{4,2}$, and the permutation $R(1234) = 1342$ from Eq. (A.3). The inverse is $R^{-1}(1234) = 1423$, which is not in $\mathcal{R}_{4,2}$.

The total number of permutations $|\mathcal{R}_{m,k}|$, i.e. the size of the set $\mathcal{R}_{m,k}$, is given by the following combinatorical argument. Let us assume that $t_{k+1}, \cdots, t_m$ are ordered by the permutation in the correct order. The number of ways we can place the k time arguments $t_1, \cdots, t_k$ among $t_{k+1}, \cdots, t_m$ is given by $m(m-1)(m-2)\cdots(m-k) = \frac{m!}{(m-k)!}$. Of all these permutations, one out of every $k!$ permutations has the arguments $t_1, \cdots, t_k$ in the right order. Dividing by $k!$ gives the size of the set $\mathcal{R}_{m,k}$ as

$$|\mathcal{R}_{m,k}| = \frac{m!}{(m-k)!k!} = \binom{m}{k}. \tag{A.4}$$

The set $\mathcal{R}_{m,k}$ can be defined in a compact manner. We note that the argument $t_{R(i)}$ is at position i in the step function on the right hand side of Eq. (A.2). Writing $l = R(i)$, the argument t_l is at position $R^{-1}(l)$. Thus, the set $\mathcal{R}_{m,k}$ can be defined as the set of permutations R that satisfy

$$\begin{aligned} (i < j) \text{ and } (i, j \leq k)) &\Rightarrow R^{-1}(i) < R^{-1}(j) \\ (i < j) \text{ and } (i, j > k)) &\Rightarrow R^{-1}(i) < R^{-1}(j). \end{aligned} \tag{A.5}$$

Writing $R^{-1}(i) = l$ in Eq. (A.5), we can equivalently define the set $\mathcal{R}_{m,k}$ to contain the permutations that satisfy

$$\begin{aligned} (R(i) < R(j)) \text{ and } (R(i), R(j) \leq k)) &\Rightarrow i < j \\ (R(i) < R(j)) \text{ and } (R(i), R(j) > k)) &\Rightarrow i < j. \end{aligned} \tag{A.6}$$

It turns out that we will need one more result, which is the multiplication of two step functions containing $t_1, \cdots, t_k$ and $t_{k+1}, \cdots, t_m$ separately, when the order of the first set of times is reversed:

$$\Theta(t_k, t_{k-1}, \cdots, t_1)\Theta(t_{k+1}, t_{k+2}, \cdots, t_m) = \sum_{T \in \mathcal{T}_{m,k}} \Theta\left(t_{T(1)}, t_{T(2)}, \cdots, t_{T(m)}\right). \tag{A.7}$$

The set $\mathcal{T}_{m,k}$ is closely related to $\mathcal{R}_{m,k}$. The size of the set is the same, $|\mathcal{T}_{m,k}| = \binom{m}{k}$, and it can be defined by either of the two relations

$$\begin{aligned} (i > j) \text{ and } (i, j \leq k) &\Rightarrow T^{-1}(i) < T^{-1}(j) \\ (i < j) \text{ and } (i, j > k) &\Rightarrow T^{-1}(i) < T^{-1}(j). \end{aligned} \tag{A.8}$$

or

$$\begin{aligned} (T(i) > T(j)) \text{ and } (T(i), T(j) \leq k) &\Rightarrow i < j \\ (T(i) < T(j)) \text{ and } (T(i), T(j) > k) &\Rightarrow i < j. \end{aligned} \tag{A.9}$$

The multiplication of step functions are related to the structure of nested commutators, as we show in the next appendix.

Appendix B. The Structure of Nested Commutators

In this section, we elucidate the structure of the nested commutator and derive some useful results. Our discussion on structure follows a similar one in Ref. [17].

The nested commutator of $m + 1$ objects, $[x, 1, 2, \cdots m]$, where each number $x, 1, \cdots, m$ represents a different object, is defined as

$$[x, 1, 2, \cdots m] = [\cdots [[x, 1], 2], \cdots, m]. \tag{B.1}$$

The nested commutator in Eq. (B.1) has 2^m terms, of which one half has a prefactor $+1$ and one half a prefactor -1. It is convenient to group the terms according to the number of objects, k, that appear to the left of x in each term. The sign of the terms is given by $(-1)^k$. Let us take the example of $m = 4$ and $k = 2$:

$$[x, 1, 2, 3, 4]_2 = 21x34 + 31x24 + 41x23 + 32x14 + 42x13 + 43x12 \tag{B.2}$$

where $_2$ denotes that two objects are to the left of x, and therefore all terms have a positive sign. In Eq. (B.2), the numbers to the left of x are in decreasing order, while the numbers to the right are in increasing order.

In general, we write a nested commutator as

$$[x, 1, 2, \cdots, m] = \sum_k [x, 1, 2, \cdots, m]_k, \tag{B.3}$$

where the terms $[x, 1, 2, \cdots, m]_k$, with k numbers to the left of x, can be written as

$$[x, 1, 2, \cdots, m]_k = (-)^k \sum_{Q \in \mathcal{Q}_{m,k}} Q(1, 2, \cdots, k) x Q(k + 1, \cdots, m), \tag{B.4}$$

where we sum over all permutations $Q \in \mathcal{Q}_{m,k}$ such that the numbers to the left of x are in decreasing order, and the numbers to the right of x in increasing order. In the example above, Eq. (B.2), we have

$$[x, 1, 2, 3, 4]_2 = \sum_{Q \in \mathcal{Q}_{4,2}} Q(12)xQ(34) \tag{B.5}$$

with

$$\sum_{Q \in \mathcal{Q}_{4,2}} Q(1234) = 2134 + 3124 + 4123 + 3214 + 4213 + 4312. \tag{B.6}$$

We see that $Q(1) > Q(2)$, while $Q(3) < Q(4)$.

The set $\mathcal{Q}_{m,k}$ can be compactly defined as containing those permutations Q that fulfill

$$\begin{aligned} &(i > j) \text{ and } (i, j \leq k) \Rightarrow Q(i) < Q(j) \\ &(i < j) \text{ and } (i, j > k) \Rightarrow Q(i) < Q(j). \end{aligned} \tag{B.7}$$

Comparing with Eq. (A.8), we see that the set $\mathcal{Q}_{m,k}$ contain exactly the inverses of the set $\mathcal{T}_{m,k}$.

We will now prove some relations between nested commutators, that are useful when working with retarded compositions. Let us now denote a nested commutator of n objects by

$$A_n = [1, \ldots, n]. \tag{B.8}$$

To begin with we observe that

$$[1, \ldots, n] = [A_{i-1}, i, \ldots, n]. \tag{B.9}$$

We will then prove that

$$\begin{aligned} [\ldots, i-1, [i, x], i+1, \ldots] = [\ldots, i-1, i, x, i+1, \ldots] \\ - [\ldots, i-1, x, i, i+1, \ldots] \qquad \text{when } i > 1. \end{aligned} \tag{B.10}$$

For Eq. (B.10), we obtain, from Eq. (B.9),

$$\begin{aligned} [\ldots, i-1, [i, x], i+1, \ldots] &= [A_{i-1}, [i, x], i+1, \ldots] \\ &= [[[A_{i-1}, [i, x]], i+1], \ldots] \end{aligned} \tag{B.11}$$

Using the Jacobi identity, Eq. (152), we find

$$[A_{i-1}, [i, x]] = [[A_{i-1}, i], x] - [[A_{i-1}, x], i]. \tag{B.12}$$

Inserting the Jacobi identity into Eq. (B.11) leads to

$$\begin{aligned} &[[[[A_{i-1}, i], x], i+1], \ldots] - [[[[A_{i-1}, x], i], i+1], \ldots] \\ &= [A_{i-1}, i, x, i+1, \ldots] - [A_{i-1}, x, i, i+1, \ldots] \\ &= [\ldots, i-1, i, x, i+1, \ldots] - [\ldots, i-1, x, i, i+1, \ldots], \end{aligned} \tag{B.13}$$

which proves Eq. (B.10).

Finally we will show that

$$\begin{aligned}&[\ldots,i,x,i+1,\ldots]\\&=[[1,x],2,\ldots]+[1,[2,x],3,\ldots]+\ldots+[\ldots,i-1,[i,x],i+1,\ldots]\end{aligned}\tag{B.14}$$

This result can be proven by induction, with the base step

$$\begin{aligned}&[[1,x],2,\ldots]+[1,[2,x],3,\ldots]\\&=[1,x,2,\ldots]+[1,2,x,3,\ldots]-[1,x,2,3,\ldots]\\&=[1,2,x,3,\ldots],\end{aligned}\tag{B.15}$$

and the induction step

$$\begin{aligned}&[\ldots,i,x,i+1,\ldots]+[\ldots,i,[i+1,x],i+2,\ldots]\\&=[\ldots,i,x,i+1,\ldots]+[\ldots,i,i+1,x,i+2,\ldots]-[\ldots,i,x,i+1,i+2,\ldots]\\&=[\ldots,i+1,x,i+2,\ldots]\end{aligned}\tag{B.16}$$

Appendix C. Expansion of Retarded Compositions in Terms of Nested Retarded Compositions

A general retarded composition can be defined as

$$O^{\check{X}R(Z_1,Z_2\cdots Z_r)\check{Y}}=\sum_{P\in S_{r-1}}\Theta_{h_1h_{P(2)}\cdots h_{P(r)}}O^{\check{X}[Z_1,Z_{P(2)},\ldots,Z_{P(r)}]\check{Y}},\tag{C.1}$$

where Z_i is some object with a defined a top element h_i. In the simplest case of $Z_i=\check{h}_i$ for all i, Eq. (C.1) reduces to the definition of a simple retarded composition in Eq. (56). If Z_i, for some i, is taken to be a retarded set, for example $Z_i=R(\mathcal{H}_i)$ for some $\mathcal{H}_i=h_i\cup I_i$, Eq. (C.1) defines a nested retarded composition. Finally Z_i itself can be nested retarded set, for example $Z_i=R(R(\mathcal{H}_i),R(\mathcal{H}_r))$. In this case the top element h_i is the top element of $\mathcal{H}_i$.

Here we will use the relations between nested commutators derived in Appendix B to derive the result expressed diagrammatically in Eq. (159). We will show that a nested retarded composition can be expanded as a sum of nested retarded compositions as

$$\bar{O}^{\check{X}R(Z_1,Z_2\cdots Z_r)\check{Y}}(t_{\mathcal{N}})=\sum_{i=1}^{r-1}\bar{O}^{\check{X}R(Z_1,Z_2\cdots Z_{i-1}R(Z_i,Z_r)Z_{i-1}\cdots Z_{r-1})\check{Y}}(t_{\mathcal{N}}).\tag{C.2}$$

Here we have expanded with respect to Z_r. Note that since the left hand side is symmetric with respect to permutations of the indices $2\cdots r$, the expansions with respect to any of the objects $Z_2,\ldots,Z_r$ give the same result.

To keep the presentation cleaner we suppress X and Y as well as the time-arguments. For the right hand side of Eq. (C.2) we define a new set of Z' objects as

$$\begin{aligned}Z'_i&=R(Z_i,Z_r)\\Z'_k&=Z_k\quad k\neq i.\end{aligned}\tag{C.3}$$

Note that the top element of Z'_n is the same as for Z_n, i.e. h_n, for all n. Using this definition the right hand side of Eq. (C.2) can be expanded using Eq. (C.1). For each i we can restrict our attention to the term that contain the unit permutation, as the other terms can be obtained by subsequent permutations at the end of the derivation. This gives

$$\begin{aligned}\sum_{i=1}^{r-1}\Theta_{h_1\cdots h_{r-1}}\bar{O}^{[Z'_1,Z'_2\cdots Z'_{i-1}Z'_iZ_{i+1}\cdots Z'_{r-1}]} &= \sum_{i=1}^{r-1}\Theta_{h_1\cdots h_{r-1}}\bar{O}^{[Z_1,Z_2\cdots Z_{i-1}R(Z_i,Z_r)Z_{i+1}\cdots Z_{r-1}]}\\ &= \sum_{i=1}^{r-1}\Theta_{h_1\cdots h_{r-1}}\Theta_{h_ih_r}\bar{O}^{[Z_1,Z_2\cdots Z_{i-1}[Z_i,Z_r]Z_{i+1}\cdots Z_{r-1}]}.\end{aligned} \tag{C.4}$$

The product of step functions can be written as a sum of step functions using

$$\Theta_{h_1\cdots h_{r-1}}\Theta_{h_ih_r} = \sum_{j=i}^{r-1}\Theta_{h_1\cdots h_jh_rh_{j+1}\cdots h_{r-1}}, \tag{C.5}$$

We then reorder the sums

$$\sum_{i=1}^{r-1}\sum_{j=i}^{r-1} \to \sum_{j=1}^{r-1}\sum_{i=1}^{j}, \tag{C.6}$$

which leads to

$$\begin{aligned}\sum_{i=1}^{r-1}\Theta_{h_1\cdots h_{r-1}}\bar{O}^{[Z'_1,Z'_2\cdots Z'_i\cdots Z'_{r-1}]} &= \sum_{j=1}^{r-1}\Theta_{h_1\cdots h_jh_rh_{j+1}\cdots h_{r-1}}\sum_{i=1}^{j}\bar{O}^{[Z_1,Z_2\cdots Z_{i-1}[Z_i,Z_r]Z_{i+1}\cdots Z_{r-1}]}\\ &= \sum_{j=1}^{r-1}\Theta_{h_1\cdots h_jh_rh_{j+1}\cdots h_{r-1}}\bar{O}^{[Z_1,Z_2,\ldots,Z_j,Z_r,Z_{j+1},\ldots,Z_{r-1}]},\end{aligned} \tag{C.7}$$

where on the last line we have used the relation between nested commutators shown in Eq. (B.14). Summing over all the permutations of $2\cdots r-1$ in Eq. (C.7) yields the right-hand side of Eq. (C.2) as a consequence of the definition of a retarded composition, Eq. (C.1). The sum over permutations yields

$$\sum_{P\in S_{r-2}}\sum_{j=1}^{r-1}\Theta_{h_1\cdots h_{P(j)}h_rh_{P(j+1)}\cdots h_{P(r-1)}}\bar{O}^{[Z_1,Z_{P(2)},\ldots,Z_{P(j)},Z_r,Z_{P(j+1)},\ldots,Z_{P(r-1)}]} \tag{C.8}$$

Here for each permutation of $2,\ldots,r-1$, one sums over all positions of r in the sequence. The effect is the same as summing over all permutations of $2,\ldots,r$. Eq. (C.8) then becomes equal to the definition of the retarded composition $\bar{O}^{R(Z_1,Z_2\cdots Z_r)}$, as given by Eq. (C.1). This completes the proof of Eq. (C.2).

As a useful example of the expansion in Eq. (C.2), we consider a case in which all objects Z_i only contain single elements, that is $Z_i = \check{h}_i$. The expansion formula in this

case is

$$\bar{O}^{\check{X}R(\check{h}_1,\check{h}_2\cdots\check{h}_r)\check{Y}}(t_{\mathcal{N}}) = \sum_{i=1}^{r-1} \bar{O}^{\check{X}R(\check{h}_1,\check{h}_2\cdots\check{h}_{i-1}R(\check{h}_i,\check{h}_r)\check{h}_{i+1}\cdots\check{h}_{r-1})\check{Y}}(t_{\mathcal{N}}). \tag{C.9}$$

Finally we will consider the case of expanding one of the nested sets. For example, suppose that we have $O^{\check{X}R(Z_1,Z_2\cdots Z_r)\check{Y}}(t_{\mathcal{N}})$ where $Z_k = R(Z'_1, Z'_2\cdots Z'_s)$. In this case it is possible to apply Eq. (C.2) on Z_k to obtain

$$\begin{aligned} &\bar{O}^{\check{X}R(Z_1,Z_2\cdots Z_{k-1}R(Z'_1,Z'_2\cdots Z'_s)Z_{k+1}\cdots Z_r)\check{Y}}(t_{\mathcal{N}}) \\ &= \sum_{i=1}^{s-1} \bar{O}^{\check{X}R(Z_1,Z_2\cdots Z_{k-1}R(Z'_1,Z'_2\cdots R(Z'_i,Z'_s)\cdots Z'_{s-1})Z_{k+1}\cdots Z_r)\check{Y}}(t_{\mathcal{N}}). \end{aligned} \tag{C.10}$$

To prove Eq. (C.10) we expand the outermost retarded set in nested commutators. After expanding also the nested commutators thus generated, one obtains a sum in which terms of the form considered above in Eq. (C.2) appear. Eq. (C.2) can then be applied to each of these terms to expand Z_k. Because in the sum of terms generated by Eq. (C.2) the top element of the expanded retarded set remains the same in each term, we can reconstruct the outermost retarded set, which leads to Eq. (C.10). Note that expanding a set deeper in the nested structure raises no further issues. In each such case expanding the outer retarded sets allows one to eventually reach a situation in which Eq. (C.2) can be applied.

Appendix D. Retarded-set Representation for Retarded Compositions

Here we will outline the proof of Eq. (87), which states that for two Keldysh-functions $\mathscr{O}$ and $\bar{\mathscr{O}}$ related by

$$\mathscr{O}(z_{\mathcal{E}}) = \int_\gamma \mathrm{d}z_{\mathcal{I}}\, \bar{\mathscr{O}}(z_{\mathcal{N}}), \tag{D.1}$$

the retarded compositions are related by

$$O^{R(\check{h}_1,\check{\mathcal{H}}_1)\cdots R(\check{h}_H,\check{\mathcal{H}}_H)}(t_{\mathcal{E}}) = \int_{t_0}^{\infty} \mathrm{d}t_{\mathcal{I}} \sum_{\mathcal{I}} \bar{O}^{R(\check{h}_1,\check{\mathcal{H}}_1\cup\check{\mathcal{I}}_1)\cdots R(\check{h}_H,\check{\mathcal{H}}_H\cup\check{\mathcal{I}}_H)}(t_{\mathcal{N}}). \tag{D.2}$$

We first prove the case for a single internal argument z_i, for which

$$\mathscr{O}(z_{\mathcal{E}}) = \int_\gamma \mathrm{d}z_i\, \bar{\mathscr{O}}(z_{\mathcal{N}}), \tag{D.3}$$

and

$$O^{R(\check{e}_1,\check{e}_2\cdots\check{e}_E)}(t_{\mathcal{E}}) = \int_{t_0}^{\infty} \mathrm{d}t_i\, \bar{O}^{R(\check{e}_1,\check{e}_2\cdots\check{e}_E\check{)}}(t_{\mathcal{N}}). \tag{D.4}$$

Suppressing the time-arguments, the proof of Eq. (D.4) proceeds as follows:

(i) We expand the left-hand side of Eq. (D.4) in terms of nested commutators using Eq. (64). This gives

$$O^{R(\check{e}_1,\check{e}_2\cdots\check{e}_E)} = \sum_{P\in S_{E-1}} \Theta_{e_1 e_{P(2)}\cdots e_{P(E)}} O^{[\check{e}_1,\check{e}_{P(2)},\ldots,\check{e}_{P(E)}]}. \tag{D.5}$$

(ii) Each Keldysh component of $\mathscr{O}$ can be written in terms of retarded compositions of $\bar{\mathscr{O}}$ using Eq. (63). This gives for example for the Keldysh component $O^{\check{e}_1\cdots\check{e}_E}$

$$O^{\check{e}_1\cdots\check{e}_E} = \int_{t_0}^{\infty} \mathrm{d}t_i \sum_{j=1}^{E} \bar{O}^{\check{e}_1\cdots R(\check{e}_j,\check{i})\cdots\check{e}_E}, \tag{D.6}$$

and similarly for each permutation of $e_1,\ldots,e_E$. Thus if in Eq. (D.5) we expand the nested commutators, apply Eq. (D.6) to each Keldysh component, and then reconstruct the nested commutator, we obtain

$$\begin{aligned} O^{R(\check{e}_1,\check{e}_2\cdots\check{e}_E)} &= \int_{t_0}^{\infty} \mathrm{d}t_i \sum_{j=1}^{E} \sum_{P\in S_{E-1}} \Theta_{e_1 e_{P(2)}\cdots e_{P(E)}} O^{[\check{e}_1,\check{e}_{P(2)},\ldots,R(\check{e}_j,\check{i}),\ldots,\check{e}_{P(E)}]} \\ &= \int_{t_0}^{\infty} \mathrm{d}t_i \sum_{j=1}^{E} O^{R(\check{e}_1,\check{e}_2\cdots R(\check{e}_j,\check{i})\cdots\check{e}_E)}, \end{aligned} \tag{D.7}$$

where on the second line we have used the definition of a nested retarded composition, Eq. (C.1).

(iii) We can now apply Eq. (C.9) derived in Appendix C to the right hand side of Eq. (D.7) to obtain Eq. (D.4), which was to be proven.

Multi-retarded compositions can be obtained by going through the same steps as above. To demonstrate this we will consider an example with four external arguments and take the component

$$O^{R(\check{a},\check{b})R(\check{c},\check{d})} = \Theta_{ab}\Theta_{cd} O^{[\check{a},\check{b}][\check{c},\check{d}]}. \tag{D.8}$$

In the second step we again write the Keldysh components of $\mathscr{O}$ in terms of retarded compositions of $\bar{\mathscr{O}}$ using Eq. (63). For four arguments we have

$$O^{abcd} = \int_{t_0}^{\infty} \mathrm{d}t_i \left[\bar{O}^{R(\check{a},\check{i})\check{b}\check{c}\check{d}} + \bar{O}^{\check{a}R(\check{b},\check{i})\check{c}\check{d}} + \bar{O}^{\check{a}\check{b}R(\check{c},\check{i})\check{d}} + \bar{O}^{\check{a}\check{b}\check{c}R(\check{d},\check{i})}\right], \tag{D.9}$$

etc. Substituting these into Eq. (D.8) leads to

$$\begin{aligned} &\Theta_{ab}\Theta_{cd} O^{[\check{a},\check{b}][\check{c},\check{d}]} \\ &= \int_{t_0}^{\infty} \mathrm{d}t_i\, \Theta_{ab}\Theta_{cd}\Big(\bar{O}^{[R(\check{a},\check{i}),\check{b}][\check{c},\check{d}]} + \bar{O}^{[\check{a},R(\check{b},\check{i})][\check{c},\check{d}]} + \bar{O}^{[\check{a},\check{b}][R(\check{c},\check{i}),\check{d}]} + \bar{O}^{[\check{a},\check{b}][\check{c},R(\check{d},\check{i})]}\Big) \\ &= \int_{t_0}^{\infty} \mathrm{d}t_i \left(\bar{O}^{R(R(\check{a},\check{i}),\check{b})R(\check{c},\check{d})} + \bar{O}^{R(\check{a},R(\check{b},\check{i}))R(\check{c},\check{d})} + \bar{O}^{R(\check{a},\check{b})R(R(\check{c},\check{i}),\check{d})} + \bar{O}^{R(\check{a},\check{b})R(\check{c},R(\check{d},\check{i}))}\right). \end{aligned} \tag{D.10}$$

Applying Eq. (C.2) in step iii) now leads to

$$\Theta_{ab}\Theta_{cd} O^{[\check{a},\check{b}][\check{c},\check{d}]} = \int_{t_0}^{\infty} \mathrm{d}t_i \left[\bar{O}^{R(\check{a},\check{b}\check{i})R(\check{c},\check{d})} + \bar{O}^{R(\check{a},\check{b})R(\check{c},\check{d}\check{i})}\right]. \tag{D.11}$$

For an arbitrary retarded composition $O^{R(\check{h}_1,\check{\mathcal{H}}_1)\cdots R(\check{h}_H,\check{\mathcal{H}}_H)}$, performing these steps leads to

$$O^{R(\check{h}_1,\check{\mathcal{H}}_1)\cdots R(\check{h}_H,\check{\mathcal{H}}_H)}(t_{\mathcal{E}}) = \int_{t_0}^{\infty} \mathrm{d}t_i \sum_{j=1}^{H} \bar{O}^{R(\check{h}_1,\check{\mathcal{H}}_1)\cdots R(\check{h}_j,\check{\mathcal{H}}_j\cup\check{\imath})\cdots R(\check{h}_H,\check{\mathcal{H}}_H)}(t_{\mathcal{N}}), \tag{D.12}$$

in which the internal argument is added to each retarded set in turn.

Having considered the case of a single internal argument, the more general situation can be handled simply by applying Eq. (D.12) repeatedly for each integral in Eq. (D.1). In this way every internal argument gets added to each retarded set, and the end result is a sum in which the internal arguments are distributed in every possible way among the retarded sets. In other words we obtain Eq. (D.2) which was to be proven.

References

[1] Danielewicz P 1984 *Ann. Phys. (N. Y).* **152** 239–304 ISSN 00034916 URL http://linkinghub.elsevier.com/retrieve/pii/0003491684900927

[2] Stefanucci G and van Leeuwen R 2013 *Nonequilibrium Many-Body Theory of Quantum Systems: A Modern Introduction* (Cambridge: Cambridge University Press) ISBN 9781107352070

[3] Fetter A L and Walecka J D 2003 *Quantum Theory of Many-Particle Theory* (New York: Dover Publications)

[4] Langreth D C and Wilkins J W 1972 *Phys. Rev. B* **6** 3189–3227 ISSN 0556-2805 URL https://link.aps.org/doi/10.1103/PhysRevB.6.3189

[5] Langreth D C 1976 Linear and Nonlinear Response Theory with Applications *Linear Nonlinear Electron Transp. Solids* ed Devreese J T and Doren V E (Boston, MA: Springer US) ISBN 978-1-4757-0877-6 URL http://link.springer.com/10.1007/978-1-4757-0875-2

[6] Pavlyukh Y, Uimonen A M, Stefanucci G and van Leeuwen R 2016 *Phys. Rev. Lett.* **117** 206402 ISSN 0031-9007 (*Preprint* 1607.04309) URL https://link.aps.org/doi/10.1103/PhysRevLett.117.206402

[7] Hedin L 1965 *Phys. Rev* **139** URL http://link.aps.org/doi/10.1103/PhysRev.139.A796

[8] Danielewicz P 1990 *Ann. Phys. (N. Y).* **197** 154–201 ISSN 00034916 URL http://linkinghub.elsevier.com/retrieve/pii/0003491690902042

[9] Hyrkäs M J, Karlsson D and van Leeuwen R 2018 *unpublished* 1–7

[10] Keldysh L 1965 *Sov. Phys. JETP* **20** 1018–1026 URL http://www.jetp.ac.ru/cgi-bin/dn/e{_}020{_}04{_}1018.pdf

[11] Kadanoff L P and Baym G 1962 *Quantum Statistical Mechanics* (Benjamin, New York)

[12] van Leeuwen R and Stefanucci G 2012 *Phys. Rev. B* **85** 115119 ISSN 1098-0121 (*Preprint* arXiv:1102.4814v2) URL http://link.aps.org/doi/10.1103/PhysRevB.85.115119

[13] van Leeuwen R and Stefanucci G 2013 *J. Phys. Conf. Ser.* **427** 012001 ISSN 1742-6588 (*Preprint* 1303.7105) URL http://stacks.iop.org/1742-6596/427/i=1/a=012001?key=crossref.963aca25f9882b062aed2745dbf22737

[14] Wagner M 1991 *Phys. Rev. B* **44** 6104–6117 ISSN 01631829

[15] Konstantinov O V and Perel' V I 1961 *Jetp* **12** 142 URL http://www.jetp.ac.ru/cgi-bin/e/index/e/12/1/p142?a=list

[16] Ness H, Dash L K, Stankovski M and Godby R W 2011 *Phys. Rev. B* **84** 195114 ISSN 1098-0121 (*Preprint* 1106.1094) URL http://arxiv.org/abs/1106.1094http://link.aps.org/doi/10.1103/PhysRevB.84.195114

[17] Zagier D B 1970 *J. Math. Phys.* **11** 3253–3257 ISSN 0022-2488 URL http://aip.scitation.org/doi/10.1063/1.1665124

II

DIAGRAMMATIC EXPANSION FOR POSITIVE SPECTRAL FUNCTIONS IN THE STEADY-STATE LIMIT

by

M. Hyrkäs, D. Karlsson and R. van Leeuwen 2019

Physica status solidi B **256** 1800615 (2019).

DOI:10.1002/pssb.201800615

Diagrammatic Expansion for Positive Spectral Functions in the Steady-State Limit

M. J. Hyrkäs[*,1], D. Karlsson[1], R. van Leeuwen[1]

[1] Department of Physics, Nanoscience Center P.O.Box 35 FI-40014 University of Jyväskylä, Finland

Key words: Non-equilibrium Green's functions, perturbation theory, spectral properties

[*] Corresponding author: e-mail markku.hyrkas@jyu.fi

Recently, a method was presented [1] for constructing self-energies within many-body perturbation theory that is guaranteed to produce a positive spectral function for equilibrium systems, by representing the self-energy as a product of half-diagrams on the forward and backward branches of the Keldysh contour. We derive an alternative half-diagram representations that is based on products of retarded diagrams. Our approach extends the method to systems out of equilibrium. When a steady-state limit exists, we show that our approach yields a positive definite spectral function in the frequency domain.

1 Introduction In Ref. [1], Stefanucci et. al. derive a diagrammatic method for generating approximations for the self-energy that are guaranteed to produce positive semidefinite (PSD) spectral functions for equilibrium systems. It was shown that such approximate self-energies can be expressed as products of half-diagrams. These results were further applied to response functions in Ref. [2]. The approach of Ref. [1] is based on deriving a Lehmann-like representation for the correlation self-energy that in effect splits the Keldysh contour between the forward and backward branches partitioning the self-energy diagrams into time ordered and anti-time ordered half-diagrams. This approach requires the assumption that the interactions are adiabatically turned off in the future, which restricts the method to systems in equilibrium.

Below we will present an alternative formulation of the method in which the adiabatic turn-off in the future is avoided. This allows for the derivation of a Lehmann-like representation for the correlation self-energy that is valid also out of equilibrium [3,4]. In this formulation the self-energy diagrams are partitioned into two retarded pieces.

A special non-equilibrium situation emerges when after application of an external potential the system reaches a steady-state in the distant future. A commonly studied case is that of steady current in quantum transport, which is reached after the application of a bias. However, we may envisage many other situations, such as the attainment of a steady photocurrent of an illuminated solid, or persistent currents after application of a magnetic field in a spatially periodic system. Other examples can be conceived of when external fields couple to, e.g., the spin degrees of freedom in a system. In these cases the steady-state limit implies that we recover time-translational invariance in the long-time limit. If a steady-state is reached, our method proves that for the exact case, the spectral function is positive semidefinite (PSD) in the frequency domain. A general diagrammatic approximation will violate the PSD property [1]. The method of repairing the PSD property by a minimal addition of diagrams is the same in our extension as in Ref. [1].

We begin by briefly presenting the theoretical context, and then derive the Lehmann-like representation for the correlation self-energy following the example of Ref. [1] with only minor modifications. In the subsequent section we rewrite the representation in terms of explicitly retarded diagrams. In the final section, we consider the GW approximation as an example, and show that it gives PSD spectral functions in the steady-state limit.

2 Theoretical Background We consider an interacting fermion system described by a Hamiltonian of the form

$$\hat{H}(t) = \int d\mathbf{x}\hat{\psi}^\dagger(\mathbf{x})h(\mathbf{x},t)\hat{\psi}(\mathbf{x}) + \frac{1}{2}\int d\mathbf{x}d\mathbf{x}'\hat{\psi}^\dagger(\mathbf{x})\hat{\psi}^\dagger(\mathbf{x}')v(\mathbf{x},\mathbf{x}')\hat{\psi}(\mathbf{x}')\hat{\psi}(\mathbf{x}). \tag{1}$$

The operators $\psi(x)$ ($\psi^\dagger(x)$) are annihilation (creation) field operators in space-spin point $\mathbf{x}$. The term $h(\mathbf{x},t)$ is a general time-dependent one-body part, while $v(\mathbf{x},\mathbf{x}')$ is a general two-body interaction.

The single-particle Green's function is defined as

$$G(\mathbf{x}_1z_1;\mathbf{x}_2z_2) = -i\langle\Psi_0|\mathcal{T}_\gamma\left\{\hat{\psi}_H(\mathbf{x}_1z_1)\hat{\psi}^\dagger_H(\mathbf{x}_2z_2)\right\}|\Psi_0\rangle, \tag{2}$$

where Ψ_0 is the initial state with n particles at time t_0, z_1 and z_2 are time-parameters on the Keldysh contour γ:

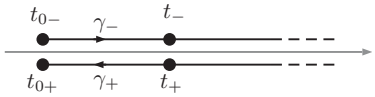

(3)

and the Heisenberg operators are given by

$$\hat{\psi}_H(\mathbf{x}t) = \hat{\mathcal{U}}(t_0,t)\hat{\psi}(\mathbf{x})\hat{\mathcal{U}}(t,t_0), \tag{4}$$

where $\hat{\mathcal{U}}(t,t_0)$ is the time-evolution operator [5]. The irreducible correlation self-energy can be expressed as [6,5]

$$\Sigma_c(\mathbf{x}_1z_1;\mathbf{x}_2z_2) = -i\langle\Psi_0|\mathcal{T}_\gamma\left\{\hat{\gamma}_H(\mathbf{x}_1z_1)\hat{\gamma}^\dagger_H(\mathbf{x}_2z_2)\right\}|\Psi_0\rangle_{\rm irr}, \tag{5}$$

with

$$\hat{\gamma}(\mathbf{x}_1) = \int d\mathbf{x}_2 v(\mathbf{x}_1,\mathbf{x}_2)\hat{n}(\mathbf{x}_2)\hat{\psi}(\mathbf{x}_1), \tag{6}$$

and similarly for the adjoint $\hat{\gamma}^\dagger(\mathbf{x}_1)$. The subscript irr denotes that all reducible diagrams (those that can be separated into two disjoint pieces by removing a single Green's function line) are to be removed from the expansion.

3 Lehmann Representation of The Self-Energy We derive a Lehmann-like representation for the correlation part of the interaction self-energy Σ_c, following closely Ref. [1]. The idea is to obtain an expression for Σ_c that consists of a sum of squared amplitudes. From this the PSD property of the resulting spectral function can be derived in the steady-state case.

The lesser component of the correlation self-energy of Eq. (5) is given by

$$\begin{aligned}\Sigma^<_c(1;2) =& i\left[\langle\Psi_0|\hat{\gamma}^\dagger_H(2)\hat{\gamma}_H(1)|\Psi_0\rangle\right]_{\rm irr}\\ =& i\Big[\langle\Psi_0|\hat{\mathcal{U}}(t_0,t_2)\hat{\gamma}^\dagger(\mathbf{x}_2)\hat{\mathcal{U}}(t_2,t_0)\\ &\times\hat{\mathcal{U}}(t_0,t_1)\hat{\gamma}(\mathbf{x}_1)\hat{\mathcal{U}}(t_1,t_0)|\Psi_0\rangle\Big]_{\rm irr},\end{aligned} \tag{7}$$

where we use the shorthand notation $1 = \mathbf{x}_1t_1$, and similarly for the primed argument. The treatment of the greater component is analogous.

To proceed, we consider a complete set of states $|\chi_i\rangle$ in Fock space and insert the unit operator

$$\mathbf{1} = \sum_i |\chi_i\rangle\langle\chi_i| \tag{8}$$

between $\hat{\gamma}_H$ and $\hat{\gamma}^\dagger_H$ in Eq. (7). Since $\hat{\gamma}_H$ ($\hat{\gamma}^\dagger_H$) removes (adds) a particle, we can restrict the sum over states to $(n-1)$–particle states. This yields

$$\Sigma^<_c(1;2) = i\Big[\sum_i S_i(2)S^*_i(1)\Big]_{\rm irr}, \tag{9}$$

where we defined the amplitudes

$$S_i(1) = \langle\Psi_0|\hat{\mathcal{U}}(t_0,t_1)\hat{\gamma}^\dagger(\mathbf{x}_1)\hat{\mathcal{U}}(t_1,t_0)|\chi_i\rangle. \tag{10}$$

In Eq. (9) the expression inside the square brackets is a Lehmann-like representation for the lesser component of reducible self-energy. To obtain a Lehmann-like representation for the irreducible self-energy Σ_c we derive the diagrammatic representation of the amplitudes S_i.

To do this, we again follow the approach of Ref. [1]. We assume that the initial state $|\Psi_0\rangle$ is the ground state of the system described by Eq. (1) at t_0. A necessary condition for having a diagrammatic expansion is the ability to use the Wick theorem. For simplicity, in this work we employ the Gell-Mann and Low theorem [7] to connect the interacting state to a non-interacting state $|\Phi_0\rangle$ at time $-\tau$, for which the limit $\tau\to\infty$ is taken at the end. This implies that the ground state can be obtained by

$$|\Psi_0\rangle = \hat{\mathcal{U}}(t_0,-\tau)|\Phi_0\rangle. \tag{11}$$

Here $\mathcal{U}(t_0,-\tau)$ is the time-evolution operator that contains an adiabatically switched two-body interaction $v(\mathbf{x},\mathbf{x}',t) = \mathrm{e}^{\eta(t-t_0)}v(\mathbf{x},\mathbf{x}')$ where η is a positive infinitesimal taken to be zero at the end. Under the adiabatic assumption, the amplitudes S_i, Eq. (10), can be written as

$$S_i(2) = \langle\Phi_0|\hat{\mathcal{U}}(-\tau,t_2)\hat{\gamma}^\dagger(\mathbf{x}_2)\hat{\mathcal{U}}(t_2,-\tau)|\chi_i\rangle. \tag{12}$$

Since $\hat{\gamma}^\dagger$ creates one particle, only the states with one particle less than $|\Phi_0\rangle$ contribute to S_i. Because $|\Phi_0\rangle$ is a non-interacting state, a complete basis can be constructed through

$$|\chi^{(N)}_{\mathcal{PQ}}\rangle = \hat{c}^\dagger_{q_N}\dots\hat{c}^\dagger_{q_1}\hat{c}_{p_{N+1}}\dots\hat{c}_{p_1}|\Phi_0\rangle, \tag{13}$$

where $\mathcal{P} = \{p_1,\dots,p_{N+1}\}$ and $\mathcal{Q} = \{q_1,\dots,q_N\}$ are lists of one-particle eigenstates of the Hamiltonian of the non-interacting system at $-\tau$. The operators $\hat{c}^\dagger_k$ and $\hat{c}_k$ creates particles and holes in the one-particle states with quantum label k. N is the number of particle-hole pairs created

on top of the single-hole state $\hat{c}_{p_1}|\Phi_0\rangle$. The states $|\chi^{(N)}_{\mathcal{PQ}}\rangle$ differ from the states $|\chi_i\rangle$ by a different normalization [1]

$$\langle\chi^{(N)}_{\mathcal{PQ}}|\chi^{(N)}_{\mathcal{PQ}}\rangle = N!(N+1)!, \tag{14}$$

and we therefore need to make the replacement

$$\sum_i |\chi_i\rangle\langle\chi_i| \to \sum_{N=0}^{\infty} \frac{1}{(N+1)!N!} \sum_{\mathcal{PQ}} |\chi^{(N)}_{\mathcal{PQ}}\rangle\langle\chi^{(N)}_{\mathcal{PQ}}|. \tag{15}$$

where the sum is over all the different lists of quantum numbers that denote either an unoccupied ($\mathcal{P}$) or an occupied ($\mathcal{Q}$) state. The prefactor is needed since different permutations of the same quantum numbers in $\mathcal{P}$ and $\mathcal{Q}$ produce the same state (up to a minus sign that gets canceled out in Eq. (15)). The replacement in Eq. (15) leads to the expression

$$\Sigma_c^<(1;2) = i\left[\sum_{N=0}^{\infty} \frac{1}{(N+1)!N!} \sum_{\mathcal{PQ}} S_{N,\mathcal{PQ}}(2) S^*_{N,\mathcal{PQ}}(1)\right]_{\rm irr}, \tag{16}$$

with the amplitude

$$S_{N,\mathcal{PQ}}(2) = \langle\Phi_0|\mathcal{U}(-\tau,t_2)\hat{\gamma}^\dagger(\mathbf{x}_2)\mathcal{U}(t_2,-\tau)|\chi^{(N)}_{\mathcal{PQ}}\rangle. \tag{17}$$

Writing the state $|\chi^{(N)}_{\mathcal{PQ}}\rangle$ as in Eq. (13) leads to

$$\begin{aligned} S_{N,\mathcal{PQ}}(2) &= \langle\Phi_0|\mathcal{U}(-\tau,t_2)\hat{\gamma}^\dagger(\mathbf{x}_2)\mathcal{U}(t_2,-\tau)\hat{c}^\dagger_{q_N}\dots\hat{c}^\dagger_{q_1}\hat{c}_{p_{N+1}}\dots\hat{c}_{p_1}|\Phi_0\rangle \\ &= \langle\Phi_0|\mathcal{T}_{\gamma_\tau}\left\{e^{-i\int_{\gamma_\tau} d\bar{z}\hat{H}(\bar{z})}\hat{\gamma}^\dagger(\mathbf{x}_2 z_2)\hat{c}^\dagger_{q_N}(-\tau_-)\dots\hat{c}^\dagger_{q_1}(-\tau_-)\hat{c}_{p_{N+1}}(-\tau_-)\dots\hat{c}_{p_1}(-\tau_-)\right\}|\Phi_0\rangle, \end{aligned} \tag{18}$$

where the contour ordering is now over the extended contour γ_τ:

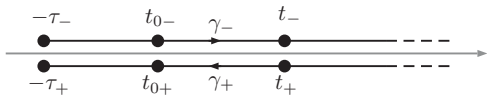

(19)

and the creation and annihilation operators have been given a time-argument to mark their position at the beginning of the contour. The contour-ordered expression, Eq. (18), is proportional to a $(N+2)$–particle Green's function, and can thus be diagrammatically expanded using standard perturbation theory with the Wick's theorem.

Next we will need to define a modified S in such a way that the product in Eq. (16) will generate only the irreducible diagrams. Here the situation is analogous to that in [1], where it was argued that this can be done by a) leaving out the term $N=0$, that contains only reducible diagrams, by starting the sum from $N=1$ and b) including only those diagrams in $S_{N,\mathcal{PQ}}(1)$ that are irreducible in the sense that the vertex 1 can not be detached from the vertices specified by $\mathcal{P}$ and $\mathcal{Q}$ by removing a single Green's function line. The part of S that is irreducible in this sense will be denoted by $\tilde{S}$. This allows the lesser self-energy to be written as

$$\Sigma_c^<(1;2) = i\sum_{N=1}^{\infty} \frac{1}{(N+1)!N!} \sum_{\mathcal{PQ}} \tilde{S}_{N,\mathcal{PQ}}(2)\tilde{S}^*_{N,\mathcal{PQ}}(1), \tag{20}$$

which can be seen as a Lehmann-like representation for the non-equilibrium irreducible correlation self-energy.

It was shown in [1] that the Fourier transform of $-i\Sigma_c$ obtained from such a representation will be PSD in equilibrium, and that therefore the resulting spectral function will be PSD as well. The same proof can be used without modifications in the more general steady-state case. This shows that the spectral function will be PSD in the steady-state limit.

For every diagram $D^{(j)}_{N,\mathcal{PQ}}$ in the expansion of $\tilde{S}_{N,\mathcal{PQ}}$, the expansion also contains all the diagrams that are obtained from $D^{(j)}_{N,\mathcal{PQ}}$ by permuting $\mathcal{P}$ and $\mathcal{Q}$ (with a minus sign for odd permutations), forming a subset of related diagrams. Let $D^{(j)}_{N,\mathcal{PQ}}$ for $j \in I_N$ form a set that contains a single diagram from each such subset. We can then rebuild $\tilde{S}$ by summing over permutations of the diagrams $D^{(j)}$:

$$\tilde{S}_{N,\mathcal{PQ}} = \sum_{j\in I_N} \sum_{\substack{P_p\in\pi_{N+1}\\ P_q\in\pi_N}} (-1)^{|P_p|+|P_q|} D^{(j)}_{N,P_p(\mathcal{P})P_q(\mathcal{Q})}, \tag{21}$$

where π_N is the symmetric group of order N and $|P_p|$ is the number of transpositions in the permutation P_p. Now in the product of $\tilde{S}$'s permuting the quantum numbers in

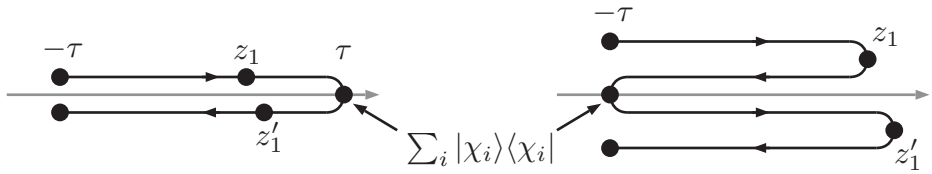

Figure 1 Left figure represents the approach of [1], where the unit operator can be thought to be placed at the end-point of the contour, splitting it into a time ordered forward branch and an anti-time ordered backward branch. In contrast we place the unit operator at $-\tau$, leaving a full Keldysh contour on both sides.

both factors in the same way always results in the same diagram. This leads to the same diagram appearing $(N+1)!N!$ times, and consequently $\Sigma^<$ can be expressed as

$$\begin{aligned}\Sigma_c^<(1;2) =& i\sum_{N=1}^{\infty}\sum_{j_1,j_2\in I_N}\sum_{\substack{P_p\in\pi_{N+1}\\P_q\in\pi_N}}(-1)^{|P_p|+|P_q|}\\ &\times\sum_{\mathcal{PQ}} D^{(j_2)}_{N,\mathcal{PQ}}(2)D^{(j_1)^*}_{N,P_p(\mathcal{P})P_q(\mathcal{Q})}(1),\end{aligned}\tag{22}$$

where the sum is only over the relative permutations between the two factors. This representation is useful for constructing PSD approximations.

Eq. (20) and Eq. (22) are closely related to the similar equations derived in [1]. We will now clarify the difference between our derivations. In [1] it is assumed that evolving the non-interacting ground state from $-\tau$ to τ produces the same state up to a phase factor, so that

$$\mathcal{U}(\tau,-\tau)|\Phi_0\rangle = e^{i\alpha}|\Phi_0\rangle.\tag{23}$$

This fact is used to write the amplitude S_i as

$$S_i(2) = \langle\Phi_0|\hat{\mathcal{U}}(-\tau,t_2)\hat{\gamma}^\dagger(\mathbf{x}_2)\hat{\mathcal{U}}(t_2,\tau)|\chi_i\rangle,\tag{24}$$

so that the basis χ_i is constructed from a non-interacting ground state in the distant future. This allows S_i to be written as a time ordered product, so that S_i^* becomes correspondingly an anti-time ordered product. One can think that placing the unit operator between the $\hat{\gamma}$ operators in effect splits the contour in two. In [1] the unit operator is placed at the end of the contour at time τ, splitting it into a time ordered forward branch and an anti-time ordered backward branch. On the other hand in this paper we deform the contour by having it return to $-\tau$ between the $\hat{\gamma}$ operators, and place the unit operator at time $-\tau$ leaving a Keldysh contour with forward and backward branches on both sides (see figure 1). Thus we avoid having to assume Eq. (23), and pay the price in having to treat S as an object on the full contour.

Since we do not assume Eq. (23), we are not restricted to equilibrium situations, and Eq. (20) and Eq. (22) are valid also out of equilibrium. We stress that the discussion of PSD properties of spectral functions only applies when $\Sigma_c(t_1,t_2)$ depends only on the time difference t_1-t_2. This is the case in equilibrium, as well as in the steady state limit.

4 Evaluation of the Half-Diagrams Considering now a half-diagram $D^{(j)}_{N,\mathcal{PQ}}$ appearing in Eq. (22), there are no interaction lines connecting to the vertices marked by $\mathcal{P}$ and $\mathcal{Q}$, and therefore these vertices are always connected to the rest of the diagram only by a Green's function line (see figure 2). Since the contour-times of the vertices $\mathcal{P}$ and $\mathcal{Q}$ are always at the beginning of the contour $(-\tau_-)$ these Green's functions are always lesser for $\mathcal{P}$ and greater for $\mathcal{Q}$. Let us index the vertices that $\mathcal{Q}$ and $\mathcal{P}$ connect to using $\mathcal{N}=\{n_1,\ldots,n_N\}$ and $\mathcal{M}=\{m_1,\ldots,m_{N+1}\}$ respectively, and denote the Green's functions by $g^>_{n_1q_1}=g^>_{\mathbf{x}_{n_1}q_1}(t_{n_1},-\tau)$ and $g^<_{p_1m_1}=g^<_{p_1\mathbf{x}_{m_1}}(-\tau,t_{m_1})$. We can then express $D^{(j)}_{N,\mathcal{PQ}}$ of Eq. (22) as

$$\begin{aligned}&D^{(j)}_{N,\mathcal{PQ}}(\mathbf{x}_2z_2)\\ &=\int d\mathbf{x}_\mathcal{N}d\mathbf{x}_\mathcal{M}\int_\gamma dz_\mathcal{N}dz_\mathcal{M}\Delta^{(j)}_N(\mathbf{x}_2z_2,\mathbf{x}_\mathcal{N}z_\mathcal{N},\mathbf{x}_\mathcal{M}z_\mathcal{M})\\ &\times g^>_{n_1q_1}\cdots g^>_{n_Nq_N}g^<_{p_1m_1}\cdots g^<_{p_{N+1}m_{N+1}},\end{aligned}\tag{25}$$

where $\Delta^{(j)}_N$ is the diagram that is left after removing the external Green's function lines from $D^{(j)}_{N,\mathcal{PQ}}$ (see figure 2).

In contrast to [1] the diagrams appearing in D are contour ordered rather than (anti)time ordered. To convert the contour expression into a real-time expression the usual Langreth [8] rules are inadequate due to the multi-integral structure, and more generalized rules have to be used [9, 10]. Here we give a brief discussion of the real-time conversion.

Let $A(z_\mathcal{N})=A(z_{n_1},\ldots,z_{n_N})$ be an arbitrary diagram containing at most two-point contour functions. We define a *contour-ordered component*

$$A^{P(n_1)\cdots P(n_N)}(t_\mathcal{N}),\tag{26}$$

with P some permutation of $\mathcal{N}=\{n_1,\ldots,n_N\}$, as the real-time diagram that is obtained by replacing each

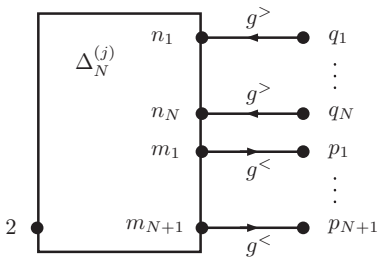

Figure 2 Diagrammatic representation of the half-diagram $D^j_{N,\mathcal{PQ}}$ (see Eq. (25)).

contour function $F(z_{n_i}, z_{n_j})$ by the greater (lesser) component if n_i is left (right) of n_j in the sequence $P(n_i)\cdots P(n_N)$. For example if

$$A(z_a, z_b, z_c) = G(z_a, z_b)G(z_b, z_c), \tag{27}$$

then

$$A^{acb}(t_a, t_b, t_c) = G^>(t_a, t_b)G^<(t_b, t_c). \tag{28}$$

Now to clean up the notation we introduce the following definitions

– $\Theta_{n_1\cdots n_N} = \Theta(t_{n_1} - t_{n_2})\Theta(t_{n_2} - t_{n_3})\cdots\Theta(t_{n_{N-1}} - t_{n_N})$ is a product of step-functions

– A sum of contour-ordered components can be written using a sum of sequences in the superscript, as in

$$A^{acb} - A^{abc} = A^{acb-abc}. \tag{29}$$

For brevity we use the commutator notation in this context, so that for example the above expression could be written as

$$A^{acb-abc} = A^{a[c,b]}. \tag{30}$$

– $[n_1, \ldots, n_N]$ denotes a nested commutator $[\cdots[[n_1, n_2], n_3], \ldots, n_N]$.

– A retarded component of a diagram $A(z_\mathcal{N})$, in which all the other arguments are retarded with respect to t_{n_1}, is defined as

$$A^{R(n_1,n_2\cdots n_N)}(t_\mathcal{N}) = \sum_{P\in S_{N-1}} \Theta_{n_1 P(n_2)\cdots P(n_N)} A^{[n_1,P(n_2),\ldots,P(n_N)]}(t_\mathcal{N}), \tag{31}$$

where the sum is over permutations of indices other than n_1, so that t_{n_1} is always the largest of the time-arguments. For a two-point function this definition reduces to

$$\begin{aligned} &A^{R(a,b)}(t_a, t_b) \\ &= \Theta_{ab}A^{[a,b]}(t_a, t_b) \\ &= \Theta(t_a - t_b)\left(A^>(t_a, t_b) - A^<(t_a, t_b)\right), \end{aligned} \tag{32}$$

which coincides with the usual definition of A^R. Note that $A^{R(b,a)} = A^A$ is the advanced component.

An integral over all but one variables of a contour-diagram

$$A'(z_i) = \int_\gamma dz_{\mathcal{N}\setminus i} A(z_\mathcal{N}), \quad i \in \mathcal{N} \tag{33}$$

is a function symmetric with respect to the branch index, so that $A'(t) = A'(t_\pm)$, that for both branch-indices is equal to the real-time integral [9, 10]

$$A'(t_i) = \int_{t_0}^{\infty} dt_{\mathcal{N}\setminus i} A^{R(i,\mathcal{N}\setminus i)}(t_\mathcal{N}). \tag{34}$$

This result can be derived by splitting the domain of integration into sub-domains of fixed contour order. In each such sub-domain one can replace $A(z_\mathcal{N})$ by a specific contour ordered component. It turn out the various terms generated can be expressed elegantly using nested commutators, which motivates the definition of a general retarded component given in Eq. (31). For a detailed derivation, see section 4 in [10].

Applying Eq. (34) to Eq. (25) tells us that $D^{(j)}_{N,\mathcal{PQ}}(\mathbf{x}_1 z_1)$ is symmetric with respect to the branch index, and can be expressed as

$$\begin{aligned} D^{(j)}_{N,\mathcal{PQ}}(\mathbf{x}_2 t_2) = \int d\mathcal{N}d\mathcal{M}\Delta^{(j)R(1,\mathcal{NM})}_{N,\mathcal{NM}}(2) \\ \times g^>_{n_1 q_1}\cdots g^>_{n_N q_N} g^<_{p_1 m_1}\cdots g^<_{p_{N+1} m_{N+1}}, \end{aligned} \tag{35}$$

where $\int d\mathcal{N} = \int d\mathbf{x}_\mathcal{N} \int_{t_0}^{\infty} dt_\mathcal{N}$ and

$$\Delta^{(j)R(2,\mathcal{NM})}_{\mathcal{N},\mathcal{NM}}(2) = \Delta^{(j)R(2,\mathcal{NM})}_{N}(\mathbf{x}_2 t_2, \mathbf{x}_\mathcal{N} t_\mathcal{N}, \mathbf{x}_\mathcal{M} t_\mathcal{M}) \tag{36}$$

is the retarded component of the diagram $\Delta^{(j)}_N$ in which all the other arguments, including all the internal arguments, are retarded with respect to t_2. The same can be done for $D^{(j)^*}$, and the result is a diagrammatic expansion for $\Sigma^<_c$ in terms of two retarded pieces that are connected by greater and lesser Green's functions. These connecting Green's functions are always either two greater or two lesser Green's functions in line in the form

$$\sum_q g^<_{\mathbf{x}_1 q}(t_1, -\tau) g^<_{q\mathbf{x}_2}(-\tau, t_2). \tag{37}$$

These can be joined to a single Green's function by using

$$\begin{aligned} \sum_q g^>_{\mathbf{x}_1 q}(t_1, -\tau) g^>_{q\mathbf{x}_2}(-\tau, t_2) &= -ig^>_{\mathbf{x}_1\mathbf{x}_2}(t_1, t_2) \\ \sum_q g^<_{\mathbf{x}_1 q}(t_1, -\tau) g^<_{q\mathbf{x}_2}(-\tau, t_2) &= ig^<_{\mathbf{x}_1\mathbf{x}_2}(t_1, t_2). \end{aligned} \tag{38}$$

These relations can be proven in the following way. The lesser Green's function can be written as [5] (the procedure for the greater component is analogous)

$$g^<_{\mathbf{x}q}(t_1,t_2) = i\sum_{i=1}^{n}\phi_{\mathbf{x}i}(t_1)\phi^*_{iq}(t_2), \tag{39}$$

where n is the number of particles so that the sum is over the occupied single-particle states ϕ (we are assuming zero temperature), non-interacting Green's functions fulfill the relation

$$\begin{aligned}&\sum_q g^<_{\mathbf{x}_1 q}(t_1,-\tau)g^<_{q\mathbf{x}_2}(-\tau,t_2)\\ &= -\sum_{i,j}^{n}\phi_{\mathbf{x}_1 i}(t_1)\sum_q\left[\phi^*_{iq}(-\tau)\phi_{qj}(-\tau)\right]\phi^*_{j\mathbf{x}_2}(t_2)\\ &= -\sum_{i}^{n}\phi_{\mathbf{x}_1 i}(t_1)\phi^*_{i\mathbf{x}_2}(t_2) = ig^<_{\mathbf{x}_1\mathbf{x}_2}(t_1,t_2).\end{aligned} \tag{40}$$

The relations (38) are a generalization of the equilibrium results found in [1].

This joining leads ultimately to the expression

$$\begin{aligned}\Sigma^<_c(1;2) = i\sum_{N=1}^{\infty}\sum_{j_1,j_2\in I_N}\sum_{\substack{P_n\in\pi_N\\P_m\in\pi_{N+1}}}(-1)^{|P_n|+|P_m|}\int d\mathcal{N}d\mathcal{N}'d\mathcal{M}d\mathcal{M}'\\ \times\Delta^{(j_2)R(2,\mathcal{N}'\mathcal{M}')}_{N,\mathcal{N}'\mathcal{M}'}(2)g^>_{n'_1P_n(n_1)}\cdots g^>_{n'_NP_n(n_N)}g^<_{P_m(m_1)m'_1}\cdots g^<_{P_m(m_{N+1})m'_{N+1}}\left[\Delta^{(j_1)R(1,\mathcal{N}\mathcal{M})}_{N,P_n(\mathcal{N})P_m(\mathcal{M})}\right]^*(1),\end{aligned} \tag{41}$$

where $g^{\lessgtr}_{n'_1n_1} = g^{\lessgtr}(\mathbf{x}_{n'_1}t_{n'_1},\mathbf{x}_{n_1}t_{n_1})$, so that the expression no longer depends on $-\tau$. Eq. (41) is an exact representation of the correlation self-energy in terms of retarded pieces. Furthermore, it can be used as a starting point for the repairing procedure to produce PSD self-energies that was presented in [1].

A given approximate self-energy can always be written in the form of Eq. (41) with some Δ, and some restrictions on the sums. By cutting the greater and lesser Green's function lines one can obtain an expression in the form of Eq. (22), now with restricted sums. Typically such an approximation is not PSD, but it can be made PSD by addition of extra diagrams. It was shown in [1] that if Eq. (22) is modified to

$$\begin{aligned}\tilde{\Sigma}^<_c(1;2) =& i\sum_{N=1}^{N_{max}}\sum_{j_1,j_2\in\tilde{I}_N}\sum_{\substack{P_p\in\tilde{\pi}_{N+1}\\P_q\in\tilde{\pi}_N}}(-1)^{|P_p|+|P_q|}\\ &\times\sum_{\mathcal{P}\mathcal{Q}}D^{(j_2)}_{N,\mathcal{P}\mathcal{Q}}(2)D^{(j_1)^*}_{N,P_p(\mathcal{P})P_q(\mathcal{Q})}(1),\end{aligned} \tag{42}$$

with $\tilde{I}_N\subset I_N$, $\tilde{\pi}_N\subset\pi_N$ and $\tilde{\pi}_{N+1}\subset\pi_{N+1}$, the resulting approximate self-energy will be PSD as long as $\tilde{\pi}_N$ and $\tilde{\pi}_{N+1}$ are subgroups of the permutation groups π_N and π_{N+1} respectively. These observations were used in [1] to set out a repairing procedure for converting a non-PSD approximation to a PSD one using a minimal number of extra diagrams. These arguments apply directly also to the non-equilibrium case here discussed.

This procedure can be extended to dressed Green's functions. The discussion regarding this in [1] is again directly applicable to our case.

5 The GW Approximation in the Steady-State Limit As an example of the results derived above, we will in this section outline the proof that the spectral functions produced by the gW_0 approximation in the steady state limit are PSD.

By gW_0 we mean the approximation in which the exchange-correlation self-energy is given by

$$\Sigma_{xc,gW_0}(\bar{1},\bar{2}) = ig(\bar{1},\bar{2})W_0(\bar{1},\bar{2}), \tag{43}$$

where $\bar{1} = \mathbf{x}_1z_1$,

$$W_0(\bar{1},\bar{2}) = V(\bar{1},\bar{2}) + \int d\bar{3}d\bar{4}V(\bar{1},\bar{3})P(\bar{3},\bar{4})W_0(\bar{4},\bar{2}) \tag{44}$$

with $V(\bar{1},\bar{2}) = \delta(z_1,z_2)v(\mathbf{x}_1,\mathbf{x}_2,z_1)$, $\int d\bar{3} = \int\mathbf{x}_3\int_\gamma z_3$ and

$$P(\bar{1},\bar{2}) = -ig(\bar{1},\bar{2})g(\bar{2},\bar{1}), \tag{45}$$

the polarization function in the random phase approximation. As explained above, to show that gW_0 is PSD we must show that $\Sigma^<_{c,gW_0}$ can be written in the form of Eq. (42).

The lesser component of Eq. (43) is (the exchange term vanishes, since it is time-local [5])

$$\Sigma^<_{c,gW_0}(1,2) = ig^<(1,2)W^<_0(1,2) \tag{46}$$

and

$$P^<(1;2) = -ig^<(1;2)g^>(2;1). \quad (47)$$

Using the equation

$$W_0^<(1;2) = \int d3d4 W_0^R(1;3)P^<(3;4)W_0^A(4;2) \quad (48)$$

we obtain

$$\Sigma^<_{c,gW_0}(1;2) = \int d3d4\, W_0^R(1;3)g^>(4,3)g^<(1;2)g^<(3,4)W_0^A(4;2) \quad (49)$$

Using the equations (38) to cut the Green's function lines, we obtain (dropping the time-arguments for brevity)

$$\Sigma^<_{c,gW_0}(1;2) = -i \sum_{q_1p_1p_2} \int d3d4 \times W_0^R(1;3)g^>_{q_1\mathbf{x}_3}g^<_{\mathbf{x}_1p_1}g^<_{\mathbf{x}_3p_2}g^>_{\mathbf{x}_4q_1}g^<_{p_1\mathbf{x}_2}g^<_{p_2\mathbf{x}_4}W_0^A(4;2) \quad (50)$$

Now if we expand the screened interaction as (repeated convolutions implied)

$$W_0^R = \sum_{j=0}^{\infty} W_0^{(j)R} = \sum_{j=0}^{\infty} (VP^R)^j V, \quad (51)$$

with j the number of polarization bubbles, we can express $\Sigma_c^<$ as

$$\Sigma^<_{c,gW_0}(1;2) = -i \sum_{j_1,j_2\in\tilde{I}_N} \sum_{\mathcal{PQ}} D^{(j_2)}_{1,\mathcal{PQ}}(2)D^{(j_1)^*}_{1,\mathcal{PQ}}(1), \quad (52)$$

with $\mathcal{P} = \{p_1, p_2\}$, $\mathcal{Q} = \{q_1\}$, $\tilde{I}_N = \{0, 1, 2, \ldots\}$ and

$$D^{(j)}_{1,\mathcal{PQ}}(2) = \int d3\, W_0^{(j)R}(2;3)g^>_{q_1\mathbf{x}_3}g^<_{\mathbf{x}_2p_1}g^<_{\mathbf{x}_3p_2}. \quad (53)$$

Now Eq. (52) matches the form of Eq. (42) for $N_{max} = 1$ and the sum over permutations including only the identity permutation. Since $\tilde{I}_N$ represents a set of diagrams not related by permutations, and since the identity permutation constitutes a sub-group by itself, it follows that $-i\Sigma^<_{c,gW_0}$ is PSD.

As mentioned, the PSD property is retained in the dressed case, meaning that the fully self-consistent GW approximation is PSD as well. Indeed numerical results yield PSD spectral functions [11,12,13].

6 Conclusions We have presented a method for obtaining approximations for the correlation self-energy that are guaranteed to result in PSD spectral functions in non-equilibrium systems in the steady-state limit. A further advantage of our approach is that, unlike the approach of [1], it is not limited to correlators of two operators, but is in principle generalizable for higher-order correlators by placing a set of basis states at distant past between each operator. As an application we showed that the steady-state spectral function within the gW_0 approximation is PSD. A more detailed exposition will be deferred to a future publication.

Acknowledgements D.K. acknowledges the Academy of Finland for funding under Project No. 308697. M.H. thanks the Finnish Cultural Foundation for support R.v.L. acknowledges the Academy of Finland for funding under Project No. 317139.

References

[1] G. Stefanucci, Y. Pavlyukh, A. M. Uimonen, and R. van Leeuwen, Phys. Rev. B **90**, 115134 (2014).

[2] A. M. Uimonen, G. Stefanucci, Y. Pavlyukh, and R. van Leeuwen, Phys. Rev. B **91**(11), 115104 (2015).

[3] C. Gramsch, K. Balzer, M. Eckstein, and M. Kollar, Phys. Rev. B **88**(23), 1–21 (2013).

[4] C. Gramsch and M. Potthoff, Phys. Rev. B **92**(23), 1–11 (2015).

[5] G. Stefanucci and R. van Leeuwen, Nonequilibrium Many-Body Theory of Quantum Systems: A Modern Introduction (Cambridge University Press, Cambridge, jul 2013).

[6] P. Danielewicz, Ann. Phys. (N. Y). **152**(2), 239–304 (1984).

[7] A. L. Fetter and J. D. Walecka, Quantum Theory of Many-Particle Theory (Dover Publications, New York, 2003).

[8] D. C. Langreth, Linear and Nonlinear Response Theory with Applications, in: Linear Nonlinear Electron Transp. Solids, edited by J. T. Devreese and V. E. Doren, (Springer US, Boston, MA, 1976).

[9] P. Danielewicz, Ann. Phys. (N. Y). **197**(1), 154–201 (1990).

[10] M. Hyrkäs, D. Karlsson, and R. van Leeuwen, arXiv:1903.03489 [math-ph].

[11] K. S. Thygesen and A. Rubio, Phys. Rev. B **77**(11), 115333 (2008).

[12] P. Myöhänen, A. Stan, G. Stefanucci, and R. van Leeuwen, Phys. Rev. B **80**(11), 115107 (2009).

[13] M. Puig von Friesen, C. Verdozzi, and C. O. Almbladh, Phys. Rev. B **82**(15), 155108 (2010).

III

CUTTING RULES AND POSITIVITY IN FINITE TEMPERATURE MANY-BODY THEORY

by

M. Hyrkäs, D. Karlsson and R. van Leeuwen 2022

Journal of Physics A: Mathematical and Theoretical **55** 335301

DOI:10.1088/1751-8121/ac802d

Cutting rules and positivity in finite temperature many-body theory

M. J. Hyrkäs, D. Karlsson, and R. van Leeuwen

Department of Physics, Nanoscience Center P.O.Box 35 FI-40014 University of Jyvaskyla, Finland

E-mail: markku.j.hyrkas@jyu.fi

Abstract. For a given diagrammatic approximation in many-body perturbation theory it is not guaranteed that positive observables, such as the density or the spectral function, retain their positivity. For zero-temperature systems we developed a method [Phys.Rev.B**90**,115134 (2014)] based on so-called cutting rules for Feynman diagrams that enforces these properties diagrammatically, thus solving the problem of negative spectral densities observed for various vertex approximations. In this work we extend this method to systems at finite temperature by formulating the cutting rules in terms of retarded N-point functions, thereby simplifying earlier approaches and simultaneously solving the issue of non-vanishing vacuum diagrams that has plagued finite temperature expansions. Our approach is moreover valid for nonequilibrium systems in initial equilibrium and allows us to show that important commonly used approximations, namely the GW, second Born and T-matrix approximation, retain positive spectral functions at finite temperature. Finally we derive an analytic continuation relation between the spectral forms of retarded N-point functions and their Matsubara counterparts and a set of Feynman rules to evaluate them.

Keywords: diagrammatic perturbation theory, non-equilibrium Green's functions, quantum many-body theory, spectral properties

Submitted to: *J. Phys. A: Math. Theor.*

1. Introduction

Non-equilibrium Green's function theory [1] is a powerful tool for calculating time-dependent properties in a variety of quantum many-particle systems. While exact in principle, in practice the formalism relies on approximate diagrammatic expansions; to finite order, or to infinite order via resummations.

For a given diagrammatic approximation, there is in general no guarantee that relevant properties of the exact solution will be retained. This, in particular, applies to the positivity of probability distributions, such as the spectral function in energy space and the particle density in position space. For example when the lowest order vertex correction in a dynamically screened expansion for the electron gas was considered, the spectral function was found to become negative [2] with a similar issue occurring for the absorption spectrum [3]. The same problems were observed also in finite systems for the case of atoms and small Hubbard lattices [4, 5]. Injudiciously chosen approximations may even result in both the spectral function and the particle density becoming negative, as was demonstrated for the Anderson model [6]. These issues have considerably hindered progress in the study of spectral properties beyond the simplest approximations.

For the case of equilibrium systems at zero temperature the problem of negative spectral densities was solved with a systematic diagrammatic method [7, 8] in which Feynman graphs are expressed in terms of so-called half-diagram products that could be derived from the Lehmann representation of the correlation functions. Diagrammatically this procedure amounts to cutting the Feynman graphs in various ways and gluing the pieces together in order to form new manifestly positive products such that a non-negative spectral function is guaranteed. Of practical importance is the possibility [7] to extend a given non-positive approximation with a minimal set of extra diagrams to enforce the positivity condition. This constitutes the so-called Positive Semi-Definite (PSD) expansion for spectral functions. Another considerable advantage of the method is that it allows for an expansion in physical scattering processes, which was successfully used to study the various contributions of particle-hole and plasmon excitations to the spectral function of the electron gas [9, 10]. A similar technique was also developed for the steady state limit of non-equilibrium systems initially in a zero-temperature equilibrium [11]. This extension is not straightforward as it required a new expansion technique in terms of so-called multi-retarded half-diagrams and appears as a special case of a general integral calculus for multi-argument contour functions, originally developed by Danielewicz [12] and extended by us [13].

The previously mentioned developments leave out the important case of systems in finite temperature equilibrium, which will form the main topic of this paper. Finite temperature many-body theory is vital for the description of excited state properties in warm dense matter systems [14], such as laser-shocked, fusion and astrophysical systems, and phase transitions in nuclear matter [15]. It is also important to describe coupled electron-boson systems, for example in the study of temperature-dependent properties

of solid state systems in which electron-phonon interactions are crucial [16, 17, 18]. Another relevant class of physical systems in this respect is that of small electronic systems coupled to baths [19], such as nanojunctions [20].

In the particle physics community several diagrammatic cutting approaches have been developed to study positive scattering amplitudes in finite temperature quantum field theory but they turn out to have undesirable features that make them unsuitable for our purpose of constructing a PSD perturbation theory. The method we develop in this paper connects and simplifies some of these approaches and it is therefore useful to give a brief overview of them.

Early works by Kobes and Semenoff [21, 22] (see also [23] for an overview) are based on the largest-time equation originally invented by Veltman [24, 25] and derive expansions in time-ordered and anti-time-ordered diagrams, containing so-called "non-cuttable" diagrams [22] which generate disconnected subdiagrams when the standard cutting rules are applied. This, in turn, leads to the appearance of disconnected vacuum diagrams in the construction of PSD approximations which is undesirable as they are absent in an exact expansion. Later work [26, 23] based on the same method managed to rearrange diagrams in such a way that non-cuttable pieces do not arise at the expense of a proliferation of extra Green's function lines making the method very laborious and equally unsuitable for our purpose of creating a finite temperature PSD perturbation theory. A very different approach was pursued by Jeon [27] based solely on Matsubara diagrams, but leading eventually to an expansion in (anti)-time ordered diagrams again with the appearance of disconnected diagrams in the same vein as earlier works. Finally Landshoff [28], with the example of bosonic particles, gave a simpler derivation purely based on Keldysh contour integrals and the Lehmann representation but also ends up with an expansion involving disconnected subdiagrams after cutting. Our earlier approach for zero-temperature systems is closely related to this derivation but in the present work we use a different and simpler procedure to generalize our earlier method [7] to the case of finite temperature systems. Furthermore, to solve the critical issue of the non-cuttable diagrams we use the technique of retarded half-diagrams [13, 11] instead of the (anti)-time ordered expansion of Landshoff.

In hindsight it is found that all earlier approaches mentioned above can be obtained in a rather simple way from the more straightforward derivation which forms the main subject of this paper. One of our goals therefore is to put earlier work into a new context and to elucidate its relations to the present work. As it turns out, our approach can also be naturally generalized to the case of finite temperature systems at initial equilibrium which are subsequently perturbed into a non-equilibrium state. We can for this general case demonstrate the positivity of spectral functions for several commonly used approximations, i.e. the GW, second Born and T-matrix approximations.

The paper is outlined as follows. In Chapter 2 we discuss the structure of exact correlators and their relation to the positivity of spectral functions. In Chapter 3 we derive a PSD perturbation theory for the self-energy of finite temperature systems in terms of retarded half-diagram products, thereby generalizing earlier work for zero-

temperature systems [7, 13]. Finally we apply the new formalism in Chapter 4 to demonstrate the positivity of the GW, second Born and the T-matrix approximations for finite temperature systems, before concluding in Chapter 5.

2. Positivity in many-body theory

2.1. General framework

We start with a brief introduction to the background theory and consider a system of fermions interacting via a two-body interaction described by the Hamiltonian

$$\hat{H}(t) = \int \mathrm{d}\mathbf{x}\ \hat{\psi}^\dagger(\mathbf{x}) h(\mathbf{x},t) \hat{\psi}(\mathbf{x}) + \frac{1}{2}\int \mathrm{d}\mathbf{x}\mathrm{d}\mathbf{x}'\ \hat{\psi}^\dagger(\mathbf{x})\hat{\psi}^\dagger(\mathbf{x}') v(\mathbf{x},\mathbf{x}')\hat{\psi}(\mathbf{x}')\hat{\psi}(\mathbf{x}), \quad (1)$$

where $h(\mathbf{x},t)$ is an unspecified time-dependent one-body operator, and $v(\mathbf{x},\mathbf{x}')$ a general two-body interaction. The field operators $\hat{\psi}^\dagger(\mathbf{x})$ and $\hat{\psi}(\mathbf{x})$ respectively create and annihilate a particle at space-spin point $\mathbf{x} = (\mathbf{r},\sigma)$. For an equilibrium system at finite temperature we can specify an initial ensemble described by a density operator of the form

$$\hat{\rho} = \frac{\mathrm{e}^{-\beta \hat{H}_M}}{Z} \quad (2)$$

with the partition function $Z = \mathrm{Tr}\left[\mathrm{e}^{-\beta \hat{H}_M}\right]$ and the Matsubara Hamiltonian

$$\hat{H}_M = \hat{H}(t_0) - \mu \hat{N}, \quad (3)$$

where $\hat{H}(t_0)$ is the Hamiltonian of (1) evaluated at an initial time t_0, $\hat{N}$ is the number operator, and μ the chemical potential. A strictly positive density operator, i.e. satisfying $\langle\varphi|\hat{\rho}|\varphi\rangle > 0$ for any non-zero state $|\varphi\rangle$, can always be written in the form of (2) albeit that $\hat{H}_M$ will then in general be an N-body operator rather than the simpler 2-body operator of (3) [1, 29, 30, 31, 32].

If $\hat{O}(t)$ is an (in general time-dependent) operator in the Schrödinger picture, then its time-dependent expectation value is given by

$$\langle O\rangle(t) = \mathrm{Tr}\left[\hat{\rho}\,\hat{U}(t_0,t)\hat{O}(t)\hat{U}(t,t_0)\right] = \mathrm{Tr}\left[\hat{\rho}\,\hat{O}_H(t)\right] \quad (4)$$

where $\hat{U}(t,t_0)$ is the time-evolution operator that evolves the system from time t_0 to time t; its explicit form involves a time-ordered exponential where for details we refer to the literature [1]. For carrying out perturbative expansions it is advantageous to re-express the expectation value in a contour ordered form as

$$\langle O\rangle(z) = \mathrm{Tr}\left[\mathcal{T}_\gamma\{\mathrm{e}^{-\mathrm{i}\int_\gamma d\bar{z}\hat{H}(\bar{z})}\hat{O}(z)\}\right] \quad (5)$$

where γ is the time-contour in Figure 1 consisting of a forward branch γ_- and a backward branch γ_+ in the time interval $[t_0,T]$ and a vertical or Matsubara track in the complex time interval $[t_0, t_0 - i\beta]$ on which the Hamiltonian is given by $\hat{H}_M$. The time T is

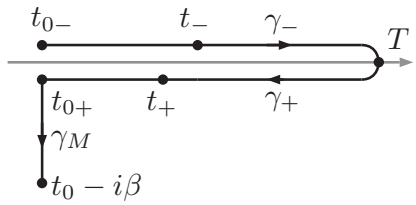

Figure 1. The contour γ, with a forward (γ_-) and backward (γ_+) real-time branches (drawn off the real axis to distinguish them) and an imaginary Matsubara branch (γ_M). Times on the forward and backward branches are denoted by t_- and t_+ respectively.

any time after which the expectation value is to be evaluated and often is taken to be infinity for convenience [1]. Perturbative expressions are then derived from this formula by expanding the time-ordered exponential in powers of the two-body interaction.

The basic ingredients of diagrammatic perturbation theory are contour ordered products of operators defined on γ, the simplest ones being strings of just two operators $\hat{O}_1$ and $\hat{O}_2$ of the general form

$$k(z,z') = \mathrm{Tr}\left[\hat{\rho}\,\mathcal{T}_\gamma\{\hat{O}_1(z)\hat{O}_2(z')\}\right] = \theta(z,z')k^>(t,t') + \theta(z',z)k^<(t,t') \tag{6}$$

where $\theta(z,z')$ is a contour Heaviside function equal to one if z is later than z' (symbolically denoted by $z > z'$) in contour ordering and zero otherwise [1]. A contour time z corresponding to real time t is denoted by t_- if it occurs on γ_- and t_+ if it occurs on γ_+. All operators that we consider satisfy $\hat{O}(t_\pm) = \hat{O}(t)$ i.e. they assume the same value on both horizontal branches. Consequently the functions $k^{\lessgtr}$ are real time functions of the explicit form

$$k^>(t,t') = \mathrm{Tr}\left[\hat{\rho}\,\hat{O}_1(t)\hat{O}_2(t')\right] \qquad k^<(t,t') = \pm\,\mathrm{Tr}\left[\hat{\rho}\,\hat{O}_2(t')\hat{O}_1(t)\right] \tag{7}$$

($+/-$ for bosonic/fermionic operators) which we will refer to as many-body correlation functions, or simply correlators. An important case is when $\hat{O}_1(z) = \hat{\psi}_H(\mathbf{x},z)$ and $\hat{O}_2(z) = \hat{\psi}^\dagger_H(\mathbf{x}',z)$ in which case the functions $k^>$ and $k^<$ correspond to the functions $\mathrm{i}G^>$ and $\mathrm{i}G^<$ representing the particle and hole Green's functions. The way these correlation functions incorporate positivity constraints on physical observables is discussed in the next section.

2.2. Positivity constraints on exact correlators

In this section we expose a general structure of non-equilibrium correlators, namely that of a positive semi-definite Hermitian form, and show that this structure is sufficient to guarantee important positivity constraints. By casting approximate diagrammatic theories in this form these properties are then automatically satisfied in the approximate theory. We delay the discussion of approximations to the following chapters and will

first discuss the case of exact correlators. Let $\hat{\rho}$ be a density operator of the form

$$\hat{\rho} = \sum_j w_j |\Psi_j\rangle\langle\Psi_j|, \tag{8}$$

where the occupation numbers $w_j \geq 0$, subject to the condition $\sum_j w_j = 1$, describe a probability distribution over a set $\{|\Psi_j\rangle\}$ of normalized initial many-body states. This defines a positive semi-definite (PSD) operator $\hat{\rho}$ by which we mean that

$$\langle\varphi|\hat{\rho}|\varphi\rangle \geq 0 \tag{9}$$

for any state $|\varphi\rangle$ in the Hilbert space. We further consider two general operators $\hat{A}$ and $\hat{B}$ in Hilbert space. These operators may depend on various parameters, such as space and time, but these will be suppressed as they are not relevant at this point of the discussion. We define the (weighted) Hilbert-Schmidt product [33] of these operators as:

$$\langle\!\langle \hat{A}|\hat{B}\rangle\!\rangle = \mathrm{Tr}\left[\hat{\rho}\hat{A}^\dagger\hat{B}\right], \tag{10}$$

where curvy angled brackets are used to distinguish the Hilbert-Schmidt product from the standard Hilbert space inner product. The Hilbert-Schmidt product is well-defined if $\hat{A}$ and $\hat{B}$ are bounded operators, as is discussed in detail by Haag, Hugenholtz and Winnink [33]. As demonstrated in Appendix A this product satisfies the properties of a positive semi-definite Hermitian form (PSDHF) when the operator $\hat{\rho}$ is positive semi-definite, and that of an inner product when $\hat{\rho}$ is strictly positive. For the purposes of this work the positive semi-definiteness is both sufficient and most practical as we will often encounter finite diagrammatic expansions that represent a PSDHF but do not possess the strict positivity property. A consequence of the PSDHF structure is that the Cauchy-Schwartz inequality

$$|\langle\!\langle \hat{A}|\hat{B}\rangle\!\rangle|^2 \leq \langle\!\langle \hat{A}|\hat{A}\rangle\!\rangle\langle\!\langle \hat{B}|\hat{B}\rangle\!\rangle \tag{11}$$

is satisfied (see Appendix A for a short proof) which leads to useful constraints on the correlators. The positive semi-definiteness of the Hilbert-Schmidt product furthermore leads to interesting corollaries by choosing particular forms of the operator $\hat{A}$. If we take

$$\hat{A} = \int \mathrm{d}\mathbf{x}\, \varphi(\mathbf{x})\, \hat{\psi}_H(\mathbf{x}, t) \tag{12}$$

we obtain

$$0 \leq \langle\!\langle \hat{A}|\hat{A}\rangle\!\rangle = \int \mathrm{d}\mathbf{x}\mathrm{d}\mathbf{x}'\, \varphi^*(\mathbf{x})\, \mathrm{Tr}\left[\hat{\rho}\, \hat{\psi}_H^\dagger(\mathbf{x}, t)\hat{\psi}_H(\mathbf{x}', t)\right] \varphi(\mathbf{x}') \tag{13}$$

which expresses the fact that at each time t the one-particle density matrix, regarded as an integral kernel acting on spatial functions, is a positive semi-definite operator. This is an important property of the density matrix. It guarantees, for example, that the

instantaneous natural orbital occupation numbers [34] obtained by diagonalizing the density matrix are non-negative. Another important case arises if we take

$$\hat{A} = \int \mathrm{d}t\, \varphi(t) \hat{O}_H(t) \tag{14}$$

where $\hat{O}_H(t)$ is the Heisenberg form of a Schrödinger operator $\hat{O}$. In that case we obtain

$$0 \leq \langle \hat{A} | \hat{A} \rangle = \int \mathrm{d}t\mathrm{d}t'\, \varphi^*(t) C(t,t') \varphi(t') = \int \frac{\mathrm{d}\omega}{2\pi} \frac{\mathrm{d}\omega'}{2\pi} \tilde{\varphi}^*(\omega) \tilde{C}(\omega,\omega') \tilde{\varphi}(\omega') \tag{15}$$

where $\tilde{\varphi}(\omega)$ is the Fourier transform of φ and we defined

$$C(t,t') = \langle \hat{O}_H(t) | \hat{O}_H(t') \rangle = \mathrm{Tr}\left[\hat{\rho}\, \hat{O}_H^\dagger(t) \hat{O}_H(t')\right] \tag{16}$$

as well as its Fourier transform

$$\tilde{C}(\omega,\omega') = \int \mathrm{d}t\mathrm{d}t'\, \mathrm{e}^{\mathrm{i}(\omega t - \omega' t')}\, C(t,t'). \tag{17}$$

Let us now investigate the equilibrium or steady-state limit. It is convenient to introduce the relative time-coordinate $\tau = t - t'$ and the average time coordinate $T = (t + t')/2$, which transforms the expression in (17) to

$$\tilde{C}(\omega,\omega') = \int \mathrm{d}\tau \mathrm{d}T\, \mathrm{e}^{\mathrm{i}(\omega-\omega')T + \mathrm{i}(\omega+\omega')\tau/2}\, C(T + \frac{\tau}{2}, T - \frac{\tau}{2}). \tag{18}$$

For equilibrium systems or in the steady state limit of a non-equilibrium system [11] the correlator is independent of T and the equation becomes

$$\tilde{C}(\omega,\omega') = 2\pi\delta(\omega - \omega')\, \mathcal{A}(\omega) \tag{19}$$

where we defined

$$\mathcal{A}(\omega) = \int \mathrm{d}\tau\, \mathrm{e}^{\mathrm{i}\omega\tau}\, C(\tau, 0) = \int \mathrm{d}\tau\, \mathrm{e}^{\mathrm{i}\omega\tau} \langle \hat{O}_H(\tau) | \hat{O}_H(0) \rangle. \tag{20}$$

For a general correlator of the form of (16) in an equilibrium or steady state regime the function $\mathcal{A}(\omega)$ defined by (20) is called the corresponding *spectral function*. If we now insert expression (19) back into (15) we find that

$$\int \frac{\mathrm{d}\omega}{2\pi}\, |\tilde{\varphi}(\omega)|^2\, \mathcal{A}(\omega) \geq 0. \tag{21}$$

Since this expression is valid for a general function $\tilde{\varphi}$ it follows that the spectral function is pointwise (for each given ω) PSD, i.e.

$$\mathcal{A}(\omega) \geq 0, \tag{22}$$

which is an important consequence of the Hilbert-Schmidt product structure of the correlator in (16). As an illustration we examine the spectral function corresponding to

i$G^>$. To this end we consider (20) and take the operator $\hat{O}$ in this expression to be of the form

$$\hat{O} = \int \mathrm{d}\mathbf{x}\, u(\mathbf{x})\, \hat{\psi}^\dagger(\mathbf{x}) \tag{23}$$

with $u(\mathbf{x})$ a general function. Equations (20) and (22) then yield

$$\mathcal{A}(\omega) = \int \mathrm{d}\mathbf{x}\mathrm{d}\mathbf{x}'\, u^*(\mathbf{x}) A^>(\mathbf{x},\mathbf{x}';\omega) u(\mathbf{x}') \geq 0 \tag{24}$$

where we defined the matrix spectral function

$$\begin{aligned} A^>(\mathbf{x},\mathbf{x}';\omega) &= \int \mathrm{d}\tau\, \mathrm{e}^{\mathrm{i}\omega\tau} \langle \hat{\psi}_H^\dagger(\mathbf{x},\tau) | \hat{\psi}_H^\dagger(\mathbf{x}',0)\rangle \\ &= \mathrm{i}\int \mathrm{d}\tau\, \mathrm{e}^{\mathrm{i}\omega\tau}\, G^>(\mathbf{x}\tau,\mathbf{x}'0) = \mathrm{i}G^>(\mathbf{x},\mathbf{x}';\omega) \end{aligned} \tag{25}$$

in which on the last line we also defined the Fourier transform of the particle propagator. Since the expression in (24) is equal to its complex conjugate it follows that $A^>$ is a Hermitian integral kernel acting in real space. Similarly we can define a spectral function $A^<$ for the hole propagator as

$$A^<(\mathbf{x},\mathbf{x}';\omega) = -\mathrm{i}G^<(\mathbf{x},\mathbf{x}';\omega) = \int d\tau\, \mathrm{e}^{\mathrm{i}\omega\tau} \langle \hat{\psi}_H(\mathbf{x}',0) | \hat{\psi}_H(\mathbf{x},\tau)\rangle \tag{26}$$

which again is a PSD operator in the same sense as in (24). In the following chapters we will simply regard the functions $G^{\lessgtr}$ as matrices and suppress the spatial labels $\mathbf{x}$ and $\mathbf{x}'$ or any other non-temporal basis labels, reintroducing them when necessary. The particular combination

$$A(\omega) = \mathrm{i}\left(G^>(\omega) - G^<(\omega)\right) \tag{27}$$

combines the spectral functions of the particle and hole propagator and is commonly referred to as the spectral function corresponding to the (retarded) Green's function. This function encodes information on the probability of many-body scattering processes as occurring in photo-emission and inverse photo-emission experiments [35, 36, 37] and its PSD structure therefore guarantees that the probabilities are always positive semi-definite.

The PSD Hermitian form structure is very general as it applies to both equilibrium and non-equilibrium systems. In the following chapters we will investigate how this structure can be build into diagrammatic perturbation theory and thereby enforce the required positivity properties.

2.3. Construction of PSD approximations

In this section we briefly review the approach that we used in our earlier works to construct PSD approximations for systems at zero temperature. In practice, the spectral functions for the Green's function are not calculated directly but from a diagrammatic

approximation to the self-energy appearing in the Dyson equation [1] written in matrix form as

$$G(z_1, z_2) = g(z_1, z_2) + \int_\gamma \mathrm{d}z_3 \mathrm{d}z_4 \, g(z_1, z_3)\Sigma(z_3, z_4)G(z_4, z_2) \tag{28}$$

where Σ denotes the self-energy, describing the irreducible particle scatterings, and g is the Green's function of the system in the absence of interactions. For equilibrium systems at zero temperature there is a simple relation between the greater and lesser Green's functions and the corresponding components of the correlation part of the self-energy, which in frequency space in matrix notation reads

$$G^{\lessgtr}(\omega) = G^R(\omega)\Sigma_c^{\lessgtr}(\omega)G^A(\omega). \tag{29}$$

Here G^R and G^A are the retarded and advanced Green's functions which are each others adjoint. Hence to ensure the PSD property of $\mathrm{i}G^>(\omega)$ and $-\mathrm{i}G^<(\omega)$ it is sufficient to establish the positivity of $\mathrm{i}\Sigma_c^>(\omega)$ and $-\mathrm{i}\Sigma_c^<(\omega)$. We showed [7] that this can be done in a diagrammatic fashion and demonstrated, for example, that the exact Σ_c can be written in a Hermitian product form in which each factor can be identified with a diagrammatic expression belonging to a cut self-energy diagram, a so-called half-diagram, a procedure that we will briefly summarize in the next section. More importantly, we further established that, if a given approximation for the self-energy does not have this structure, the diagrammatic series can be extended by construction of Hermitian products to form a new approximation that is PSD.

The central open question now is whether this procedure can be extended to finite temperature systems. For this we will need cutting rules that can be applied to diagrams on the extended contour and which allow for the derivation of a PSD expression. In the next chapter we will derive such rules.

3. Self-energy cutting rules at finite temperature

The purpose of this chapter is threefold. First, we generalize our original derivation of cutting rules [7], based on the Lehmann representation and the adiabatic assumption, from zero temperature to finite temperature. This is insightful since it shows that the finite temperature correction for the Lehmann amplitudes can be interpreted as an additional interaction with heat bath particles. Second, in the subsequent section we present an alternative derivation that uses neither the Lehmann representation nor requires the adiabatic assumption and moreover is valid for non-equilibrium final states. Both derivations lead to the same expansion in time-ordered and anti-time-ordered Green's functions. However, unlike the zero-temperature case we find that at finite temperature it is in general difficult to derive approximate positive definite expressions without introducing unwanted vacuum diagrams in the expansion. Third, we then demonstrate how this issue can be resolved using an expansion in so-called retarded half-diagrams [13, 11] with a clear physical interpretation as collective contributions of past scattering processes.

3.1. Cutting rules from the Lehmann representation

The correlation self-energy at finite temperature can be written as (see [38] or [1] section 9.1.)

$$\Sigma_c(\mathbf{x}_1 z_1, \mathbf{x}_2 z_2) = -\mathrm{i}\mathrm{Tr}\left[\hat{\rho}\,\mathcal{T}_\gamma\left\{\hat{\gamma}_H(\mathbf{x}_1 z_1)\hat{\gamma}_H^\dagger(\mathbf{x}_2 z_2)\right\}\right]_{\mathrm{irr}}, \tag{30}$$

where the sub-index irr denotes an operation that removes all reducible diagrams, i.e. those in which the external vertices 1 and 2 (corresponding to $\mathbf{x}_1 z_1$ and $\mathbf{x}_2 z_2$ respectively) can be disconnected from each other by removing a single g-line. The contour γ consists of forward and backward real-time branches (see Figure 1) where in this case we do not introduce the Matsubara branch but instead work directly with the density matrix $\hat{\rho}$. The operator $\hat{\gamma}_H$ is the Heisenberg form of the operator

$$\hat{\gamma}(\mathbf{x}) = \int \mathrm{d}\mathbf{x}'\, v(\mathbf{x},\mathbf{x}')\hat{\psi}^\dagger(\mathbf{x}')\hat{\psi}(\mathbf{x}')\hat{\psi}(\mathbf{x}) = \sum_{j_1 j_2 j_3} \gamma_{j_1 j_2 j_3}(\mathbf{x})\,\hat{c}_{j_1}^\dagger \hat{c}_{j_2}\hat{c}_{j_3}, \tag{31}$$

where the second equality expresses the operator in a single particle basis $\varphi_j(\mathbf{x})$ where

$$\gamma_{j_1 j_2 j_3}(\mathbf{x}) = \int \mathrm{d}\mathbf{x}' v(\mathbf{x},\mathbf{x}')\varphi_{j_1}^*(\mathbf{x}')\varphi_{j_2}(\mathbf{x}')\varphi_{j_3}(\mathbf{x}) \tag{32}$$

and $\hat{c}_j$ and $\hat{c}_j^\dagger$ are the creation and annihilation operators in one-particle basis. To establish a connection to our earlier work we start with a short description of the zero-temperature case and subsequently point out the problems that arise when attempting to generalise to the finite temperature case.

In the zero-temperature limit the density matrix $\hat{\rho}$ reduces to $\hat{\rho} = |\Psi_0\rangle\langle\Psi_0|$ where $|\Psi_0\rangle$ is the many-body ground state. Taking the lesser component of the self-energy we can then write

$$-\,\mathrm{i}\Sigma_c^<(1,2) = \langle\Psi_0|\hat{\gamma}_H^\dagger(2)\hat{\gamma}_H(1)|\Psi_0\rangle_{\mathrm{irr}} \tag{33}$$

where we used the short-hand notation $1 = \mathbf{x}_1 t_1$ and $2 = \mathbf{x}_2 t_2$. Following [7] we first use the Gell-Mann-Low theorem [39] and a time-evolution operator $\hat{U}$ to connect $|\Psi_0\rangle$ adiabatically to a non-interacting ground state $|\Phi_0\rangle$ at time $-T$, i.e. $|\Psi_0\rangle = \hat{U}_\eta(t_0,-T)|\Phi_0\rangle$, where eventually we let T approach infinity and η is an adiabatic parameter. This allows us to write

$$-\mathrm{i}\Sigma_c^<(1,2) = \langle\Phi_0|\hat{U}(-T,t_2)\hat{\gamma}^\dagger(\mathbf{x}_2)\hat{U}(t_2,T)\hat{U}(T,t_1)\hat{\gamma}(\mathbf{x}_1)\hat{U}(t_1,-T)|\Phi_0\rangle_{\mathrm{irr}} \tag{34}$$

where we have split the evolution operator $\hat{U}(t_2,t_1) = \hat{U}(t_2,T)\hat{U}(T,t_1)$ between the $\hat{\gamma}$ and $\hat{\gamma}^\dagger$ operators. Then we consider a complete set of non-interacting many-body eigenstates $|L,N\rangle$ of the form

$$|L,N\rangle = \hat{c}_{i'_1}\ldots\hat{c}_{i'_{N+1}}\hat{c}_{i_N}^\dagger\ldots\hat{c}_{i_1}^\dagger|\Phi_0\rangle \tag{35}$$

where $L = (I, I')$ is a multi-index with $I = (i_1,\ldots,i_N)$ and $I' = (i'_1,\ldots,i'_{N+1})$. We only consider states that contain one more removed particle than an added one, as due to

the specific form of $\hat{\gamma}$ only such states give a non-vanishing contribution when we insert them later using a completeness relation. The states $|L, N\rangle$ satisfy the orthonormality relations

$$\langle L_1, N_1 | L_2, N_2 \rangle = \delta_{N_1,N_2} \sum_P (-1)^{|P|} \delta_{L_1,P(L_2)} \tag{36}$$

where $P(L) = (P_1(I), P_2(I'))$ consists of all permutations P_1 and P_2 of the labels I and I' in L separately and $|P| = |P_1| + |P_2|$ is the overall sign of the permutation. There are $N!(N+1)!$ of such permutations and the completeness relation in the relevant Hilbert space for our states is therefore given by

$$\sum_{N=0}^{\infty} \sum_L \frac{1}{N!(N+1)!} |L, N\rangle\langle L, N| = 1 \tag{37}$$

where the summation index $L = (I, I')$ runs over all orderings of the indices in the multi-labels I and I'. We now insert the completeness relation (37) in between the operators $\hat{U}(t_2, T)$ and $\hat{U}(T, t_1)$ in (34) to obtain the expression

$$-\mathrm{i}\Sigma_c^<(1,2) = \sum_{N=1}^{\infty} \sum_L \frac{1}{N!(N+1)!} A_{L,N}(1) B_{L,N}(2) \tag{38}$$

which is in so-called Lehmann representation form and where we defined

$$A_{L,N}(1) = \langle L, N | \hat{U}(T, t_1) \hat{\gamma}(\mathbf{x}_1) \hat{U}(t_1, -T) | \Phi_0 \rangle_{\mathrm{irr}} \tag{39}$$

$$B_{L,N}(2) = \langle \Phi_0 | \hat{U}(-T, t_2) \hat{\gamma}^\dagger(\mathbf{x}_2) \hat{U}(t_2, T) | L, N \rangle_{\mathrm{irr}}. \tag{40}$$

These functions are related by complex conjugation, i.e $A_{L,N}(1) = B^*_{L,N}(1)$, but we give them different names since they have different diagrammatic expansions; the function $A_{L,N}$ can be expanded in time-ordered Green's functions while the function $B_{L,N}$ can be expanded in anti-time ordered Green's functions. The terms in the expansion are called half-diagrams and the sub-index irr in (39) and (40) indicates that we remove all half-diagrams that will lead to a reducible self-energy by a gluing procedure that we will describe in more detail later; this also implies that the sum over particle-hole pairs in (38) starts at $N = 1$. The diagrammatic expansion of $A_{L,N}$ and $B_{L,N}$ is most easily performed using the known Feynman rules (see Appendix B) of the contour-ordered n-particle Green's function, which is defined as [1]

$$G_n(1, \ldots n; 1' \ldots n') = \frac{1}{\mathrm{i}^n} \langle \mathcal{T}_\gamma [\hat{c}_{1,H}(z_1) \ldots \hat{c}_{n,H}(z_n) \hat{c}^\dagger_{n',H}(z'_n) \ldots \hat{c}^\dagger_{1',H}(z'_1)] \rangle \tag{41}$$

where $\hat{c}_{j,H}$ and $\hat{c}^\dagger_{j,H}$ are the Heisenberg forms of $\hat{c}_j$ and $\hat{c}^\dagger_j$. Using this definition we obtain the expressions

$$A_{L,N}(1) = \mathrm{i}^{N+2} \sum_{j_1 j_2 j_3} \gamma_{j_1 j_2 j_3}(\mathbf{x}_1) G^T_{N+2}(j_2, j_3, i_1, \ldots i_N; j_1^+, i'_1, \ldots, i'_{N+1}) \tag{42}$$

$$B_{L,N}(2) = \mathrm{i}^{N+2} \sum_{j_1 j_2 j_3} \gamma^*_{j_1 j_2 j_3}(\mathbf{x}_2) G^{\bar{T}}_{N+2}(j_1^+, i'_1, \ldots, i'_{N+1}; j_2, j_3, i_1, \ldots i_N) \tag{43}$$

where all the operators with indices in I and I' have time-coordinate T and the operators with labels in the set $\{j_1, j_2, j_3\}$ have time t_1 in $A_{L,N}$ and t_2 in $B_{L,N}$. The Green's function G^T_{N+2} denotes an $(N+2)$-particle Green's function ordered on the forward contour γ_- while $G^{\bar{T}}_{N+2}$ denotes an $(N+2)$-particle Green's function ordered on the backward contour γ_+. This gives the diagrammatic expression

$$-\mathrm{i}\Sigma^<_c(1,2) = \sum_{N=1}^{\infty} \frac{(-1)^{N+1}}{N!(N+1)!} \sum_L \Bigg[\quad \Bigg]_{\mathrm{irr}} \tag{44}$$

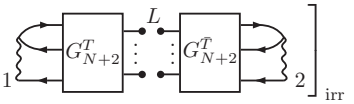

where the $(-1)^{N+1}$ arises from multiplication of the two factors i^{N+2} in (42) and (43) along with an additional prefactor -1 that arises from assigning a factor i for the two explicitly drawn interaction lines in the bracket to be able to use the Feynman rules for the two amputated $(N+1)$-particle Green's functions that emerge after joining of the $\hat{\gamma}$ operators. In Appendix B we specify the precise Feynman rules for the diagrammatic terms in brackets and demonstrate that a gluing procedure leads to the standard Feynman rules for the self-energy [1].

The factorization of the self-energy into half-diagrams in equations (38) and (44) was the crucial starting point of the PSD perturbation theory for positive spectra in our previous work [7]. Let us now investigate whether we can generalize this derivation to the case of finite temperature systems. Instead of using the Gell-Mann-Low theorem we follow Keldysh [40] in making the adiabatic assumption

$$\hat{\rho} = \hat{U}_\eta(t_0, -T)\hat{\rho}_0\hat{U}_\eta(-T, t_0), \tag{45}$$

where ρ_0 is the density operator of a noninteracting system and $\hat{U}_\eta$ includes an adiabatic switch-on of the interactions from a distant time $-T$ in the past with η an adiabatic parameter. This is a much stronger assumption than the Gell-Mann-Low theorem as it assumes that all eigenstates are adiabatically connected and that no level crossings occur that lead to degeneracies [1]. For the moment we explore the consequences of this assumption but we will demonstrate later that the same results can be derived under weaker assumptions. Under the adiabatic assumption the lesser self-energy takes the form

$$-\mathrm{i}\Sigma^<_c(1,2) = \mathrm{Tr}\left[\hat{\rho}_0\hat{U}_\eta(-T,t_0)\hat{\gamma}^\dagger_H(2)\hat{\gamma}_H(1)\hat{U}_\eta(t_0,-T)\right]_{\mathrm{irr}}. \tag{46}$$

We introduce a suitable basis of non-interacting many-body eigenstates $|J\rangle$ to perform the trace and place a completeness relation for a complete set of states $|L\rangle$ between the $\hat{\gamma}$-operators. This allows the density-matrix, expressed as $\hat{\rho}_0 = \frac{e^{-\beta(\hat{H}_0-\mu\hat{N})}}{Z_0}$, to be brought outside the trace, leading to an expression for the self-energy of the form

$$-\mathrm{i}\Sigma^<_c(1,2) = \sum_{L,J} \frac{e^{-\beta(E_J-\mu N_J)}}{Z_0} \langle J|\hat{\gamma}^\dagger_H(2)|L\rangle_{\mathrm{irr}}\langle L|\hat{\gamma}_H(1)|J\rangle_{\mathrm{irr}}. \tag{47}$$

We could now try and follow the derivation for the zero-temperature case to expand the Lehmann amplitudes $\langle L|\hat{\gamma}_H(1)|J\rangle$ in Feynman diagrams. However, these can not

be expressed straightforwardly in terms of finite temperature Green's functions as the amplitudes neither involve traces over a density matrix nor satisfy appropriate Kubo-Martin-Schwinger boundary conditions. Instead the zero-temperature Wick theorem could be used to expand in diagrams for a zero-temperature many-particle Green's function, but this procedure turns out to be cumbersome and we will therefore follow a much more direct alternative approach.

We first expand Σ in Feynman diagrams with finite-temperature Green's functions for all its g-lines. Then to connect to the Lehmann expression above we expand each diagram in terms of the zero-temperature Green's functions by writing $g = g_0 + \delta g$ where g is the non-interacting Green's function at finite temperature and g_0 is the non-interacting Green's function at zero temperature. Their difference δg can conveniently be expressed in terms of g_0 along with Fermi factors. We illustrate the procedure with an example.

Let us consider the lesser component of the following diagram that appears in the T-matrix approximation for the self-energy

$$D^<(1,2) = \Bigg[\quad \Bigg]^< \tag{48}$$

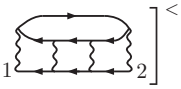

in which the Green's function lines now denote finite temperature Green's functions. This component of the self-energy is obtained by taking z_1 to be on the forward branch γ_- and z_2 to be on the backward branch γ_+. Its expansion in terms of (anti)time-ordered Green's functions is obtained by splitting each internal contour-time integral explicitly into its forward and backward parts, giving

$$D^<(1,2) = \quad + \quad + \quad + \tag{49}$$

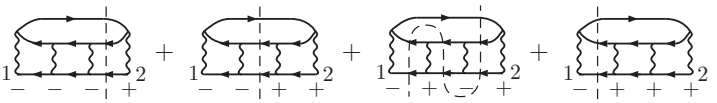

where $-/+$ denotes that the time-argument is taken to be on the forward/backward branch, and the dashed line marks the separation between the two branches. The Green's functions connecting times on γ_- and γ_+ are either time-ordered (g_{--}) and anti-time-ordered (g_{++}) or given by $g_{+-} = g^>$ and $g_{-+} = g^<$. These are the only Green's functions that appear since the two-body interaction is only present in the evolution operators on the real time axis and no interactions occur on the Matsubara branch as we replaced the density matrix by $\hat{\rho}_0$ using the adiabatic assumption [40].

To connect the self-energy to its Lehmann expansion we write the contour-ordered single-particle Green's function on γ_- and γ_+ at finite temperature as

$$g_i(z_1, z_2) = g_{0,i}(z_1, z_2) + \delta g_i(t_1, t_2), \tag{50}$$

where i labels a state in the eigenbasis of the one-body Hamiltonian and $g_{0,i}$ is the zero-temperature Green's function

$$\begin{aligned} g_{0,i}(z_1, z_2) &= \theta(z_1, z_2) g^>_{0,i}(t_1, t_2) + \theta(z_2, z_1) g^<_{0,i}(t_1, t_2) \\ &= \theta(z_1, z_2)(-\mathrm{i})\bar{n}_i \mathrm{e}^{-\mathrm{i}\epsilon_i(t_1 - t_2)} + \theta(z_2, z_1)\mathrm{i} n_i \mathrm{e}^{-\mathrm{i}\epsilon_i(t_1 - t_2)}, \end{aligned} \tag{51}$$

where n_i is the occupation number of one-particle state i and $\bar{n}_i = 1 - n_i$. The finite temperature correction term δg_i can be expressed as

$$\begin{aligned}\delta g_i(t_1,t_2) &= \mathrm{i}(f_i - n_i)\mathrm{e}^{-\mathrm{i}\epsilon_i(t_1-t_2)} = \mathrm{i}\left[\bar{n}_i f_i - n_i \bar{f}_i\right]\mathrm{e}^{-\mathrm{i}\epsilon_i(t_1-t_2)} \\ &= -f_i\, g^{>}_{0,i}(t_1,t_2) - \bar{f}_i\, g^{<}_{0,i}(t_1,t_2),\end{aligned} \tag{52}$$

where $f(\omega) = \frac{1}{\mathrm{e}^{\beta\omega}+1}$ and $\bar{f}(\omega) = 1 - f(\omega)$ are the Fermi- and anti-Fermi-functions, and we have used the shorthand notation $f_i = f(\epsilon_i - \mu)$ and similarly for $\bar{f}_i$. The correction terms do not involve any temporal step-functions, and consequently the same correction applies to the greater and lesser components individually. This allows us to express the finite temperature diagrams as linear combinations of zero-temperature diagrams weighted by Fermi factors. In particular using (50) and (52), along with the relations

$$\begin{aligned}\mathrm{i}g^{<}(t_1,t_2) &= g_{--}(t_1,T)g_{++}(T,t_2) = g_{++}(t_1,-T)g_{--}(-T,t_2) \\ -\mathrm{i}g^{>}(t_1,t_2) &= g_{++}(t_1,T)g_{--}(T,t_2) = g_{--}(t_1,-T)g_{++}(-T,t_2),\end{aligned} \tag{53}$$

we can write for example the greater component of the finite temperature Green's function as

$$\begin{aligned}-\mathrm{i}g^{>}_i(t_1,t_2) &= g_{0,i,++}(t_1,T)g_{0,i,--}(T,t_2) \\ &\quad + f_i\, g_{0,i,++}(t_1,T)g_{0,i,--}(T,-T)g_{0,i,++}(-T,T)g_{0,i,--}(T,t_2) \\ &\quad - \bar{f}_i g_{0,i,++}(t_1,-T)g_{0,i,--}(-T,T)g_{0,i,++}(T,-T)g_{0,i,--}(-T,t_2),\end{aligned} \tag{54}$$

which can be expressed diagrammatically as (using a double-line to denote the finite temperature g-line)

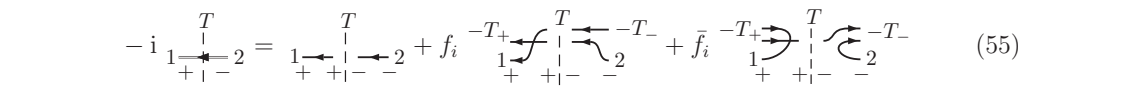

(55)

where the cut is made at time T. Note that the last two diagrams here belong to a two-particle Green's function, and the differences in signs of the terms appearing in (54) are absorbed into the corresponding diagram prefactors. Diagrammatically the correction term (52) therefore generates two additional diagrams for each g-line. These additional diagrams can be interpreted to result from the fact that one can not differentiate between excitations created by interaction with the propagating particle, and those present in the finite temperature ensemble state. Therefore we need to include the processes in which the propagating particle/hole is either exchanged with an ensemble particle/hole excitation or combines with an ensemble hole/particle.

If we consider, for example, the second diagram in (49) and insert (55) into one of the g-lines which connect the + and − halves of the diagram, we generate the diagrams

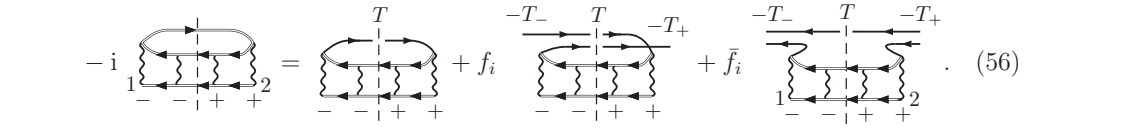

(56)

By repeating these steps for each of the g-lines crossing the cut in (56) one can achieve a factorization in terms of fully time-ordered and anti-time-ordered half-diagrams at finite temperature.

In an analogous manner the internal finite temperature g-lines in the half-diagrams can also be expanded in zero-temperature g-lines. Suppose, for example, that we have factorized all the connecting g-lines in (56) and we take the diagram with no coupling to the ensemble excitations. An internal g-line can be expanded as

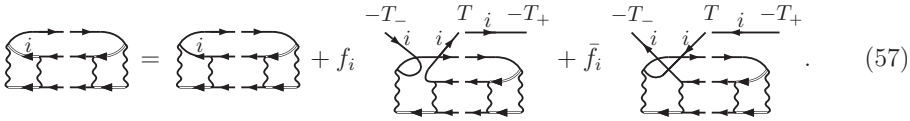

(57)

In order to group the half-diagrams into Hermitian products, the Fermi factors need to be expressed in a way that allows them to be taken out as common factors. This can be achieved by noting that for example the diagram multiplied by f_i in (57) contains $g_i^>$ and is therefore non-zero only when the state i is unoccupied in the ground-state, i.e. $\bar{n}_i = 1$. We can thus write the prefactor as $f_i = \bar{n}_i f_i + n_i \bar{f}_i$. Similar reasoning works also for the diagram with prefactor $\bar{f}_i$ in (57), which allows us to pull $\bar{n}_i f_i + n_i \bar{f}_i$ out as a common factor.

We could then, in theory, construct PSD self-energy approximations by expanding the g-lines connecting the half-diagrams, and building Hermitian products such as

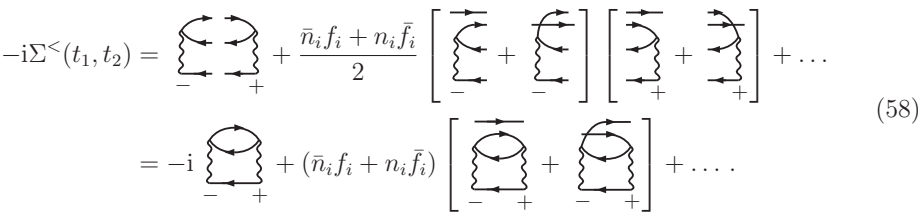

(58)

Terms such as in (58) can be connected to the Lehmann amplitudes appearing in (47) by noting that for example a $g_i^>$ line starting at $-T$ corresponds to a state $|J\rangle$ in (47) with the single-particle state i occupied. An excitation to one-particle state i can only occur in $|J\rangle$ when that state is unoccupied in the ground state. Similarly a de-excitation from one-particle state i can only occur in $|J\rangle$ when that state is occupied in the ground state. We can therefore express the prefactor as $\bar{n}_i f_i + n_i \bar{f}_i = n_i^J f_i + \bar{n}_i^J \bar{f}_i$, where n_i^J is the occupation of the single-particle state i in the non-interacting many-body eigenstate $|J\rangle$. In general such terms appear as products, which can be expressed as

$$\prod_i \left[n_i^J f_i + \bar{n}_i^J \bar{f}_i \right] = \prod_i \frac{\mathrm{e}^{-\beta n_i^J \epsilon_i}}{1 + \mathrm{e}^{-\beta \epsilon_i}} = \frac{\mathrm{e}^{-\beta \sum_i n_i^J \epsilon_i}}{\prod_i (1 + \mathrm{e}^{-\beta \epsilon_i})}, \tag{59}$$

and thus be related to the Boltzmann factor for the state $|J\rangle$ appearing in (47). In this manner one could, by careful accounting of all the diagrams and prefactors, work one's way back to a diagrammatic expression of the form of (47), which would constitute a

finite temperature generalization of (44) containing additional connections between the half-diagrams that are weighted by Boltzmann factors corresponding to the sum over the J-states. This is equivalent to defining the J and L states in (47) in a suitable manner to write the Lehmann amplitudes $\langle J|\cdots|L\rangle_{\rm irr}$ as multi-particle Green's functions at zero temperature. We have therefore succeeded in deriving a diagrammatic expansion for the self-energy based on Lehmann amplitudes which generalizes our earlier work and reduces to it in the zero temperature limit. The finite temperature corrections of this expansion can be interpreted as additional interactions by which particles enter and leave a heat bath [28]. Although physically insightful and feasible to derive a PSD perturbation theory, the approach is not very practical; as follows from (55) each cut g-line leads to three zero-temperature diagrams. In the following section we discuss a much more viable approach to PSD approximations at finite temperature.

3.2. Factorization of the self-energy and the issue of non-vanishing vacuum diagrams

In the previous section we provided a generalisation of the zero-temperature cutting procedure that can be directly related to the Lehmann amplitudes $\langle L|\gamma(1)|J\rangle_{\rm irr}$. However, this required a formulation in terms of zero temperature Green's functions and is, although possible [41, 42], not very practical for deriving PSD approximations for applications of many-body perturbation theory. We therefore advance here another procedure for factorizing self-energy diagrams.

We consider again the standard finite temperature diagrammatic expansion of the self-energy from the previous section. We expand each diagram in (anti)time ordered components as in (49) and then algebraically factorize the g-lines connecting the forward and backward branches using the relation

$$g^{\lessgtr}(t,t') = g^R(t,t_0)g^{\lessgtr}(t_0,t_0)g^A(t_0,t') \tag{60}$$

where g^R and g^A are the retarded and advanced Green's functions and t_0 is a suitably chosen time. Since $g^<(t_0,t_0) = \mathrm{i}\rho_0$ and $g^>(t_0,t_0) = -\mathrm{i}(1-\rho_0) = -\mathrm{i}\bar{\rho}_0$ where ρ_0 is the one-particle density matrix at time t_0, we can write

$$-\mathrm{i}g^<(t,t') = [g^R(t,t_0)\rho_0^{\frac{1}{2}}][g^R(t',t_0)\rho_0^{\frac{1}{2}}]^\dagger = \tilde{g}^<(t,t_0)[\tilde{g}^<(t',t_0)]^\dagger \tag{61}$$

$$\mathrm{i}g^>(t,t') = [g^R(t,t_0)\bar{\rho}_0^{\frac{1}{2}}][g^R(t',t_0)\bar{\rho}_0^{\frac{1}{2}}]^\dagger = \tilde{g}^>(t,t_0)[\tilde{g}^>(t',t_0)]^\dagger \tag{62}$$

where the $\tilde{g}^{\lessgtr}$ are defined by these equations and $\rho_0^{\frac{1}{2}}$ and $\bar{\rho}_0^{\frac{1}{2}}$ are the square roots of ρ_0 and $\bar{\rho}_0$ as spatial operators, which are well-defined since these operators are PSD; in case we use the eigenbasis of the one-body Hamiltonian of (1) they are diagonal matrices with diagonal elements given by the square roots of the (anti)-Fermi functions. We thus see that we can factorize the lesser and greater functions as $\mp\mathrm{i}g^{\lessgtr} = \tilde{g}^{\lessgtr}\tilde{g}^{\lessgtr\dagger}$ which, as shown in Appendix B, allows the self-energy to be written as

$$-\mathrm{i}\Sigma_c^<(1,2) = \sum_{N=1}^{\infty}\sum_{a,b,I,P}(-1)^{|P|}A^{(a)}_{N,I}(1,t_0)A^{(b)*}_{N,P(I)}(2,t_0) \tag{63}$$

where $A^{(a)}_{N,I}$ represents a diagrammatic expression of a half-diagram of topology a. The label N denotes the number of particle-hole line pairs connecting the half-diagrams and I is a multi-index for the spatial labels of all connecting lines. The permutations P run over all permutations of the particle and hole lines separately and since for $\Sigma^<$ there is one hole line more than a particle line there are $N!(N+1)!$ of such permutations. The main difference with the derivation in the previous section is that the diagram $A^{(i)}_{N,I}(1,t_0)$ can not directly be associated with a Lehmann amplitude; it rather consists of a term in an expansion of the $(N+1)$-particle Green's function in which the Green's functions on cut external legs have been replaced by the functions $\tilde{g}^{\lessgtr}$, and the remaining leg corresponding to vertex 1 has been removed. In Appendix B we prove that we recover the correct expansion of the self-energy when these modified diagrams obey the same Feynman rules as the $(N+1)$-particle Green's function. From expression (63) it also becomes clear that the expansion is PSD; defining

$$S^{(a)}_{N,I}(1,t_0) = \sum_P (-1)^{|P|}\, A^{(a)}_{N,P(I)}(1,t_0) \tag{64}$$

we see that the self-energy can be written as the explicitly positive semi-definite expression

$$-\,\mathrm{i}\Sigma^<_c(1,2) = \sum_{N=1}^{\infty} \frac{1}{N!(N+1)!} \sum_{a,b,I} S^{(a)}_{N,I}(1,t_0) S^{(b)*}_{N,I}(2,t_0). \tag{65}$$

So far the discussion concerned the exact self-energy. However, in contrast to the exact self-energy, a given diagrammatic approximation, such as that in (49), will in general not lead to a positive definite spectral function. To solve this problem we can attempt to repeat the procedure for the zero temperature case [7] to construct a PSD perturbation series. The first step is to write the expansion as a product of factors containing the time and anti-time-ordered parts; again using our factorization procedure with the functions $\tilde{g}$ of equations (61) and (62). The factors that result from this procedure have then to be re-assembled into Hermitian products to obtain the PSD form of (65). For systems at finite temperature a complication arises from the presence of diagrams with islands consisting solely of time or anti-time ordered vertices of the form

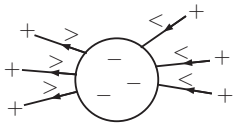

(66)

such as in the third diagram in (49). At zero-temperature such islands vanish, as demonstrated by the following argument. All the g-lines entering an island will be greater/lesser, and all the g-lines leaving will be lesser/greater. At zero temperature a greater/lesser Green's function always carries an energy above/below the Fermi level and the island formally has a net energy flow in or out. This is, however, forbidden by energy conservation that is mathematically enforced by the presence of Heaviside functions whereby the island vanishes. At finite temperature this is not true anymore

due to the smearing of the Heaviside functions to continuous Fermi functions. This is problematic when it comes to constructing PSD approximations out of half-diagrams, which is best illustrated with the example of the third diagram in (49). The diagram has the following structure

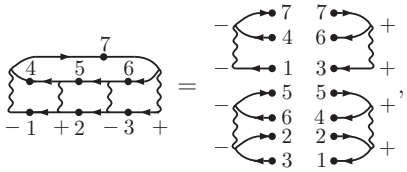

(67)

which we have cut into time and anti-time ordered parts using the factorization of the greater and lesser Green's functions, and where two islands appear that are disconnected from external vertices. In the notation of (63) the diagrammatic product on the right-hand side corresponds to the term

$$(-1)^2 A^{(a)}_{3,(3265147)}(1,t_0) A^{(a)*}_{3,(1245367)}(2,t_0) \tag{68}$$

where the half-diagrams on both sides of the cut are of the same topology a, have cut lines with $N=3$ particle hole pairs and cut labels $I=(3265147)$ and $P(I)=(1245367)$ corresponding to an even permutation $(13)(46)$ consisting of two transpositions. In order to obtain a PSD self-energy containing this diagram we need to construct a PSD form from the separate half-diagrams as derived in our earlier work [7]. If the half-diagrams have the same topology and only differ in the labeling of the cut legs, this is achieved by adding the half-diagrams corresponding to the smallest permutation subgroup containing the permutation of the legs in question. This procedure amounts to the construction of additional terms in (63) which allows for a rewriting of the equation in a PSD form as is done in (65). In our case the halves differ by the permutation $\sigma=(13)(46)$ of the external legs and the smallest subgroup containing it is $\{\iota,\sigma\}$ where ι is the identity permutation. This yields the following minimal PSD extension of the given diagram

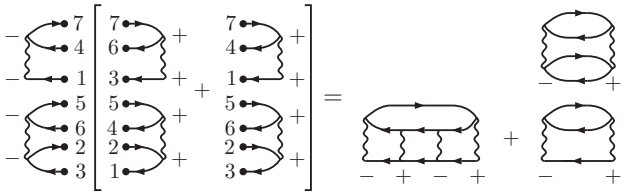

(69)

We therefore see that the construction introduces a new self-energy diagram containing a disconnected vacuum diagram. This is readily seen to be a general feature; the minimal PSD extension of diagrams containing + or − islands necessarily introduces disconnected vacuum diagrams into the self-energy. However, such vacuum diagrams do not contribute to the exact self-energy, since a sum over all their different time/anti-time ordered components corresponds to an integral over the loop contour on all

vertices, which vanishes as a closed integral. The minimal PSD extension procedure, however, creates only specific time-ordered components of the vacuum diagram, and therefore introduces a finite contribution that would eventually be cancelled in the exact expansion. It is clearly undesirable to include in an approximate expansion terms that should ultimately not contribute. This issue has been prominently discussed in the particle physics literature [21, 27, 28, 26, 23] where diagrams containing + or − islands are referred to as "non-cuttable" diagrams [22, 23]. In section 3.4 we will resolve this issue using the concept of retarded half-diagrams.

However, before addressing that problem we will first derive a generalization of the result of this section that is even valid for non-equilibrium final states and does not require the adiabatic assumption. It will also allow us to make a connection to earlier work of Jeon [27] which is thereby put into a different context.

3.3. Time-ordered cutting rules from the Riemann-Lebesque lemma

The derivation of the finite temperature expansion for the self-energy in section 3.1 was based on the assumption that the interacting density matrix can be adiabatically connected to a non-interacting one [40]. This assumption is stronger than needed and in this section we derive the result in a more direct and simpler fashion by applying the Riemann-Lebesque (RL) lemma for Fourier transforms to the case of systems with a continuous one-particle spectrum. In the second part of this section we will show that even the assumption of a continuous spectrum is not needed, at least when we confine ourselves to finite temperature systems in thermodynamic equilibrium.

Our starting point is the full contour of Figure 1 which contains also a Matsubara branch. Throughout this section we use as an example the diagram

$$D^<(1,2) = \Big[$$ 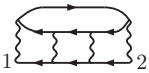 $$\Big]^<$$ (70)

The lesser component is obtained by taking the external time z_1 on the forward branch γ_- and the external time z_2 on the backward branch γ_+. The time-ordered expansion of a contour diagram at finite temperature is achieved by splitting each internal contour-time integral explicitly into its forward, backward and Matsubara parts (see Figure 1)

$$\int_\gamma dz = \int_{\gamma_-} dz + \int_{\gamma_+} dz + \int_{\gamma_M} dz = \int_{t_{0-}}^{\infty} dz + \int_{\infty}^{t_{0+}} dz + \int_{t_{0+}}^{t_0 - \mathrm{i}\beta} dz \qquad (71)$$

and summing over all the resulting real-time integrals. For our example diagram (using

$-/+$ to denote the γ_-/γ_+ branches) we have

$D^<(1,2) =$ 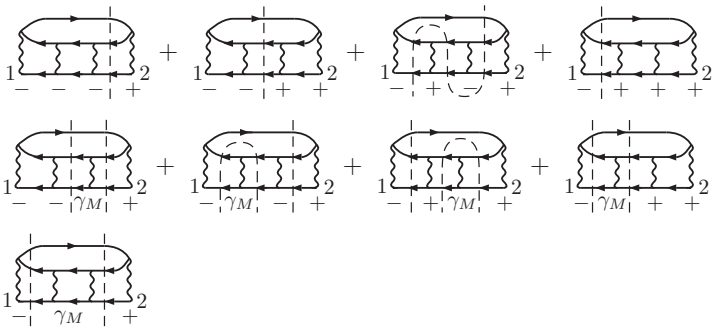

(72)

where dashed lines mark the cuts between the distinct branches. The Green's functions that connect a real time to a time on the Matsubara branch are denoted by $g(t_0 - \mathrm{i}\tau, t_\pm) = g^\ulcorner(\tau, t)$ and $g(t_\pm, t_0 - \mathrm{i}\tau) = g^\urcorner(t, \tau)$ (see [1] for a thorough discussion) and a Green's function connecting two times on the Matsubara branch is denoted by the Matsubara Green's function $g^M(\tau, \tau')$. We will now demonstrate that for a system with a continuous energy spectrum the so-called left and right Green's functions $g^\ulcorner$ and $g^\urcorner$ give a vanishing contribution to the Feynman diagrams provided we assume the system to be in equilibrium before a given time t_0. Practically this implies that we can disregard the Matsubara branch in the diagrams provided we let all real time integrals commence at $-\infty$ instead of the finite time t_0.

In the following we assume that the system is in equilibrium for times $t \leq t_0$ while for $t > t_0$ there may be external perturbations that bring the system into a non-equilibrium state. From time translation invariance it follows that for a system in equilibrium the value of an observable cannot depend on the wait time between state preparation and the start of the measurement. Therefore we can extend the contour to a past time $t = -T \leq t_0$ (see Figure 2). Now for any time t we have the decomposition (see [1] for details),

$$g^\ulcorner(\tau, t) = -\mathrm{i}g^M(\tau, 0)g^A(-T, t) \qquad g^\urcorner(t, \tau) = \mathrm{i}g^R(t, -T)g^M(0, \tau) \tag{73}$$

where $g^{R/A}$ denotes the retarded/advanced Green's function. For $t > t_0$ it will be useful to use a semi-group property [1] of the retarded and advanced functions

$$g^A(-T, t) = -\mathrm{i}g^A(-T, t_0)g^A(t_0, t) \qquad g^R(t, -T) = \mathrm{i}g^R(t, t_0)g^R(t_0, -T). \tag{74}$$

The functions $g^{R/A}$ are in general expressed in terms of time-ordered exponentials [1] but for times t and t' in the equilibrium time interval $[-T, t_0]$ they acquire a simple form with respect to a basis of non-interacting one-particle eigenstates of the one-body part of the Hamiltonian

$$g_i^R(t, t') = -\mathrm{i}\theta(t - t')\mathrm{e}^{-\mathrm{i}\epsilon_i(t-t')} \qquad g_i^A(t, t') = \mathrm{i}\theta(t' - t)\mathrm{e}^{-\mathrm{i}\epsilon_i(t-t')} \tag{75}$$

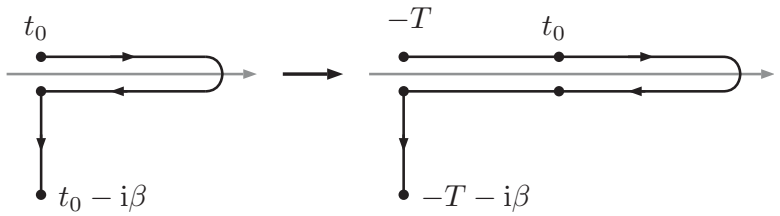

Figure 2. In a system initially in equilibrium, the wait time between state preparation and measurement does not affect the result. One can therefore extend the contour to a past time $t = -T$.

where ϵ_i is the eigenenergy of the one-particle state labeled by i. The key ingredient of our derivation is the Riemann-Lebesque (RL) lemma (see Th.7.5 of [43]) which states that

$$0 = \lim_{T\to\pm\infty} \int \mathrm{d}\epsilon\, F(\epsilon)\, \mathrm{e}^{\mathrm{i}\epsilon T} \tag{76}$$

whenever F belongs to the space of integrable functions $L^1(\mathbb{R})$ (for example F can be a piecewise continuous function). If the one-particle spectrum ϵ_i is continuous, as is generally the case for an infinite system, the summations over the labels i in the Feynman diagrams can be replaced by integrals over the energy ϵ where a density of states $d(\epsilon)$ appears in the integration volume element. If $d(\epsilon)$ belongs to $L^1(\mathbb{R})$ the RL lemma and (74) can be invoked to establish that diagrams that contain $g^{\rceil}$ and $g^{\lceil}$ vanish in the limit $T \to \infty$.

Applying the RL lemma we therefore retain only the first row of (72) provided that in these diagrams we let the lower bound of all time integrations be equal to $-\infty$. We see that in this way we derived precisely the same self-energy expansion as in the previous section with two important differences. First, we needed a much weaker assumption (a continuous spectrum instead of the adiabatic assumption). Second, the expression derived above is valid for general systems in initial equilibrium up to some finite time but exposed to a time-dependent external perturbation after it.

In the following we will show that even the assumption of having a continuous one-particle spectrum can be disposed off when we restrict ourselves to systems in thermodynamic equilibrium. This will be done by making a connection to the work of Jeon[27]. We can write the self-energy in an alternative version of (63) as follows

$$-\mathrm{i}\Sigma_c^<(t_1,t_2) = \sum_{N=1}^{\infty} \sum_{a,b,I,P} (-1)^{|P|} \int_{\gamma_-} \mathrm{d}t_{\mathcal{I}} \int_{\gamma_+} \mathrm{d}t'_{\mathcal{I}}\, B^{(a)}_{N,I}(t_1,t_{\mathcal{I}}) \Upsilon^<_I(t_{\mathcal{I}},t'_{\mathcal{I}}) B^{(b)*}_{N,P(I)}(t_2,t'_{\mathcal{I}}), \tag{77}$$

where the terms $B^{(a)}_{N,I}$ are obtained from the terms $A^{(a)}_{N,I}$ by removing the legs of the cut lines and $t_{\mathcal{I}}$ and $t'_{\mathcal{I}}$ are sets of time labels for the endpoints of the cut lines. The cut

lines are assembled in a new term Υ_I of the form

$$\Upsilon_I^<(t_\mathcal{I}, t'_\mathcal{I}) = \prod_{p\in J}^{N} -\mathrm{i}g_p^>(t'_p, t_p) \prod_{q\in K}^{N+1} \mathrm{i}g_q^<(t_q, t'_q) \tag{78}$$

where the index set $I = (J, K)$ for the cut lines has been divided into sets of indices J referring to particle lines and indices K referring to hole lines (we always choose a one-particle basis in which the zeroth-order Green's functions are diagonal).

If we specialize to systems that are in equilibrium at all times then all quantities are time-translation invariant and we can do Fourier transforms to find lower dimensional expressions in frequency space. Fourier transforming (77) one obtains

$$-\mathrm{i}\Sigma_c^<(\omega) = \sum_{N=1}^{\infty} \sum_{a,b,I,P} (-1)^{|P|} \int \frac{\mathrm{d}\omega_\mathcal{I}}{(2\pi)^I} B_{N,I}^{(a)}(\omega_\mathcal{I}) 2\pi\delta(\omega - \Omega) \Upsilon_I^<(\omega_\mathcal{I}) B_{N,P(I)}^{(b)*}(\omega_\mathcal{I}), \tag{79}$$

where we defined the total energy flowing to the left through the cut lines as $\Omega = \sum_{i\in\mathcal{I}} \omega_i$ and

$$B_{N,I}^{(a)}(\omega_\mathcal{I}) = \int \mathrm{d}t_\mathcal{I}\, B_{N,I}^{(a)}(t_1, t_\mathcal{I}) \mathrm{e}^{\mathrm{i}\omega_\mathcal{I}\cdot(t_1 - t_\mathcal{I})} \tag{80}$$

(using the notation $\omega_\mathcal{I} \cdot (t_1 - t_\mathcal{I}) = \sum_{i\in\mathcal{I}} \omega_i(t_1 - t_i)$) so that the time-convolutions between the half-diagrams are replaced by simple products. The function $\Upsilon_I^<(\omega_\mathcal{I})$ with the explicit form

$$\Upsilon_I^<(\omega_\mathcal{I}) = \prod_{p\in J}^{N} -\mathrm{i}g_p^>(-\omega_p) \prod_{q\in K}^{N+1} \mathrm{i}g_q^<(\omega_q) \tag{81}$$

is a PSD integral operator in spatial indices for all $\omega_\mathcal{I}$. If we consider the explicit form of $g^\lessgtr$ (see (51)) the Fourier transform of $\Upsilon^<$ is readily expressed in terms of delta distributions and with the relations above we can express the lesser self-energy as

$$-\mathrm{i}\Sigma_c^<(\omega) = \sum_{N=1}^{\infty} \sum_{a,b,I,P} (-1)^{|P|} B_{N,I}^{(a)}(\tilde{\epsilon}_\mathcal{I}) 2\pi\delta(\omega - \mathcal{E}) F^<(\epsilon_\mathcal{I}) B_{N,P(I)}^{(b)*}(\tilde{\epsilon}_\mathcal{I}), \tag{82}$$

where we defined $\epsilon_\mathcal{I}$ the set of one-particle energies ϵ_i for the cut lines and we further defined

$$F^<(\epsilon_\mathcal{I}) = \prod_{p\in J}^{N} \bar{f}(\epsilon_p - \mu) \prod_{q\in K}^{N+1} f(\epsilon_q - \mu). \tag{83}$$

We also defined the energy $\mathcal{E} = \sum_{q\in K} \epsilon_q - \sum_{p\in J} \epsilon_p$ and $\tilde{\epsilon}_\mathcal{I}$ is an argument list consisting of the energies ϵ_q for the hole lines and $-\epsilon_p$ for the particle lines. Expression (82) is of a physically appealing Fermi golden rule form [12], involving products of scattering amplitudes $B_{N,I}^{(i)}$, occupation functions incorporated in $F^<$ and an overall energy conservation enforced by a delta function. A rearrangement of the expression as in (65) will make this even more apparent but the expression above is closer to the expressions that would actually be used in practice.

In equilibrium the fluctuation dissipation theorem gives that $-\mathrm{i}\Sigma_c^<(\omega) = f(\omega - \mu)\Gamma(\omega)$ and $\mathrm{i}\Sigma_c^>(\omega) = \bar{f}(\omega - \mu)\Gamma(\omega)$ where $\Gamma(\omega)$ is the spectral function of the self-energy (also known as the rate function) which can be expressed as

$$\Gamma(\omega) = \mathrm{i}(\Sigma_c^>(\omega) - \Sigma_c^<(\omega)) = \mathrm{i}(\Sigma_c^R(\omega) - \Sigma_c^A(\omega)). \tag{84}$$

If we use that in equilibrium (see for example [1] section 9.5)

$$\Sigma_c^{R/A}(\omega) = \Sigma_c^M(\omega - \mu \pm \mathrm{i}\eta), \tag{85}$$

with η a positive infinitesimal and μ the chemical potential we can write

$$-\mathrm{i}\Sigma_c^<(\omega) = \mathrm{i}f(\omega - \mu)(\Sigma_c^M(\omega - \mu + \mathrm{i}\eta) - \Sigma_c^M(\omega - \mu - \mathrm{i}\eta)). \tag{86}$$

This relation was used by Jeon [27] to derive an expression of the form of (82) (for the Green's function instead of the self-energy) using an expansion in Matsubara Green's functions (see equations (3.4a) and (3.4b) in [27]). Jeon's derivation proceeds via the following steps:

(i) Each Matsubara diagram is expanded in its time-ordered components in imaginary time.

(ii) Each time-ordered component is expressed in frequency space using the rules derived originally by Balian and De Dominicis [44] and later by Baym and Sessler [45].

(iii) For each of the obtained expressions the limit $\eta \to 0$ is taken for a difference of terms as in (86).

(iv) The final expression obtained this way can be interpreted as a sum over cut diagrams and factors to the left and right of the cut can be expressed in terms of time-ordered and anti-time-ordered Green's functions (this uses (D.22) of Appendix D).

Importantly this derivation nowhere uses the Riemann-Lebesque lemma, and therefore does not need to assume continuous spectra. Its main ingredient is analytic continuation and the use of fluctuation dissipation relations such as $g^>(\omega) = -\mathrm{e}^{\beta(\omega-\mu)}g^<(\omega)$. It is therefore similar in spirit to the derivation that proves that the equilibrium limit of the Kadanoff-Baym equations is independent of the initial time of time-propagation (section 9.6 of [1]). It follows from Jeon's derivation that in equilibrium the removal of Matsubara track integrals in the expansion of $\Sigma_c^{\lessgtr}$ is justified even for systems with a discrete energy spectrum provided we extend the time-integrals to the infinite past. The information about the initial density matrix is not lost, as it is still preserved in the functions $g^{\lessgtr}$ that contain the Fermi functions depending on the temperature and the chemical potential. For additional discussion of these relations see Appendix D; they play a more important role in the next section in which we use a more elegant approach to derive the result.

The above cutting rules still retain the issues relating to disconnected pieces in half-diagrams leading to unwanted vacuum diagrams, as we discussed below (66). In

the following section we propose how this crucial issue can be solved by a different kind of expansion of the contour diagram, replacing time-ordered half-diagrams by retarded ones.

3.4. Retarded cutting rules

The problems posed by disconnected pieces in half-diagrams are created because cutting the diagram between the forward and the backward branches limits each half-diagram to a single branch on which vacuum diagrams do not integrate to zero. The most straightforward way to deal with this issue is therefore to start by deforming the contour to a double loop so that it returns to $-T$ between the external time arguments located at the end of each loop as follows

(87)

Each time integration can therefore be written as a sum of two time integrations on each separate loop. When this is done for the time-integrals in a Feynman diagram disconnected sub-diagrams vanish as they are integrated from $-T$ to $-T$ on a loop and only the contribution from terms connecting to external vertices survive. This elimination does not rely on any physical properties of the system, such as energy-conservation, and therefore happens also at finite temperature and in non-equilibrium systems.

Internal loop integrals over a sub-diagram up to the external times representing the entry or exit point of the self-energy can be expressed in terms of real-time integrals over retarded functions [13, 11]. Accordingly we define a multi-argument retarded component of a general Feynman diagram with integrand $D(z_{\mathcal{N}}) = D(z_1, \ldots, z_N)$ and external vertex at time z_1 as follows

$$\int_\gamma \mathrm{d}z_2 \cdots \mathrm{d}z_N D(z_{\mathcal{N}}) = \int_{t_0}^{\infty} \mathrm{d}t_2 \cdots \mathrm{d}t_N D^{R(1,2\cdots N)}(t_{\mathcal{N}}), \tag{88}$$

where γ is a loop contour and the multi-retarded function $D^{R(1,2\cdots N)}(t_{\mathcal{N}})$ with respect to argument 1 is a real-time function such that equality holds in the equation above. The multi-retarded functions allow for convenient conversion from contour to real-time integration and capture, in effect, the back-and-forth integration on the contour within a single real-time function. We show how to evaluate these functions in Appendix C and Appendix D, although for the purpose of developing PSD approximations they feature mainly as building blocks and it is sufficient to evaluate the final self-energy directly once it is obtained from the PSD construction. If we now split our time-integrations as sums of integrations on each of the loops of (87) and on the Matsubara branch γ_M and

apply this to our example diagram we have

$D^<(1,2) =$ 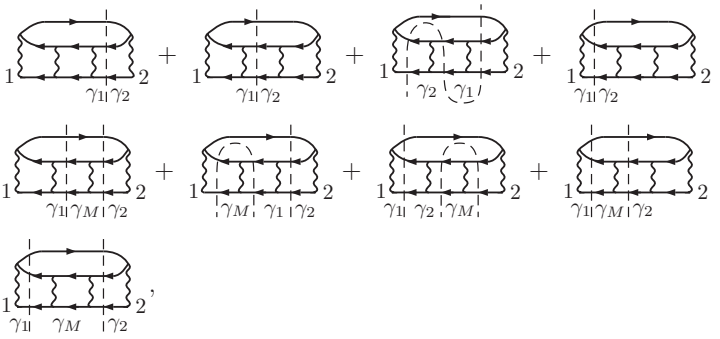

(89)

where in the figure the time integrations over the loops γ_1, γ_2 (see Figure 87) and the Matsubara branch γ_M are indicated for each interaction line. The lesser component was selected by taking z_1 to be on loop γ_1 and z_2 to be on loop γ_2 which occurs later in contour ordering. We will assume that our system has a continuous spectrum such that we can apply the Riemann-Lebesque lemma. Then as before the Matsubara diagrams can be discarded when time-integrals commence at $-\infty$, so that we retain only the first line of diagrams in (89). Now since internal vertices are integrated over the separate loops γ_1 and γ_2, any half-diagram with disconnected parts vanishes and therefore also the third diagram in the first line of (89) is eliminated. The remaining three diagrams are the same one would obtain in a time-ordered zero temperature treatment, only now with retarded half-diagrams and internal g-lines at finite temperature. The example clearly illustrates the strategy outlined in the beginning of this section, by the use of retarded half-diagrams the bothersome diagram of equation (69) no longer appears in the expansion.

Similar to the time-ordered case the self-energy generally takes the form

$$-\mathrm{i}\Sigma_c^<(t_1,t_2) = \sum_{N=1}\sum_{a,b,I,P}(-1)^{|P|}\int_{\gamma_1}\mathrm{d}z_{\mathcal{I}}\int_{\gamma_2}\mathrm{d}z'_{\mathcal{I}}\,B^{(a)}_{N,I}(t_1,z_{\mathcal{I}})\Upsilon^<_I(t_{\mathcal{I}},t'_{\mathcal{I}})B^{(b)*}_{N,P(I)}(t_2,z'_{\mathcal{I}}), \tag{90}$$

with $\Upsilon^<$ as in (78) (see Appendix B) where instead of integrations over the branches γ_- and γ_+ of equation (77) we now have integrations on the loops γ_1 and γ_2. In (90) we can first focus our attention to the part integrated over γ_1, which by applying (88) can be written as

$$\int_{\gamma_1}\mathrm{d}z_{\mathcal{I}}\,B^{(a)}_{N,I}(t_1,z_{\mathcal{I}})\Upsilon^<_I(t_{\mathcal{I}},t'_{\mathcal{I}}) = \int\mathrm{d}t_{\mathcal{I}}\,B^{(a)R}_{N,I}(t_1,t_{\mathcal{I}})\Upsilon^<_I(t_{\mathcal{I}},t'_{\mathcal{I}}), \tag{91}$$

with the shorthand notation $B^R(t_1,t_{\mathcal{I}}) = B^{R(1,\mathcal{I})}(t_1,t_{\mathcal{I}})$. Here the $\Upsilon^<$ function can be left out of the retarded function since it does not depend on the branch indices for $z_{\mathcal{I}}$, but only on the real-times $t_{\mathcal{N}}$ since all times on loop γ_1 are earlier than those on loop γ_2. This follows from the definition of the retarded component as a sum over the possible distributions of $z_{\mathcal{I}}$ between the two branches (see Appendix C), which leaves $\Upsilon^<$ the

same in every term of the sum allowing it to be pulled out as a common factor. After an analogous argument for the integrals over γ_2, (90) takes the form [12]

$$-\mathrm{i}\Sigma_c^<(t_1,t_2) = \sum_{N=1}\sum_{a,b,I,P}(-1)^{|P|}\int \mathrm{d}t_{\mathcal{I}}\mathrm{d}t'_{\mathcal{I}}\, B^{(a)R}_{N,I}(t_1,t_{\mathcal{I}})\Upsilon^<_I(t_{\mathcal{I}},t'_{\mathcal{I}})B^{(b)R*}_{N,P(I)}(t_2,t'_{\mathcal{I}}). \quad (92)$$

This equation is similar in form to (77) and for the case of equilibrium systems it can analogously be Fourier transformed as

$$-\mathrm{i}\Sigma_c^<(\omega) = \sum_{N=1}\sum_{a,b,I,P}(-1)^{|P|}\int \frac{\mathrm{d}\omega_{\mathcal{I}}}{(2\pi)^I}B^{(a)R}_{N,I}(\omega_{\mathcal{I}})2\pi\delta(\omega-\Omega)\Upsilon^<_I(\omega_{\mathcal{I}})B^{(b)R*}_{N,P(I)}(\omega_{\mathcal{I}}). \quad (93)$$

Similar to the time-ordered case, equation (93) can be derived for equilibrium systems without having to use the assumption of a continuous spectrum to argue that Matsubara integrals vanish from the expansion of $\Sigma_c^<$. This relies on an important result from Appendix D where we derive spectral representations for general retarded and Matsubara diagrams, and show that these are directly related by analytical continuation. The crucial result is that for equilibrium systems there exists a general relation between the spectral form $\mathscr{D}^R(\omega_{\mathcal{N}})$ of a multi-retarded function describing a given Feynman diagram and the spectral form $\mathscr{D}^M(\omega_N)$ of the corresponding multi-argument Matsubara function for the same Feynman diagram; this relation is given by

$$\mathscr{D}^{R(1,2,\ldots,N)}(\omega_{\mathcal{N}}) = \mathscr{D}^M(\omega_{\mathcal{N}}-\mu-\mathrm{i}\eta_{\mathcal{N}}) \quad (94)$$

where $\omega_{\mathcal{N}} = \{\omega_1,\ldots,\omega_N\}$ represents a set of N frequencies and $\eta_{\mathcal{N}}$ is a set of positive infinitesimals. The precise form of these functions is defined by equations (D.20) and (D.30) in Appendix D which for our discussion here represent spectral forms of half-diagrams. A relation of the form (94) was also derived by Baier and Niégawa [46] but this required the implicit assumption of a continuous spectrum to make certain terms vanish. Our derivation in Appendix D does not require this assumption and is instead directly based on fluctuation-dissipation relations for Matsubara functions; additionally it yields a set of useful Feynman rules to evaluate multi-retarded functions in frequency space. Relation (94) is a generalization of (85) and can in particular be applied to the half-diagrams appearing in the retarded expansion for the self-energy. In connection with step (iv) of Jeon's derivation [27] that we outlined in the previous section this allows us to convert half-diagrams appearing in the expansion of the Matsubara self-energy to retarded half-diagrams which then precisely yields the retarded cutting rules that we derived above. The final result is that, for the case of finite temperature equilibrium systems, equation (93) is also valid without the assumption of a continuous spectrum, which means that in equilibrium the result holds also for finite systems.

Let us illustrate the Feynman rules derived in Appendix D for the evaluation of the

retarded half-diagrams in expressions like (93). For example, in the cut diagram

$$-\mathrm{i}D^<(\omega) = \quad = \int \frac{\mathrm{d}\omega_{\mathcal{I}}}{(2\pi)^I} B^{(a)R}_{1,(123)}(\omega_{\mathcal{I}}) 2\pi\delta(\omega-\Omega)\Upsilon^<(\omega_{\mathcal{I}}) B^{(b)R*}_{1,(123)}(\omega_{\mathcal{I}}) \tag{95}$$

where $\Omega = \omega_1+\omega_2+\omega_3$, the explicit form of $B^{(a)R}_{1,(123)}(\omega_{\mathcal{I}})$ follows from the rules given below (D.22) in Appendix D. We obtain

$$\begin{aligned} &\left[\quad\right]^{R(1,1'22')} \\ &= -2\pi\mathrm{i}\delta(\omega+\Omega)\int \frac{\mathrm{d}\nu\mathrm{d}\nu'}{4\pi^2} \frac{g^>(\nu)g^>(\nu') - g^<(\nu)g^<(\nu')}{\omega_1+\omega_2+\nu+\nu'-\mathrm{i}\eta} v_1 v_2 = D^{(a)R}(\omega,\omega_{\mathcal{I}}), \end{aligned} \tag{96}$$

which is related to $B^{(a)R}_{1,3}(\omega_{\mathcal{I}})$ (defined as in (80)) by

$$D^{(a)R}(\omega,\omega_{\mathcal{I}}) = \int \mathrm{d}t_1 \mathrm{d}t_{\mathcal{I}}\, B^{(a)R}_{1,(123)}(t_1,t_{\mathcal{I}}) \mathrm{e}^{\mathrm{i}\omega t_1 + i\omega_{\mathcal{I}}\cdot t_{\mathcal{I}}} = 2\pi\delta(\omega+\Omega) B^{(a)R}_{1,(123)}(-\omega_{\mathcal{I}}). \tag{97}$$

These expressions contain the interaction lines v_1 and v_2 as well as the functions $g^{\lessgtr}(\nu)$ which are the Fourier transforms of the functions $g^{\lessgtr}$ with respect to the difference of their time arguments, where in all the expressions we suppressed spatial integrations for clarity of presentation.

We further note that it is always possible to expand a retarded half-diagram in terms of time-ordered Green's functions by splitting the loop integral into an integration on a forward and on a backward branch, but since we have two half-diagrams now we have two γ_- branches and two γ_+ branches to keep track of. Consider for example the second term in (89); expanding the half-diagrams leads to

$$= + + + + . \tag{98}$$

The designation of the external vertices is irrelevant since they are at end points of the loops in (87). Note that in evaluating these diagrams the Green's functions crossing the cut are independent of the +'s and the −'s, they are determined separately by the ordering of the loops. Alternatively, one could remove the dashed lines and use a different mark for each of the four branches, along with rules for the resulting $4^2 = 16$ Green's function components. An approach along these lines was developed by Bedaque, Das and Naik in [26] starting from the latest time equation [24, 25] rather than referring to integration branches (see [23] for an extensive discussion). Either way, the time-ordered expansion leads to a very large number of diagrams, especially for higher order

functions since each new external parameter comes with another forward and backward branch. It is therefore both more convenient, as well as physically more appealing, to make use of retarded half-diagrams; they have the advantage of giving only a single real-time diagram for each cut.

In summary: the use of retarded half-diagrams solves the crucial issue of non-vanishing vacuum diagrams while retaining the construction procedure of PSD approximations just as in the time-ordered formalism. It has the additional advantage that retarded half-diagrams have a physical interpretation as scattering amplitudes by past processes such that Hermitian products of retarded half-diagrams can be interpreted as scattering probabilities [12]. In the following chapter we will apply this approach to some commonly employed approximations to show that they are PSD.

4. Application: positivity of diagrammatic approximations

It is known (see e.g. section 9.7 in [1]) that equation (29) is valid for finite temperature systems in equilibrium or for non-equilibrium systems in a steady state limit when the Riemann-Lebesque lemma applies. It therefore follows directly that a PSD self-energy with a positive rate function $\Gamma(\omega)$ leads to a PSD Green's function with positive spectral function $A(\omega)$, and therefore it is sufficient to consider the PSD approximations for the self-energy in order to obtain them for the spectral function.

In the following we will prove that some commonly used approximations for the self-energy, namely the second Born, T-matrix and GW approximations, preserve positivity also for finite temperature systems. The derivation illustrates the fact that the cutting rules derived for zero-temperature systems can be directly applied, provided we interpret the half-diagrams to be retarded rather than time-ordered functions. Consequently all methodology discussed in earlier work [7], such as the construction of a minimal PSD-extension, apply directly to the finite temperature case as well.

4.1. The T-matrix approximation

The T-matrix approximation comes in two flavors, the T-matrix approximation in the particle-particle channel and the T-matrix approximation in the particle-hole channel. The first one plays an important role in the study of systems with short range interactions such as Bose/Fermi gases in cold atom traps [47, 48, 49] and nuclear matter [50, 51, 52, 53], as well as in the description of Hubbard systems [17, 54, 55], to name a few examples. The second is important to describe excitations in semi-conductors [56, 57], and in particular for the study of exciton states [58]. The derivation below is given in the particle-particle channel but a completely analogous approach applies to the particle-hole channel.

The particle-particle T-matrix approximation is given by

$$\Sigma(1,2) =$$

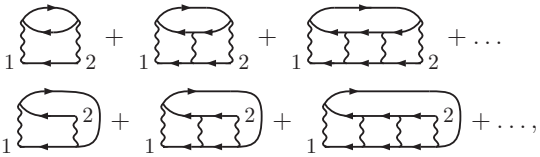

(99)

where the first line contains the direct part and the second line the exchange part. Performing the retarded expansion, and leaving out any diagrams with Matsubara integrals or disconnected half-diagrams, gives for the direct part

$$-\mathrm{i}\Sigma_d^<(1,2) =$$

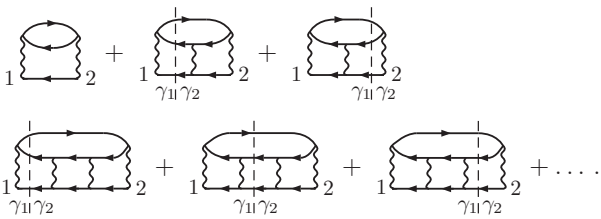

(100)

Note that in the case of the T-matrix the ability to discard disconnected half-diagrams reduces the number of diagrams generated by n-th order contour diagram from 2^{n-2} in the time-ordered formalism to $n-1$ in the retarded formalism.

We factorize the Green's functions crossing the dashed line in (100) using the relations (61) and (62) to obtain for the direct part

$$-\mathrm{i}\Sigma_d^<(1,2) =$$

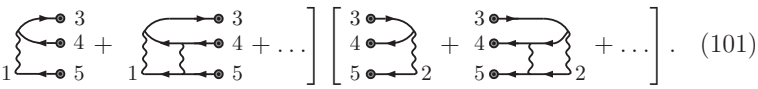

(101)

The expansion and factorization of the exchange part is analogous, expect that on the right hand half-diagram the labels 4 and 5 are exchanged. We therefore have

$$-\mathrm{i}\Sigma_x^<(1,2) =$$

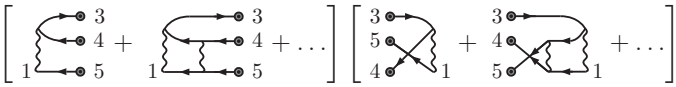

(102)

and the full self-energy can be written as

$$-\mathrm{i}\Sigma^<(1,2)$$

$$=$$

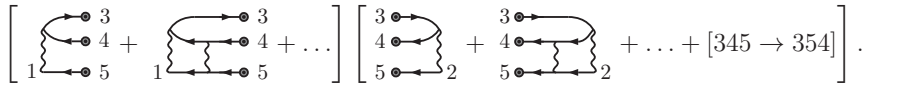

(103)

As discussed in [7], this is PSD since the right-hand side is a sum of terms where the cut labels are permuted according to the subgroup $\{\iota,(45)\}$ of the full permutation group. We finally remark this also proves that the second Born approximation is PSD since it is the subset of the particle-particle T-matrix approximation corresponding to the second order diagrams.

4.2. The GW approximation

The *GW* approximation is one of the most prevalent approximations in electronic structure theory [59, 60]. It can be applied at different levels of self-consistency [61], leading to various flavors of the approximation designated as the G_0W_0, GW_0 and the fully self-consistent *GW* approximation, which often are all grouped under the term *GW* approximation. The physics of long range screening and plasmon dynamics that is incorporated in this approximation plays an important role not only in electronic systems but also in charged plasmas at elevated temperatures [62, 63]. An in-depth study of the finite temperature GW_0 approximation for high temperature plasmas was performed by Fortmann [63] while a combination of the *GW* approximation and cumulant expansion was recently studied by Kas and Rehr for warm dense matter[14]. Furthermore, the finite temperature *GW* approximation was recently studied for the calculation of the Helmholtz free energy and spin response functions [64].

The *GW* approximation for the self-energy, given by

$\Sigma_{GW}(1,2) =$ 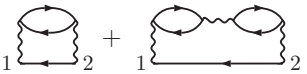 $+ \ldots,$ (104)

can be expressed in terms of retarded half-diagrams as

$-\mathrm{i}\Sigma^{<}_{GW}(1,2) =$ 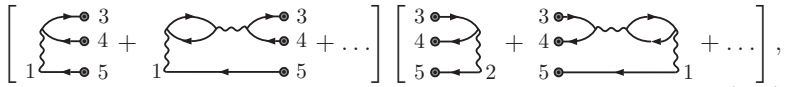 , (105)

which shows that the expansion is positive. This result is in agreement with the numerical results of Fortmann [63] for the GW_0 approximation. The dressing of the base line of the self-energy diagram, that is required to deal with the GW_0 approximation, is readily included in our method since positivity is preserved during the self-consistency iteration and the dressed line can therefore be cut as a Hermitian product. Similar arguments for the zero-temperature case were presented in [7]. A completely analogous reasoning applies to the fully self-consistent *GW* approximation.

We finally remark that both the GW and T-matrix approximations are not only PSD but also conserving [1]. However, a general conserving approximation will typically not be PSD as it need not have the form of a Hermitian product. A minimal PSD extension of the approximation typically leads to the introduction of only specific cuts of additional higher order diagrams which render it PSD but not Φ-derivable [1]. The situation at finite temperature is thus fully analogous to the one discussed in the zero-temperature case [7].

5. Conclusions

In this work we addressed the question how to enforce important positivity constraints on spectral functions obtained from approximate diagrammatic expansions in many-body theory of quantum systems at finite temperature. We showed that this is possible using

a finite temperature generalization of earlier work [7] that was based on cutting rules for Feynman diagrams and the construction of minimal PSD extensions. A straightforward expansion of that work, directly based on the Lehmann representation, was shown to be possible but turned out to be cumbersome for applications. An alternative formulation starting from self-energy diagrams, and the use of a factorization of Green's function lines along a cut, was found to be much more suitable. This lead to the consideration of half-diagrams with modified external legs which can be used to build finite temperature PSD approximations. However, when used in conjunction with the standard (anti)-time ordered formulation of many-body theory the PSD construction results in the appearance of vacuum diagram contributions which are absent in an exact expansion and which therefore should not contribute in any approximate expansion. This issue was finally resolved by a reformulation based on a deformation of the integration contour, which leads to an expansion in retarded half-diagrams for which such vacuum diagram contributions automatically vanish. Apart from providing an attractive physical interpretation the formalism also extends to non-equilibrium systems in initial equilibrium and thus allows us to study physical processes such as the steady-state limit of quantum transport situations, thereby generalizing earlier work for zero-temperature systems [11]. Our derivations furthermore provide a unified view of various earlier studies that addressed cutting rules in finite temperature systems and which can be related to each other by means of contour deformations. Additionally we derived a generalized connection between retarded and Matsubara multi-argument functions and provided a useful set of Feynman rules for multi-retarded functions in frequency space. Finally we established that important commonly used approximations, namely the GW, second Born and T-matrix approximation, retain positive spectral functions at finite temperature. The work opens up new fields for application of finite temperature many-body theory, notably in studying vertex corrections and higher order processes in finite temperature many-particle systems as was done in the zero-temperature version of the theory [9, 10].

Acknowledgments

D.K. acknowledges the academy of Finland for funding under Project No. 308697. M.H. thanks the Finnish Cultural Foundation for support. R.v.L. acknowledges the academy of Finland for funding under Project No. 317139.

Appendix A. Positive semi-definite Hermitian forms

In this appendix we will show that the (weighted) Hilbert-Schmidt product

$$\langle \hat{A} | \hat{B} \rangle = \mathrm{Tr}\left[\hat{\rho}\hat{A}^\dagger \hat{B}\right], \tag{A.1}$$

satisfies the properties of a positive semi-definite Hermitian form and the Cauchy-Schwartz inequality. It is readily seen that (A.1) satisfies the properties of a Hermitian

form. We have

$$\langle\hat{A}|\lambda_1\hat{B}_1+\lambda_2\hat{B}_2\rangle=\lambda_1\langle\hat{A}|\hat{B}_1\rangle+\lambda_2\langle\hat{A}|\hat{B}_2\rangle \tag{A.2}$$

$$\langle\hat{A}|\hat{B}\rangle=\langle\hat{B}|\hat{A}\rangle^* \tag{A.3}$$

where λ_1 and λ_2 are complex numbers. We further have that

$$\langle\hat{A}|\hat{A}\rangle=\mathrm{Tr}\left[\hat{\rho}\,\hat{A}^\dagger\hat{A}\right]\geq 0 \tag{A.4}$$

which makes our Hermitian form positive semi-definite. This is readily derived as follows. Since $\hat{\rho}$ is a PSD operator, it can be uniquely written as $\hat{\rho}=\hat{\rho}^{\frac{1}{2}}\hat{\rho}^{\frac{1}{2}}$. Furthermore, since $\hat{\rho}$ is self-adjoint, $\hat{\rho}^{\frac{1}{2}}$ is self-adjoint as well. Using the cyclic property of the trace we can write

$$\langle\hat{A}|\hat{A}\rangle=\mathrm{Tr}\left[\hat{\rho}^{1/2}\hat{A}^\dagger\hat{A}\hat{\rho}^{1/2}\right]=\mathrm{Tr}\left[\hat{F}^\dagger\hat{F}\right], \tag{A.5}$$

with $\hat{F}=\hat{A}\hat{\rho}^{1/2}$. Since any operator of the form $\hat{F}^\dagger\hat{F}$ is PSD, the trace is non-negative, which means that $\langle\hat{A}|\hat{A}\rangle\geq 0$. To make the Hilbert-Schmidt product a proper inner product we also need the property

$$\langle\hat{A}|\hat{A}\rangle=0\quad\Rightarrow\quad\hat{A}=0. \tag{A.6}$$

However, from (A.5) we can only prove that

$$\langle\hat{A}|\hat{A}\rangle=0\quad\Rightarrow\quad\hat{A}\hat{\rho}^{1/2}=0. \tag{A.7}$$

If $\hat{\rho}$ is a strictly positive operator this implies $\hat{A}=0$ and we are indeed dealing with a proper inner product, as was proven by Haag et al [33]. This is, for example, the case if $\hat{\rho}$ represents a grand canonical ensemble. However, if $\hat{\rho}$ is only a positive semi-definite operator then we do not in general have an inner product but instead what is known in the mathematical literature as a positive semi-definite Hermitian form (PSDHF). This structure is sufficient to derive the Cauchy-Schwartz inequality

$$|\langle\hat{A}|\hat{B}\rangle|^2\leq\langle\hat{A}|\hat{A}\rangle\langle\hat{B}|\hat{B}\rangle. \tag{A.8}$$

Equation (A.8) is obviously true if $\langle\hat{A}|\hat{B}\rangle=0$ so it is sufficient in the following to assume that $\langle\hat{A}|\hat{B}\rangle\neq 0$. We use property (A.4) and consider

$$0\leq\langle\hat{A}-\lambda\hat{B}|\hat{A}-\lambda\hat{B}\rangle=\langle\hat{A}|\hat{A}\rangle-\lambda\langle\hat{A}|\hat{B}\rangle-\lambda^*\langle\hat{B}|\hat{A}\rangle+|\lambda|^2\langle\hat{B}|\hat{B}\rangle \tag{A.9}$$

where λ is a complex number that we can choose freely. Let us now write $\langle\hat{A}|\hat{B}\rangle=|\langle\hat{A}|\hat{B}\rangle|\mathrm{e}^{\mathrm{i}\phi}$ and choose $\lambda=s\,\mathrm{e}^{-\mathrm{i}\phi}$ where s is real. Then (A.9) becomes

$$0\leq\langle\hat{A}|\hat{A}\rangle-2s\,|\langle\hat{A}|\hat{B}\rangle|+s^2\,\langle\hat{B}|\hat{B}\rangle. \tag{A.10}$$

Since $\langle\hat{A}|\hat{B}\rangle\neq 0$ it follows immediately that also $\langle\hat{B}|\hat{B}\rangle\neq 0$ since otherwise (A.10) would represent a non-constant linear function in s bounded from below which does not

exist. The quadratic polynomial in s on the right hand side of the inequality in (A.10) is therefore a positive semi-definite parabola-shaped function which can at most have one real zero. It therefore follows that its corresponding discriminant is zero or negative, i.e.

$$|\langle \hat{A}|\hat{B}\rangle|^2 - \langle \hat{A}|\hat{A}\rangle\langle \hat{B}|\hat{B}\rangle \leq 0 \tag{A.11}$$

which is equivalent to (A.8).

The Cauchy-Schwartz inequality can be used to obtain bounds on various correlators. As an example, let us consider the lesser Green's function given by

$$-\mathrm{i}G^<(1,2) = \mathrm{Tr}\left[\hat{\rho}\,\hat{\psi}_H^\dagger(2)\hat{\psi}_H(1)\right] = \langle \hat{\psi}_H(2)|\hat{\psi}_H(1)\rangle, \tag{A.12}$$

with the shorthand notation $1 = \mathbf{x}_1 t_1$ etc. Applying the Cauchy-Schwartz inequality to (A.12) yields the upper bound

$$|G^<(1,2)|^2 \leq n(1)n(2). \tag{A.13}$$

As such, the magnitude of the lesser Green's function is bounded from above by the density in a general time-dependent system. In systems where the density decays exponentially for large distances, such as in atoms and molecules, (A.13) states that also the lesser Green's function decays exponentially (or faster). The upper bound is more familiar for the time diagonal, $t_1 = t_2$, where (A.13) yields a well-known [65] upper bound for the time-dependent single-particle density matrix.

Appendix B. Feynman rules for half-diagrams

The main goal of this appendix is to show that (63) is valid provided that we assign a proper topological pre-factor to each half-diagram. We are concerned about this since each half-diagram $A^{(a)}_{N,I}$ contains modified external legs $\tilde{g}^{\lessgtr}$ which replaced the standard Green's functions g and therefore is not obtained directly from an expansion involving Wick's theorem, as was the case for the Lehmann amplitudes in the zero-temperature formulation. We thus need to assure that we can assign pre-factors to the half-diagrams such that the gluing operation leads to the correct prefactors for the self-energy. In order to clearly distinguish the external vertices of the self-energy from the labels of the cut lines we will label them α and β instead of 1 and 2, i.e. we consider the self-energy $-i\Sigma^<(\alpha,\beta)$.

The pre-factor that we will use for the half-diagrams is determined by the following rule. For a given half-diagram $A^{(a)}_{N,I}(\alpha)$ attached to external self-energy vertex α we denote the entrance lines by j' and the exit ones by j. Since α corresponds to an exit vertex there are N labels j and $N+1$ labels j'. For any such labeling the half-diagram is interpreted as belonging to an expansion of $G_{N+1}(\alpha, J; J')$ where J and J' are the sets of labels for j and j'. We then assign to the half-diagram the topological pre-factor [66]

$$\mathrm{i}^{n_v}(-1)^{N+1+l+\tilde{l}} \tag{B.1}$$

where n_v is the number of v-lines, l the number of loops formed by the g-lines and $\tilde{l}$ the number of extra loops created when we imagine each entrance vertex from the set J' to be merged with the exit vertex from (α, J) with the same position in the argument list. It follows from our definition that the topological pre-factor for the diagram $A^{(a)}_{N,P(I)}(\alpha)$ changes with a relative factor $(-1)^{|P|}$ compared to that of $A^{(a)}_{N,I}(\alpha)$ since every interchange of external vertices changes the number of loops for $\tilde{l}$ by one. Note, however, that the actual value of the permuted diagram does not just differ by a sign from the non-permuted one as it represents a topologically different diagram. The central statement that we will demonstrate is that (63) gives the correct expansion for the self-energy, i.e. with the proper topological pre-factor of the Feynman rules for the self-energy. To show this we need two ingredients; the first one (proven in Appendix C) is that

$$A^{(a)\dagger}_{N,I}(\alpha) = (-1)^N \tilde{A}^{(a)}_{N,I}(\alpha) \tag{B.2}$$

where we defined $\tilde{A}^{(a)}_{N,I}$ to be the non-conjugated half-diagram but with all directions of the Green's function lines reversed and the $\tilde{g}$ legs replaced by $\tilde{g}^\dagger$ and vice versa. Such a reversed diagram represents the right-hand side of a cut self-energy diagram.

The second ingredient is a topological rule that we state as follows. Let $l(ab)$ be the number of loops created when two half diagrams of topology a and b are glued together, then

$$(-1)^{\tilde{l}(a)+\tilde{l}(b)} = (-1)^{N+l(ab)} \tag{B.3}$$

where $\tilde{l}(a)$ and $\tilde{l}(b)$ are the factors from our rule stated above for the two separate half-diagrams. We postpone the demonstration of the latter statement and first establish that it implies the desired result in combination with (B.2). We consider the product

$$\sum_I (-1)^{|P|} A^{(a)}_{N,I}(\alpha) A^{(b)\dagger}_{N,P(I)}(\beta), \tag{B.4}$$

which amounts to a gluing operation. As we outlined above, for the purpose of determining the topological pre-factor it is sufficient to consider the particular product

$$\sum_I A^{(a)}_{N,I}(\alpha) A^{(b)\dagger}_{N,I}(\beta) \tag{B.5}$$

since permutation of the external vertices changes the topological prefactor by $(-1)^{|P|}$. From (B.2) it follows that conjugation gives a diagram with reversed Green function lines which is accompanied with a pre-factor $(-1)^N$ while the gluing of the $\tilde{g}$ lines using (61) and (62) produces an overall factor of $-\mathrm{i}$ as we glue one more hole line than a particle line. The gluing procedure thus yields a net factor of $-\mathrm{i}(-1)^N$ and the overall factor of the diagram is therefore

$$C = -\mathrm{i}(-1)^N \mathrm{i}^{n_v} (-1)^{l(a)+l(b)+\tilde{l}(a)+\tilde{l}(b)} \tag{B.6}$$

where $n_v = n_v(a) + n_v(b)$ is the total number of interaction lines. Then equation (B.3) immediately gives that

$$C = -\mathrm{i}(-\mathrm{i})^{n_v} (-1)^l \tag{B.7}$$

where l is the total number of loops in the glued self-energy diagram. Given that we were considering a diagram for $-\mathrm{i}\Sigma^<$ we see that we precisely recover the usual Feynman rule prefactor $(-\mathrm{i})^{n_v}(-1)^l$ for the self-energy diagram, which thereby proves the desired relation (63).

To prove (B.3) we consider the factorization of a general self-energy diagram in terms of half-diagrams from (B.5). For the left hand diagram we label the entrance vertices of the cut lines with labels i'. If a path of directed Green's function lines starting at entrance vertex i' exits the half-diagram at a given vertex we label that exit vertex by i. This ensures that connecting i to i' in the left-hand diagram always creates one loop, and therefore $(-1)^{\tilde{l}(a)} = (-1)^{N+1}$. For example:

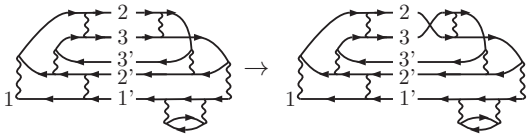

(B.8)

The right hand side can always be obtained by a permutation Q of the external vertices from a diagram with $\tilde{l}(b) = N + 1$ loops (as shown graphically in (B.8)) which yields a factor $(-1)^{\tilde{l}(b)} = (-1)^{N+1+|Q|}$. Every permutation that changes $\tilde{l}(b)$ by one also changes $l(ab)$ by one and therefore $(-1)^{l(ab)} = (-1)^{N+|Q|}$ since we do not glue the entrance and exit vertices of the self-energy diagram. We thus obtain $(-1)^{\tilde{l}(a)+\tilde{l}(b)} = (-1)^{N+l(ab)}$ as was to be proven.

Appendix C. Multi-retarded functions and their adjoints

The multi-retarded N-point function occurring in equation (88) is defined as (see [12, 13])

$$D^{R(1,2\cdots N)}(t_{\mathcal{N}}) = \sum_P \theta(t_1, t_{P(2)}, \ldots, t_{P(N)}) D^{[1,P(2),\ldots,P(N)]}(t_{\mathcal{N}}) \tag{C.1}$$

where $t_{\mathcal{N}} = (t_1, \ldots, t_N)$ and $\theta(t_1, \ldots, t_N)$ is defined to be equal to one when $t_1 > \ldots > t_N$ and zero otherwise. Since t_1 is always the latest time such a function is called a retarded function with respect to top element 1. Here the sum is over all permutations P of $2, \ldots, N$ and $[1, 2, \ldots, N] = [[[1, 2], 3], \ldots, N]$ is a nested commutator represented by a formal sum of strings of integers such as $[1, 2] = 12 - 21$. In general the commutator is of the form $L = \sum_i \sigma_i l_i$ where $\sigma_i = \pm 1$ and l_i is a string of N integers and we define

$$D^L = \sum_i \sigma_i D^{l_i} \tag{C.2}$$

where D^{l_i} corresponds to a real time function for the contour ordering l_i. For example for $N = 3$ we would have

$$D^{R(1,23)}(t_1, t_2, t_3) = \theta(t_1, t_2, t_3) D^{[1,2,3]}(t_1, t_2, t_3) + \theta(t_1, t_3, t_2) D^{[1,3,2]}(t_1, t_2, t_3), \tag{C.3}$$

where

$$D^{[1,2,3]} = D^{[[1,2],3]} = D^{123-312-213+321} = D^{123} - D^{312} - D^{213} + D^{321}. \tag{C.4}$$

The string of indices in the superscript gives the contour order of the time arguments with the latest argument to the left. For example, D^{312} corresponds to a real-time function for the contour ordering $z_3 > z_1 > z_2$.
The aim is to derive a useful expression for the adjoint of the multi-retarded function D^R

$$\left[D^{R(1,2\cdots N)}(t_{\mathcal{N}})\right]^\dagger = \sum_P \theta(t_1, t_{P(2)}, \ldots, t_{P(N)}) \left[D^{[1,P(2),\ldots,P(N)]}(t_{\mathcal{N}})\right]^\dagger, \tag{C.5}$$

which requires us to consider the adjoint of its various components D^J where $J = j_1 \ldots j_N$ is a reordering of the labels $1 \ldots N$. Let us take $D_n^J(t_{\mathcal{N}})$ (where we added a sub-index n) to be a specific ordered component of an un-integrated Feynman diagram for a many-particle Green's function G_n. By un-integrated diagram we mean that we apply all Feynman rules to it apart from integrating over internal times; the diagram therefore depends on $N = 2n + n_v$ times where n_v is the number of interaction lines in D_n^J. By taking the adjoint of such a component every internal g-line is transformed to

$$g^{\lessgtr\dagger}(1,2) = -g^{\lessgtr}(2,1), \tag{C.6}$$

which thus reverses the direction of each g-line, thereby reserving the time-ordering of D_n^J and since the diagram prefactor contains an i for each interaction line, we get a minus sign for each interaction as well. The adjoint for an ordered diagram with n_g Green's function lines and n_v interaction lines is therefore given by

$$D_n^{J\dagger}(t_{\mathcal{N}}) = (-1)^{n_g+n_v} \tilde{D}_n^{\bar{J}}(t_{\mathcal{N}}) = (-1)^{N-n} \tilde{D}_n^{\bar{J}}(t_{\mathcal{N}}) \tag{C.7}$$

where $\tilde{D}_n^J$ is the diagram obtained from D_n^J by reversal of all the g-lines and $\bar{J}$ is string J in reverse order. We further used that $n_g = 2n_v + n$ and $N = n_v + 2n$ to rewrite the prefactor in the second step of equation (C.7). We now employ this relation in the expression (C.5). If a nested commutator $[1, \ldots, N] = \sum \sigma_i l_i$ contains a specific ordering of l_i, it also contains the reverse ordering $\bar{l}_i$, with a relative $+/-$ sign if N is odd/even; consequently reversing the ordering in every string l_i yields an overall factor $(-1)^{N-1}$. Together with equation (C.7) we thus obtain

$$\left[D_n^{R(1,2\cdots N)}(t_{\mathcal{N}})\right]^\dagger = (-1)^{n-1} \tilde{D}_n^{R(1,2\cdots N)}(t_{\mathcal{N}}). \tag{C.8}$$

This result can now be employed to deduce similar relations for the half-diagrams $B_{N,I}^{(a)R}(t_1, t_{\mathcal{I}})$ appearing in the retarded expansion of self-energy diagrams (92). They are (now integrated) G_{N+1} diagrams with their external legs amputated, but still follow the relation (C.8) as can be checked by following the same steps as outlined above. Thus we have for these half-diagrams

$$[B_{N,I}^{(a)R}(t_1, t_{\mathcal{I}})]^\dagger = (-1)^N \tilde{B}_{N,I}^{(a)R}(t_1, t_{\mathcal{I}}). \tag{C.9}$$

The half-diagrams $A^{(a)R}_{N,I}$ are obtained from $B^{(a)R}_{N,I}$ by attaching $\tilde{g}^{\lessgtr}$-functions as external legs for the cut vertices I; from (C.9) it then follows that

$$[A^{(a)R}_{N,I}(t_1,t_0)]^\dagger = (-1)^N \tilde{A}^{(a)R}_{N,I}(t_1,t_0), \tag{C.10}$$

when we define $\tilde{A}^{(a)R}_{N,I}$ as the diagram with the $\tilde{g}^{\lessgtr}$ legs replaced by $[\tilde{g}^{\lessgtr}]^\dagger$ and vice versa. As a final remark we note that a similar relation can be derived for (anti)-time-ordered diagrams. Since $(g_{--})^\dagger = -g_{++}$ this would have a given a factor $(-1)^{N+1}$ in the equation above. The gluing rule for the (anti)-time ordered functions (53) then generates an additional minus sign yielding a correct pre-factor for every diagram in the expansion of the self-energy from the considerations in Appendix B.

Appendix D. Analytic continuation and Feynman rules for multi-argument retarded and Matsubara functions

The aim of this appendix is to derive the important relation (94) and to give the Feynman rules for the evaluation of retarded half-diagrams in frequency space. To obtain a spectral representation of a multi-retarded function we define the Fourier transform

$$\mathcal{D}^{R(e,\mathcal{I})}(\omega_\mathcal{N}) = \int \mathrm{d}t_\mathcal{N}\, \mathrm{e}^{\mathrm{i}\omega_\mathcal{N}\cdot t_\mathcal{N}} D^{R(e,\mathcal{I})}(t_\mathcal{N}) \tag{D.1}$$

where $\mathcal{N} = \{1,\ldots,N\}$ is an ordered set of labels and $t_\mathcal{N}$ and $\omega_\mathcal{N}$ are sets of arguments labeled with $\mathcal{N}$, e is the label for the external time and $\mathcal{I} = \mathcal{N}\setminus e$ is the set $\mathcal{N}$ with label e removed. We further used the shorthand notation

$$\omega_\mathcal{N}\cdot t_\mathcal{N} = \omega_1 t_1 + \omega_2 t_2 + \ldots + \omega_N t_N. \tag{D.2}$$

When D^R represents the integrand of a half-diagram we can set some of ω_j's to zero to recover the Fourier representation of any desired half-diagram discussed in the main text. To carry out the Fourier integral it will be useful to use the relation (see [13] for more details)

$$\int_\gamma \mathrm{d}z_{\mathcal{N}\setminus e}\, D(z_\mathcal{N}) = \int_{t_0}^\infty \mathrm{d}t_{\mathcal{N}\setminus e}\, D^{R(e,\mathcal{I})}(t_\mathcal{N}), \tag{D.3}$$

where $D(z_\mathcal{N})$ is a contour function that can explicitly be written as a sum over contour-orderings as

$$D(z_\mathcal{N}) = \sum_P \theta(z_{P(\mathcal{N})}) D^{P(\mathcal{N})}(t_\mathcal{N}), \tag{D.4}$$

where the sum is over all permutations $P(\mathcal{N})$ of the ordered set $\mathcal{N}$. The contour dependence only occurs in the contour Heaviside function $\theta(z_\mathcal{N})$ defined to be one for $z_1 > ... > z_N$ on the contour and zero otherwise. We take $D^{P(\mathcal{N})}(t_\mathcal{N})$ in (D.4) to have the structure

$$D^{P(\mathcal{N})}(t_\mathcal{N}) = \left[C \prod_L g_L(z_{L_f}, z_{L_i}) \prod_I v_I \right]^{P(\mathcal{N})}, \tag{D.5}$$

where the term on the right hand side is a product of Green's functions g_L and interaction lines v_I and the superscript $P(\mathcal{N})$ denotes the ordering of the contour times used to evaluate this product. Hereby the Green's functions become greater and lesser functions and consequently the resulting expression is a function of real times only. We furthermore denoted by C the topological prefactor given by the Feynman rules for this diagram, and L runs over all g-lines in the diagram starting from initial time z_{L_i} and ending at final time z_{L_f}. Position-spin arguments are here suppressed and the interaction lines are taken to be time-independent. A half-diagram can always be assumed to be in this form for time-local interactions $v(z_1, z_2) = v\,\delta(z_1, z_2)$ as the delta-functions can already be integrated out in the original self-energy diagram that gave rise to the half-diagram under consideration.

We express the permuted set as $P(\mathcal{N}) = \{\mathcal{N}_+^P, e, \mathcal{N}_-^P\}$, where $\mathcal{N}_+^P/\mathcal{N}_-^P$ are ordered sets of labels ordered after/before e. The contour-times $z_{\mathcal{N}_+^P}/z_{\mathcal{N}_-^P}$ are therefore placed on the backward/forward branch. This corresponds to

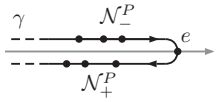

(D.6)

Taking an integral over the internal times for (D.4) then involves integration over the step-functions which can be expressed as

$$\begin{aligned}\int_\gamma \mathrm{d}z_{\mathcal{N}\setminus e}\,\theta(z_{P(\mathcal{N})}) &= \int_{\gamma_-}\mathrm{d}z_{\mathcal{N}_-^P}\int_{\gamma_+}\mathrm{d}z_{\mathcal{N}_+^P}\,\theta(t_e, t_{\bar{\mathcal{N}}_+^P})\theta(t_e, t_{\mathcal{N}_-^P}) \\ &= \int_{-\infty}^{\infty}\mathrm{d}t_{\mathcal{N}\setminus e}\,(-1)^{N_+^P}\theta(t_e, t_{\bar{\mathcal{N}}_+^P})\theta(t_e, t_{\mathcal{N}_-^P}),\end{aligned} \tag{D.7}$$

where $\bar{\mathcal{N}}$ is a set of reversed order and $(-1)^{N_+^P} = (-1)^{|\mathcal{N}_+^P|}$ comes from the direction of integration on the backward branch [13]. Note that the contour γ is here taken to extend to $-\infty$, and can be taken to extend to $+\infty$ since the integral is cut off by the step-functions at t_e. We can thus express the retarded component as

$$D^{R(e,\mathcal{I})}(t_\mathcal{N}) = \sum_P (-1)^{N_+^P}\theta(t_e, t_{\bar{\mathcal{N}}_+^P})\theta(t_e, t_{\mathcal{N}_-^P})D^{P(\mathcal{N})}(t_\mathcal{N}). \tag{D.8}$$

This relation can now be inserted into (D.1). Each g-line in the term (D.5) corresponds to either a lesser or a greater component which we rewrite in frequency space as

$$g_L^{\lessgtr}(t, t') = \int \frac{\mathrm{d}\nu}{2\pi} g_L^{\lessgtr}(\nu)\mathrm{e}^{-\mathrm{i}\nu(t-t')} \tag{D.9}$$

and thus obtain

$$\begin{aligned}D^{P(\mathcal{N})}(t_\mathcal{N}) &= \left(\prod_L \int \frac{\mathrm{d}\nu_L}{2\pi}\mathrm{e}^{-\mathrm{i}\nu_L(t_{L_f}-t_{L_i})}\right)\left[C\prod_L g_L(\nu_L)\prod_I v_I\right]^{P(\mathcal{N})} \\ &= \int \frac{\mathrm{d}\nu_\mathcal{L}}{2\pi^{|\mathcal{L}|}}\mathrm{e}^{-\mathrm{i}\nu_\mathcal{L}\cdot(t_{\mathcal{L}_f}-t_{\mathcal{L}_i})}\mathcal{D}^{P(\mathcal{N})}(\nu_\mathcal{L}),\end{aligned} \tag{D.10}$$

where $|\mathcal{L}|$ is the number of g-lines in the diagram and $\nu_{\mathcal{L}}$ is the set of the corresponding frequencies ν_L. This allow us to rewrite (D.1) as

$$\mathcal{D}^{R(e,\mathcal{I})}(\omega_{\mathcal{N}}) = \sum_P \int \frac{\mathrm{d}\nu_{\mathcal{L}}}{(2\pi)^{|\mathcal{L}|}} \Lambda_{eP(\mathcal{N})}(\sigma_{\mathcal{N}}) \mathcal{D}^{P(\mathcal{N})}(\nu_{\mathcal{L}}), \tag{D.11}$$

where

$$\Lambda_{eP(\mathcal{N})}(\sigma_{\mathcal{N}}) = (-1)^{N_+^P} \int \mathrm{d}t_{\mathcal{N}}\, \theta(t_e, t_{\bar{\mathcal{N}}_+^P}) \theta(t_e, t_{\mathcal{N}_-^P}) \mathrm{e}^{\mathrm{i}\sigma_{\mathcal{N}} \cdot t_{\mathcal{N}}}. \tag{D.12}$$

Here $\sigma_{\mathcal{N}} = \{\sigma_1, \ldots, \sigma_N\}$ where σ_j is to the total energy leaving the vertex/vertices at time t_j (in the example diagram given here black lines belong to the diagram and grey lines are potential external connections)

$$\sigma_j = \omega_j + \sum_{L, L_i = j} \nu_L - \sum_{L, L_f = j} \nu_L \tag{D.13}$$

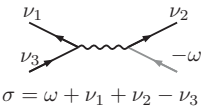

Here ω_j is the energy leaving the diagram at interaction line j, and therefore in a Feynman diagram we label the frequency on an incoming external line with $-\omega_j$ as in the figure of (D.13). The first sum adds the energy being carried away by internal g-lines, and the second sum subtracts the energy being brought in by internal g-lines. The integrals in (D.12) can be evaluated using the expression

$$\begin{aligned} &\int \mathrm{d}t_1 \cdots \mathrm{d}t_k\, \theta(t, t_k, \ldots, t_1) \mathrm{e}^{\mathrm{i}\sigma_1 t_1 + \ldots + \mathrm{i}\sigma_k t_k} \\ &= (-\mathrm{i})^k \frac{\mathrm{e}^{\mathrm{i}(\sigma_1 + \ldots + \sigma_k)t}}{(\sigma_1 - \mathrm{i}\eta_1)(\sigma_1 + \sigma_2 - \mathrm{i}\eta_2) \cdots (\sigma_1 + \ldots + \sigma_k - \mathrm{i}\eta_k)} \end{aligned} \tag{D.14}$$

which can be derived by writing each step-function as

$$\theta(t, t_k, \ldots, t_1) = \theta(t - t_k)\theta(t_k - t_{k-1}) \cdots \theta(t_2 - t_1), \tag{D.15}$$

and substituting the representation

$$\theta(t) = -\lim_{\eta \to 0} \frac{1}{2\pi i} \int_{-\infty}^{\infty} \mathrm{d}\xi \frac{\mathrm{e}^{-\mathrm{i}\xi t}}{\xi + \mathrm{i}\eta}. \tag{D.16}$$

After using equation (D.14) in equation (D.12) we further use

$$\int \mathrm{d}t_e \mathrm{e}^{\mathrm{i}(\sigma_1 + \ldots + \sigma_N)t_e} = 2\pi\delta(\sigma_1 + \ldots + \sigma_N) = 2\pi\delta(\omega), \tag{D.17}$$

where $\omega = \sum_i \omega_i = \sum_i \sigma_i$ since all internal energy flows cancel by summing over all vertices. Defining a sum over the l first or the l last elements in $\sigma_{\mathcal{N}}$

$$\Omega_l^{\mathcal{N}} = \sum_{i=1}^{l} \sigma_i, \qquad \Omega_l^{\bar{\mathcal{N}}} = \sum_{i=1}^{l} \sigma_{N+1-l} \tag{D.18}$$

then leads to

$$\Lambda_{eP(\mathcal{N})}(\sigma_{\mathcal{N}}) = \frac{(-1)^{N_+^P}(-\mathrm{i})^{N-1}\,2\pi\delta(\omega)}{\prod_{k=1}^{N_-^P}(\Omega_k^{\overline{P(\mathcal{N})}} - \mathrm{i}\eta_k)\prod_{l=1}^{N_+^P}(\Omega_l^{P(\mathcal{N})} - \mathrm{i}\eta_l)}. \tag{D.19}$$

A multi-retarded diagram (D.11) therefore has the spectral representation

$$\mathcal{D}^{R(e,\mathcal{I})}(\omega_{\mathcal{N}}) = 2\pi\delta(\omega)\mathscr{D}^{R(e,\mathcal{I})}(\omega_{\mathcal{N}}) \tag{D.20}$$

where we defined the analytic function

$$\mathscr{D}^{R(e,\mathcal{I})}(\omega_{\mathcal{N}}) = \sum_P \int \frac{\mathrm{d}\nu_{\mathcal{L}}}{(2\pi)^{|L|}} \frac{(-1)^{N_+^P}(-\mathrm{i})^{N-1}}{\prod_{k=1}^{N_-^P}(\Omega_k^{\overline{P(\mathcal{N})}} - \mathrm{i}\eta_k)\prod_{l=1}^{N_+^P}(\Omega_l^{P(\mathcal{N})} - \mathrm{i}\eta_l)} \mathcal{D}^{P(\mathcal{N})}(\nu_{\mathcal{L}}). \tag{D.21}$$

We can now also easily work out the spectral representation for a time-ordered diagram. The lack of the backward branch means that $N_+^P = 0$, which leads to

$$\mathcal{D}^{T}(\omega_{\mathcal{N}}) = 2\pi\delta(\omega)\sum_P \int \frac{\mathrm{d}\nu_{\mathcal{L}}}{2\pi^{|L|}} \frac{(-\mathrm{i})^{N-1}}{\prod_{n=1}^{N-1}(\Omega_n^{\overline{P(\mathcal{N})}} - \mathrm{i}\eta_n)} \mathcal{D}^{P(\mathcal{N})}(\nu_{\mathcal{L}}). \tag{D.22}$$

Setting $N_-^P = 0$ leads to a similar expression for an anti-time ordered diagram. These are the types of expressions used by Jeon [27] to derive cutting rules for Matsubara functions. The terms in the sum in (D.21) can be evaluated with the help of the following diagrammatic rules.

(i) Draw the v-lines/vertices at the N times in the order of increasing contour time from bottom to top as in figure a) below.

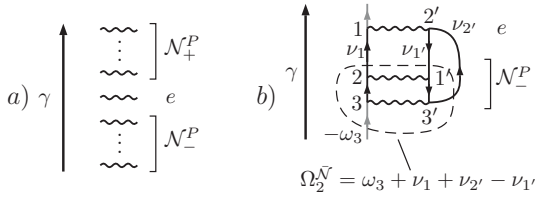

(D.23)

(ii) Draw the lines between the vertices according to the structure of the diagram. Assign to an ascending g-line a greater component $g_L^>(\nu_L)$ and to a descending g-line a lesser component $g_L^<(\nu_L)$. Assign to each v-line v_I.

(iii) For each $n \leq N_-^P$ draw a circle around the first n vertices in contour order. For each circle multiply the denominator by the factor $(\Omega - i\eta)$, where Ω is the total energy flowing outwards through the circle. See figure b) above for an example.

(iv) For each $n \leq N_+^P$ draw a circle around the last n vertices in contour order. For each circle multiply the denominator by the factor $(\Omega - i\eta)$, where Ω is the total energy flowing outwards through the circle.

(v) Multiply with $C(-1)^{N_+^P}(-\mathrm{i})^{N-1}$, where C is the prefactor for the diagram given by the applicable Feynman rules.

(vi) Integrate over the frequencies ν_j.

Let us consider as an example the retarded diagram

$$T^{R(1,2)}(t_1,t_2) = \left[\begin{array}{cc} 1' & 2' \\ & \\ 1 & 2 \end{array}\right]^{R(1,2)}, \qquad \begin{array}{ccccccc} & & & & & & \omega_{1'} \\ 1' & & \nu' & & 2' & & -\omega_{2'} \\ \omega_1 & 1 & \nu & 2 & & & -\omega_2 \end{array} \tag{D.24}$$

that appears as a half-diagram in the retarded expansion for the T-matrix approximation. Since time-local interactions connect the vertices pairwise, there are only two contour orderings to consider since t_2 is either earlier or later than t_1 on the contour. Following our rules these give

$$\gamma \left\uparrow \begin{array}{l} 1(e) \\ \\ 2 \end{array}\right. \begin{array}{ccc} & \nu & \nu' \\ & & \\ -\omega_2 & & -\omega_{2'} \end{array} \quad \to \int \frac{\mathrm{d}\nu \mathrm{d}\nu'}{(2\pi)^2} \frac{(-1)^0(-\mathrm{i})^1 g^>(\nu) g^>(\nu') v_1 v_2}{\omega_2 + \omega_2' + \nu + \nu' - \mathrm{i}\eta_2} \tag{D.25}$$

$$\gamma \left\uparrow \begin{array}{l} 2 \\ \\ 1(e) \end{array}\right. \begin{array}{ccc} -\omega_2 & & -\omega_{2'} \\ & & \\ & \nu & \nu' \end{array} \quad \to \int \frac{\mathrm{d}\nu \mathrm{d}\nu'}{(2\pi)^2} \frac{(-1)^1(-\mathrm{i})^1 g^<(\nu) g^<(\nu') v_1 v_2}{\omega_2 + \omega_2' + \nu + \nu' - \mathrm{i}\eta_2} \tag{D.26}$$

where we have substituted $C = 1$ as given by the Feynman rules for our labeling of the external vertices (see Appendix B). Summing over the orderings we therefore have

$$\mathcal{T}^{R(1,2)}(\bar\omega_1, \bar\omega_2) = -2\pi\mathrm{i}\delta(\bar\omega_1 + \bar\omega_2) \int \frac{\mathrm{d}\nu \mathrm{d}\nu'}{4\pi^2} \frac{g^>(\nu) g^>(\nu') - g^<(\nu) g^<(\nu')}{\bar\omega_2 + \nu + \nu' - \mathrm{i}\eta_2} v_1 v_2, \tag{D.27}$$

where $\bar\omega_1 = \omega_1 + \omega_{1'}$ and $\bar\omega_2 = \omega_2 + \omega_{2'}$.

Let us now compare the frequency representation for a retarded diagram derived above to the corresponding expression for a Matsubara diagram. The general expression for an N-point Matsubara function in frequency space is defined to be

$$\mathcal{D}^M(\omega_\mathcal{N}) = \int_0^{-\mathrm{i}\beta} \mathrm{d}z_\mathcal{N}\, \mathrm{e}^{\mathrm{i}\omega_\mathcal{N}\cdot z_\mathcal{N}} D^M(z_\mathcal{N}) \tag{D.28}$$

where $\omega_\mathcal{N} = \{\omega_1, \ldots, \omega_N\}$ is an ordered set of discrete frequencies of the general Matsubara form $\omega_j = 2\pi\mathrm{i}m/\beta$ with m running over odd integers and $z_\mathcal{N} = \{z_1, \ldots, z_N\}$ is a set of times $z_j = -\mathrm{i}\tau_j$ on the Matsubara branch. Due to time translation invariance $D^M(-\mathrm{i}\tau_\mathcal{N}) = D^M(-\mathrm{i}\tau'_\mathcal{N})$ with $\tau'_j = \tau_j - \tau_e$, which gives $\tau'_e = 0$ on argument position e. A change of integration variable to τ'_j and use of (anti)-periodic boundary conditions [1] then produces an overall Kronecker delta multiplied with the factor $-\mathrm{i}\beta$ resulting from an imaginary time integral [46]. This yields

$$\mathcal{D}^M(\omega_\mathcal{N}) = 2\pi\delta_\omega\, \mathscr{D}^M(\omega_\mathcal{N}) \tag{D.29}$$

in which we defined $\delta_\omega = \delta_{\omega,0}/(2\pi i/\beta)$ where $\delta_{\omega,0}$ is a Kronecker delta for the sum $\omega = \omega_1 + \ldots + \omega_N$ of all Matsubara frequencies. We further defined the analytic function

$$\mathscr{D}^M(\omega_\mathcal{N}) = (-\mathrm{i})^{N-1} \int_0^\beta \mathrm{d}\tau_{\mathcal{N}\setminus e}\, \mathrm{e}^{\omega_\mathcal{N}\cdot\tau_\mathcal{N}} D^M_e(-i\tau_\mathcal{N}) \tag{D.30}$$

where D_e^M denotes the Matsubara N-point function $D^M(-\mathrm{i}\tau_{\mathcal{N}})$ in which we put $\tau_e = 0$; since $\tau_e = 0$ the integral in (D.30) and therefore $\mathscr{D}^M$ is independent of ω_e. For the specific diagrammatic form of D^M we assume an identical expression as in (D.5) where now the contour variables are on the vertical Matsubara track. The Green's function lines can be written as the integrals [1]

$$g_L^{\lessgtr}(\tau,\tau') = \int \frac{\mathrm{d}\nu}{2\pi} g_L^{\lessgtr}(\nu)\mathrm{e}^{-(\nu-\mu)(\tau-\tau')}. \tag{D.31}$$

Inserting these expressions then gives

$$\mathscr{D}^M(\omega_{\mathcal{N}}) = \sum_{\mathcal{M}} \int \frac{\mathrm{d}\nu_{\mathcal{L}}}{(2\pi)^{|L|}} \left[C \prod_L g_L(\nu_L) \prod_I v_I \right]^{\mathcal{M}e} \Lambda_{\mathcal{M}}(\sigma_{\mathcal{M}}) \tag{D.32}$$

where the sum is over all orderings of the $N-1$ times in $\mathcal{M} = \mathcal{N} \setminus e$ (since we set $z_e = 0$ to be the earliest time) and where we defined

$$\Lambda_{\mathcal{M}}(\sigma_{\mathcal{M}}) = (-\mathrm{i})^{N-1} \int_0^\beta \mathrm{d}\tau_{\mathcal{M}}\, \theta(\tau_{\mathcal{M}}, 0) e^{\sigma_{\mathcal{M}}\cdot\tau_{\mathcal{M}}} \tag{D.33}$$

where

$$\sigma_j = \omega_j + \sum_{L=L_i} \bar{\nu}_L - \sum_{L=L_f} \bar{\nu}_L, \tag{D.34}$$

with $\bar{\nu}_L = \nu_L - \mu$. The latter term can be evaluated using the expression

$$\int_0^\beta \mathrm{d}\tau_n \ldots \mathrm{d}\tau_2\, \theta(\tau_n,\ldots,\tau_2,0)\mathrm{e}^{\sigma_n\tau_n+\ldots+\sigma_2\tau_2} = \sum_{\mathrm{div}(\mathcal{M})} \frac{(-1)^{M_+}\mathrm{e}^{\beta\Omega^-_{M_-}}}{\prod_{l=1}^{M_-}\Omega_l^- \prod_{k=1}^{M_+}\Omega_k^+} \tag{D.35}$$

where the sum is over all n divisions $\mathrm{div}(\mathcal{M})$ of the set $\mathcal{M} = \{n,\ldots,2\} = \{\mathcal{M}_-, \mathcal{M}_+\}$ into two disjoint subsets of size M_- and M_+ where we ordered the index corresponding to the latest time to the left. Here Ω_l^- and Ω_l^+ are defined to be the sum over the first l elements and the last l elements of $\sigma_{\mathcal{M}} = \{\sigma_n,\ldots,\sigma_2\}$ respectively. This expression can be conveniently derived using Laplace transforms [67, 27] or directly [45] by repeated integration and rearrangement of the resulting terms. This finally gives

$$\mathscr{D}^M(\omega_{\mathcal{N}}) = \sum_{\mathcal{M}} \sum_{\mathrm{div}(\mathcal{M})} \int \frac{\mathrm{d}\nu_{\mathcal{L}}}{(2\pi)^{|L|}} \frac{(-\mathrm{i})^{N-1}(-1)^{M_+}\mathrm{e}^{\beta\Omega^-_{M_-}}}{\prod_{l=1}^{M_-}\Omega_l^- \prod_{k=1}^{M_+}\Omega_k^+} \left[C \prod_L g_L(\nu_L) \prod_I v_I \right]^{\mathcal{M}e}. \tag{D.36}$$

Now

$$\mathrm{e}^{\beta\Omega^-_{M_-}} \left[\prod_L g_L(\nu_L) \prod_I v_I \right]^{\mathcal{M}_-\mathcal{M}_+e} = \left[\prod_L g_L(\nu_L) \prod_I v_I \right]^{\mathcal{M}_+ e\,\mathcal{M}_-} \tag{D.37}$$

so the product with the Boltzmann factors causes an effective cyclic permutation of the Matsubara times from $(\mathcal{M}_-, \mathcal{M}_+, e)$ to $(\mathcal{M}_+, e, \mathcal{M}_-)$. This is a consequence of the fluctuation-dissipation relations for the greater and lesser Green's functions:

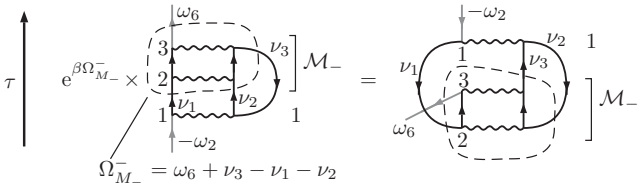

Figure D1. Example diagram for (D.37). In this case $\mathcal{M}_- = \{3, 2\}$, $\mathcal{M}_+ = \emptyset$, $e = 1$ and $\Omega^-_{M_-} = \omega_6 + \nu_3 - \nu_2 - \nu_1$. Multiplying by $e^{\beta\Omega^-_{M_-}}$ converts the left diagram into the right one in which the particle-hole lines that enter the circled region enclosing the vertices labeled by $\mathcal{M}_-$ are reversed in direction thereby inducing the cyclic set permutation $(\mathcal{M}_-, \mathcal{M}_+, 1) \to (\mathcal{M}_+, 1, \mathcal{M}_-)$

$e^{\beta\bar{\nu}} g^<(\nu) = -g^>(\nu)$ [45]. This is best illustrated with the example of Figure D1, where on the left hand side we consider a particular self-energy diagram for a given time-ordering. In this example the cut lines carry frequencies ν_1, ν_2 and ν_3 and we have an external vertex with outflowing frequency ω_6. In this case multiplication with $e^{\beta\Omega^-_{M_-}}$ has the effect

$$e^{\beta(\omega_6+\bar{\nu}_3-\bar{\nu}_2-\bar{\nu}_1)} g^>(\nu_1) g^>(\nu_2) g^<(\nu_3) = g^<(\nu_1) g^<(\nu_2) g^>(\nu_3) \tag{D.38}$$

where since ω_6 denotes an odd Matsubara frequency we have $e^{\beta\omega_6} = -1$. The particle lines along the cut have turned into hole lines and vice-versa leading to a contribution that diagrammatically corresponds to the right hand side of Figure D1 which amounts to a cyclic permutation of the times of the vertices. Since the orderings in $\mathcal{M}$ correspond to all orderings of the times $z_2, \ldots, z_N$ and we also sum over all ways to insert e into $\mathcal{M}$ we therefore sum over all orderings of $\mathcal{N} = (\mathcal{N}^+, e, \mathcal{N}^-)$ and the expression can be rewritten as

$$\mathscr{D}^M(\omega_\mathcal{N}) = \sum_\mathcal{N} \int \frac{\mathrm{d}\nu_\mathcal{L}}{(2\pi)^{|L|}} \frac{(-\mathrm{i})^{N-1}(-1)^{N_+}}{\prod_{k=1}^{N_-} \Omega^\mathcal{N}_k \prod_{l=1}^{N_+} \Omega^\mathcal{N}_l} \left[C \prod_L g_L(\nu_L) \prod_I v_I \right]^\mathcal{N} . \tag{D.39}$$

This is a generalisation to multiple external vertices of an expression derived by Balian and De Dominicis [44] and Baym and Sessler [45] for the frequency representation of the Matsubara self-energy diagrams. Our expression is of identical form to the one obtained from the Fourier transform of the retarded function (D.21). Writing $\omega_i = \bar{\omega}_i + \mu$ in (D.34) we see that this equation becomes identical to (D.13) apart from a shift with μ. It then follows that the functions $\mathscr{D}^M$ and $\mathscr{D}^R$ are equal if we replace each ω_i in $\mathscr{D}^M$ by $\omega_i - \mu - \mathrm{i}\eta_i$, i.e.

$$\mathscr{D}^{R(e,\mathcal{I})}(\omega_\mathcal{N}) = \mathscr{D}^M(\omega_\mathcal{N} - \mu - \mathrm{i}\eta_\mathcal{N}), \tag{D.40}$$

where η_i are positive infinitesimals (and there is no dependence on η_e). This analytic continuation formula is a generalization of (85) for general diagrams. Let us see how this relates to the very familiar example of the analytic continuation of the retarded and Matsubara Green's function. Evaluating the spectral representation of

$G^R(t_1,t_2) = G^{R(1,2)}(t_1,t_2)$ using the rules derived above gives for the two contour-orderings

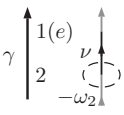

$$\rightarrow \int \frac{\mathrm{d}\nu}{2\pi} \frac{(-1)^0(-\mathrm{i})^1 g^>(\nu)}{\omega_2+\nu-\mathrm{i}\eta_2},$$

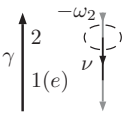

$$\rightarrow \int \frac{\mathrm{d}\nu}{2\pi} \frac{(-1)^1(-\mathrm{i})^1 g^<(\nu)}{\omega_2+\nu-\mathrm{i}\eta_2} \tag{D.41}$$

which give using the spectral function $A(\nu) = \mathrm{i}(g^>(\nu) - g^<(\nu))$

$$\begin{aligned} G^{R(1,2)}(\omega_1,\omega_2) &= -2\pi\delta(\omega_1+\omega_2)\int \frac{\mathrm{d}\nu}{2\pi}\frac{A(\nu)}{\omega_2+\nu-\mathrm{i}\eta_2} \\ &= 2\pi\delta(\omega_1+\omega_2)\int \frac{\mathrm{d}\nu}{2\pi}\frac{A(\nu)}{\omega_1-\nu+\mathrm{i}\eta_2} = 2\pi\delta(\omega_1+\omega_2)G^R(\omega_1). \end{aligned} \tag{D.42}$$

The rules for evaluating Matsubara functions are exactly the same as those for retarded functions, except that instead of $(\Omega - i\eta)$ the factors appearing in the denominator have the form $(\Omega + \mu)$. These rules therefore give for G^M the spectral representation

$$G^M(\omega_1,\omega_2) = 2\pi\delta(\omega_1+\omega_2)\int \frac{\mathrm{d}\nu}{2\pi}\frac{A(\nu)}{\omega_1-\nu+\mu} = 2\pi\delta(\omega_1+\omega_2)G^M(\omega_1). \tag{D.43}$$

Here $G^R(\omega_1)$ and $G^M(\omega_1)$ are the usual retarded and Matsubara components of the single-particle Green's function in frequency space, and comparing (D.42) and (D.43) we find the familiar result

$$G^R(\omega) = G^M(\omega - \mu + \mathrm{i}\eta). \tag{D.44}$$

An expression similar to (D.40) was also derived by Baier and Niégawa [46] based on the assumption that certain mixed imaginary-real time integrals vanish, which is akin to the assumption of a continuous spectrum in combination with the Riemann-Lebesque lemma. They formulate the relation (D.40) as

$$\mathcal{D}^{R(e,\mathcal{I})}(\omega_{\mathcal{N}}) = \mathcal{D}^M(\omega_{\mathcal{N}} - \mu - \mathrm{i}\eta_{\mathcal{N}}), \tag{D.45}$$

where η_i for $i \neq e$ are positive and $\eta_e = -\sum_{i\neq e}\eta_i$. Our derivation is both more well-defined and more general and has the additional advantage of not requiring the assumption of having a continuous spectrum which we used in deriving the finite temperature cutting rules (Section 3.3). The main result (D.40) can now be employed together with the technique of Jeon [27] to derive the retarded cutting rules directly from the Matsubara ones without the assumption of having a continuous spectrum.

References

[1] G. Stefanucci and R. van Leeuwen. *Nonequilibrium Many-Body Theory of Quantum Systems: A Modern Introduction*. Cambridge: Cambridge University Press, July 2013. ISBN: 9781107352070.

[2] P. Minnhagen. "Vertex correction calculations for an electron gas". In: *J. Phys. C Solid State Phys.* 7.17 (Sept. 1974), pp. 3013–3019. DOI: 10.1088/0022-3719/7/17/011.

[3] F. Brosens and J.T. Devreese. "Dynamical exchange effects in the dielectric function of jellium from perturbative and variational methods". In: *Phys. Rev. B* 29 (2 Jan. 1984), pp. 543–546. DOI: 10.1103/PhysRevB.29.543.

[4] M. Hellgren and U. von Barth. "Exact-exchange kernel of time-dependent density functional theory: Frequency dependence and photoabsorption spectra of atoms". In: *The Journal of Chemical Physics* 131.4 (2009), p. 044110. DOI: 10.1063/1.3179756.

[5] A. Schindlmayr and R.W. Godby. "Systematic Vertex Corrections through Iterative Solution of Hedin's Equations Beyond the *GW* Approximation". In: *Phys. Rev. Lett.* 80 (8 Feb. 1998), pp. 1702–1705. DOI: 10.1103/PhysRevLett.80.1702.

[6] D. Karlsson and R. van Leeuwen. "Partial self-consistency and analyticity in many-body perturbation theory: Particle number conservation and a generalized sum rule". In: *Phys. Rev. B* 94.12 (Sept. 2016), p. 125124. DOI: 10.1103/PhysRevB.94.125124.

[7] G. Stefanucci et al. "Diagrammatic expansion for positive spectral functions beyond GW: Application to vertex corrections in the electron gas". In: *Phys. Rev. B* 90 (2014), p. 115134. DOI: 10.1103/PhysRevB.90.115134.

[8] A.-M. Uimonen et al. "Diagrammatic expansion for positive density-response spectra: Application to the electron gas". In: *Phys. Rev. B* 91.11 (Mar. 2015), p. 115104. DOI: 10.1103/PhysRevB.91.115104.

[9] Y. Pavlyukh et al. "Vertex corrections for positive-definite spectral functions of simple metals". In: *Physical Review Letters* 117.20 (2016). DOI: 10.1103/PhysRevLett.117.206402.

[10] Y. Pavlyukh, G. Stefanucci, and R. van Leeuwen. "Dynamically screened vertex correction to *GW*". In: *Phys. Rev. B* 102 (4 July 2020), p. 045121. DOI: 10.1103/PhysRevB.102.045121.

[11] M. Hyrkäs, D. Karlsson, and R. van Leeuwen. "Diagrammatic Expansion for Positive Spectral Functions in the Steady-State Limit". In: *Phys. status solidi* 256.7 (July 2019), p. 1800615. DOI: 10.1002/pssb.201800615.

[12] P. Danielewicz. "Operator expectation values, self-energies, cutting rules, and higher-order processes in quantum many-body theory". In: *Ann. Phys. (N. Y).* 197.1 (Jan. 1990), pp. 154–201. DOI: 10.1016/0003-4916(90)90204-2.

[13] M. Hyrkäs, D. Karlsson, and R. van Leeuwen. "Contour calculus for many-particle functions". In: *J. Phys. A Math. Theor.* 52.21 (May 2019), p. 215303. DOI: 10.1088/1751-8121/ab165d.

[14] J. J. Kas and J. J. Rehr. "Finite Temperature Green's Function Approach for Excited State and Thermodynamic Properties of Cool to Warm Dense Matter". In: *Phys. Rev. Lett.* 119 (17 Oct. 2017), p. 176403. DOI: 10.1103/PhysRevLett.119.176403.

[15] A. Rios et al. "Liquid-gas phase transition in nuclear matter from realistic many-body approaches". In: *Physical Review C* 78.4 (Oct. 2008). DOI: 10.1103/physrevc.78.044314.

[16] F. Giustino. "Electron-phonon interactions from first principles". In: *Rev. Mod. Phys.* 89 (1 Feb. 2017), p. 015003. DOI: 10.1103/RevModPhys.89.015003.

[17] Y. Pavlyukh et al. "Time-linear scaling nonequilibrium Green's function method for real-time simulations of interacting electrons and bosons. II. Dynamics of polarons and doublons". In: *Phys. Rev. B* 105 (12 Mar. 2022), p. 125135. DOI: 10.1103/PhysRevB.105.125135.

[18] D. Karlsson et al. "Fast Green's Function Method for Ultrafast Electron-Boson Dynamics". In: *Physical Review Letters* 127.3 (July 2021). DOI: 10.1103/physrevlett.127.036402.

[19] D. Zgid and E. Gull. "Finite temperature quantum embedding theories for correlated systems". In: *New Journal of Physics* 19.2 (Feb. 2017), p. 023047. DOI: 10.1088/1367-2630/aa5d34.

[20] M. Galperin et al. "Cooling mechanisms in molecular conduction junctions". In: *Phys. Rev. B* 80 (11 Sept. 2009), p. 115427. DOI: 10.1103/PhysRevB.80.115427.

[21] R. L. Kobes and G. W. Semenoff. "Discontinuities of green functions in field theory at finite temperature and density". In: *Nuclear Physics B* 260.3 (1985), pp. 714–746. DOI: 10.1016/0550-3213(85)90056-2.

[22] R. L. Kobes and G. W. Semenoff. "Discontinuities of green functions in field theory at finite temperature and density (II)". In: *Nuclear Physics B* 272.2 (1986), pp. 329–364. DOI: 10.1016/0550-3213(86)90006-4.

[23] F. Gelis. "Cutting rules in the real-time formalisms at finite temperature". In: *Nuclear Physics B* 508.1 (1997), pp. 483–505. DOI: 10.1016/S0550-3213(97)80023-5.

[24] M. Veltman. "Unitarity and causality in a renormalizable field theory with unstable particles". In: *Physica* 29.3 (1963), pp. 186–207. DOI: 10.1016/S0031-8914(63)80277-3.

[25] M. Veltman. *Diagrammatica: The Path to Feynman Diagrams*. Cambridge Lecture Notes in Physics. Cambridge University Press, 1994. DOI: 10.1017/CBO9780511564079.

[26] P. F. Bedaque, A. Das, and S. Naik. "Cutting rules at finite temperature". In: *Modern Physics Letters A* 12.33 (1997), pp. 2481–2496. DOI: 10.1142/S0217732397002612.

[27] S. Jeon. "Computing spectral densities in finite temperature field theory". In: *Phys. Rev. D* 47 (10 May 1993), pp. 4586–4607. DOI: 10.1103/PhysRevD.47.4586.

[28] P.V. Landshoff. "Simple physical approach to thermal cutting rules". In: *Physics Letters B* 386.1 (1996), pp. 291–296. DOI: 10.1016/0370-2693(96)00919-7.

[29] R. van Leeuwen and G. Stefanucci. "Wick theorem for general initial states". In: *Phys. Rev. B* 85 (11 Mar. 2012), p. 115119. DOI: 10.1103/PhysRevB.85.115119.

[30] R. van Leeuwen and G. Stefanucci. "Equilibrium and nonequilibrium many-body perturbation theory: a unified framework based on the Martin-Schwinger hierarchy". In: *Journal of Physics: Conference Series* 427 (Mar. 2013), p. 012001. DOI: 10.1088/1742-6596/427/1/012001.

[31] M. Garny and M. M. Müller. "Kadanoff-Baym equations with non-Gaussian initial conditions: The equilibrium limit". In: *Phys. Rev. D* 80 (8 Oct. 2009), p. 085011. DOI: 10.1103/PhysRevD.80.085011.

[32] M. Wagner. "Expansions of nonequilibrium Green's functions". In: *Phys. Rev. B* 44 (12 Sept. 1991), pp. 6104–6117. DOI: 10.1103/PhysRevB.44.6104.

[33] R. Haag, N. M. Hugenholtz, and M. Winnink. "On the equilibrium states in quantum statistical mechanics". In: *Communications in Mathematical Physics* 5.3 (1967), pp. 215–236. DOI: 10.1007/BF01646342.

[34] H. Appel and E. K. U. Gross. "Time-dependent natural orbitals and occupation numbers". In: *EPL (Europhysics Letters)* 92.2 (Oct. 2010), p. 23001. DOI: 10.1209/0295-5075/92/23001.

[35] F. Reinert and S. Hüfner. "Photoemission spectroscopy—from early days to recent applications". In: *New Journal of Physics* 7 (Apr. 2005), pp. 97–97. DOI: 10.1088/1367-2630/7/1/097.

[36] C.O. Almbladh and L. Hedin. *Beyond the one-electron model: many-body effects in atoms, molecules, and solids,* in Handbook of Synctrothron radiation vol. 1b. Ed. by E.E. Koch. North-Holland, 1983, pp. 607–904.

[37] C.O. Almbladh. "Photoemission beyond the sudden approximation". In: *Journal of Physics: Conference Series* 35 (Apr. 2006), pp. 127–144. DOI: 10.1088/1742-6596/35/1/011.

[38] P. Danielewicz. "Quantum theory of nonequilibrium processes, I". In: *Ann. Phys. (N. Y).* 152.2 (Feb. 1984), pp. 239–304. DOI: 10.1016/0003-4916(84)90092-7.

[39] M. Gell-Mann and F. Low. "Bound States in Quantum Field Theory". In: *Phys. Rev.* 84 (2 Oct. 1951), pp. 350–354. DOI: 10.1103/PhysRev.84.350.

[40] L. V. Keldysh. "Diagram technique for nonequilibrium processes". In: *Sov. Phys. JETP* 20.4 (1965), pp. 1018–1026. URL: www.jetp.ras.ru/cgi-bin/e/index/e/20/4/p1018?a=list.

[41] T. Blažek and P. Maták. "Cutting rules on a cylinder: a simplified diagrammatic approach to quantum kinetic theory". In: *The European Physical Journal C* 81.12 (2021), p. 1050. DOI: 10.1140/epjc/s10052-021-09874-3.

[42] T. Blažek and P. Maták. "Mass-derivative relations for leptogenesis". In: *The European Physical Journal C* 82.3 (2022), p. 214. DOI: 10.1140/epjc/s10052-022-10165-8.

[43] W. Rudin. *Functional Analysis*. McGraw-Hill, 1991.

[44] R. Balian and C. De Dominicis. "Sur la fonction de green à une particule en mécanique statistique quantique". In: *Nuclear Physics* 16.3 (1960), pp. 502–517. DOI: 10.1016/S0029-5582(60)81010-3.

[45] G. Baym and A.M. Sessler. "Perturbation-Theory Rules for Computing the Self-Energy Operator in Quantum Statistical Mechanics". In: *Phys. Rev.* 131 (5 Sept. 1963), pp. 2345–2349. DOI: 10.1103/PhysRev.131.2345.

[46] R. Baier and A. Niégawa. "Analytic continuation of thermal N-point functions from imaginary to real energies". In: *Phys. Rev. D* 49 (8 Apr. 1994), pp. 4107–4112. DOI: 10.1103/PhysRevD.49.4107.

[47] H. Shi and A. Griffin. "Finite-temperature excitations in a dilute Bose-condensed gas". In: *Physics Reports* 304.1 (1998), pp. 1–87. DOI: 10.1016/S0370-1573(98)00015-5.

[48] A. Perali et al. "BCS-BEC Crossover at Finite Temperature for Superfluid Trapped Fermi Atoms". In: *Phys. Rev. Lett.* 92 (22 June 2004), p. 220404. DOI: 10.1103/PhysRevLett.92.220404.

[49] Q. Chen et al. "BCS–BEC crossover: From high temperature superconductors to ultracold superfluids". In: *Physics Reports* 412.1 (2005), pp. 1–88. DOI: 10.1016/j.physrep.2005.02.005.

[50] W.H. Dickhoff and C. Barbieri. "Self-consistent Green's function method for nuclei and nuclear matter". In: *Progress in Particle and Nuclear Physics* 52.2 (Apr. 2004), 377–496. DOI: 10.1016/j.ppnp.2004.02.038.

[51] T. Alm et al. "Nucleon spectral function at finite temperature and the onset of superfluidity in nuclear matter". In: *Phys. Rev. C* 53 (5 May 1996), pp. 2181–2193. DOI: 10.1103/PhysRevC.53.2181.

[52] P. Bożek. "Self-consistent solution of Galitskii-Feynman equations at finite temperature". In: *Phys. Rev. C* 59 (5 May 1999), pp. 2619–2626. DOI: 10.1103/PhysRevC.59.2619.

[53] T. Frick and H. Müther. "Self-consistent solution to the nuclear many-body problem at finite temperature". In: *Phys. Rev. C* 68 (3 Sept. 2003), p. 034310. DOI: 10.1103/PhysRevC.68.034310.

[54] M. Puig von Friesen, C. Verdozzi, and C.-O. Almbladh. "Kadanoff-Baym dynamics of Hubbard clusters: Performance of many-body schemes, correlation-induced damping and multiple steady and quasi-steady states". In: *Phys. Rev. B* 82 (15 Oct. 2010), p. 155108. DOI: 10.1103/PhysRevB.82.155108.

[55] N. Schlünzen and M. Bonitz. "Nonequilibrium Green Functions Approach to Strongly Correlated Fermions in Lattice Systems". In: *Contributions to Plasma Physics* 56.1 (2016), pp. 5–91. DOI: 10.1002/ctpp.201610003.

[56] N. H. Kwong, G. Rupper, and R. Binder. "Self-consistent T-matrix theory of semiconductor light-absorption and luminescence". In: *Phys. Rev. B* 79 (15 Apr. 2009), p. 155205. DOI: 10.1103/PhysRevB.79.155205.

[57] G. Strinati. "Application of the Green's functions method to the study of the optical properties of semiconductors". In: *La Rivista del Nuovo Cimento (1978-1999)* 11.12 (1988), pp. 1–86. DOI: doi.org/10.1007/BF02725962.

[58] C. Piermarocchi and F. Tassone. "Role of bound pairs in the optical properties of highly excited semiconductors: A self-consistent ladder approximation approach". In: *Phys. Rev. B* 63 (24 June 2001), p. 245308. DOI: 10.1103/PhysRevB.63.245308.

[59] L. Hedin. "New Method for Calculating the One-Particle Green's Function with Application to the Electron-Gas Problem". In: *Phys. Rev.* 139 (3A Aug. 1965), A796–A823. DOI: 10.1103/PhysRev.139.A796.

[60] F. Aryasetiawan and O. Gunnarsson. "The GW method". In: *Reports on Progress in Physics* 61.3 (Mar. 1998), pp. 237–312. DOI: 10.1088/0034-4885/61/3/002.

[61] A. Stan, N. E. Dahlen, and R. van Leeuwen. "Levels of self-consistency in the GW approximation". In: *The Journal of Chemical Physics* 130.11 (2009), p. 114105. DOI: 10.1063/1.3089567.

[62] A. Wierling and G. Röpke. "One-Particle Spectral Function of Electrons in a Hot and Dense Plasma". In: *Contributions to Plasma Physics* 38.4 (1998), 513–524. DOI: 10.1002/ctpp.2150380405.

[63] C. Fortmann. "Self-consistent spectral function for non-degenerate Coulomb systems and analytic scaling behaviour". In: *Journal of Physics A: Mathematical and Theoretical* 41.44 (Oct. 2008), p. 445501. DOI: 10.1088/1751-8113/41/44/445501.

[64] P. Pokhilko et al. "Evaluation of two-particle properties within finite-temperature self-consistent one-particle Green's function methods: Theory and application to GW and GF2". In: *The Journal of Chemical Physics* 155.2 (2021), p. 024119. DOI: 10.1063/5.0054661.

[65] W. Kutzelnigg and D. Mukherjee. *Reduced-Density-Matrix Mechanics: With Application to Many-Electron Atoms and Molecules*. Ed. by D. A. Mazziotti. Advances in Chemical Physics. Hoboken, NJ, USA: John Wiley & Sons, Inc., Mar. 2007. ISBN: 9780470106600. DOI: 10.1002/0470106603.

[66] J.W. Negele and H. Orland. *Quantum Many Particle Systems*. Boca Raton: CRC Press, 1995. ISBN: 9780201410471.

[67] C. Bloch and C. De Dominicis. "Un développement du potentiel de gibbs d'un système quantique composé d'un grand nombre de particules". In: *Nuclear Physics* 7 (1958), pp. 459–479. DOI: 10.1016/0029-5582(58)90285-2.